National Centre
for the Replacement
Refinement & Reduction
of Animals in Research

Evaluation of the potential of *Xenopus laevis* as a novel model organism for the detection of drug-induced cardiotoxicity

Thesis submitted for the degree of Doctor of Philosophy (PhD)

University of East Anglia

School of Biological Sciences

Saskia Wyville

47,484 Words

September 2025

Abstract

As animal use in science decreases the need for models to accurately predict drug-induced cardiotoxicity increases. *Xenopus laevis* embryos provide the potential for initial molecule screening on a medium- to high-throughput scale, allowing toxic molecules to be removed earlier in development, reducing the number and expense of later mammalian trials.

To investigate *X. laevis* models two factors were examined- the effect on heart rate and the detection or change in expression of miRNA biomarkers. To determine heart rate, embryos were treated with known cardiotoxic drugs such as doxorubicin and terfenadine at a range of concentrations at NF stage 38 and grown in drug-containing media until NF stage 45 before being anaesthetised and imaged. Video footage was used to determine heart rate through movement of blood between heart chambers and a novel program in R Studio. Biomarkers from the literature that indicated cardiotoxicity, miRNA-208, miRNA-499, and miRNA-143 were used. Embryos were exposed in the same manner until NF stage 45, before being harvested into 'head' and 'tail' samples; with head sample containing the heart and major organs and tail sample containing highly vascular tail tissue, before being assessed using qRT-PCR to determine expression levels of target miRNAs.

When exposed to doxorubicin and terfenadine, heart rate decreased and incidence of arrhythmia increased at the higher concentrations of the drug, mirroring the effects seen in mammalian models of cardiotoxicity. The qRT-PCR results were varied, with strong indications of increasing expression of miRNA-499 and miRNA-143 in the embryos exposed to the highest concentrations of terfenadine, and a reduction in expression of miRNA-499 and miRNA-143 in embryos exposed to the highest concentrations of doxorubicin.

The results obtained in this study indicate that *X. Laevis* would make a suitable model for assessing drug-induced cardiotoxicity and the methodologies employed lend themselves well to scaling for industrial applications.

Contents

List of Figures

List of Tables

Acknowledgements

My thanks go to my supervisory team of Professor Grant Wheeler, Dr Amer Rana and Professor Sam Fountain, for their support and insights over the course of this thesis, as well as helping me to develop as a person.

I would also like to thank Dr Timothy Grocott for his invaluable help with all things mathematics and software related.

A very specific thanks goes to Dr Claudia Buhigas, I could never have managed to work out the coding aspects of this thesis without your help and patience with me as I tried to catch up with your level of knowledge.

Further thanks go to the other members of the lab who I have worked alongside during my time here- Amy, Marco, Emily, Joe, Magda and everyone else. We always found time to have a laugh, even when things felt like they were falling down around us.

I am grateful to the team at NC3R's, especially Dr Natalie Duggett, for arranging funding for the project and continued support through training, summer schools and more.

Dr Alice Godden is also deserving of thanks, as you turned from fellow PhD student to mentor and friend, I am thankful you have been part of my journey.

My gratitude is also directed towards my family, who have helped from the start with moving across the country and back, always being at the end of the phone and a constant source of support and encouragement- especially Mum, Elana, and Dave. Thank you also to my loving partner, Scott. You really are the other side of my coin, and I am glad I met you when I did, as I don't think this would have been as successful without you at my side.

Covid-19 and Disruption Statement

The author began their PhD on October 1, 2020. At the point of arrival at the University of East Anglia, Covid-19 restrictions were in force. The University had entered lockdown in March 2020 alongside most other businesses and academic institutions in the UK, and the European Xenopus Resource Centre (EXRC) had stopped shipping in January 2020. Fresh *Xenopus laevis* and *Xenopus tropicalis* had been intended for ordering/delivery in mid-2020, and at the onset of the Covid-19 pandemic these orders were cancelled by the EXRC. This fresh breeding stock was required as the current frog colony were beginning to get older, and as the frogs got older the fertility and quality of eggs laid is reduced.

The University reopened for essential work with strict restrictions in June 2020. These restrictions included occupancy restrictions, mandatory face masking and regular testing 2x weekly as routine, with additional tests being taken following exposure to virus or on showing symptoms. In the laboratory, these restrictions led to the creation of a rota system to ensure only one lab group would be in at any given time, as the facilities were shared between the chick lab and the frog lab (Figure 0.1). This was intended to limit the amount of people each person would be exposed to, and to minimise risk of transmission should Covid-19 enter the laboratory. This led to difficulties with planning experiments, as being restricted to set times meant that there was no flexibility in embryo development and access to equipment. Daily care for embryos also had to be performed outside of lab hours on days that the frog group were not scheduled in, and on weekends times to enter the laboratory had to be co-ordinated to ensure there was minimal crossover. Altogether, this was quite restrictive and not conducive to sustained positive advances.

Figure 0.1: Initial laboratory rota. *This shows the allocation of time between the Chick group (C- yellow) and the Frog group (F- green) for the initial period when the University reopened following the Covid-19 lockdown.*

In February 2021, the EXRC began shipping products again, namely frozen *Xenopus sp.* sperm- the shipping of live frogs was planned to be reintroduced later in the year and the previously cancelled order would be fulfilled. The authors first vaccination for Covid-19 was in May 2021, ahead of the general vaccine rollout in the UK, due to underlying health conditions leading them to be considered clinically vulnerable. In July of the same year, Covid-19 restrictions were lifted slightly at the University, with social distancing guidelines and masking remaining as the major restrictions remaining. At the same time, the EXRC began reporting illness amongst some of the *Xenopus* populations and that shipping live frogs may be delayed. By the start of January 2022, the illness frequency was higher than expected and requests for spleen and liver samples of any frogs culled during research were requested to be sent over for assistance in identifying the potential spread of the unknown disease. During this time, embryo generation had been done by use of frozen *Xenopus* sperm and what few male *X. laevis* remained in the colony. As the number of males reduced to zero, all fertilisation was done using frozen sperm, which gave much lower rates of fertilisation compared to fresh sperm harvested from testes.

There was a period of time leading up to June 2022 when there were several weeks in a row where fertilisation rates were near 0% and research stalled due to this. By June 2022, the fertilisation issues with frozen *X. laevis* sperm had been reported to the EXRC and an agreement was reached that they would cull males and ship fresh testes when required, as the disease outbreak at the centre had been identified and was under control. Orders for shipping live animals and replenishing the colony of breeding females were able to be made starting from August 2022, but these did not arrive until May 2023, when the research period had concluded. A timeline covering these major points of disruption is included in Figure 0.2.

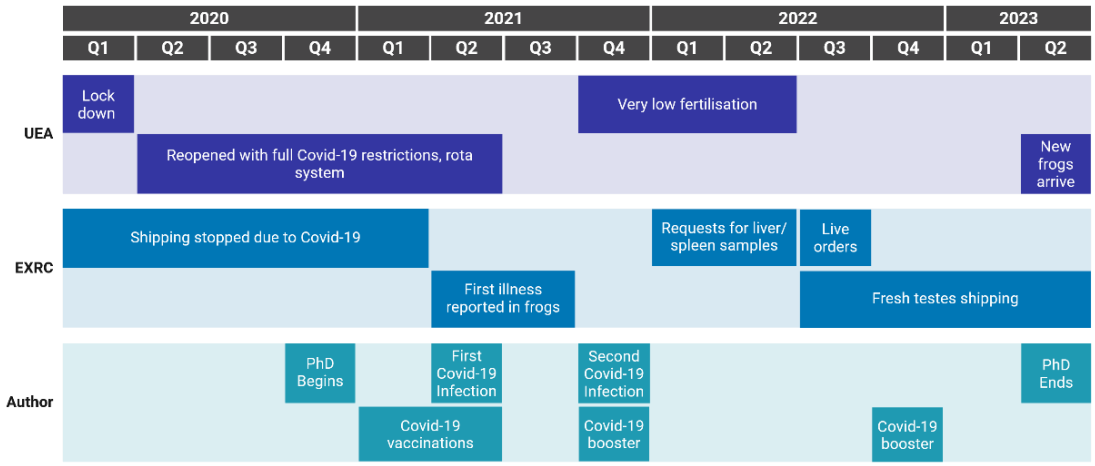

Figure 0.2: Disruption timeline. *Figure shows major disruptions involving the University, EXRC and the Author personally. These are largely caused by the Covid-19 pandemic, particularly with regards to shipping frogs and testes from the EXRC and illness due to the infection. Not included are general impacts such as shipping delays.*

Chapter 1: Introduction

1.1 Overview of drug development

Drug development is a complex, time-consuming process that as a result costs billions of dollars per year. New drugs must not only treat the specific disease they are designed for but must also be carefully tested to ensure they do not cause additional harm and as a consequence an extensive, multi-stage process is conducted on each potential compound to ensure drugs that come onto the market are as safe as possible (Figure 1.1).

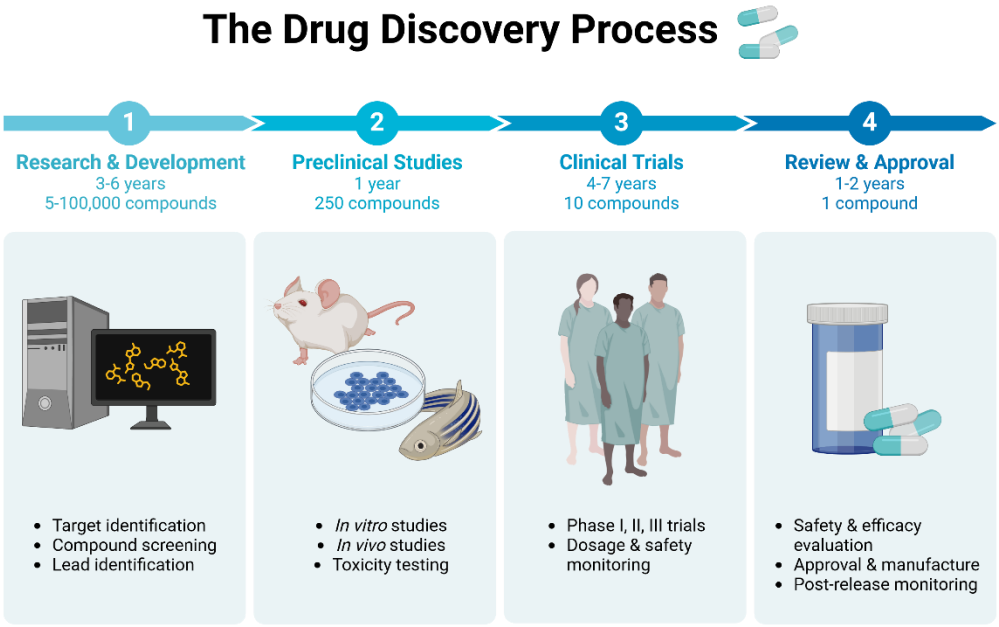

Figure 1.1: The drug discovery process. *Time taken for each stage of bringing a drug to market from initial target discovery can be anywhere from 9- 16 years; most compounds identified in the earliest stages fail before coming to review (Blass, 2015; Brunning, 2016; U.S Food & Drug Administration, 2018). Created with Biorender.*

Drug development starts with an assessment of the current state of pharmacological knowledge and identifying a need for improvement. Target identification begins with novel compounds being designed or identified as a

potential new therapeutic for a chosen disease. Over recent years this process has become highly automated, and it is possible to screen tens of thousands of compounds using very high-throughput screening methodologies. These compounds tend to fall into two categories- completely novel targets for the disease of interest or using an existing target for which a drug or drugs already exist to treat and searching for a compound that improves on the existing drug, be it greater efficacy in treatment or reduction in side effects. The latter category is much more likely to yield consistent results as it uses an existing knowledge base, whereas the creation of an entirely novel target for treating the disease generates a lot more uncertainty and so increases risk that a product will fail in this process. The compounds with the strongest potential are further optimised to be more target-specific and maximise potency of effect, to give the compound the best chance of success in the ensuing clinical stages. At this stage it is possible to conduct very early toxicity studies, and recent developments mean *in silico* simulations based on existing knowledge of similar and existing compounds are as likely to be used as living models (Blass, 2015; Eakins and Xu, 2009; Lu and Kacew, 2002).

Preclinical development is where most potential compounds fail, and most of these failings occur during *in vivo* tests using animal models such as mice. The reason for such a large attrition rate at this point specifically is in part due to the historical lack of *in vitro* tests that are sufficiently representative of real human physiology. While progress is being made in this area, the fact remains that moving from *in vitro* tests into a living organism, even with the advent of organoid and IPSC technology, is a jump in complexity that has yet to be artificially replicated, and for as long as the complexities of whole organisms remain beyond replication, the need for *in vivo* testing will remain. Indeed, it is a legal requirement for most of the world to carry out *in vivo* testing prior to human testing.

The progression through clinical trials occurs over multiple phases. Phase 1 is performed on a very small cohort, usually less than 100 people, using participants that are in good health. The aims for these trials are to discover any immediate side effects that were unable to be predicted or discovered previously, as well as initial human measurements such as how quickly the drug is metabolised. Phase 2 is conducted on a larger scale but with usually less than 500 people involved, and these are typically patients with the disease the drug is seeking to treat. This stage allows the efficacy of the drug to be determined as trials are typically performed with placebos alongside the active compound. Phase 3 is usually a wider scale operation with thousands of participants and is used to determine an accurate efficacy rate, conduct dosage experiments, and comparisons with other existing drugs to be performed. Throughout all stages a strong emphasis on safety will be in place as adverse reactions, potentially severe in effect, are a very real possibility (Moonen *et al*., 2017).

Following human trials the drug undergoes a review process, where data collected is analysed and final calculations made to determine whether the drug is effective and meets the aims set out in the initial stage of drug development. All the data produced so far is collated and submitted to the relevant regulatory body for assessment and if successful the drug will be approved for market release. If unsuccessful, additional trials and experiments may be conducted to cover the areas of concern noted by the regulatory body and then resubmitted for approval. Following approval post release monitoring occurs to ensure any additional side effects are detected and reported. These may occur due to the larger number of patients taking the drug or through long term exposure, something unable to be tested during clinical trial phases.

1.2 Safety assessment and checks

Drug development, and more importantly the safety assessments, that are expected to be performed before a drug is approved is a highly regulated area of legislation worldwide.

The regulatory system used within the UK for drug safety assessment is still based around the EU regulations following their withdrawal from the EU. While this may change as time passes, this is unlikely as the EU medicines regulatory process is designed to perform as a gold standard, with multiple countries around the world adopting the recommendations provided. Many of these recommendations stem from collaboration and discussion between the three major contributors (the EU, USA and Japan) at the International Conference on Harmonisation (ICH), established in 1990 with the aim to integrate and standardise regulations across the globe. Some of the regulations deal with drug development prior to beginning trials (clinical or otherwise) such as Q8(R2) which focusses on the development of the drug product itself and the ideal properties that should be searched for when choosing candidates.

The main aim for these recommendations is to improve public safety. This is achieved through standardisation of tests that should be performed for new drug products, minimising the risk of unsafe drugs being passed for approval, and removing them from the development process at the earliest point possible. It is important to consider that these are guidelines for best practise and are not legislatively mandated, the idea behind this is to allow drug manufacturers flexibility in performing studies and to encourage adoption of new methodologies and approaches as they are developed.

Initially, most drugs will undergo what are known as exploratory toxicology studies- these are used to determine which organs are affected by the drug, and through using a range of doses and exposure times this can help

determine at what dosage the drug will begin to cause toxicity. Once these rough estimations of dosages have been made, more detailed *in vivo* studies can be conducted through regulatory toxicological studies, which are performed following good laboratory practise (GLP) and good manufacturing practice (GMP).

ICH guidelines are varied in their scope, with the bulk of relevant guidelines covered below:

S7A- Safety Pharmacology Studies for Human Pharmaceuticals covers the area of study design, encouraging choices that test the effects of novel compounds on the most relevant organ systems, such as cardiovascular or respiratory systems. Stipulations include that the highest tested doses should be chosen which produce moderate adverse effects to fully understand the risk potential of novel compounds (ICH Harmonised Tripartite Guideline, 2000).

S7B- The Non-Clinical Evaluation of the Potential for Delayed Ventricular Repolarization (QT Interval Prolongation) by Human Pharmaceuticals evaluates the potential for delayed ventricular repolarisation, a factor that is a regulatory requirement and not a guideline. Repolarisation disruption is the reason so many novel developments into modelling cardiotoxicity focus on the electrophysiologic effects of a novel drug (ICH Harmonised Tripartite Guideline, 2005a).

S9- Nonclinical Evaluation for Anticancer Pharmaceuticals discusses the various types of toxicity that should be tested for, such as reproductive toxicity, genotoxicity, carcinogenicity and generalised toxicity (ICH Harmonised Tripartite Guideline, 2009b).

S3A- Note for Guidance on Toxicokinetics: The Assessment of Systemic Exposure in Toxicity Studies discusses how to quantify exposure to a novel compound using variables such as plasma concentrations or looking for metabolites.

E4- Dose Response Information to Support Drug Registration makes the point that dose response studies are vital for determining the minimum dose of drug required to provide the maximum effect, as continually increasing a dose without changing the therapeutic effect is a waste of money and may increase the likelihood of toxic side effects (ICH Harmonised Tripartite Guideline, 1994).

E14- The Clinical Evaluation of QT/QTc Interval Prolongation and Proarrhythmic Potential for Non-Antiarrhythmic Drugs covers the clinical evaluation of QT/QRT interval prolongation and proarrhythmic potential for non-antiarrhythmic drugs, predominately to cover clinical trials (ICH Harmonised Tripartite Guideline, 2005b).

S4- Duration of Chronic Toxicity Testing in Animals (Rodent and Non-Rodent Toxicity Testing) covers the experiments that should be conducted to explore chronic toxicity in animal models. Primarily these are rodents (6-month study period) and non-rodents (9-month study period) (ICH Harmonised Tripartite Guideline, 1998).

The culmination of all the pre-clinical experiments and studies are used to inform initial clinical trials, as explained in **M3(R2) Guidance on Nonclinical Safety Studies for the Conduct of Human Clinical Trials and Marketing Authorisation for Pharmaceuticals**. This offers guidance on which nonclinical safety studies to consider when determining how to perform clinical trials. It covers the repeated dose toxicity studies that should have

been performed on animal models and how the length of time spent on those studies can inform the length of a clinical trial. If the full 6 months exposure in rodents was performed as per S4 guidelines, this would likely produce results supporting a 6 months or longer clinical trial in humans. If a shorter period such as 2 weeks was performed, this would only support a clinical trial of around the same time period for the safety of the patients involved (ICH Harmonised Tripartite Guideline, 2009a).

Although the guidelines listed govern the development and approval of novel drugs within the UK, other countries have taken note of the flaws within the existing system and sought to progress their own development and approval process to overcome the existing challenges. For instance, in 2022 the USA signed into law the FDA Modernization Act 2.0. The purpose of this bill is to repeal the previously existing requirements for animal testing prior to drug approval, and to allow alternative methods to be utilised to indicate drug safety instead. This explicitly creates the space for drug developers to offer non-animal methods for drug approval that is only implied in the ICH guidelines, and will hopefully encourage drug developers to pursue these non-animal alternatives (Han, 2023).

1.3 Flaws with the current system

The current system of drug development has become more robust over time, and while we are at the point where drug certification is the best and safest it ever has been, it is not above criticism and further improvement.

One of the more pressing issues facing any company seeking to develop a new drug is the fact that costs for doing so are rising year on year, making research and development into novel drugs less appealing without a higher guarantee on return. One method that is being used to encourage development is government sponsoring of research via schemes such as USAID’s neglected tropical diseases program or subsidising some of the

development costs. Another way that drug manufacturers can combat this is by adopting new methods of drug testing that can offer a reduced cost outlay- this is an area where new methodologies can offer great advances as many of the established systems, particularly *in vivo* methods, come at a great cost.

The largest issue however remains with drug attrition, with the biggest cause of attrition being toxicity of the novel drug across all phases of the drug development process. This has encouraged companies to focus their safety studies on the earlier stages of development, identifying and discarding compounds that are most likely to cause toxicity at the earliest opportunity, thereby reducing the amount of time and money spent on a non-viable drug. This means that new methodologies encouraging early removal of drugs from the pipeline by indicating toxicity earlier would be welcomed by the industry for these reasons, with the caveat that they can be proven to be effective and more efficient than existing offerings.

A factor tempering the ready acceptance of novel methodologies is the need to prove a new method's effectiveness in toxicity testing, as resistance towards adoption of said new methods can be slow, often due to concern that regulatory authorities would not recognise them as accurate and acceptable representations of the novel compounds' effects in humans. This is where the ICH guidelines can be utilised to their best effectiveness, as the fact they are very specifically created as guidelines and not strict regulations creates the flexibility for new methods to be incorporated.

Another potential flaw in the system, and one that prompts the creation of non-animal methods specifically, is the potential for failure of translation from animal model to human. This is not something that can escaped but can be mitigated as much as possible by making careful considerations as to the animals being used for modelling and toxicity studies. It is essential to ensure

that models are as reflective of human physiology as possible, and the positive or negative responses seen in the animal are likely to be recapitulated in humans. This can be assessed in numerous ways, but looking for genetic orthologues across species and for proteins that are conserved across species is often a good indicator. This is a factor driving the E14 regulations specifically surrounding the use of QT/QRT interval elongation as a specific cardiotoxicity marker, as the genes responsible for the electrophysiological response in the heart are often conserved between humans and animal model species (Salkoff et al., 1992).

1.4 Cardiotoxicity

"Cardiotoxicity" can refer to anything that is toxic and causes damage to the heart. In this study, we are focussing on drug-induced cardiotoxicity and as such will ignore other contributors such as dietary and environmental factors.

1.4.1 The healthy heart

The proper functioning of the heart is so intrinsic to life that during embryo development the heart is the first organ to develop, and indeed a human heartbeat can be detected from as early as 6 weeks of gestation. The primary function of the heart is to facilitate movement of blood around the body, via a pumping mechanism in which blood enters the heart and electrical impulses stimulate contraction of the cardiac muscle, forcing the blood from the chamber it currently is in and into the next chamber or out through the blood vessels.

The nature of said chambers and specific anatomy depends on which organism the heart belongs to. For the purposes of this study, we will focus on comparing the mammalian, amphibian and fish hearts as seen in Figure 1.2.

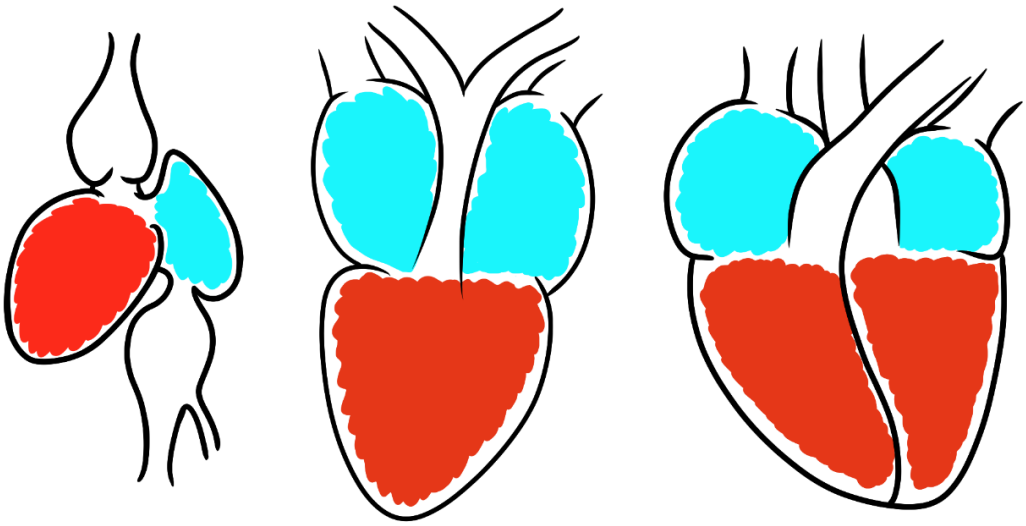

Figure 1.2: Comparative anatomy of hearts. *Fish heart, amphibian heart and mammalian heart, with the atria in blue and the ventricles in red. Illustration created by Collyer, Edward (2024).*

Mammalian heart

The mammalian heart is found throughout all species under the class *Mammalia*, including dogs (*Canis lupus familiaris*), mice (*Mus musculus*), and humans (*Homo sapiens*). In humans, the size of a person's heart can be estimated by using the size of their fist, but a measurement of approximately 12x9 cm long and wide, and 6cm thick is considered average for an adult (Tortora and Derrickson, 2014). The mammalian heart consists of 4 chambers, two atria and two ventricles, and is divided roughly down the middle into two halves. The walls of the ventricles are much thicker than those of the atria, with the left ventricle having the thickest of all due to the necessity of creating a higher pressure for pumping blood from this chamber around the body. The heart tissue is multi-layered, with an inner layer (endocardium), middle layer (myocardium) and the outer layer (epicardium). The myocardium constitutes the bulk of cardiac tissue and is the location of cardiac muscle fibres.

The cardiovascular system of mammals is considered a double circulatory system, as oxygenated and deoxygenated blood are kept separate and dealt with in a separate system of arteries (primarily transporting oxygenated blood) and veins (primarily transporting deoxygenated blood). In a mammalian heart, deoxygenated blood enters the right atrium via the vena cava, passes through the atrioventricular valves into the right ventricle and then out of the heart through a semilunar valve into the pulmonary artery, where it travels to the lungs to become reoxygenated. After oxygenation, blood returns to the heart through the pulmonary vein and enters the left atrium, passes through another set of atrioventricular valves into the left ventricle and out through a semilunar valve and into the aorta to be transported to the rest of the body. The valves within the heart act to create a one-way system, preventing backflow of the blood as it travels between chambers and are held closed due to the pressure of the blood in the now filled chamber (Giunti Editorial Group, 2005).

The pumping action is controlled by the generation and proliferation of action potentials, originating in the autorhythmic cells of the sinoatrial node (in the right atrial wall). These cells spontaneously depolarise and repolarise, triggering an action potential when it passes a threshold, which propagates through the cardiac tissue and leads to the contraction of the atria initially, before being transmitted to the atrioventricular node in the interatrial wall, then continuing to the bundle of His- another group of cardiac cells that are specially adapted to conduct electrical charges. The bundle of His propagates the action potential through the tissues before branching and developing into Purkinje fibres that branch across the ventricular walls, leading to synchronised and consistent contraction of cardiac tissue, allowing the heart to pump blood effectively.

The action potential of cardiomyocytes occurs over 5 distinct phases. A visual interpretation of both action potential and relevant ionic currents is shown in Figure 1.3. In human cardiomyocytes, the baseline membrane

potential is approximately -90mV, with phase 0 being the rapid influx of Na+ ions as the voltage gated sodium ion channels activate, depolarising the membrane potential to approximately +20mV. This in turn triggers phase 1, in which potassium ion channels are opened to cause rapid repolarisation with K+ ion removal. The repolarisation is slowed and levels off as Ca^2+ and slow delayed rectifier K+ channels open to allow Ca^2+ inflow and further K+ outflow in phase 2. Phase 3 occurs when further K+ rectifier channels open to increase the outflow of K+ ions, eventually returning the membrane potential back to -90mV at phase 4, where the cardiomyocytes remain until the next cycle begins from phase 0 again (Darbar and Roden, 2013; Li et al., 2016).

Shown in Figure 1.3 are the genes responsible for or associated with the α-subunit of each ion channel. These are particularly important when considering cardiac disorders, as mutations within these are often associated with changes in cardiac rhythm. Darbar and Roden (2013) note that mutations in several of the studied genes are associated with atrial fibrillation- particularly several members of the KCN group of genes responsible for the potassium ion currents. One of these in particular- KCNH2- has strong associations with cardiac arrythmias. Due to the functional importance of these channels, the genes responsible for producing them are often well conserved between species, with many having homologues of the gene. Despite this apparent similarity, there are cases where the presence of similar genes and similar ion channels do not lead to similar behaviours in models, particularly between human and animal model responses. A mouse model of long QT syndrome was developed using a mutation in the KCNH2 gene, but despite the same mutation in humans leading to severe negative impacts in humans the mouse model remained unaffected (Nerbonne et al., 2001). Incidents such as these serve as a reminder that the presence of similar channels do not necessarily indicate similar outcomes.

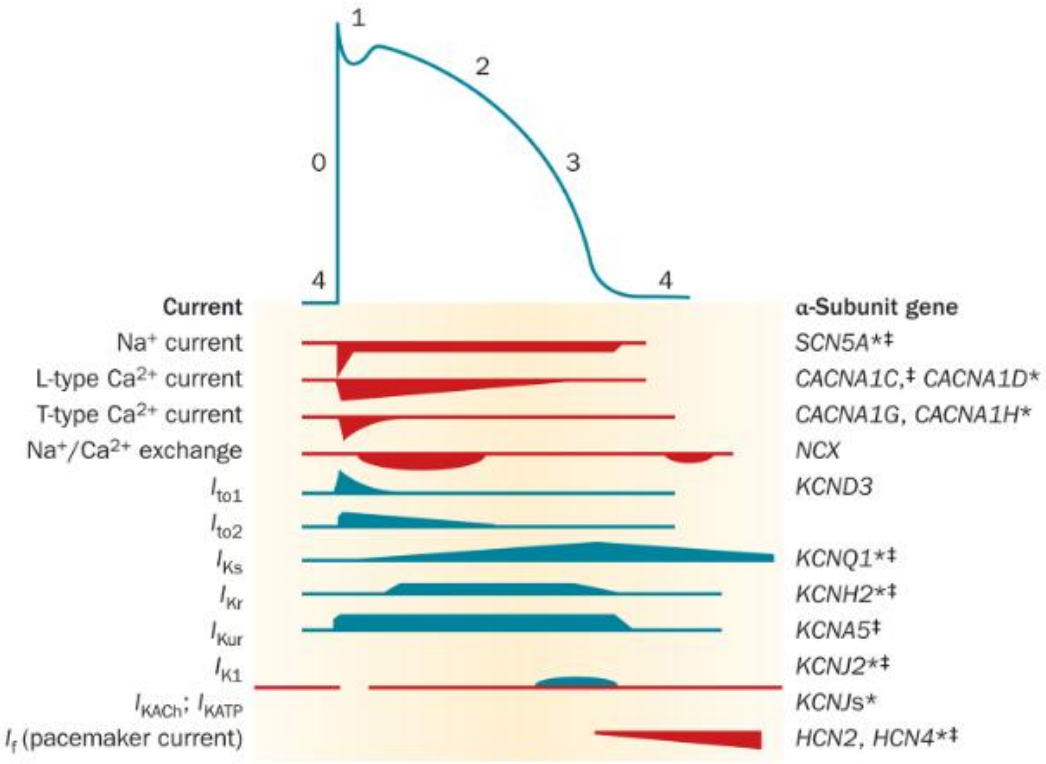

Figure 1.3: Cardiomyocyte action potential and ionic currents. *Genes associated with the α-subunit are included, and polarisation indicated in both time and intensity, with incoming ion transport shown by red graphs and outgoing ion movement shown by blue. Baseline membrane potential of approximately -90mV in phase 4 and remains so until Na+ ions enter the cell, triggering rapid depolarisation in phase 0. A period of rapid repolarisation occurs in phase 1 as K+ ions move out of the cell, before plateauing in phase 2 as Ca^2+ ions begin to enter the cell, balancing out the K+ outflow. This is overcome in phase 3 as more K+ ion channels are opened furthering the exodus of K+ ions before the cell membrane reaches the baseline action potential once more. Figure from* (Darbar and Roden, 2013).

The electrical activity of hundreds of action potentials traveling across the heart generates an electrical current that can be detected using an electrocardiograph and visualised as an electrocardiogram (ECG), an example of which is shown in Figure 1.4. Annotated on the diagram are specific points of interest of the ECG, beginning with the P wave, which indicates atrial depolarisation, followed by the QRS complex where the

ventricle is depolarised, followed by the T wave which is ventricular repolarisation. The most relevant part of the ECG to this study is the QT interval, the time taken between points Q and T, which is usually between 350-440ms in a healthy adult human. A QT interval of over 500ms is used as a clinical indicator of an unhealthy heart (Li *et al*., 2016). There are multiple factors that could trigger QT elongation such as genetic predisposition, but the most relevant to this study is that it is often a side effect of cardiotoxic drugs.

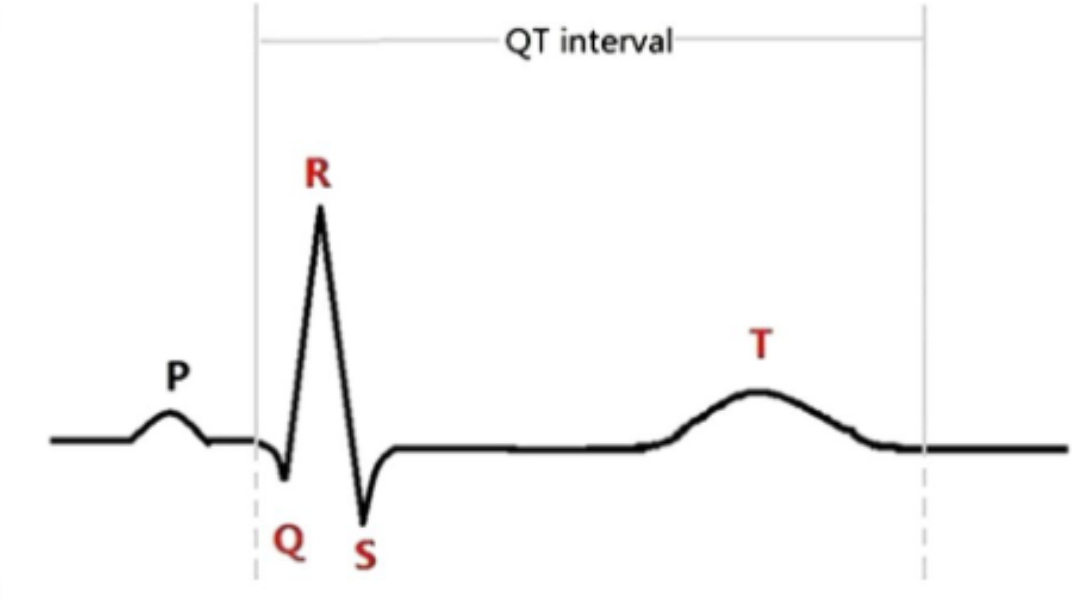

Figure 1.4: Human electrocardiogram trace. *Points of interest labelled are the P wave, corresponding with atrial depolarisation, the QRS complex which indicates ventricular depolarisation and the T wave where the ventricle is repolarised. The QT interval is the time between points Q and the end of the T wave. Figure from Li et al. (2016).*

Piscine heart

The piscine heart is found in all classes of fish, from cartilaginous fish such as the sharks and rays (*Chondrichthyes*) to bony fish such as the zebrafish (*Danio rerio*). Of the three heart types discussed in this project, the fish heart is the simplest in construction as it has two pumping chambers- one ventricle

and one atrium. There is a single circulatory system as there are no separate vascular systems for oxygenated and deoxygenated blood. There is a single loop in which the blood travels from the body into the atrium of the heart, passing through a valve to the muscular ventricle where it is then pumped back out to the gills and onward towards the main body following reoxygenation (D'Amico *et al*., 2011). As with mammals and amphibians, the heart is the earliest organ to form during embryo development due to the need for a functional circulatory system to provide oxygen and nutrients to the rest of the developing embryo (Wolpert *et al*., 2015). Embryos feature a functional beating heart as early as 2 days post fertilisation allowing them to be utilised in cardiovascular studies- including those covering cardiotoxicity (D'Amico *et al*., 2011).

Amphibian heart

The amphibian heart is simultaneously more and less complex than the mammalian heart due to the nature of amphibian development. While amphibians such as salamanders are included in this category, this thesis focusses on the frog heart, in particular the heart of the African Clawed frog (*Xenopus laevis)* tadpole. Early embryos have a cardiac system like fish, but as the embryo matures and moves towards metamorphosis the heart develops a more complex anatomy that is retained as a mature adult. The amphibian heart at this later embryo stage has a single ventricle and two atria, with some mixing of oxygenated and deoxygenated blood occurring, but this is kept as low as possible through timing of the contractions between the different chambers. The blood enters through the atria, one handling deoxygenated blood and the other oxygenated, then is pumped through the ventricle which transports the blood around the body. Amphibians' ability to perform gas exchange through their skin, coupled with their relatively small sizes, are the primary reasons they can survive without the strict separation of oxygenated and deoxygenated blood required by mammals (Mohun, 2003; Mohun et al., 2000).

1.4.2 The toxic heart

Cardiotoxicity most commonly presents in one of two ways, but they can occur simultaneously. The first of these is through physical damage of the heart where structural changes lead to loss of function, as seen in events following myocardial infarction (MI), where heart tissue is starved of oxygen and physically damaged. It can also present through changes in cellular function without necessarily causing cellular damage, such as drugs that affect the heart's electrophysiology and lead to arrhythmias.

Drugs that have been found to cause cardiotoxic effects can either cause immediate, acute effects or chronic effects that are detected months or even years after the drug treatment has ended. The potential for delayed onset of toxicity is why such a strong emphasis is made on testing for electrophysiological effects in drug development. The main identifier of electrophysiological effects is QT elongation, indicative of a delayed repolarisation response, which could also potentially develop into arrhythmia.

One of the main causes for QT elongation, particularly if it is drug-induced, is the inhibition of the rapidly activating delayed rectifier potassium ion current (IKr), which often occurs through blocking of the voltage gated potassium channel linked to the current. One of the subunits of this channel is alpha subunit KV11.1, which is a protein containing 6 α-helical transmembrane segments. The gene responsible for encoding this protein is the human Ether-à-go-go-related gene (hERG), also known in the literature as KCNH2 (Darbar and Roden, 2013; Sanguinetti et al., 1995). This gene is highly conserved in evolution, as many animal models having homologues of the gene present which also controls the IKr in said animal.

Another cause of QT elongation is the inhibition of the slow delayed rectifier current (IKs) (Kodama *et al*., 1997; Salata *et al*., 1995). The IKs current is primarily controlled by the KV7.1 voltage-gated potassium channel, with the

major subunit being encoded by the KCNHQ1 gene (Jost *et al*., 2007). This gene has been associated with multiple mutations that trigger long QT syndrome and so has seen use in drug testing for QT-shortening compounds (Obiol-Pardo *et al*., 2011).

Torsade de Pointes (TdP) is a feature seen on ECGs as changing QRS complexes occur. TdP is indicative of extra ventricular beats, which can be caused by early depolarisation of the ventricle, initiated in the Purkinje fibres or midmyocardial cells (Dessertenne, 1966). This can lead to a life-threatening arrhythmia called tachycardia, defined as a resting heart rate of 100 beats per minute or higher. People treated with drugs associated with TdP have been found to have blood plasma concentrations of the drug compound at levels that would be enough to cause hERG channel blockage/interference (Redfern *et al*., 2003).

Aside from changes in electrophysiology, biomarkers are a method of detecting cardiotoxicity. Possibly the most important and widely used biomarker is cardiac troponin (cTn). cTn is a protein found in heart muscle, and when the heart is damaged, either through events such as a heart attack or drug induced cardiac toxicity, the protein is released into the blood stream and can be detected through a blood test. cTn is extensively used in clinical settings as well as research environments as a marker of cardiotoxicity or cardiac damage because it has been shown to have a strong correlation between blood concentration and cardiac damage (Zhang *et al*., 2022).

Another protein family used as cardiac damage biomarkers are natriuretic peptides (NPs). There are multiple forms of NP, including atrial (ANP), cerebral (BNP) and type C (CNP) that are produced in the atria, ventricles and endothelial cells respectively. These are an effective predictor of cardiotoxicity in cancer treatment (Zhang *et al*., 2022).

1.5 The need for non-animal alternatives

The use of animals in scientific research is and will continue to be controversial, as definitions of sentience and understanding of how animals perceive pain change over time. The current use of animals in research in the UK is highly controlled under the Animals (Scientific Procedures) Act (ASPA) 1986 (Animals (Scientific Procedures) Act, 1986), and the restrictions imposed in this piece of legislation are some of the strictest in the world. In summary, animals that are sensate to pain can only be used in research when no alternative is available to generate the required results. This means that use of an *in vitro* model or an alternative non-protected animal would not provide the necessary information for the research. This act protects all vertebrate species other than humans and cephalopods; specifically, after 2/3 of the gestation or incubation period respectively has passed for mammals or birds/reptiles, or capable of independently feeding itself when referring to fish and amphibians. This means that the only animals able to be used in research without the research falling under the licensing of ASPA (1986) are early embryonic forms of mammals, amphibians, fish and cephalopods, or any other invertebrate. To provide some examples, this means that zebrafish after 5.2 days post fertilisation, *Xenopus* sp. At NF stage 46 and beyond and chicken embryos beyond day 14 of development are all protected under ASPA (1986) rules.

Elsewhere there are similar laws such as the Statute on the Administration of Laboratory Animal Use 1988 and Guideline on the Humane Treatment of Laboratory Animals 2006 in China (Ministry of Science and Technology, 1988; Ministry of Science and Technology, 2006); Laboratory Animal Welfare Act 1966 and additional policies beyond this in the USA (Laboratory Animal Welfare Act, 1966); and while in the EU each country has its own laws they are influenced and informed by EU Directive 2010/63/EU (European Commission, 2003). These regulations all vary but cover the use of animals in scientific research and impose minimum standards of care they should receive.

In the UK and EU the guidelines and care standards follow the 3R's Principle- Replacement, Reduction and Refinement:

- **Replacement**- Accelerating the development and use of predictive and robust models and tools, based on the latest science and technologies, to address important scientific questions without the use of animals.
- **Reduction**- Appropriately designed and analysed animal experiments that are robust and reproducible, and truly add to the knowledge base.
- **Refinement**- Advancing research animal welfare by exploiting the latest *in vivo* technologies and by improving understanding of the impact of welfare on scientific outcomes.

This guiding principle indicates that research on animals should only be conducted when there is no suitable alternative non-animal methodology. If animal use cannot be avoided the experiments should be conducted to utilise them in the most efficient way to generate the maximum amount of data from the minimum number of animals (Hubrecht and Carter, 2019). While research on animals still does and must continue for now, alternatives are actively being developed. Many of these seek to actively remove animals from scientific experimentation and replace them completely.

It is often external forces driving the push for animal replacement, such as animal rights groups, that seek to eliminate all animal experimentation regardless of reason. This is often the more publicised approach due to the methods chosen (demonstrations etc.) and if only the efforts shown in the media were considered it would be understandable to conclude that external pressures are the main driving force of change in this area- this is not the case. When looking at the industry from within it is clear there is an equal if not greater push towards non-animal alternatives, with efforts made to reduce the number of animals used in situations where there is no

acceptable replacement. The removal of animals in scientific research will not happen suddenly. Following the 3Rs principles, modifying the use of animals to improve the experiments being conducted will thereby improve the quality of data provided from animal use. This is key because it allows for improved quality of life for the animals that must be utilised in research, while making steps to reduce the numbers used until such a time that non-animal alternatives are viable.

1.6 Non-animal methods

Typically before *in vivo* testing there are multiple methods of testing a novel drug that do not require the use of animals, however in some cases the methods are used side by side. This section provides an overview of some of the more commonly used methods and techniques and the pros and cons of each system, as each has its own strengths and weaknesses.

1.6.1 *In silico* testing

As computer power increases and utilisation improves there is a push to create novel methods of performing drug development entirely within virtual environments. The recent adoption of AI technology and the ability for computers to draw from a huge database of information to make decisions in simulations has high potential to become influential tools in the drug development process. *In silico* technology is already in use for target detection and initial virtual screens for novel drugs (Dhingra *et al*., 2023); but applications already exist for more detailed analysis, such as molecular modelling, binding site prediction, and automated analysis of databases of enzyme data (Khan *et al*., 2023; Mittal *et al*., 2023; Sharma *et al*., 2023).

In silico technology can be used from the very earliest stages of drug development through using databases of interactions between target proteins and existing drugs. Identifying potential leads with the best chances of successful creation and testing can be done on a much larger scale than previously thought (Khan *et al*., 2023). The improvements of *in silico*

techniques have helped push drug discovery towards a target-based approach which offers a cheaper and often more robust outcome than the more traditional phenotype-based approach (Sharma *et al*., 2023).

The largest restriction in utility of *in silico* methods are due to the dependency on and availability of existing data for the program to draw from. Computer simulations of drug-target interactions can only extrapolate from existing knowledge, and if that initial knowledge is not complete then the program's accuracy will be severely curtailed. An additional problem seen in this area is that oftentimes *in silico* models struggle to predict minor metabolites formed from less common synthesis pathways, as these minor metabolites can be a cause of toxicity (Pathak *et al*., 2023).

1.6.2 iPSCs

Induced pluripotent stem cells (iPSCs) are a relatively recent development by Yamanaka *et al.* (2006). Their method involved reprogramming adult somatic cells to become pluripotent stemlike cells through induction of expression of transcription factors that are responsible for maintaining a pluripotent stage in embryonic stem cells during development. The transcription factor delivery led to the loss of somatic characteristics of the cells and a reversion to a state similar to embryonic stem cells. More importantly, it was discovered that from this state, these cells can be differentiated to specific cell phenotypes and utilised in research requiring a specific cell type. This model is a popular choice for areas such as neurone research (Bonaventura *et al*., 2021).

By differentiating iPSCs into cardiomyocytes, they can be used in drug development. An advantage of this method is the ability to utilise human IPSCs, leading to a representative response to drug exposure akin to that in the human organism (Lian *et al*., 2010). IPSC derived cardiomyocytes display many of the qualities of cardiomyocytes that are in the heart-specifically their ability to spontaneously contract. Their ability to be created

in large numbers allows them to be utilised in high-throughput drug screening, particularly in the assessment of changes to the electrophysiology of the cardiac system (Lian *et al*., 2010).

A cardiac microphysiological system was developed by Mathur *et al*. (2015), in which they showed that a physiologically realistic iPSC-derived cardiac tissue model was possible to create. Their model utilised human derived cells, physiologically relevant tissue structure and perfusion designed to mimic human vasculature. They were able to keep the tissue viable and functional for multiple weeks and performed tests utilising model drugs to measure the cardiac response. Their findings were supportive of the model being able to successfully and confidently indicate cardiotoxic effects of drugs in an *in vitro* system (Mathur *et al*., 2015).

Before these developments, many *in vitro* toxicity screens were dependant on artificial expression of cardiac ion channels in cell lines, often human embryonic kidney cell lines or Chinese hamster ovary cell lines. These are not able to accurately model the correct genetic, cellular and biochemical characteristics seen in the heart. The use of these lines in assessing cardiotoxicity are falling out of favour as better models, such as those discussed here, are created and developed as they can more accurately model the complexity of cardiac cells in human cardiomyocytes (Cheng and Force, 2010; Ferreira *et al*., 2008; Liang *et al*., 2013).

In recent years, further advances to IPSC models of cardiotoxicity have been developed, with additional support from regulatory authorities to encourage this as an alternative or alongside animal models. The Comprehensive in vitro Proarrythmia Assay (CiPA) initiative was developed in 2013, following a workshop at the FDA in the United States. The aim of this initiative is to develop an in vitro assay that can be used to determine if a compound causes arrythmia, using a mixture of approaches. The initiative has been

very productive over the past decade, producing research advancing each of the four components. Work for the initiative could fall under: ion channel development, in silico model approaches, myocyte assays to confirm in silico findings and finally human phase 1 ECGs to determine any unanticipated effects from novel compounds. Recent work by Strauss et al., (2021) summarises several of the advances made by the initiative and emphasises the strengths of these methods as alternatives to the more traditional animal based processes dictated by legislation. These advances have also been sought by researchers on a more global scale, with the Japan iPSC Cardiac Safety Assessment (JiCSA) also working towards similar goals, with extensive industry support as many companies have begun to incorporate these new approaches into their development pipelines. Indeed, there has been significant overlap in the work performed under CiPA and JiCSA (De Korte et al., 2020; Sakai et al., 2017) which has no doubt helped inform the legislative changes occurring currently to enable greater acceptance of iPSC methods to assess cardiac safety of novel compounds.

1.6.3 Organoids

Organoids are simplified, miniature organs produced *in vitro*. These are typically 3 dimensional, with multiple cell types specific to the organ that group and organise in the space provided in the same manner as in the natural organ. Importantly, they are capable of replicating functions found within the organ. Cardiac organoids have been created that replicate a human ventricle that can beat spontaneously, allowing measurements and changes in values such as internal pressure and electrophysiology to be performed (Li *et al*., 2018a). An introductory review discussing this new technology was created by Zhao *et al*. (2021), in which they discuss the opportunities offered by cardiac organoids for preclinical research. Cardiac organoids have shown strong potential for many areas of medical research, being able to be used as models for myocardial infarction, genetic diseases of the heart, and arrhythmia. There have been multiple methods developed to enable varying construction techniques of organoids, enabling more complex and realistic organoids to be used in research, some with layers of

different cell lines that more closely mimic a real heart (Andrysiak *et al*., 2021).

This technology is constantly developing, with new advances being found every year as more specialised organs are modelled by organoids and a wider range of uses are found for them. The biggest advantage to organoids as a model is the ability to create them from human cell lines, making them biologically representative of the organ being modelled. The largest disadvantage to be overcome with organoids are that at a certain size the lack of vasculature and media/blood circulation leads to cell death in the centre of the organoid as the cells there are starved of nutrition. Another disadvantage is that as organoids are such a new technology there is no reference database to work from, so the knowledge base is being created from the ground up and will only be improved with time. The novelty of the method also means there is likely to be some reluctance to accept it in place of existing methodologies for toxicity testing without extensive research, and proof generated to show their effectiveness and the accuracy of results will be paramount. These disadvantages are not insurmountable, with the largest hurdle to overcome them being time and energy spent in developing the organoid model further.

1.6.4 Organ-on-a-chip

Organ-on-a-chip technology is cell culture grown on a microfluidic surface (or chip) that simulates mechanics and physiological responses of organs or in more elaborate examples, multiple organs as part of the same system. The great benefit of this system is that it offers modularity and excellent environmental control, allowing culture of cells to be carefully modulated with regards to oxygenation level, pH and the flow rate of the culture medium (Andrysiak *et al*., 2021; Berg, 2019).

Another advantage of this technology is the ability to automate the conditions as well as the monitoring of the experiment, allowing for continuous,

simultaneous measurement of physiological responses, providing exceptional data generation. Additionally, researchers have been developing models that culture cells from various organ systems together to generate additional data and better improve understanding of inter-organ effects of compounds. Examples of these include culturing neuronal cells alongside cardiac cells (Sakai et al., 2017) and a model culturing four cell types together to represent the heart, brain, liver and skeletal muscle (Oleaga et al., 2016). These advancements represent the likely direction of this field, as the creation of a more comprehensive human system is more likely to generate results comparable to those seen in the body system as a whole, rather than focusing on organs in isolation (Andrysiak et al., 2021)

The largest drawback of organ-chip technology is the relatively high cost when compared to other methods, the currently lower throughput generated from these methods and the limited validation data available. Additionally, utilisation of these methods often requires a significant engineering skillset which may require biology labs wishing to expand into this area to acquire specialists with these skills and the equipment required to utilise this technology (Andrysiak *et al*., 2021).

In conclusion, at the outset of this project it is clear that although non-animal techniques are considered newer approaches -to varying extents- there is constant development and improvement within this area, with significant progress being made within the last decade. Indeed, the collaboration and shared outcomes seen on a global scale between industry and research leaders has helped lead to novel methods and improvements on existing techniques. Although there are still disadvantages of these models when compared to each other and to animal models, these are constantly being addressed and the adoption of them alongside animal and existing methods by industry and growing acceptance of the validity of the results produced by regulatory bodies shows these methods have a strong future. The strengths and weaknesses of these models are summarised in Table 1.1. It is likely

that as time progresses and further investment continues the strengths of these models will increase as the disadvantages lessen, with the likelihood being that at some point in the future these alternatives will surpass animal methods entirely in their use, and the work done in this study in developing *Xenopus* as a model for cardiotoxicity should be done with this in mind and assessment of the *Xenopus* model should consider this likely possibility.

	In silico	iPSC	Organoid	Organ-on-a-chip
Advantages	Can be used at scale Can be done early into the development process Can be very cheap to use Constantly developing and improving	Human cell-based methods Can be done in layers to accurately represent cardiac tissue Medium to high throughput Established models approved by CiPA etc	Human cell-based methods Potential for medium-high throughput	Human cell-based methods Flow present and controllable Integrated sensor availability Mechanical and electrical stimulus control
Disadvantages	Requires significant existing data banks Predictions can be inaccurate Must be used alongside other methods	Limited physiological accuracy Can be high cost depending on methods	Struggling to develop effective cardiac organoids Lack of vascularisation Existing models relatively simple	Sometimes gives false negatives Chip material not inert Can be expensive Requires heavily specialised training

Table 1.1: Analysis of non-animal methods of cardiotoxicity at the outset of the project.

1.7 Animal methods

A popular animal-derived *ex vivo* model for cardiotoxicity assessment of novel drugs is the Langendorff Screenit model. The Langendorff model is an

old methodology, developed in 1895 which has been continually developed and refined in the following century of use. The model consists of a heart, removed from the animal's body and perfused with an oxygen rich solution to maintain function.

This model is advantageous as it is relatively simple to prepare and easily reproducible, allowing experimentation to occur that maintains the structure and electrophysiology of the heart, while being much more accessible than a heart still inside a living organism, with the natural caveat that the heart can only be sustained for so long following removal (Bell *et al*., 2011). This model has been adapted across multiple species and can be performed using rodents, rabbits and larger mammals such as dogs and pigs, and has been developed into a fully automated methodology that tracks and reports the effect of various drug concentrations on the heart electrophysiology (Bell *et al*., 2011; Valentin *et al*., 2004). The Langendorff heart is maintained through either constant pressure or constant flow perfusion into the aorta; and multiple measurements can be taken from the heart in this state. The most study-relevant measurements that can be taken are myocardial contractility- measured through linear force contraction with a tie positioned through the apex attached to an isometric force transducer, or from the insertion of a balloon in the left ventricle- and the measurement of electrophysiological changes through use of appropriately placed ECG electrodes (Bell *et al*., 2011). Another *ex vivo* model for cardiotoxicity testing is isolated Purkinje fibres taken from dogs or pigs- these can be used to assess the proarrhythmic potential of novel compounds; with compounds known to cause QT-prolongation causing prolongation of action potential in the isolated Purkinje fibres (Gintant *et al*., 2001).

A recent review by Podyacheva *et al.* (2021) highlights the effectiveness of rodent models in studying doxorubicin-induced cardiotoxicity. Rat models covered were exposed to either single dose short term exposure or longer-term repeated doses over multiple weeks. Assessment of toxicity was

performed using a variety of methods including ECG, histology, troponin tests, and echocardiography (ECHO). Some of these methods were performed while the rat was alive and multiple measurements were taken over the period of the study, such as troponin tests and ECGs, but others such as histology were only able to be performed postmortem as they specifically looked at cardiac tissue to assess damage.

Mice were also used for doxorubicin-induced cardiotoxicity studies in much the same way as rats but with notable differences. For instance, mice were more often used for single exposure studies, and the toxicity assessment was more often ECHO and histology with occasional troponin and BNP analysis, where only a single paper utilised an ECG analogue (Van Acker *et al*., 1996). The reasons for this disparity are potentially size related as ECGs could be more complicated to perform on smaller animals, whereas an ECHO utilises an ultrasound probe and is therefore more straightforward. It is also important to note that with the histology assessment there were strong similarities between models, as myocardial fibrosis, inflammation, disorganisation and vacuolisation of myocardial fibres were present across species and concentrations (Podyacheva *et al*., 2021). Another likely reason suggested by Deshmukh *et al*. (2012) is the fact that rodents have a distinctively high heart rate compared to humans (310-840bpm in mouse and 250-493bpm in rat), so testing to detect arrhythmias may be difficult to perform and has potential to be inaccurate or not reflect human responses, a known problem within the drug development process as a whole.

Multiple non-rodent models of cardiotoxicity have been characterised. Leporine models of chronic cardiotoxicity are assessed by postmortem histopathology, with myocardial cells presenting lysis, necrosis and degeneration, alongside alterations in cardiac troponin and BNP levels in the blood and behavioural indications of illness (Meng *et al*., 2022). Canine models show increased serum BNP levels, alterations in ventricular ejection fraction and vacuolar myocardial cells in postmortem histology.

Zebrafish (*Danio rerio*) are a newer model organism and are rising in popularity in their use for *in vivo* research over the past few decades. They are favoured over rodents due to the relatively lower cost of maintaining a breeding colony, ease of breeding and large number of eggs laid in a single spawning which can be hundreds at a time. Wild-type embryos are easy to image, are transparent and develop outside the mother. Imaging can be improved further through genetic manipulation and insertion of fluorescent protein expression at areas of interest, allowing complex internal structures to be imaged throughout development using fluorescent microscopy (Bowley et al., 2022).

These traits have led to widespread use of zebrafish as a research model, and this is inclusive of cardiac research. In particular, the large number of embryos generated and relative ease of imaging has been a large driver of consideration into using them for drug-induced cardiotoxicity studies. They offer a cheaper, higher throughput *in vivo* model when compared to rodent models such as mice. The zebrafish heart is two chambered and heart rate can be measured visually through a light microscope, as performed in (D'Amico *et al*., 2011). D'Amico found that zebrafish recapitulated cardiotoxic effects of drugs known to cause cardiotoxicity in humans, specifically with changes in heart rate and changes in atrioventricular rhythmicity- the ratio of heart beats in the atrium compared to the ventricle. In a healthy individual it would be a ratio of 1:1, in an unhealthy individual this ratio would be higher or lower.

Further development of zebrafish as a model of cardiotoxicity was performed by (Milan and MacRae, 2011), as they sought to record an electrocardiogram (ECG) from adult zebrafish, something that was not previously done due to the difficulty of performing the procedure on an animal the size of a zebrafish. The ability to routinely perform this procedure would improve the assessment of cardiotoxicity as it would allow accurate examination of the electrophysiological effects of drugs given to the animals, particularly if they

interfere with the QT length, one of the major indicators of cardiotoxicity. The ECG was obtained through restraint of the adult zebrafish in a ventral position outside of a fish tank environment, with a perfusion needle present in the mouth to ensure water and oxygen is pumped over the gills to facilitate continued survival. Two electrodes were placed into the fish, an anterior and posterior electrode, with the posterior electrode acting as a reference electrode for base signal levels and the anterior electrode detecting the signals generated in the heart. They found that the initial recordings had noise from both skeletal muscle artefacts as although the fish was restrained there was still miniscule movements and noise generated through gill movement. They partially combated this through signal averaging and explored the use of a paralytic agent (μ-conotoxin GIIIB) to further reduce the noise with some success, and a recognisable ECG was generated. Following the success of this method with untreated zebrafish, they performed experiments in which the zebrafish were perfused with drugs that were known to cause prolonged QT interval in humans to ascertain if these results were recapitulated in zebrafish and were able to be detected using the ECG methodology. Their results indicated a statistically significant change in QT length in all QT elongating drugs tested. The largest drawback of this method is that it required the use of an adult zebrafish and is not as easy to perform on embryonic zebrafish due to the much smaller size. This may impact their suitability of use as a high-throughput model for drug induced cardiotoxicity testing, as embryonic zebrafish are preferred to adult zebrafish in high-throughput methodologies. This is due to the relatively low costs and high abundance of embryo generation, as well as the lack of coverage in the ASPA (1986), meaning reduced need for licensing and approval for experimentation to occur.

The most used animal models of cardiotoxicity are, unsurprisingly, those with the most research performed into them and the greatest level of development. While this allows for a good understanding of the pros and cons of these models, over reliance on them does hinder acceptance of novel models and reduces the likelihood of development time being spent on

said new models. One of the largest pitfalls shared across all models discussed in this section is the determination of a suitable dose of drug to use when investigating drug induced cardiotoxicity, as even with known cardiotoxic compounds like doxorubicin the minimal dose required to induce cardiotoxicity without causing additional toxic effects has been shown to vary from study to study and between animal models (Meng *et al*., 2022). Indeed, while the FDA has guidance documents that provide information on converting a dose of drug from animal to human and the reverse, the list of species covered is restricted to those most likely to be used in research, meaning that utilising a new species for drug research would need to develop a new method of calculating drug equivalencies. This would be particularly important in smaller animals such as *Xenopus* tadpoles or zebrafish embryos as the standard mg/kg dosing method would be difficult to employ with an animal with less than 1 gram of mass (Morais *et al*., 2024).

1.8 *Xenopus* as a model organism

Xenopus laevis and *Xenopus tropicalis* are two species of aquatic frog, commonly known in the pet trade as the African Clawed Frog and the Western Clawed Frog respectively. They are both popular aquarium pets and widely utilised in scientific research, with methods dating back to the 1950's and their extensive use in pregnancy testing. The widespread use of *Xenopus* in this manner was enabled due to their ease of housing and feeding, enabling colonies to be set up at major hospitals and universities across the country. This provided a readily available animal model from which to use in experiments, allowing for development further into a model organism. *Xenopus laevis* is the species this project is most concerned with and unless specified as *X. tropicalis*, any further generalised references to *Xenopus* can be assumed to refer to *X. laevis* specifically.

Figure 1.5: Adult Xenopus laevis females. *These females are in a holding bucket ready to receive an injection of hCG to induce egg laying behaviour. The variety of colour and pattern differences between individuals is clear, and it is possible to identify each individual by its patterning.*

1.8.1 *Xenopus* life cycle and biology of the adult frog

Xenopus laevis are found natively across sub-Saharan Africa, with introduced populations in North and South America, Europe and Asia, where in many areas it is considered an invasive species due to its adaptability. The adult *Xenopus* is highly sexually dimorphic, with the females being much larger in size than males. Figure 1.6 shows freshly laid *Xenopus* eggs under magnification in a lab environment.

Figure 1.6: Freshly laid Xenopus laevis eggs. *These eggs have just been laid by a female Xenopus and placed in a petri dish; the animal (dark coloured) and vegetal (lighter coloured) poles of the eggs can clearly be seen, as can the jelly coat surrounding the eggs that offers protection in the wild. Following fertilisation this jelly coat can be removed from the eggs using a 2% cysteine solution, allowing greater ease of physical manipulation of the eggs. Image was taken at 10x magnification.*

In captivity, breeding occurs typically through two methods depending on the requirements of the study being conducted, with the first replicating natural mating behaviour. The second method- *in vitro* fertilisation, is often preferred as the more controlled fertilisation time allows precise development staging which is vital for many areas of research, including this project.

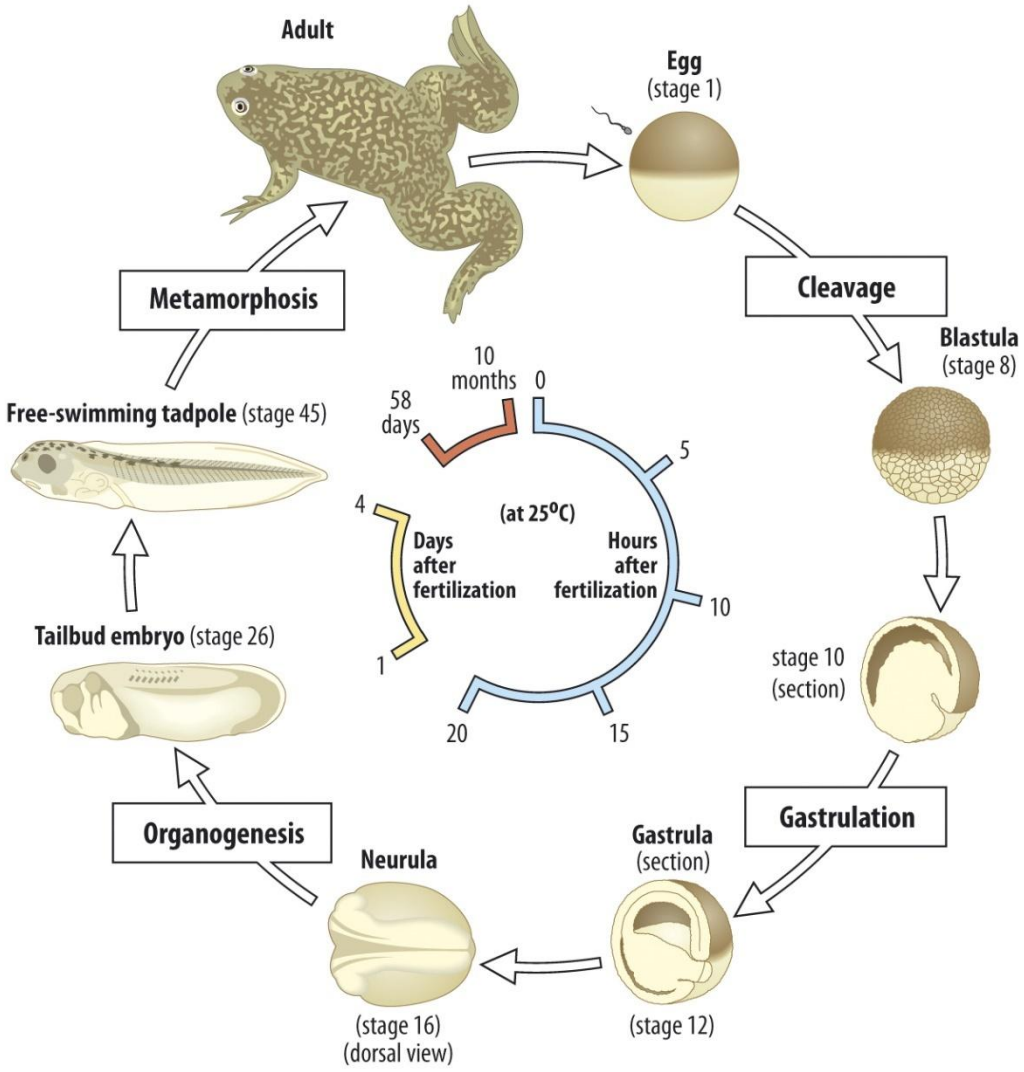

Figure 1.7: Life cycle of Xenopus laevis. *Life cycle shown from fertilised egg through the major development stages as an early embryo in the first 20 hours after fertilisation and the major stages as an older embryo in the days following this. Taken from Wolpert, Tickle and Arias, 2015.*

1.8.3 Development of the tadpole

The various stages of *Xenopus* development from zygote to adult frog has been carefully observed and categorised under the 'Normal table of *Xenopus laevis*' by Nieuwkoop and Faber (1958). Since its printing this table has been the standard reference from which all *Xenopus* studies have referenced their study organisms, and each development stage is given a number, leading to standard nomenclature of NF stage 1 or simply NF 1 as commonly utilised throughout the field. The normal table contains images to graphically

illustrate the changing appearance of the embryos as they grow, which while beneficial was somewhat incomplete in terms of every stage having ventral and lateral views, for example. Zahn *et al*. (2022) have produced a new graphical resource to supplement and update the normal table to complete the resource. Easy access to these staging maps alongside other information useful to the *Xenopus* researcher is found on an online resource facility called Xenbase (Fisher et al., 2023). *Xenopus* development speed can be altered by the temperature at which they are kept, and for the reference material and times provided, a room temperature of 23°C is assumed to be the case, with cooler environments leading to longer development times and warmer environments increasing the speed at which embryos develop.

The *Xenopus* zygote is single celled, with two distinct 'halves', the animal pole and vegetal pole. These have varying levels of pigment- the animal pole being darker and the vegetal pole being paler. The zygote will initially begin to divide approximately 90 minutes after fertilisation occurs, and the zygote reaches 4 cell stage approximately 30 minutes after this. This doubling every half-hour while still maintaining size and ability to count the number of cells continues until NF stage 6, at which point the embryo has 32 cells, with the cells in the animal half of the embryo being noticeably smaller than those of the vegetal half.

NF stage 6.5, the morula stage, signifies a change in pace for *Xenopus* development as the cell division becomes asynchronous across the animal cells and vegetal cells, with the animal cells dividing at a faster rate than those of the vegetal pole. By NF stage 7 it is no longer possible to count the number of individual cells in the embryo and as such other characteristics become more important for marking the stage of development, particularly the relative size of the animal cells, particularly between NF 8 and NF 9 (mid-blastula and late blastula respectively).

Gastrulation- which involves the internalisation of the mesoderm and endoderm and expansion of the ectoderm- begins when the embryo reaches NF stage 10, and when viewed vegetally it is possible to see the blastopore lip of the embryo, which serves as a staging marker through to NF stage 12.5, as the blastopore diameter decreases through these stages as the vegetal cells are internalised until the blastopore closes fully at NF stage 12.5.

The neurula stages between 13-21 (Figure 1.8) follows the development of the neural plate as it deepens along the midline and folds into itself to form the neural tube- the earliest development stages of the spinal cord and brain. The differences between each stage from NF stage 13 to NF stage 19 are subtle and depend on the characteristics of the neural folds and stage of neural tube closure.

NF stages 22-28 are referred to as the early tailbud stages of development, characterised as the embryo lengthens and becomes more recognisable as a tadpole, with pigmentation starting to increase in the eye, the cement gland becoming more clearly developed and increased movement of the embryo. Internally, somites, pronephric kidney and particularly the heart are beginning to develop, with the heart at NF stage 28 consisting of an endocardial tube surrounded by myocardial tissue.

Late tailbud and free-swimming tadpoles occur between NF stages 29 and 38, with the primary identifying factors for differentiation being the eye, gut and tail development. The eye develops darker pigment as the stages progress, the tailbud lengthens, the gut develops and grows in length, melanophores begin to appear on the head and the anterior trunk. Internally, the neural tube has formed the spinal cord by NF stage 29/30, the lung buds become visible by NF stage 32, the pronephric kidney and duct is formed by

NF stage 33/34, the liver bud is visible at NF stages 35/36 and by NF stage 38 the pronephric kidney is functional.

By NF stage 40 blood is visible circulating through the gills and tadpoles will begin to exhibit breathing behaviour, despite their lungs not being functional at this stage. The most distinct visual indications of staging between NF stages 41 and 45 is the shape of the gut as it proceeds to coil in a distinct and consistent pattern; an example of what a NF stage 45 embryo looks like is shown in Figure 1.8.

At NF stage 46, the embryos are freely feeding and at this point are developed to the stage that they are offered protection under the Animals (Scientific Procedures) Act 1986. Development beyond this stage is linked to metamorphosis as the hind limbs begin developing, followed by the forelimbs, the gills are resorbed into the body and the tail begins to shorten and become absorbed back into the body, until it becomes a fully-fledged froglet by NF stage 66.

Figure 1.8*: NF Stage *45 Xenopus laevis tadpole. *At this stage the embryo is fully formed with a functional cardiac system as well as the other major organs such as the liver and digestive system.*

1.8.5 *Xenopus* as a model organism

Xenopus have many traits that make them a very suitable model organism for drug toxicity research (Wheeler and Brändli, 2009). Physiologically, the embryos of *Xenopus* sp. have relatively similar organs to humans that develop early such as liver and heart. This allows them to be modelled as adult human equivalent at an early enough stage in development that it is still an embryo and to the best of current knowledge does not experience a pain response or suffer as with older frogs or other animal models. Genetically, *Xenopus tropicalis* have a diploid genome making them similar to humans, allowing knock down and manipulation of their gene expression. Genetic homology between *Xenopus* and humans is good, approximately 80% of human genes have an orthologue in the *Xenopus*, and resources such as Xenbase enable easy navigation around the parts of the genome that have been mapped. *Xenopus* sp. lay eggs and undergo external fertilisation allowing embryos to develop wholly outside the mother, giving easy access and control over the development of the embryos unlike placental mammals. The embryos are highly transparent in the wild type which can be enhanced further by using albino colour morphs of the frog, reducing pigmentation to minimal amounts. This allows easy visibility of the internal organs of the embryo without invasive imaging and can be used to reduce pigmentation interference with techniques such as *in situ* hybridisation, where darkened areas of pigment could interfere or be mistaken for staining (Wheeler and Brändli, 2009). A comparison summary of animal models used in research is included in Table 1.2.

	Rodent	Zebrafish	*Xenopus*
Positive	Closest cardiac system to humans. Genome very amenable to manipulation. Physiological response to drugs similar to humans. Very established model. Strong confidence in model from industry.	Externally developing embryos. Relatively cheap to maintain breeding population. Genetically tractable in terms of imaging and genetic manipulation. Able to be used for larger scale, high throughput methodology. Many existing mutant lines for reproducing disease phenotypes	Externally developing embryos. Relatively cheap to maintain breeding population. Bridges the physiological gap between fish and mammalian hearts. Diploid genome on *X. tropicalis* lends itself to genetic manipulation. Able to be used for larger scale, high throughput methodology. Small but growing number of mutants available to reproduce disease phenotypes.
Negative	Relatively expensive to maintain breeding population. Internally developing embryos. Ethical considerations surrounding 3Rs	Physiologically furthest away from mammalian cardiac system. Potential for different physiological responses to drugs compared to humans. Emerging model organism. Reduced confidence in model from industry.	Tetraploid genome on *X. laevis* makes genetic manipulation more difficult. Potential for different physiological responses to drugs compared to humans. Emerging model organism. Reduced confidence in model from industry.

Table 1.2: A summary comparison between rodent, fish and Xenopus model organisms*. Each model has areas they excel in and areas that are currently weak, but careful choice of model and methodology creates research spaces in which each model may be utilised to the best extent possible.*

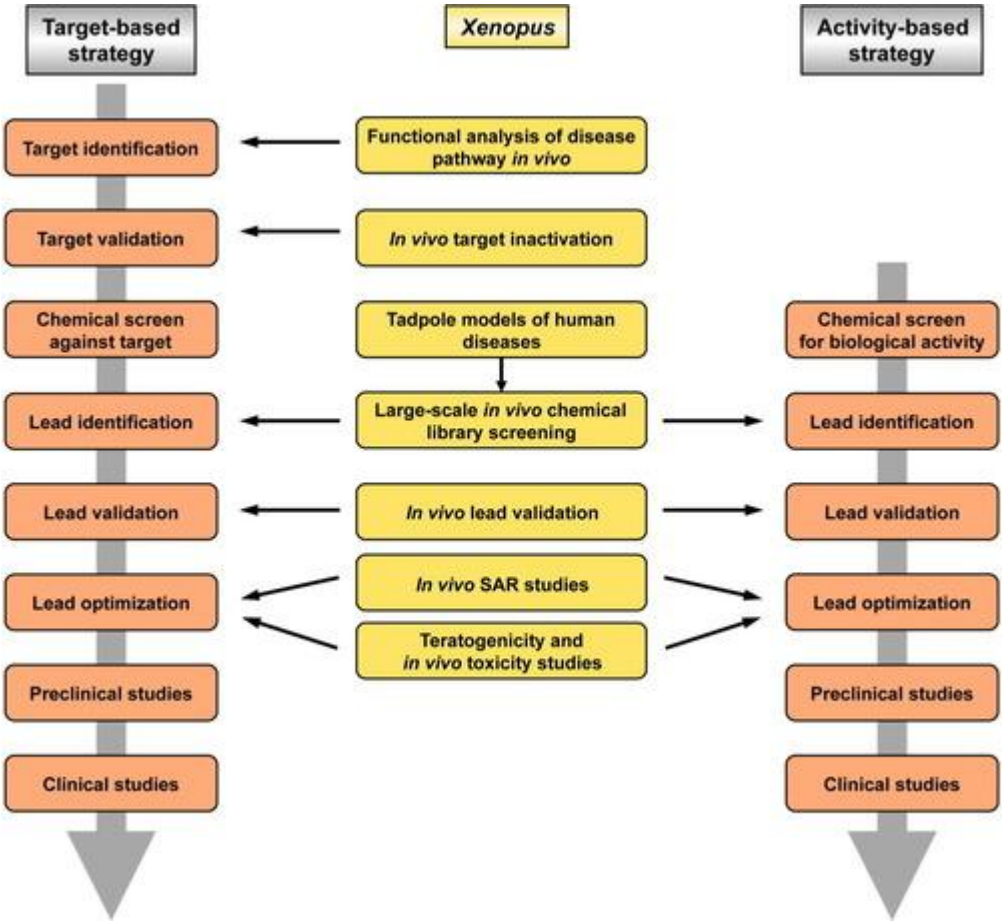

Figure 1.9: Potential uses of Xenopus in drug development. *The current process of drug development vitally under-utilises the resources available in the Xenopus model, likely due to lack of supporting experimentation in some areas- something that this project hopes to address. Taken from Wheeler and Brändli (2009).*

1.8.6 Current use of *Xenopus* in toxicity research

The Frog Embryo Teratogenesis Assay *Xenopus* (FETAX) is likely the largest use of *Xenopus* in toxicity research at the present time. This assay is designed to allow relatively quick determination of developmental toxicity using only a small amount of drug or compound (Mouche *et al*., 2011). The FETAX methodology involves placing *Xenopus* eggs at the mid-blastula stage in a solution containing the target compound at varying concentrations for 96 hours and assessing any altered development that occurs from this. FETAX was originally developed utilising *X. laevis* as the model species, but work from Fort *et al*. (2004) and Ok Song *et al*. (2003) have assessed the

suitability of *X. tropicalis* as the model for the test. The rationale driving this consideration was the faster development speed of *X. tropicalis*, which allowed the FETAX assay to be performed in 48 hours instead of 96. Other factors that could influence *X. tropicalis'* potential advantages include the faster maturation of *X. tropicalis* (reaching sexual maturity as early as 4 months instead of the 1-2 years for *X. laevis*), creating the potential for faster generation of transgenic lines.

In Ok Song's 2003 work it was noted that although *X. tropicalis* responded similarly to *X. laevis* to the three test compounds used, there was greater variability in the lethality expressed by *X. tropicalis*, which was likely influenced by the temperature the embryos were grown at. A temperature of 23 ± 1°C used to allow for a more direct comparison between the two species, but *X. tropicalis* is much more suited to growth at around 27°C. Aside from this potential issue, their findings suggested that *X. tropicalis* could be suitable for use in FETAX assays.

Fort *et al*. (2004) took note of this and as part of their work incorporated a third study group of *X. tropicalis* reared at 26.5 ± 0.5°C to address this. They found that while there was some variation in malformations across temperatures as per Ok Song *et al*. (2003), the overall results were generally similar regardless of culture temperature. The variation most often observed was predominantly found with the compounds 6-AN and semicarbizide, with the higher temperature *X. tropicalis* showing a reduced sensitivity to the compounds. This was possibly due to a slowed development speed at lower temperatures leading to increased exposure length to the toxic compounds at critical points of development.

Despite the potential shown by *X. tropicalis* for use in the FETAX assay, work over the past two decades has utilised the original format of the assay and *Xenopus laevis* as the model of choice. The use of the FETAX assay for

assessment of drugs has continued, with research into the developmental toxicity of caffeine-pseudoephedrine interactions (Moser and Rayburn, 2007), diclofenac (Cardoso-Vera *et al*., 2017) and ibuprofen (Park *et al*., 2024) being a small selection of the many studies performed in this area. Additionally, research has been conducted beyond drugs intended for human use, with FETAX being used as a way to assess potential environmental toxicity of veterinary medicines present in livestock waste (Martini *et al*., 2012).

As well as drug toxicity, *Xenopus* have also shown use in assessing metal toxicity, with Marín-Barba *et al*. (2018) utilising *X. laevis* as a model for testing iron oxide nanoparticle toxicity to great success- with increased abnormalities observed for higher levels of nanoparticle exposure. Metal toxicity in *Xenopus* was also assessed by Carotenuto *et al.* (2023) in their paper studying the effects of commercial gold and silver nanoparticles. Their findings were similar to those of Marín-Barba *et al*. (2018) in that while lethality was low development was profoundly affected.

Beyond FETAX, there are constant improvements in the scope of using *Xenopus* in research, particularly within developmental biology. Godden *et al*. (2022) have recently published a technique developed to create genetic knockouts of miRNAs in *Xenopus*, with the goal of understanding how miRNAs affect development.

A recent review by Carotenuto *et al*. (2023a) summarises the use of *Xenopus laevis* as a model organism in developmental biology and highlights the increase in published research utilising them in the past two decades, with specific focus on organogenesis, nanoparticles and toxicity. This builds upon and emphasises the comments made in Wheeler and Brändli (2009), where the specific use of *Xenopus* in drug discovery was discussed and *Xenopus* was found to have several advantages over other animal models.

They went into detail assessing the potential use cases for *Xenopus* across the entire drug development timeline, a summary of which can be seen in Figure 1.11. It is clear there is plenty of scope for *Xenopus* to be utilised in drug development far more than it currently is, and a large driver of this lack of use is likely to be a perceived lack of supporting evidence for their viability in this area.

1.8.7 *Xenopus* as a model for liver toxicity

The Wheeler lab has extensive experience with *Xenopus* as a model organism including using *Xenopus* for drug discovery screens (Saide, 2018; Saide et al., 2019; Tomlinson et al., 2005; Tomlinson et al., 2009; Wheeler and Brändli, 2009). The Wheeler lab has begun to develop *Xenopus* as a model for early screening of toxicity of small molecules and nanoparticles (Marín-Barba et al., 2018; Tomlinson et al., 2005; Tomlinson et al., 2009; Webster et al., 2016). As well as looking at general toxicity the Wheeler lab has also used *Xenopus* to study drug induced toxicity (Saide *et al*., 2019). Saide, Sherwood and Wheeler (2019) utilised paracetamol as their drug of choice to trigger drug induced liver injury (DILI) due to its high contribution rate to liver failure, being the leading cause of liver failure in the US and UK (Ostapowicz, 2002). The compound that leads to liver injury is a compound called N-acetyl-p benzoquinone imine (NAPQI), created when paracetamol is metabolised in the liver. At safe doses, NAPQI is neutralised by cellular glutathione (GSH) and so poses little risk, but in overdose situations the GSH is saturated, leaving excess NAPQI free to interact with other inter-cellular proteins, triggering eventual hepatocyte death and liver failure which if left untreated can lead to patient death.

As paracetamol has a dose-dependent effect in humans it was hypothesised that *Xenopus laevis* would exhibit a similar dose dependant response indicating liver injury. Liver injury was determined to occur if a reduction in free GSH was detected in the *Xenopus* tissue or if an increase in expression of liver-specific miR-122 was detected.

Multiple methods were utilised in this study. Common to all methods were that *Xenopus* embryos were exposed to varying concentrations of paracetamol at NF stage 38 of development as the embryonic liver was fully formed by that stage, and exposure continued until the embryo reached NF stage 45 where it was harvested for analysis. As paracetamol concentration increased abnormal phenotypes increased in frequency, with damaged/bent tails, abnormal gut and oedema all present in the highest concentrations of paracetamol, alongside outright embryo death.

The major marker of DILI used in this study was the amount of free GSH in *Xenopus* embryos following paracetamol exposure. *Xenopus* embryos were exposed to paracetamol at varying concentrations for 24 hours and then harvested to ascertain the amount of free GSH, and additional embryos were exposed to paracetamol for a longer period totalling 72 hours before being harvested. There was no significant change in free GSH levels in the 24-hour exposure groups but a significant decrease in free GSH for the 72-hour exposure, at all concentrations of paracetamol between 3-5mM, with the amount of free GSH dropping from 47nmol/mg in the control group to 22 nmol/mg in the 5mM group.

The other method explored in this study was the expression of miR-122 in *Xenopus* embryos. Wang *et al*. (2010) had noted that elevated mir-122 levels in the bloodstream could be an indication of liver damage, as the liver specific biomarker is released from the liver into the blood when damage takes place. Mir-122 is a liver specific microRNA and confirmation of its expression in *Xenopus* was conducted utilising a whole mount *in situ* (WISH) assay (Ahmed *et al*., 2015). The results of the WISH showed expression in the liver, confirmed through an additional WISH looking at alpha-1-microglobulin/bikunin precursor (AMBP), another protein with liver specific expression in the *Xenopus* (Zorn and Mason, 2001). Using qRT-PCR, miR-122 levels were detected after performing dissection on embryos to separate the highly vascular tail area from the liver containing torso, with the tail

sample in the control group being negative for miR-122. The expression of miR-122 in the tail was increased significantly at the 3 and 4mM concentrations of paracetamol exposure, indicating that DILI had occurred (Saide *et al*., 2019).

The results from this study taken together support the use of *Xenopus laevis* as a suitable model organism for modelling drug induced liver injury. The reduction of free GSH following high doses of paracetamol indicates that the drug is metabolised in a manner like that of humans, and the increase in abnormal phenotype presentation and reduction of free GSH as the dose of paracetamol is increased supports the results indicating that they respond in a dose dependant manner.

1.8.4 *Xenopus* heart development

As the heart is the focal point of the research conducted in this study, it is appropriate to consider the development of the heart separately and in greater detail than the overall tadpole development.

Development of the *Xenopus* heart begins as early as NF stage 6, where the embryo has 32 cells. Experiments into fate mapping indicate that there are 4 blastomeres that can be identified at this stage that go on to develop into the rest of the heart tissue (Hoppler and Conlon, 2020), remaining together as a group through gastrulation and being the first to specialise into cardiac cells (Mohun *et al*., 2000). The cells migrate to the ventral midline at the tailbud stage of development, around NF stages 26-28 (Lohr and Yost, 2000), and at around this time tropomyosin can be detected through antibody staining in these cells; as shown in Figure 1.10. At NF stages 31-33, the tailbud stage, the cells are beginning to coalesce into a heart tube which is maintained until NF stage 35 where cardiac tube looping starts, forming an anticlockwise spiral, as can be seen in Figure 1.10. At this point, co-ordinated contraction begins but there is no clear indication of where the heart chambers will be forming- no obvious sections of thickened myocardium and in molecular tests

there are no clear markers of chamber differentiation at this point (Lohr and Yost, 2000; Mohun *et al*., 2000). Chamber differentiation and formation is detectable by NF stage 39/40, as the myocardium thickens up more in the ventricle compared to the atria. At the same time as this occurs, spiral valve and atrioventricular valve formation begins and is completed by NF stage 45/46 alongside atrial septation. The division of the atria is unequal, with the right atrium being larger than the left, but by the time the embryo reaches NF stage 46 the adult configuration of the heart is complete (see Figure 1.10), the only changes occurring from this point onward being increasing in size as the tadpole goes through metamorphosis and becomes and adult frog (Hempel and Kühl, 2016; Lohr and Yost, 2000; Mohun *et al*., 2000).

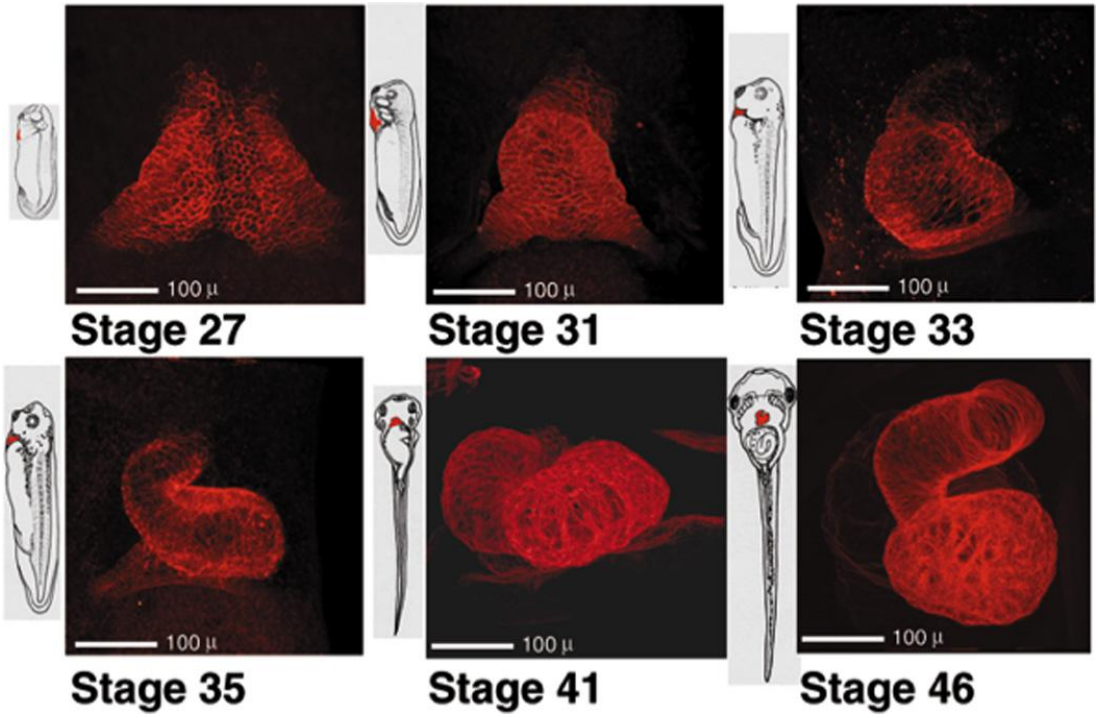

Figure 1.10: Cardiac muscle development in Xenopus laevis. *Embryos were labelled with anti-tropomyosin (CH1) prior to imaging for NF stages 27 to 33 and anti-cardiac troponin T (CT3) for NF stages 35-46. A secondary antibody, Cy5, was used for all stages. Images were taken using confocal microscopy with 30-53 optical sections taken for each image, 5-7 microns apart, in grayscale before being artificially coloured to red. All images were taken at the same magnification and are shown with the anterior of the embryo at the top of the figure. The scale bar is 100 microns. Taken from Kolker, Tajchman and Weeks, (2000).*

1.8.8 *Xenopus* as a model for cardiac research

Xenopus research is continuing to develop in scope, and in particular studies on the *Xenopus* heart are increasing as more people begin to appreciate what the model can offer.

Much of the work done regarding the *Xenopus* heart is studying its development, as covered in section 1.8.4. Lohr and Yost (2000) produced an early review collating the work known so far about *Xenopus* heart development, particularly that performed by Mohun *et al*. (2000) on the

physical development of the heart. Lohr and Yost (2000) also performed a comparison between *Xenopus* and zebrafish heart development, assessing each models' strengths and weaknesses as models. The Mohun lab continued their work on *Xenopus* heart development, with a paper detailing the origin of cardiac tissue, following the lineage as early as the gastrula stage of development (Mohun (2003). Other research has focussed on the signalling pathways that stimulate and regulate heart development, such as Abu-Elmagd, Mulvaney and Wheeler (2017) which focussed on frizzled-7's expression and its effects on heart development through morpholino knockdown, in which it was clear that knockdown of frizzled-7 has severe negative effects on heart development, up to and including complete absence of heart development completely. Research has also been carried out to study what occurs after heart damage has taken place and how *Xenopus* can be used to model heart disease, a good summary of which can be found in Hoppler and Conlon (2020). Hoppler and Conlon (2020) discuss the options available for study of the cardiac system in *Xenopus*, building on the 20 years of progress since the earlier review by Lohr and Yost (2000). These options include the advances made in genetic manipulation, such as transgenic *Xenopus*, knock-in and knock-out methodologies which add or remove genetic expression respectively, as well as studies focussed on the embryonic *Xenopus'* ability to regenerate damaged heart tissue, something that does not present in adult *Xenopus*. The review also covers the various uses of *X. laevis* and *X. tropicalis*, noting that each species is best suited to different areas of research, particularly noting that the diploid genome of *X. tropicalis* is much more suited to manipulation than the tetraploid genome of *X. laevis*, and the methodologies being developed for this becoming more sophisticated year on year- indeed much work in the last decade has been performed exploring the utilisation of CRISPR-Cas9 techniques to study knock-down and knock-out genetic mutations that lead to cardiac disease in humans (Hoppler and Conlon, 2020).

While the *Xenopus* model offers much potential in cardiac research, this potential has not been fully realised. The majority of the work done in this

area has focused on cardiac development, with relatively recent work focussing on the disruption of normal development and analysis of these effects in *Xenopus* sp. Relatively little has been done to study the effects of toxins on the healthy *Xenopus* heart, particularly in the field of drug development and what the *Xenopus* model could offer in this area.

Overall, *Xenopus* offers a solid model of cardiovascular research with great potential for success, offering several advantages over both rodent and fish models. While there are areas in which the model is perhaps less developed than the others referenced, many of the weaknesses could be addressed with additional time and attention being given to the model to combat these.

1.9 Aims

This chapter has laid down a sound foundation of the current state of drug development and has indicated there are some clear opportunities for developing new models of toxicity and cardiotoxicity, especially in the pre-clinical stage of drug development.

We hypothesise that *Xenopus laevis* could be a good model organism to take advantage of these opportunities and to examine questions of toxicity and particularly cardiotoxicity early in the drug development pipeline, potentially as one of the first *in vivo* preclinical studies conducted. To examine the soundness of this hypothesis, the Wheeler lab has already conducted extensive experimentation into the suitability of *Xenopus laevis* as a model for general toxicity, nanoparticle toxicity and drug-induced hepatotoxicity, with results indicating strong support for the model.

To continue this work and provide further evidence in the support of *Xenopus* as a multi-organ model of toxicity, this project seeks to address the use of

Xenopus in drug induced cardiotoxicity. To this end, the aims of this thesis are:

- To determine if drugs known to cause cardiotoxicity in humans can be observed to cause cardiotoxicity in embryonic amphibians.
- To evaluate the appropriateness of an embryonic amphibian model of cardiotoxicity and its potential for use in an industrial setting.

To meet these aims, drugs with a known cardiotoxicity in humans were chosen and given to *Xenopus laevis* embryos, before carrying out various methods to determine if cardiotoxicity has occurred. Chapter 3 contains the results of performing a heart rate assay in which the heart rate of *Xenopus* embryos was measured using video technology, and Chapter 4 contains the results of a biomarker assay, in which novel biomarkers for cardiotoxicity were tested. With these results together, discussion surrounding what the next steps are for developing the assay further or adjusting it for increasing scale and scope are found in Chapter 5.

Chapter 2: Materials and Methods

2.0 Solutions

Antibody solution- α-Digoxigenin-AP (Sigma), 1:3000 or α-FITC-AP (Sigma), 1:1000 in blocking solution

BCIP solution- 50mg/ml in 100% dimethylformamide (DMF)

Blocking solution- 2% Boerhinger Mannheim blocking reagent (BBR) in MABTween

BMB (10% solution)- 10% (w/v) in 1X MAB, preheated at 50°C, stirred until dissolved and then autoclaved, aliquoted and stored at -20°C

Colour solution- 45µl NBT solution, 175µl BCIP solution

Cysteine solution- 3% L-Cysteine in 0.1X MMR, adjusted to pH 7.6

DEPC solutions- 200µl DEPC (Sigma) per 1l of solution

DEPC-H_2O- 200µl DEPC per 1l of H_2O

DEPC-PBS 1X- 10 PBS Tablets (Sigma) in 1l DEPC-H_2O

Fixing solution- 3.7% PFA in DEPC-PBS

Hybridisation buffer (HYB)- 50% (v/v) formamide, 5X SSC, 1mg/ml torula RNA, 100µg/ml heparin, 1X Denharts solution, 0.1% (v/v) Tween, 0.1% (w/v) CHAPS, 5mM EDTA in deionised H_2O, adjusted to pH 8.0

LB Agar- 10g NaCl, 5g Yeast Extract, 10g Tryptone in 1l deionised H_2O + 1.5% Agar

LB Ampicillin- 1:1000 Ampicillin (Sigma) in LB Broth or Agar.

LB Broth- 10g NaCl, 5g Yeast Extract, 10g Tryptone in 1l deionised H_2O

MAB 10X- 116g Maelic acid, 87g NaCl, 60g NaOH in 800ml deionised H_2O, adjusted to pH 7.5

MABTween- MAB 1X with 0.1% v/v Tween

MEM salts 10X- 0.1M MOPS, 2mM EGTA, 1mM $MgSO_4$, adjusted to pH 7.4

MEMFA- 40ml DEPC H_2O, 5ml 36% formaldehyde, 5ml MEM salts

MMR 10X- 1M NaCl, 20mM KCl, 10mM $MgCl_2$, 20mM $CaCl_2$, 50mM HEPES, in deionised H_2O, buffered to pH7.5

NBT solution- 75mg/ml in 70% DMF

NTMT- 82ml deionised H_2O, 1ml Tween, 5ml 1M $MgCl_2$, 10ml TrisCl, 2ml 5M NaCl

PBS 1X- 10 PBS Tablets (Sigma) in 1l deionised H_2O

PBSTween- 1X PBS with 0.1% v/v Tween

Proteinase K (10µg/ml)- 1µl proteinase K, 1ml PBSTween

SSC 20X- 125.3g NaCl, 87.5g NaOH in 800ml deionised H_2O. Adjust to pH 7.0 with HCl, top up to 1l volume with deionised H_2O

TBST- 125ml 1M Tris, 40g NaCl, 1g KCl, 450ml H_2O, 50ml Tween

Testes buffer - 8ml foetal bovine serum (FBS), 2ml 1X Marc's Modified Ringer's (MMR), 10µl gentamycin (Sigma, 1:1,000U)

X-Gal Plates- LB-ampicillin plates with 50µl X-Gal spread over surface.

2.1 *Xenopus* Husbandry

Work involving *Xenopus laevis* was conducted on a Home Office Project license held by Professor Grant Wheeler, and experimental work detailed in this report was conducted under a Home Office Personal License held by the author (I71501072).

Adult *X. laevis* were maintained under current ethical guidelines as laid out by the Home Office and University of East Anglia, being maintained at a temperature of 20°C and fed a diet of commercial pellets.

2.2 Egg Collection and Fertilisation

Adult female *X. laevis* were primed 5-7 days before experiment with a 0.1ml injection of Pregnant Mare Serum Gonadotrophin (PMSG, Intervet, 5,000 iu).

The evening before egg collection primed frogs were given injections of 0.25ml Human Chorionic Gonadotrophin (hCG Chorulon, Intervet, 1,500 iu), one injection in each dorsal lymph sac.

Eggs were obtained from induced females by manual manipulation of the abdomen, encouraging expulsion of unfertilised eggs from the cloaca, which were then collected in a petri dish.

Sperm from adult male *X. laevis* were obtained from testes, either purchased from EXRC (European *Xenopus* Resource Centre, Portsmouth) or harvested in-house. This was done by anaesthetising with a lethal dose of 0.5mg/ml MS-222 (Ethyl 3-aminobenzoate methanesulfonate, Sigma) for two hours followed by complete destruction of the spinal column and removal of the heart. Euthanasia procedures were carried out by competent persons and following Schedule 1 of the Animals (Scientific Procedures) Act 1986. Post-removal or on delivery, testes were stored at 4°C in testes buffer.

For egg fertilisation, a portion of the testes was dissected with forceps and homogenised in 0.5ml of 1X MMR using a pestle and 1.5ml Eppendorf tube. This solution was immediately spread over a monolayer of freshly collected eggs and solution left for 10 minutes at 20°C. After this, the petri dishes were flooded with 0.1X MMR and left to fully fertilise for the next 20-30 minutes at 20°C. Fertilisation was indicated by rotation of the eggs in the dish so the darker animal cap was dorsally positioned, and vegetal pole was ventrally positioned.

The removal of the extracellular layer, a jelly-like substance that protects the embryo and causes fertilised eggs to stick together, was facilitated by the removal of MMR solution and addition of a 2-4% cysteine (Sigma) solution, buffered to pH 7.8 followed by gentle agitation on a roller plate for

approximately 5 minutes. The process was complete when the eggs moved freely and independently of each other. Once this was achieved, eggs were washed twice in 1X MMR followed by a further two washes in 0.1X MMR before being transferred into a fresh petri dish of 0.1x MMR and placed in an incubator set to an appropriate temperature to develop. Appropriate temperatures were determined by the experiment being conducted, by default the standard temperature for *X. laevis* was 23°C. During development, deceased embryos were removed and the 0.1X MMR solution was changed out on a regular basis.

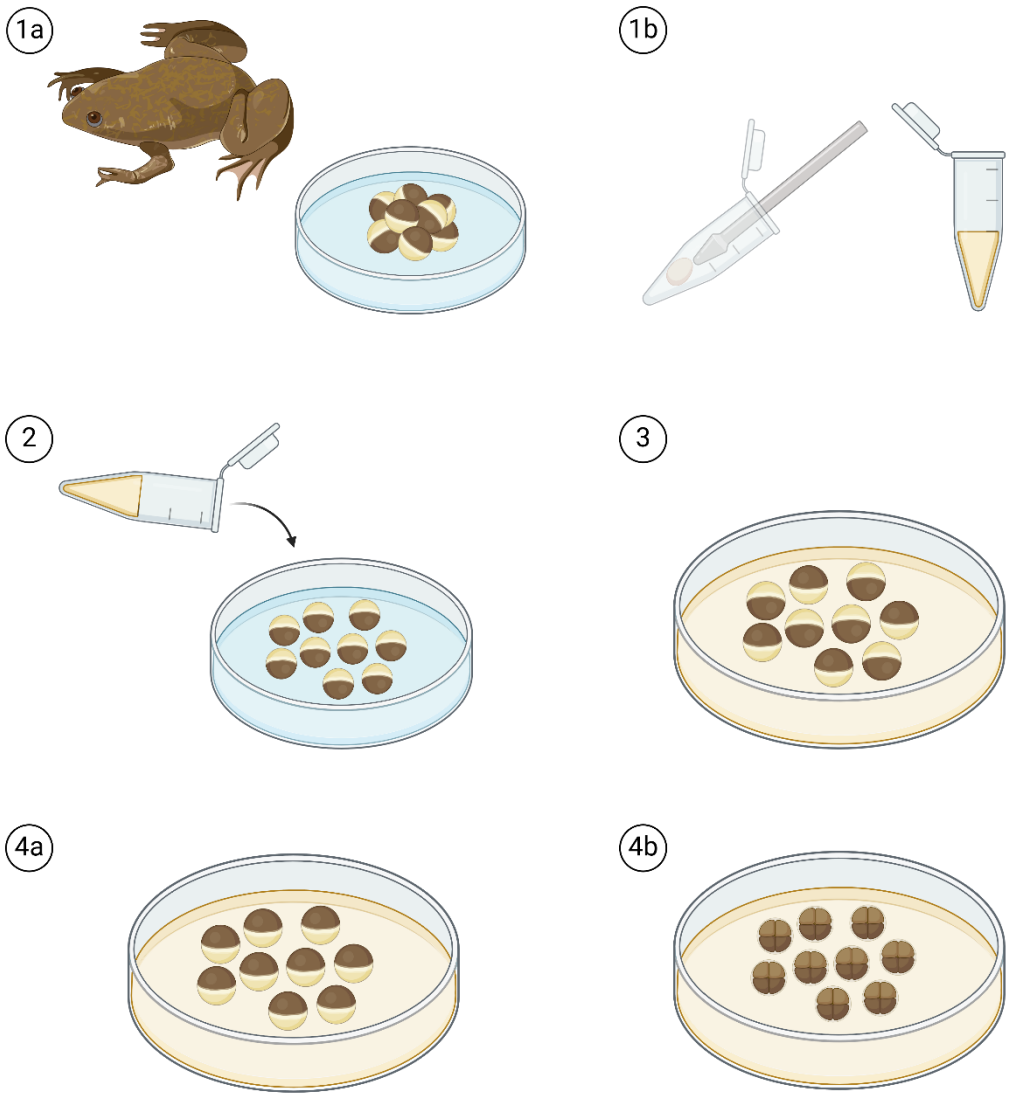

Figure 2.1: The fertilisation process. *Shown in order: harvesting eggs (1a) and preparing testes (1b), fertilisation of the eggs (2), the change in appearance as eggs fertilise and undergo cortical rotation so that the animal pole is facing upwards (3, 4a) where they remained until division and development of the embryo (4b). Cysteine treatment to remove the jelly coat can be carried out once cortical rotation is complete. Created with Biorender.*

2.3 Drug Administration

Stock solutions with a concentration of 10mM were created for each drug to allow dilution to experimental levels and allow for dissolution in a carrier solution if required- terfenadine, for example, required dissolution in dimethyl sulfoxide (DMSO) before being diluted into experimental concentrations. For

compounds which required DMSO as a carrier, the maximum concentration used was 0.5% DMSO (v/v) to minimise toxicity caused by the carrier. Where the DMSO was utilised, an additional control group was created with MMR media and DMSO only, at the highest concentration utilised for the drug-containing groups, to allow for any DMSO-induced toxicity to be determined. Embryos were exposed by introduction of the drug to the MMR media they were housed in.

2.4 Video Assay

The video assay used in this research project has been developed from previous work done by Saide (2018) and Bartlett *et al.* (2004).

2.4.1 Video Acquisition

Embryos were anaesthetised in 0.2mg/ml MS-222 dissolved into the drug solution the embryos were incubated for 15 minutes at 20°C before being manipulated into position as indicated by Figure 2.2, with the heart as clearly visible as possible.

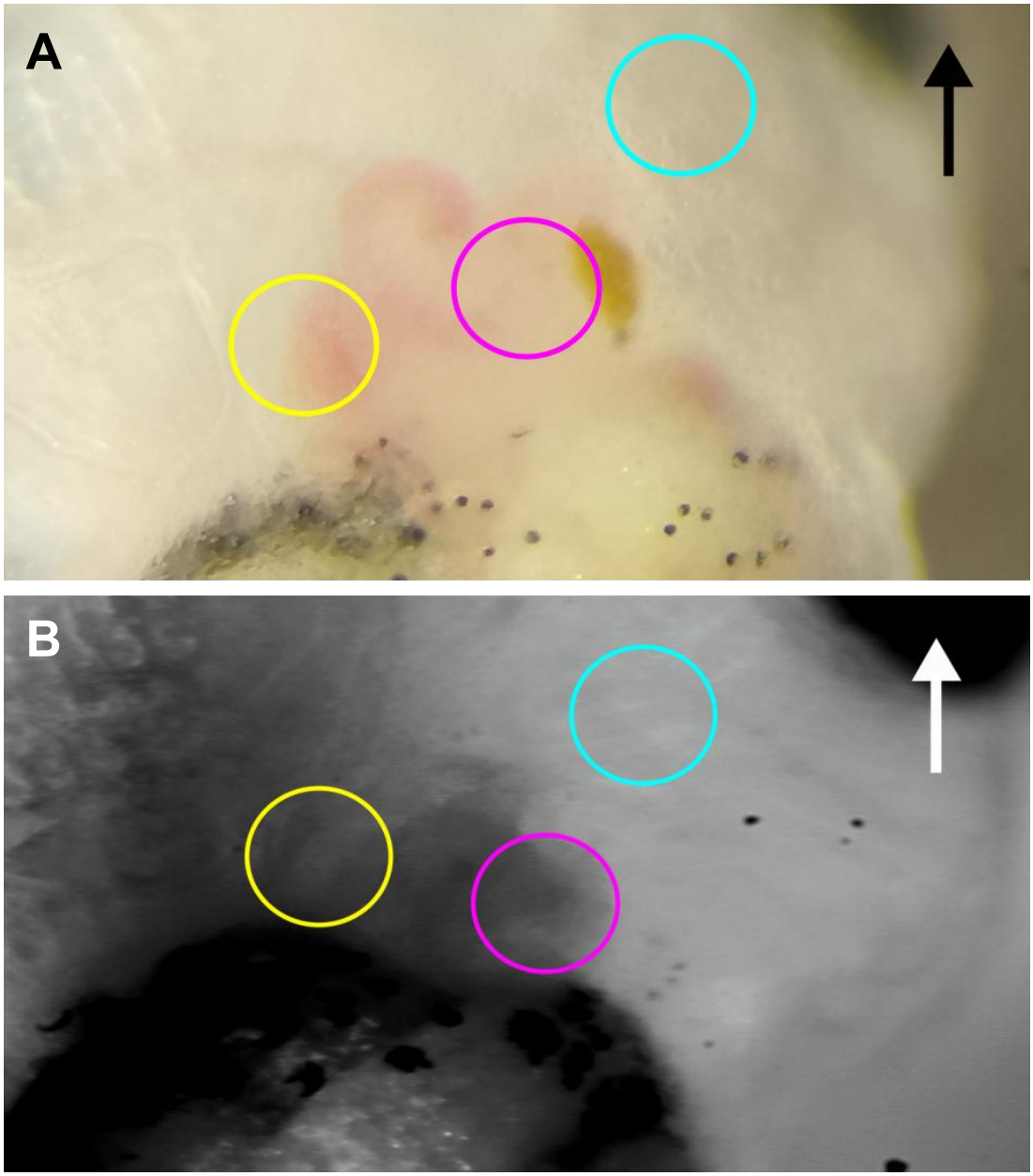

Figure 2.2: Embryos in position for heart rate recording. *A shows a view down the microscope view, B shows the image captured by the recording equipment. Arrows point to the head of the embryo, and regions of interest (ROI) are indicated by coloured circles- visible atrium (yellow), ventricle (magenta) and control region (cyan).*

Black and white video footage was recorded at 50 frames per second (fps) at the highest resolution of 720p using a Pulnix TM-840 CCD camera mounted onto a Zeis CCD upright microscope. Footage was recorded to give 30 seconds of usable footage per embryo.

2.4.2 Video analysis

Videos recorded in this study were imported into Adobe Media Encoder CC and each frame converted into a TIFF image, to create a sequence of 1500 images. This image sequence was imported into ImageJ (Schindelin *et al*., 2012) and processed using the Time Series Analyser Plugin (Balaji, 2006).

Three regions of interest (ROI) were selected, one in the visible atrium of the heart, one in the ventricle and a third ROI in an area outside of the heart but still within the embryos body. The third ROI was used to correct for any changes of intensity of the image caused by external factors. These ROI were circular and 70 pixels in diameter, with the ImageJ plugin used to generate average intensity of each ROI for each image in the 1500 image long sequence.

The data from this process was then imported into Microsoft Excel and normalised values for each heart chamber imaged in each frame were obtained by the following calculation:

$$\frac{Average\ heart\ chamber\ ROI\ Intensity}{Average\ Control\ ROI\ Intensity}$$

This was then plotted against the time point that each frame corresponded to in seconds. This generated a graph with peaks and troughs as blood flowed through one chamber into the next and caused the intensity to change, a representative example of which is shown in Figure 2.3

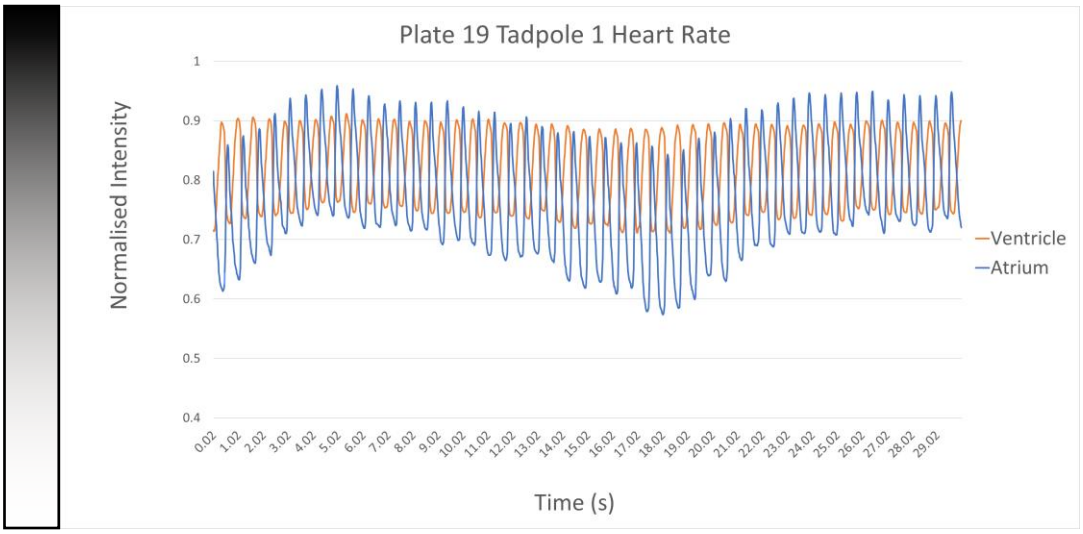

Figure 2.3: An example of the graphs created after normalising the colour intensity of the ROIs. *The darker areas created as the blood filled the ROI had a higher relative intensity, likewise the lighter areas as the blood emptied from the ROI had a lower relative intensity, creating a peak and trough as the heart completed a single beat.*

2.4.3 Automation of analysis

Very early into the research process it was decided that manual calculation of the heart rate from the video assay would be very impractical for this project and would affect the scalability of the assay. To this end, automation of the process was attempted, initially utilising ImageJ software for curve fitting, then moving into RStudio for curve fitting before settling on utilising RStudio for Fourier transformation.

To prepare the data for computational analysis, the video was processed as per Section 2.4.2; then each embryos data in the columns for the normalised atrial intensity and normalised ventricle intensity was saved in an individual .CSV file with consistent naming notation to enable relocation of specific embryo data.

These .CSV files were stored and when required for analysis, placed in a specific “working” folder that the code was designed to pull the data from for processing. After processing, the code was written to output a new .CSV file with the calculated heart rate and/or if the data was irregular for that specific embryo.

2.5 Biomarker Assay

2.5.1 Sample Collection

NF stage 45 embryos that had been exposed to drugs as described in Section 2.3 were anaesthetised in MS-222 and dissected using fine-tipped forceps as per Figure 2.4. Posterior and anterior samples from 15 embryos per concentration were pooled and gathered in 1.5ml Eppendorf tubes with any excess liquid removed. Samples were snap frozen in liquid nitrogen and stored at -80°C.

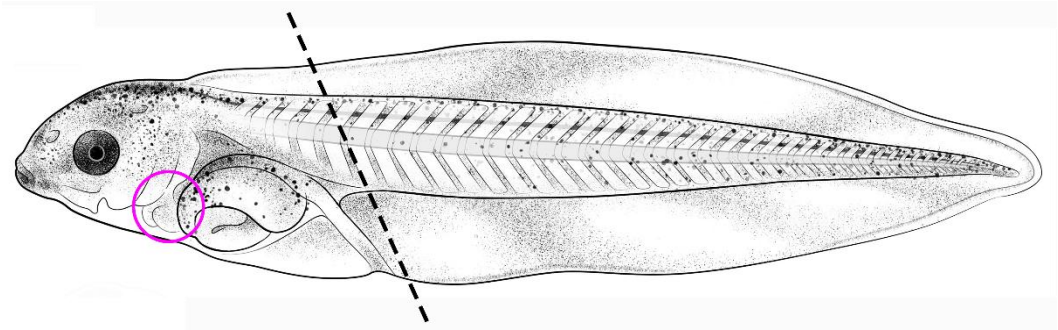

Figure 2.4: Dissection of NF stage 45 embryos. *Dissection was performed along the dotted line, leaving a tail sample filled with the maximum amount of vasculature and a head sample including the heart and liver (magenta). Image of X. laevis embryo taken from Zahn, Natalya et al., (2022)*

2.5.2 RNA Extraction

RNA and miRNA extraction was conducted using the miRNeasy Tissue/Cells Advanced Mini Kit (Qiagen, 217604). Samples of embryo tissue were homogenised using a pestle and 1.5ml Eppendorf in 260µl Buffer RLT before the addition of 80µl Buffer AL and incubation at room temperature for 3

minutes. Samples were transferred to gDNA eliminator spin columns placed in a 2ml collection tube before being centrifuged at 8,000x g for 30 seconds. Column was discarded and flow through transferred to a new 2ml reaction tube, with equal volume of isopropan-2-ol added and mixed thoroughly using pipette. Samples were transferred to an RNeasy® mini column and centrifuged at 8,000x g and flow through discarded. 700µl Buffer RWT was added to the RNeasy® mini column and centrifuged for 15 seconds at 8,000x g and flow through discarded. 500µl Buffer RPE was added to the spin column and centrifuged at 8,000x g for 15 seconds and flow through discarded. 500µl 80% ethanol was added to the spin column and centrifuged at 8,000x g for 30 seconds and flow through discarded. The miRNeasy spin column was added to a new 2ml collection tube and centrifuged at full speed for 1 minute to dry the membrane.

Final extraction of RNA was performed by the addition of 20µl RNAse free water (Sigma) to the centre of the membrane of the spin column and incubation at room temperature for 3-5 minutes, then centrifuged at full speed for 1 minute. This final step was repeated to ensure maximum yield, and RNA quantity was measured using a nanodrop to allow for dilution calculations for further steps. If cDNA synthesis was not immediately performed, RNA was stored at -80°C.

2.5.3 cDNA Synthesis

cDNA synthesis was conducted using the miRCURY® LNA® RT Kit (Qiagen, 339340). Frozen reagents were defrosted and stored on ice. Template RNA concentration was adjusted to 5ng/µl, and reaction mix prepared as listed in Table 2.1. Reaction mix was kept on ice while conditions were programmed onto thermocycler (BioRad). The conditions for the reverse transcriptase reaction were 60 minutes at 42°C followed by 5 minutes at 95°C to inactivate the reaction. If not used immediately, cDNA was stored at -20°C.

Component	Volume (µl)
5x RT SYBR Green Reaction Buffer	2
RNAse-free water	5
10x miRCURY RT Enzyme mix	1
Template RNA	2
Total Reaction Volume	10

Table 2.1: Reverse transcriptase reaction mix.

2.5.4 qRT-PCR

qRT-PCR was initially conducted using 96 well plates on the Applied Biosystems 7500 fast machine. Each individual component listed in Table 2.2 was thawed on ice and master mix created following the amounts shown, excluding cDNA. cDNA was diluted 40X before adding to relevant reaction mises, and 'no template controls' (NTC) were created by replacing the cDNA component with RNAse-free water.

Component	Amount (µl)
2x miRCURY SYBR Green Master Mix	5
ROX Reference Dye	0.05
PCR Primer Mix	1
cDNA Template (1:40 dilution)	3
RNAse-free water	1
Total Reaction volume	10

Table 2.2: Component list for qRT-PCR.

Completed reaction mixes were added to MicroAmp optical 96 well plates (Applied Biosystems) and plate layouts were designed to include 3 technical repeats for each sample.

As the project progressed a change was made to use a machine with greater capacity, Microamp enduraplate optical 384 well clear reaction plates (Applied Biosystems) were used under the same operating conditions and reaction volumes. An example plate layout is shown in Figure 2.5.

Final reaction volumes in each well was 10µl, and plates were sealed and spun briefly in a centrifuge to ensure liquid was well mixed and in the bottom of each well. The qRT-PCR machine was set up following the conditions in Table 2.3, and after completion of experimental run a subsequent melt curve analysis was conducted.

Step	**Temperature (°C)**	**Time (seconds)**	
Initial heat activation	95	120	
Denaturation	95	10	Repeat 40x
Combined Annealing/Extending	56	60	

Table 2.3: Conditions for qRT-PCR.

Various options were explored for quantitative controls and a full list of all primers used in this research is shown in Table 2.4.

samples	primers		1	2	3	4	5	6	7	8	9	10	11	12	13	14	15	16	17	18	19	20	21	22	23	24
		A	ch	ch	ch	ct	ct	ct	20h	20h	20h	20t	20t	20t	40h	40h	40h	40t	40t	40t	60h	60h	60h	60t	60t	60t
		B	80h	80h	80h	80t	80t	80t	100h	100h	100h	100t	100t	100t												
ch	5s rna	C	ch	ch	ch	ct	ct	ct	20h	20h	20h	20t	20t	20t	40h	40h	40h	40t	40t	40t	60h	60h	60h	60t	60t	60t
ct	u6 rna	D	80h	80h	80h	80t	80t	80t	100h	100h	100h	100t	100t	100t												
20h	mir-208	E	ch	ch	ch	ct	ct	ct	20h	20h	20h	20t	20t	20t	40h	40h	40h	40t	40t	40t	60h	60h	60h	60t	60t	60t
20t	mir-122	F	80h	80h	80h	80t	80t	80t	100h	100h	100h	100t	100t	100t												
40h	mir-499	G	ch	ch	ch	ct	ct	ct	20h	20h	20h	20t	20t	20t	40h	40h	40h	40t	40t	40t	60h	60h	60h	60t	60t	60t
40t	mir-103	H	80h	80h	80h	80t	80t	80t	100h	100h	100h	100t	100t	100t												
60h	mir-143	I	ch	ch	ch	ct	ct	ct	20h	20h	20h	20t	20t	20t	40h	40h	40h	40t	40t	40t	60h	60h	60h	60t	60t	60t
60t	mir-133	J	80h	80h	80h	80t	80t	80t	100h	100h	100h	100t	100t	100t												
80h		K	ch	ch	ch	ct	ct	ct	20h	20h	20h	20t	20t	20t	40h	40h	40h	40t	40t	40t	60h	60h	60h	60t	60t	60t
80t		L	80h	80h	80h	80t	80t	80t	100h	100h	100h	100t	100t	100t												
100h		M	ch	ch	ch	ct	ct	ct	20h	20h	20h	20t	20t	20t	40h	40h	40h	40t	40t	40t	60h	60h	60h	60t	60t	60t
100t		N	80h	80h	80h	80t	80t	80t	100h	100h	100h	100t	100t	100t												
		O																								
		P	ntc	ntc	ntc	ntc	ntc	ntc	ntc	ntc	ntc	ntc	ntc	ntc	ntc	ntc	ntc	ntc	ntc	ntc	ntc	ntc	ntc			

Figure 2.5: Example qRT-PCR plate layout created in Microsoft Excel. *Colour coding was used to indicate the gene of interest/miRNA of interest. Abbreviations were used to reduce cluttering of the table; with the h and t indicating if a sample was head or tail and then either a letter or number to indicate the concentration of the drug the embryos were exposed to- so 60t, for example, would indicate the tail sample of embryos exposed to 60μM of the experimental drug.*

qRT-PCR target	Product Name	Product Number (Genglobe)	Target Sequence 5'-3'
miR-208	xtr-miR-208 miRCURY LNA miRNA PCR Assay	YP02111404	AUAAGACGAGCAUAAAGCUUGU
miR-103	hsa-miR-103a-3p miRCURY LNA miRNA PCR Assay	YP00204063	AGCAGCAUUGUACAGGGCUAUGA
miR-122-5p	ssc-miR-122-5p miRCURY LNA miRNA PCR Assay	YP02101912	UGGAGUGUGACAAUGGUGUUUGU
miR-133-3p	dme-miR-133-3p miRCURY LNA miRNA PCR Assay	YP00205954	UUGGUCCCCUUCAACCAGCUGU
miR 17-5p	gga-miR-17-5p miRCURY LNA miRNA PCR Assay	YP00205960	CAAAGUGCUUACAGUGCAGGUAGU
miR-31-5p	gga-miR-31-5p miRCURY LNA miRNA PCR Assay	YP02106253	AGGCAAGAUGUUGGCAUAGCUG
miR-143	bta-miR-143 miRCURY LNA miRNA PCR Assay	YP02115709	UGAGAUGAAGCACUGUAGCUCG
miR-499-5p	dre-miR-499-5p miRCURY LNA miRNA PCR Assay	YP02110648	UUAAGACUUGCAGUGAUGUUUA
U6 RNA	U6 snRNA miRCURY LNA miRNA PCR Assay	YP00203907	Sequence not provided
5s RNA	5S rRNA miRCURY LNA miRNA PCR Assay	YP00203906	Sequence not provided.
miR-16	Xtr-miR-16a miRCURY LNA miRNA PCR Assay	YP02106865	UAGCAGCACGUAAAUAUUGGUG
Rnu1a1	RNU1A1 miRCURY LNA miRNA PCR Assay	YP00203909	Sequence not provided

Table 2.4: qRT-PCR Primers used, sourced from Qiagen.

2.6 Embryo fixation

2.6.1 Embryo Fixing

Embryos at the appropriate Nieuwkoop and Faber (NF) stage of development (Nieuwkoop and Faber, 1958) were collected and fixed in MEMFA for either 2 hours at room temperature, or overnight at 4°C, with gentle rocking. After this, embryos were washed in 100% ethanol or methanol 3 times and then either stored in the alcohol of choice at -20°C or used immediately.

2.7 Whole Mount In Situ Hybridisation (WISH)

2.7.1 WISH Probe creation

Bacterial Transformation

A 100µl aliquot of competent *Escherichia coli* cells were thawed on ice and 4µl of plasmid was pipetted into the tube. This mixture was then incubated on ice for 30 minutes before being heat shocked at 42°C for 90 seconds with tube agitation every 15s before being returned to the ice for 2 minutes. 900µl antibiotic-free Luria Broth (LB) was added to the tube and mixture incubated and shaken at 37°C and 250rpm in the heat shaker. After incubation, mixture was centrifuged for 5 min at 6000x g. Following removal of 950µl supernatant, pellet was resuspended using a pipette. This 50µl mixture was spread on an LB agar plate with appropriate antibiotic and incubated overnight at 37°C.

Primer Design

Primer design was conducted using data collected from Xenbase and the primer blast tool from NCBI (www.ncbi.nlm.nih.gov/tools/primer-blast/).

Firstly, Xenbase was used to determine the information for the gene of interest, when the expression was highest and which chromosome it was

most expressed on (if applicable). The CDS was copied and pasted into the primer blast website and the following parameters set for blasting:

- PCR Product size: between 500 and 1,000 bp
- Primer melting temperature: between 59.0 and 61.0°C
- Organism: *Xenopus*

After blast finished, primer pairs were examined and the best suited for the experiment were chosen and ordered for purchase.

RNA Extraction and cDNA synthesis

3-4 embryos were collected at the appropriate stage where mRNA of each gene of interest was most highly expressed and placed inside a 1.5ml Eppendorf tube. These were then snap frozen in liquid nitrogen for 30 seconds and stored at -80°C if not proceeding immediately to next stage. RNA extraction was done using the RNease Micro Kit (Qiagen, 74004) following the manufacturers protocol. The amount of RNA extracted was quantified using the Nanodop and cDNA created using SuperScript™ IV Reverse Transcriptase 10,000IU (Invitrogen, 18090010) following the manufacturers protocol. cDNA was stored at -20°C until required.

Amplification of Gene of Interest

cDNA was taken and the following PCR reaction conducted: 12.5µl 2X TaqBiomix, 2µl cDNA, 1µl primer mix (forward and backwards, 10µM) and 9.5ml H_2O. Thermocycler was set as shown in Table 2.5.

Step	Temperature (°C)	Time (min:sec)	
Initial Heat Activation	95	05:00	
Denaturing	95	00:30	37x
Annealing	*	00:30	
Extension	72	**	
Final extension	72	07:00	

Table 2.5: PCR reaction for amplification of gene of interest. *Annealing temperature (*) was determined by the primer pair used in the reaction. To determine time of extension step (**), length of cDNA was taken. Taq polymerase worked at a speed of approx. 1,000bp/min, therefore elongation time depends on length of cDNA, however even on short fragments this should be no less than 1 minute to ensure appropriate time for extension.*

To confirm reaction success, 4µl of PCR product was ran on a 1.5% agarose gel for 40 minutes at 90V. When imaged, a single clear band was visible at the length of the cDNA product. Multiple bands would indicate issues with the PCR reaction and experiment should be repeated.

PCR product was then purified using QIAquick PCR Purification Kit (Qiagen, 28104) following manufacturers protocol and purified fragment quantified on nanodrop. This could then be stored at -20°C.

Fragment could then be cloned using pGEM-T Easy Vector System (Promega, A1360) using the following reaction parameters: 5µl 2X Rapid Ligation Buffer, 0.5µl pGEM-T Easy Vector (50ng), 1µl T4 DNA ligase, PCR Product (Quantity calculated following below instructions) and up to 10µl H_2O to create a final volume of 15µl.

PCR product required was determined using the website https://nebiocalculator.neb.com/#!/ligation with the following parameters set:

- Insert DNA Length- The length of the PCR product.
- Vector DNA Length- the length of the pGEM-T vector, 3015bp
- Vector DNA mass- 25ng

The online tool will then give suggestions for ratios of the required insert mass and in this experiment the 3:1 value was typically taken. Volume to add to the mix was calculated using the concentration obtained previously using the nanodrop. Reaction mixture was incubated for 2 hours at room temperature or overnight at 4°C and then stored at -20°C.

Transformation and colony PCR

Bacterial transformation was conducted on X-Gal LB-agar plates following protocol. After incubation, blue and white colonies were visible, with white colonies containing the insert. PCR was conducted by removing part of a white colony from the plate using a 10µl tip and pipetting up and down into the following reaction mixture: 10µl 2X TaqBiomix, 1µl M13Fw/M13Rv mix (10uM each), 9µl H_2O. At least 3 colonies were sampled, and PCR conducted for each plate, with the colonies sampled indicated on the lid of the plate and plate retained.

Step	Temperature (°C)	Time (min:sec)	
Initial Heat Activation	95	05:00	
Denaturing	95	00:30	35x
Annealing	59	00:30	
Extension	72	*	
Final extension	72	07:00	

Table 2.6: PCR condition table for bacterial transformation*. Extension (*) time was calculated using methodology mentioned in Table 2.5, with consideration of the 200bp addition in length.*

5µl of PCR product was ran on a 1.5% agarose gel for 40min at 90V. A single band of the insert size+200bp indicated successful transformation and the rest of the colony was sampled was taken and placed into 5ml LB broth with ampicillin and grown overnight at 37°C.

MINI preps were conducted with the LB broth following manufacturer's instructions, then samples were sent for sequencing using either M13fw or M13rv as primers to determine directionality of the insert. When results were obtained, probe synthesis was performed using either of the following methods.

<u>Probe Synthesis by Plasmid Linearisation</u>

Restriction reaction was conducted in conditions suited for plasmid and restriction enzyme appropriate to experiment, with the reaction assembled as follows: 2.5µg plasmid, 2.5µl appropriate 10X Restriction Buffer, 2.5µl appropriate restriction enzyme, with H_2O added to bring the final volume to 25µl.

- Normal Restriction Enzyme- overnight at 37°C
- Time Saving Restriction Enzyme- 2h at 37°C

1µl of linearised product and 1µl circular plasmid were ran on a 1% agarose gel to determine if linearisation was successful. When success was confirmed, linearised plasmid was purified using QIAquick PCR Purification kit (Qiagen, 28104) following manufacturer's instructions. Purified sample was then quantified using a Nanodrop.

For riboprobe synthesis, reaction was assembled as follows: 4µl of 5X transcription buffer, 2µl DTT (100mM), 2µl DIG, 1µl RNA inhibitor (RNasin®), 2µl appropriate RNA polymerase (T7, T3, SP6), 100ng of purified PCR product and H_2O to a final volume of 20µl. The reaction was then incubated at the following conditions, depending on which polymerase was used:

- For T7 polymerase, overnight at 37°C
- For T3 polymerase, 3 hours at 37°C
- For SP6 polymerase, 4 hours at 40°C

Final product was checked by using a 1.5% agarose gel and 1µl of reaction product. When visible probe was confirmed, purification was conducted using G50 Purification column (Illustra, ProbeQuant G-50 Micro Columns, GE Healthcare) following manufacturer's instructions.

Purified riboprobe was quantified on Nanodrop and then diluted in hybridisation buffer to a concentration of 1µg/ml and stored at -20°C.

<u>Probe Synthesis by PCR Reaction</u>

Appropriate plasmid was selected, and a PCR reaction set up with the following reagents: 12.5µl 2X TaqBiomix, 1µl appropriate primers (10µM), 100ng of plasmid and H_2O to 25µl volume. The thermocycler was set following the conditions in Table 2.7.

Step	Temperature (°C)	Time (min:sec)	
Initial Heat Activation	95	05:00	
Denaturing	95	00:30	35x
Annealing	59	00:30	
Extension	72	1:30	
Final extension	72	07:00	

Table 2.7: Conditions of the PCR reaction for probe synthesis.

5µl of PCR product was then ran on a 1.5% agarose gel for approx. 35 minutes at 90V, then checked to confirm correct product is visible. When confirmed, purification using QIAquick PCR Purification kit (Qiagen, 28104) following manufacturer's instructions. Purified sample was then quantified using a Nanodrop.

For riboprobe synthesis, reaction was assembled as follows: 4µl of 5X transcription buffer, 2µl DTT (100mM), 2µl DIG, 1µl RNA inhibitor (RNasin®), 2µl appropriate RNA polymerase (T7, T3, SP6), 100ng of purified PCR product and H_2O to a final volume of 20µl. The reaction was then incubated at the following conditions, depending on which polymerase was used:

- For T7 polymerase, overnight at 37°C
- For T3 polymerase, 3 hours at 37°C
- For SP6 polymerase, 4 hours at 40°C

Final product was checked by using a 1.5% agarose gel and 1µl of reaction product. When visible probe was confirmed, purification was conducted using G50 Purification column (Illustra, ProbeQuant G-50 Micro Columns, GE Healthcare) following manufacturer's instructions.

Purified riboprobe was quantified on Nanodrop and then diluted in hybridisation buffer to a concentration of 1µg/ml and stored at -20°C.

2.7.2 WISH protocol

Experiment was conducted at room temperature and with gentle rocking applied at all stages unless specified. Samples were sequentially washed with decreasing concentrations of ethanol and DEPC-PBSTween for 5 minutes per stage (75% ethanol, 50% ethanol, 25% ethanol) and then washed twice in DEPC-PBSTween solution for 5 minutes each. Samples were treated with proteinase K solution for 20 minutes with no rocking applied before being washed twice more with DEPC-PBSTween for 5 minutes each.

Samples were placed in fixing solution for 20 minutes before being washed with DEPC-PBSTween for a further 5 minutes and then transferred into pre-heated hybridisation buffer (HYB) and left without rocking at 60°C, until embryos settled at the bottom of the sample container. HYB was replaced with fresh HYB and incubated for 1 hour at 60°C before transferring embryos to probe solution which was then left to incubate overnight at 60°C.

Samples were washed with HYB buffer for 10 minutes at 60°C, then three further washes in 2X SSC for 20 minutes each at 60°C. Samples were transferred to RNase A solution for 30 minutes at 37°C before being washed with 2X SSC for 10 minutes. Samples were then washed at 60°C with 0.2X SSC and rinsed with MAB for 10 minutes. Samples were then placed in antibody solution and incubated overnight at 4°C.

Samples were washed twice with MAB for 5 minutes each time, then washed a further 6 times in MAB for 30 minutes per wash. Samples were left to wash in MAB overnight at 4°C.

Samples were washed 3 times with MAB for 5 minutes each time, then twice with NTMT solution for 10 minutes, then transferred to colour solution and incubated in the dark at room temperature until the control probe developed colour. If the colour solution darkened before the probe, darkened solution was replaced with fresh colour solution. Colour reaction was stopped by washing 3 times with PBST for 10 minutes per time. Samples were then ready for imaging.

If background staining was high, samples could be incubated overnight at 4°C in 100% methanol to reduce background staining. Embryos then needed to be rehydrated by washing twice in PBS for 10 minutes before imaging.

2.7.3 LNA WISH

Experiment was conducted at room temperature and with gentle rocking applied at all stages unless specified (Ahmed *et al*., 2015).

Samples were sequentially washed with decreasing concentrations of ethanol and DEPC-PBSTween for 5 minutes each stage (75% ethanol, 50% ethanol, 25% ethanol) and then washed twice in DEPC-PBSTween solution for 5 minutes each. Samples were treated with proteinase K solution for 20 minutes with no rocking applied before being washed twice more with DEPC-PBSTween for 5 minutes each.

Samples were placed in fixing solution for 20 minutes before being washed with DEPC-PBSTween for a further 5 minutes and then transferred into pre-heated HYB and left without rocking at 54°C until embryos settled at the

bottom of the sample container. HYB was replaced with fresh HYB and incubated for 3 hours at 54°C before transferring embryos to LNA-probe solution which was then left to incubate overnight at 54°C.

Samples were washed with HYB for 10 minutes at 54°C, then three further washes in 2x SSC for 20 minutes each at 54°C. Then they were washed twice with 0.2x SSC for 30 minutes at 54°C and rinse with MAB for 10 minutes. Samples were then placed in blocking solution and incubated for at least 1 hour. Then they were transferred to antibody solution and incubated overnight at 4°C.

Samples were washed twice with MAB for 5 mins each time, then a further 6 30min washes in MAB were performed. Samples were then washed in MAB overnight at 4°C.

Samples were washed 3 times with MAB for 5 minutes each time, then twice with NTMT solution for 10 minutes, then transferred to colour solution and incubated in the dark at room temperature until the control probe developed colour. If the colour solution darkened before the probe, it was replaced with fresh colour solution. Reaction was stopped by washing 3 times with PBST for 10 minutes. Samples could then be imaged.

If background staining was high, samples were incubated overnight at 4°C in 100% methanol to reduce background staining, but embryos needed to be rehydrated by washing twice in PBS for 10 minutes before imaging.

2.8 Statistical Analysis

2.8.1 Video assay analysis

When final data collection was complete, data was collated across all repeats and merged to create a pooled dataset in GraphPad Prism. Outliers

were identified using the in-built outlier identifier and highlighted datapoints removed from the dataset.

Normality tests were conducted to determine distribution of the data, and although multiple tests were able to be conducted the results for D'Agostino-Pearson were used, following software guidance. If one of the concentration datasets was determined to be lognormal, all datasets for that drug were processed for statistical significance as if they were lognormal. If datasets were normal, one-way ANOVA would be performed to determine if the results for each group are significantly different to the control group. For lognormal data, Kruskal-Wallis test was chosen instead of one-way ANOVA. P values of 0.05 and below were considered significant.

2.8.2 Biomarker Assay analysis

Ct values were taken from qRT-PCR data and collated in a table in Microsoft Excel. The Livak method was determined to be the most appropriate method to analyse the data for gene/miRNA expression (Livak and Schmittgen, 2001).

Ct values above 35 and below 15 were treated as outliers and removed from the dataset. Mean values were taken for the triplicate technical repeats across each biological repeat performed, as well as a mean value for the complete dataset including all biological repeats. After this, the ΔCT value was found by subtracting the housekeeping miRNA repeat average from the repeat average of the target gene for each sample. Then the ΔΔCT value was calculated using minus average of the repeat from the average from all the repeats of the control head sample. Then 2 ^ -ΔΔCT was done to determine fold change compared to the control head sample of the gene of interest.

Had there been multiple biological repeats then standard deviation could have been calculated alongside determining if there was a statistically significant difference between the drug exposed groups and the control group. Unfortunately, as this was not the case statistical significance could not be determined.

Chapter 3: Assay Development and Optimisation

3.1 Introduction

The project began with an assessment of existing methodologies and understanding which would be the most suitable for obtaining the results necessary to answer the questions posed in the introduction. Foundational work on this topic had been conducted previously and results can be found in (Saide, 2018; Saide et al., 2019). In this work, the author had focussed on development of a liver toxicity assay and then followed this up with the first stages of utilising the biomarker liver assay methodology to detect cardiotoxicity in *Xenopus*, alongside a method to detect changes in heart rate that correspond with cardiotoxicity. The biomarker assay using microRNAs as biomarkers showed great promise, especially with the potential to couple this with the liver toxicity assay methodology as this would increase the scope of testing available and increase the number of results from a single experiment. Improving this method to expand the number and range of biomarkers tested would improve the results generated from the assay and provide a more robust assay.

The heart rate methodology built upon work carried out by Bartlett et al., (2004) and consisted of incubating *Xenopus* embryos with cardiotoxic drugs, anaesthetising the embryos and then recording video of the heart beating. These video recordings were then processed and the heart rate determined, and arrhythmic heart rates identified. The heart rate assay was fully manual and required human interpretation to determine arrhythmic patterns of heart beat, and this was a driving factor of developing the method further in the research covered by this report as the introduction of an automated or semi-automated methodology would allow for increased throughput and less subjective results.

The methodology also studied exposure to compounds from NF stages 38 to 45, which was approximately 3 days following standard incubation temperatures. This exposure period can be considered to be a mid-range of

exposure time, as it is longer than would be anticipated for acute exposure and performing a chronic exposure with this model would be difficult due to the development of the frog after NF stage 45.

As part of the development of both heart rate and biomarker assays, decisions had to be made as to which drugs to utilise as benchmarks to build the assay and test its suitability for use.

3.2 Drugs used in the study

The choice of drugs to be administered to the embryos was carefully considered. Ideally, a range of drugs that cause cardiotoxicity through different mechanisms would be used for the experimentation but additionally one or more negative controls should be included too. This would allow for improved comparison between the drugs where toxicity is anticipated to ensure toxicity is due to the drugs rather than any environmental changes caused through dissolution of compounds or carriers. The drugs doxorubicin, terfenadine E4031 and paclitaxel were chosen for their cardiotoxic properties to use in the assay, alongside paracetamol which had been used in developing the liver toxicity assay. Although the choice of these compounds were dictated by accessibility and previous use within the research group, there have been compound libraries assembled in the literature that have been created to cover a range of mechanisms of cardiotoxicity action and designed for use in developing new models. A 12 drug selection by De Korte et al., (2020) is one such example, shown in Table 3.1. This selection covers a range of mechanisms of action as well including drugs that affect the cardiomyocytes more distinctly than others, allowing for a determination of the sensitivity of the method being developed. This drug library was set up with the intention of use by researchers using iPSC-based assays, and so there may be an unequal effectiveness when attempting to use in an in vivo assay like the one in this report.

Class	Drug	Mechanism of action in cardiomyocytes
Positive inotropes	Isoprenaline	Nonselective β-adrenergic agonist
	Levosimendan	Calcium sensitizer
	Milrinone	Phosphodiesterase (PDE) III inhibitor
	Bay K 8644	L-type Ca^{2+} channel activator
	Omecamtiv mecarbil	Myosin activator
	CDN1163	SERCA activator
	Ouabain	Na^{+}/K^{+}-ATPase inhibitor
Negative inotropes	Doxorubicin	Impairs Ca2+ transport mechanisms in sarcoplasmic reticulum
	Nifedipine	L-type Ca2+ channel blocker
	Blebbistatin	Myosin inhibitor
	Sorafenib	Multitargeted tyrosine kinase inhibitor
No effect	Aspirin	N/A

Table 3.1: Suggested 12 drug library to use for developing cardiotoxicity models. Reproduced from De Korte et al., (2020).

Alongside the choice of compounds used in this project, the method of delivery required some consideration. Many of the drugs used are delivered through IV in humans, but the size of the *Xenopus* embryos in this study and the time required to perform such a series of microinjections makes this unlikely to be suitable in this assay. In previous work, drug delivery has taken place by dissolving into the growth media, and this seems to be the most logical method to use in this study too.

Some compounds do not dissolve readily into water-based solutions and so would require a different solvent. There are several hydrocarbon options available to use as a solvent for this purpose, but many would be unsuitable for this specific piece of research. Due to the precise pH of the growth media the embryos must be kept in, acids could potentially disrupt this and cause unintended toxicity. Alcohols would also be likely to cause independent toxicity of the embryos and interfere with any results generated. Alkanes,

such as chloroform and hexane, are toxic to aquatic life and even in small concentrations could interfere with the experiments. For these reasons, the decision was made to use Dimethyl sulfoxide (DMSO) as a vehicle where necessary.

DMSO was chosen due to the previous success utilising it as a vehicle for delivering compounds to *Xenopus* embryos. Previous work performed in the Wheeler lab (unpublished data) trialled different concentrations of DMSO and discovered that an optimal, minimally toxic concentration was 0.5% (v/v), and so has been utilised by researchers both within and external to the laboratory with success (Brändli, 2004; Saide, 2018).

Throughout the length of this project, whenever a drug has utilised DMSO as a vehicle, an additional control group was included within that experiment containing only the incubation media and DMSO, at the highest concentration used in the experiment. The heart rate results were collected and pooled across several experiments and analysis was performed to determine if DMSO affected the heart rate of the *Xenopus* embryos, with results shown in Figure 3.1.

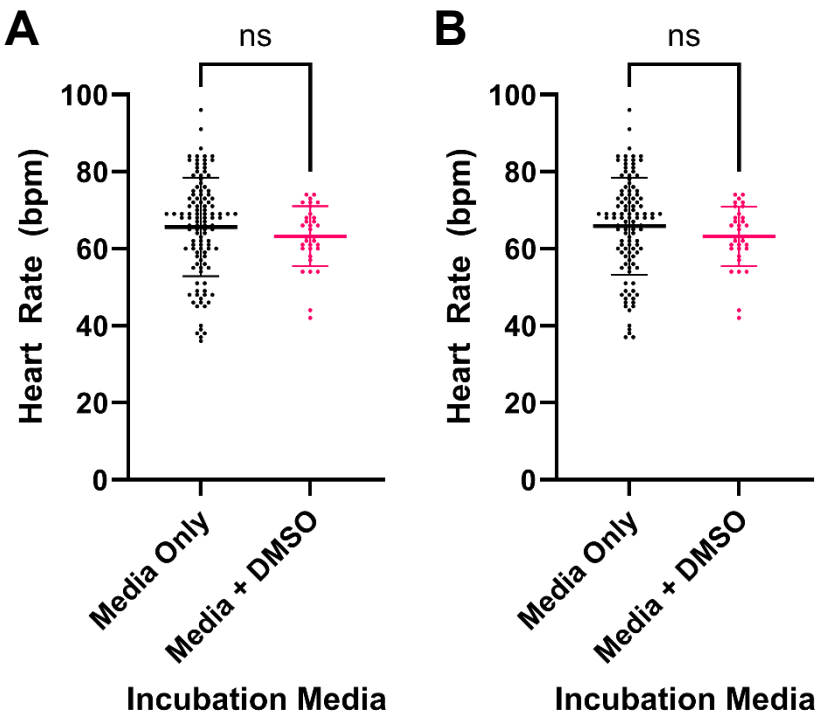

Figure 3.1: Atrial (A) and ventricular (B) heart rate of Xenopus embryos exposed to DMSO. *Xenopus embryos treated between NF stages 38 and 45 with 0.5% DMSO and kept at 23°C, then heart rate measured after 15-minute treatment with MS-222 by determining number of times the heart beat for 30 seconds and adjusted into beats per minute. Average atrial heart rate ± SD of treated embryos was compared to untreated embryos using Mann-Whitney test. n= 114 (atrial) 113 (ventricular) for untreated embryos, n= 33 for treated embryos. One datapoint for the untreated embryos was removed using GraphPad Prisms outlier detection function.*

The results from this analysis indicates that the presence of DMSO at experimental concentrations did not affect the heart rate of the *Xenopus* embryos.

As part of the research, survivability assays were performed to determine which concentrations of each drug would be most suitable to use for the experiments. While several of the drugs used have therapeutic and toxic doses in humans and mammalian models already documented in the

literature, these were often unable to be directly translated into a dissolved product for the *Xenopus* model. Doxorubicin, for example, has several therapeutic doses as it's use varies depends on the treatment plan for the cancer it is treating, but it is not unreasonable to see dosages of 75mg/m^2 as an IV bolus, with a maximum lifetime cumulative dose of 450mg/m^2 according to the NHS, and a review by Podyacheva et al., (2021) covered several different dosages in rat models that cause toxicity, given in values of mg/kg. It is due to the difficulty in converting these values to something usable in a dissolution that survivability was chosen as a method of preparing a dosage curve for the *Xenopus*. Embryos were determined to have died when they either stopped developing compared to controls, changed colour, stopped responding to stimuli, developed a 'fuzzy' appearance, the heart stopped beating, the embryo stopped moving or any combination of the above. These were checked twice daily and removed when discovered. These same signifiers of death were used to remove embryos in the experimental assays and so only embryos showing life signs were taken forward for imaging.

3.2.1 Doxorubicin

Doxorubicin is an anthracycline medication primarily used in anti-cancer treatment, discovered in the early 1960s. The anticancer effects of doxorubicin were determined very early, alongside clear instances of its toxic side effects. The mechanism used to fight cancer, upregulating the expression of death receptors causing apoptosis, can also trigger apoptosis in cardiac cells (Zhao and Zhang, 2017). Doxorubicin-induced cardiotoxicity is often triggered in a dose-dependent manner, meaning the more doxorubicin a patient is exposed to the more likely they are to develop cardiotoxicity and the more severe the cardiotoxicity is likely to be. These side effects include hypotension, tachycardia, arrhythmia and potentially congestive heart failure (Singal and Iliskovic, 1998). The cardiotoxic events are broadly split into acute events, occurring after a single dose and often a fast-onset development, and chronic toxicity which has been documented as occurring up to years after the final dose taken. Acute cardiac events tend

towards arrhythmias and inflammatory disorders such as myocarditis (Bristow *et al*., 1978). These may be treatable with early diagnosis and can be detected in-clinic during treatment session through simple ECG monitoring- they are often associated with T-wave flattening, reduced QRS voltage and QT prolongation (Singal and Iliskovic, 1998). Chronic toxicity is much more serious, with the greatest mortality of up to 50%, often tied to the presence of congestive heart failure (Chatterjee *et al*., 2010). Another common expression of cardiotoxicity that is linked to chronic doxorubicin exposure is chronic dilated cardiomyopathy (CDM) and has been noted as developing over 10 years after treatment ended (Steinherz *et al*., 1991).

To determine the appropriate concentrations of doxorubicin to study, the previous work from Saide (2018) was used as a baseline to work from. The previous work performed a survivability test using concentrations between 0 and 150μM and found limited survivability beyond 90μM concentration.

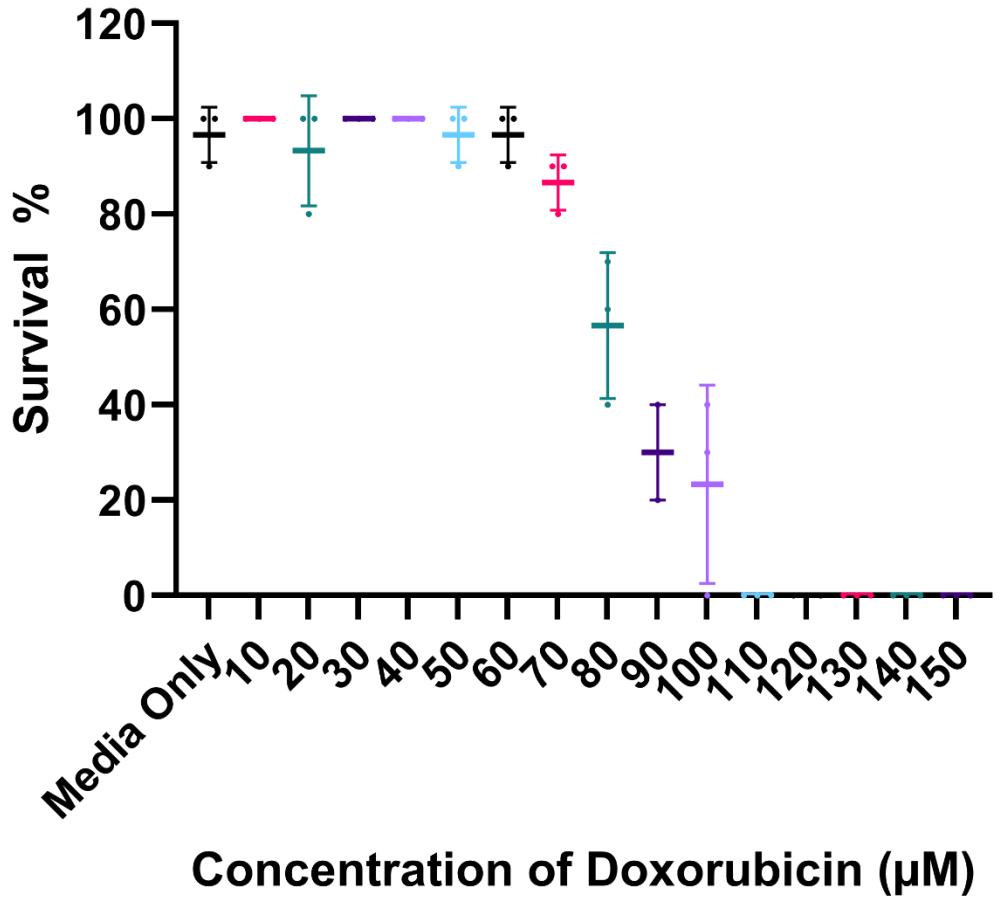

Figure 3.2: Embryo survival at doxorubicin concentrations between 0-150μM. *10 embryos were used per concentration with minimum 3 technical repeats for a total n= 30, graph shows mean and SEM as there were not enough datapoints to accurately determine standard deviation.*

This experiment showed that survival is high in the control group and at concentrations up 60μM, with survival dropping steadily up to 80μM. Survival was low (<50%) at the 90-100μM concentration and there was 100% fatality for embryos at concentrations beyond 100μM (Figure 3.2). Following these results, it was decided that for the rest of the study embryos would be exposed to concentrations up to 100μM, with the anticipation that poor survivability at the highest concentrations may lead to difficulty generating volume of results.

3.2.2 Terfenadine

Terfenadine is an antihistamine drug, originally developed in 1973 as a tranquilizer. It failed as a tranquilizer but was found to be a useful antihistamine, working as a H1 receptor antagonist, where it competes with histamine to bind to the H1 receptor. Due to its lack of sedative properties, it became very popular when brought to market and approved by the FDA in 1985, but issues arose as early as 1990 with reports of cardiovascular side effects from those taking the medication. The cardiovascular events reported were linked to QT prolongation, cardiac arrhythmia and Torsade de Pointes (Monahan *et al*., 1990; Zimmerman *et al*., 1992). Initial investigations into the mechanism of action for this pointed towards inhibition of the potassium Kv1.5 channel- when the channel is open, terfenadine may enter and block the channel preventing flow of potassium ions and so disrupting the hearts electrophysiology (Crumb *et al*.; Yang *et al*., 1995). Further investigation revealed that the Kv1.5 channel has a greater expression in the atrium rather than the ventricle, and the primary arrhythmia being reported was ventricular arrhythmia. An alternative suggestion was raised that the mechanism involved the hERG potassium ion channel instead, and further research into this ion channel showed that hERG channels were 10-fold more sensitive to a terfenadine blockage compared to the Kv1.5 channel (Roy *et al*., 1996; Woosley *et al*., 1993). Unusually, it was terfenadine itself that caused the toxicity, as it's metabolite fexofenadine- the active molecule that performs the histamine receptor inhibition- was noted to have a much lower incidence of causing toxicity (Roy *et al*., 1996), leading to the FDA approving fexofenadine and recommending withdrawal of terfenadine from the market in 1997.

To determine the appropriate concentrations of terfenadine to study, the previous work from Saide (2018) was used as a baseline to work from. The previous work performed a survivability test using concentrations between 0-100μM and found strong survivability up to 10μM with a noticeable decrease in survival between 20-80μM and no surviving embryos at the highest concentrations.

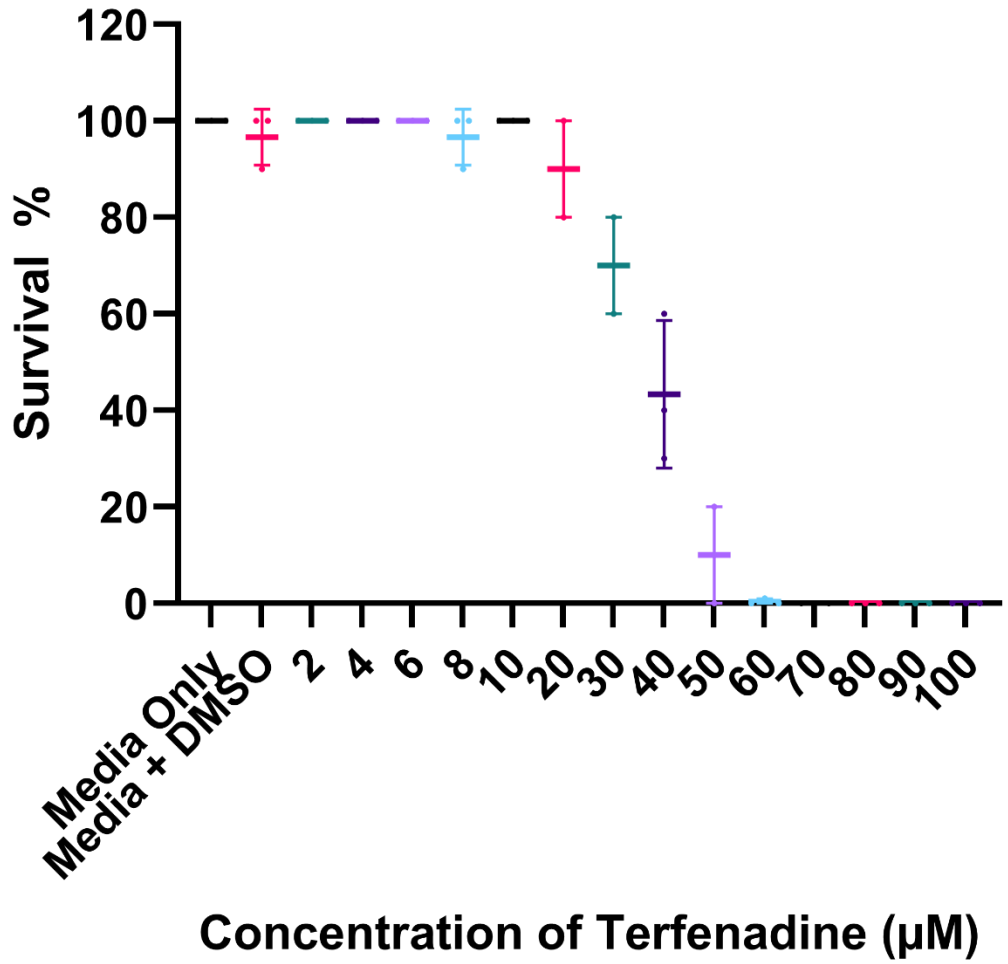

Figure 3.3: Embryo survival at terfenadine concentrations between 0-100µM*. 10 embryos were used per concentration with minimum of 3 technical repeats for a total n= 30, graph shows mean and SEM as there were not enough datapoints to accurately determine standard deviation.*

This experiment found 100% survival of embryos in the control group and at concentrations up 10µM survival remains consistently around 100%, before dropping from 20µM to 50µM, leading to 100% fatality for embryos at concentrations beyond 50µM (Figure 3.3). Survival dropped below 50% at 40µM concentration. This informed the rest of the experiments to be conducted at concentrations between 0-50µM, with the understanding that additional repeats may need to be conducted at the higher concentrations

due to the reduction in survivability leading to lower levels of data being collected.

3.2.3 Paracetamol

Paracetamol is a pain relief and fever reducing medication commonly used throughout the world without need of a prescription. This ease of access no doubt contributes to the high incidence of paracetamol-induced liver failure globally. The way it triggers hepatotoxicity is by generation of N-acetyl-p-benzoquinone (NAPQI) through a minor metabolic pathway, which builds up when high doses are consumed and instigates cell death through generation of reactive oxygen species, stimulation of Ca2+ activated degradative enzymes and lipid peroxidation (McGill and Jaeschke, 2013). It is not known to cause cardiotoxicity directly.

Paracetamol was chosen as a negative control for this project as the interactions between paracetamol and major organs are quite well documented and the link between paracetamol and liver toxicity is well studied, and research has shown there is no direct link between paracetamol and cardiac toxicity. This means that it can be used as a model for liver toxicity without overlapping into cardiotoxicity, and as such we can determine if the effects of drug exposure seen are due to specific organ toxicity (whether liver or heart) or a generalised toxicity affecting the whole embryo.

To determine the appropriate concentrations of paracetamol to study, the previous work from Saide (2018) was used as a baseline to work from. The previous work performed a survivability test using concentrations between 0-5mM and found strong survivability throughout. Further experiments were carried out using concentrations of 5.5-10mM which showed much higher levels of mortality. Due to the increased mortality a concentration range of 1-5mM was chosen to perform the following survival trial.

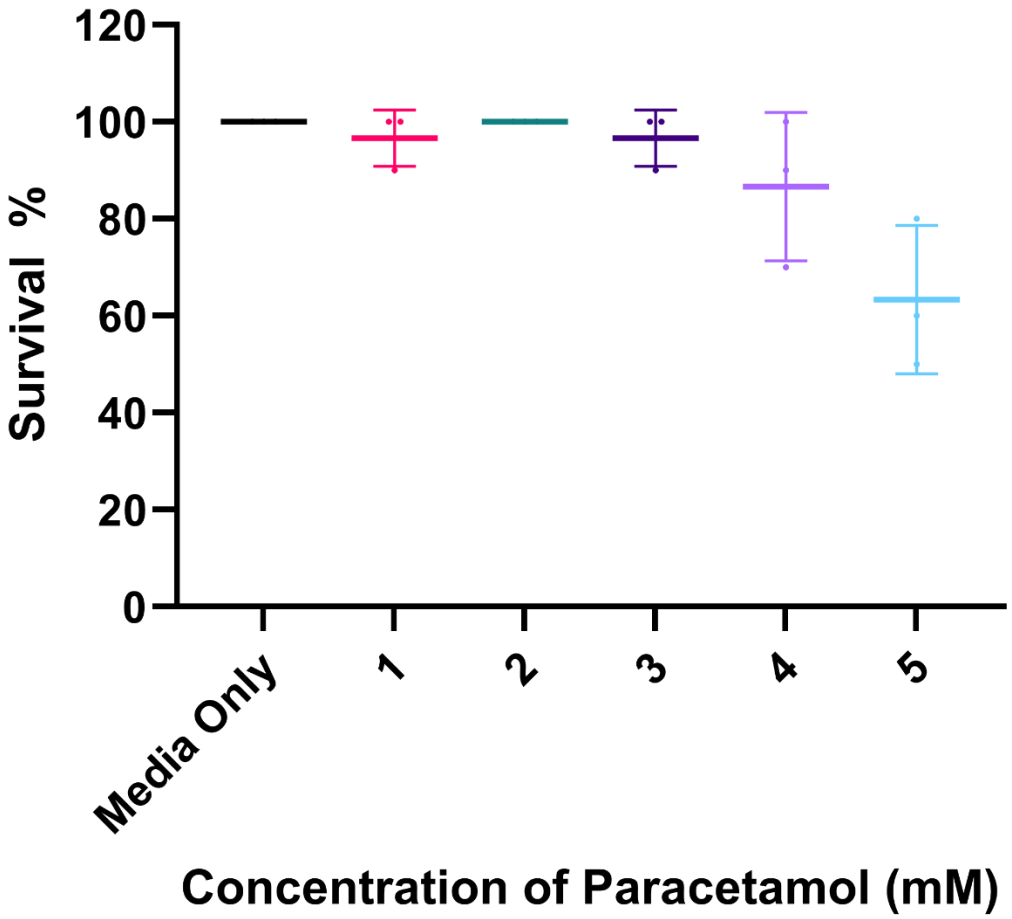

Figure 3.4: Embryo survival at paracetamol concentrations between 0-5mM*. 10 embryos were used per concentration with minimum of 3 technical repeats for a total n= 30, graph shows mean and SEM as there were not enough datapoints to accurately determine standard deviation.*

The results from this test showed 100% survival in the control group and survival remained high throughout the concentrations tested, with a reduction to 86% at 4mM and 63% at 5mM (Figure 3.4). These concentrations were chosen based on the results of Saide *et al*. (2019) although the results from this study indicated a much higher survival rate. These concentrations were maintained throughout the experiments around paracetamol exposure based on the results of Saide *et al*. (2019) indicated these dosages would be high enough to induce hepatotoxicity.

3.2.4 Paclitaxel

Paclitaxel, much like doxorubicin, is used as a chemotherapy agent used in a variety of cancer treatments. It's method of action is to target tubulin and inhibit spindle function in cells, which arrests cell division and encourages apoptosis. These effects, while beneficial in cancer treatment as it destroys cancer cells, are incredibly damaging in healthy cells and as a result instances of cardiac damage have occurred on patients receiving the drug. This cardiac damage can present as extended QT interval (long QT syndrome), bradycardia or atrial fibrillation (Pizzino et al., 2014; Valiyaveettil et al., 2023). Additional presentations such as ejection fraction and cardiac ischemia are beyond the scope of this study to monitor (Osman and Elkady, 2017).

Data for this experiment was gathered by a final year undergraduate student within the lab, who determined that a concentration range of 0.005-0.1μM would be initially trialled, following the results found in Gutiérrez-Lovera et al., (2019). This concentration range proved to have no effect on embryo survivability and therefore did not appear to induce toxicity, so a range of 0-100μM was trialled instead to induce a level of toxicity that would allow for analysis. The results from this are presented in Figure 3.5.

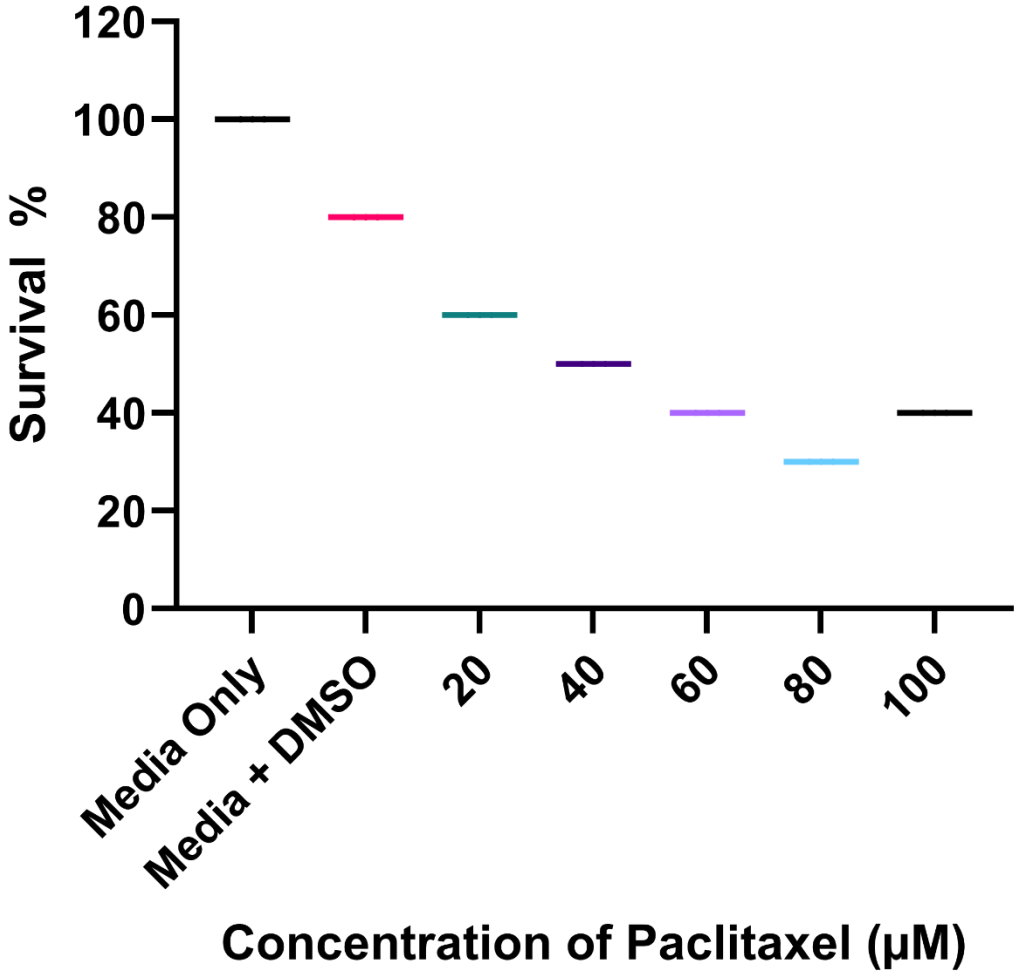

Figure 3.5: Mean embryo survival at paclitaxel concentrations between 0-100µM. *10 embryos were used per concentration with 3 technical repeats for a total n= 30.*

This experiment showed that 100% survival was found in the control group with survival reducing steadily until 80µM where it reached 30% survival, before rising again to 40% for the highest concentration of 100µM. There was a decrease in survival (from 100% to 80%) between the control and vehicle control, which could be suggestive of the DMSO causing toxicity; but the concentration of DMSO in the vehicle control was the same as the highest drug-containing concentration and as the 100µM survival was lower still at 40% it did appear that the drug itself was having an effect on survival rate rather than the DMSO, but this should be taken into consideration

alongside any other results drawn from this data. Ideally, this experiment would have been repeated with more attention paid to concentrations below 20μM, to determine where the toxicity begins.

3.2.5 E4031

Unlike the rest of the toxic agents in this study, E4031 is not a drug that has been used for medicinal purposes but was specifically designed to create cardiotoxicity. It works by binding to open hERG channels in myocardial cells, prolonging the cardiac action potential and initiating long QT syndrome (Kim et al., 2005; Weinsberg et al., 1997). Long QT syndrome presents as a cardiac arrhythmia and as such the scope of this project was to see if arrhythmias could be firstly induced in *Xenopus* embryos and if these arrhythmias could be detected by our methodology.

Data for this drug was gathered by a final year undergraduate student within the lab, who determined that a concentration range of 10-100μM would be used based on the concentrations used in the doxorubicin experiment (Figure 3.2) and a survival curve was not performed.

3.3 Heart Rate Assay Development

The initial methodology of performing the video assay was adapted from a previous PhD student (Saide, 2018) who in turn had adapted the methodology from Bartlett *et al*. (2004). It was thought that the methodology could be expanded upon and improved in certain areas, as although the previous methods worked, they were not suitable for scaling up and throughput was relatively low.

One of the key areas of the method was the use of a third imaging zone as a control ROI, which was used to normalise the data generated and account for variations of brightness in the imaging room and within the embryo. There

may be ways in which this could be improved but this was not explored in this study.

3.3.1 Anaesthesia time

To accurately film the embryos, they needed to be immobile. Previous work (Saide, 2018) in the lab utilised the anaesthetic MS-222/Tricaine (Sigma) for this purpose, and the time the embryo was exposed to the anaesthetic before filming was set at 1 hour, based on adult *Xenopus laevis* anaesthesia times. The concentration of 0.2mg/ml MS-222 was also determined in the same thesis, as higher concentrations indicated a reduction in heart rate (Figure 3.6). Despite the apparent minor increase in heart rate at 0.2mg/ml compared to 0.1mg/ml, the latter did not sufficiently anaesthetise the embryos to prevent movement.

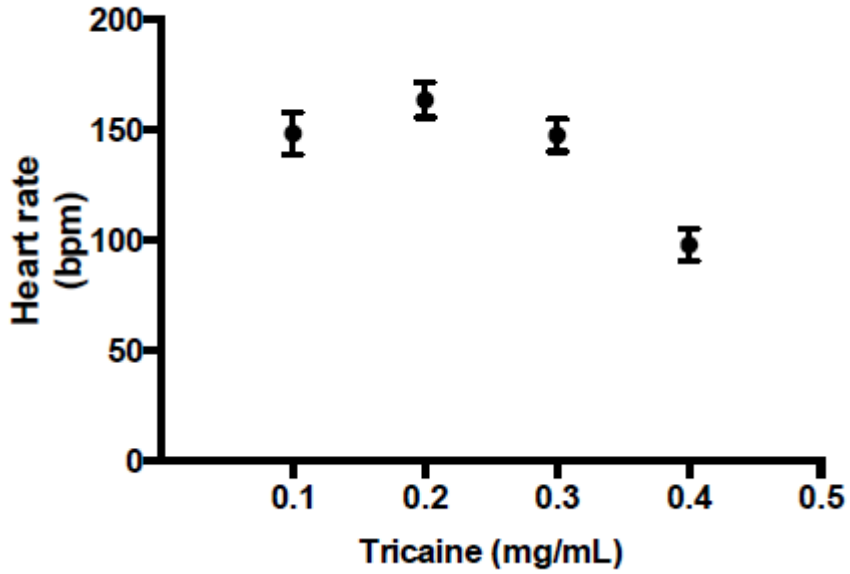

Figure 3.6: Investigation of anaesthetic concentration and heart rate. *The heart rate of NF Stage 45 Xenopus embryos after 1 hour incubation with different concentrations of MS-222/Tricaine. Taken from Saide (2018).*

With the logic that *Xenopus* embryos are much smaller than adult frogs, experiments were undertaken to see if a shorter time could be used for anaesthesia whilst still being effective. It was found that an exposure of 15 minutes at a concentration of 0.2mg/ml MS-222 (Sigma) was sufficient to fully anesthetise an embryo, tested by manipulating the embryo into position using pipette tips and the embryo not reacting to the stimulus, but with the ability to fully recover within an hour after removal from a 30 minute submersion in the MS-222 (Sigma) (Results not shown).

3.3.2 Immobilisation of the embryos

Anaesthesia, in high enough doses, can lead to a reduction in heart rate and previous work (Saide, 2018 and Figure 3.6) was used to inform the concentration of the anaesthetic used in this study to avoid this. It is important to take into consideration however, that an accurate measurement of heart rate for unanaesthetised *Xenopus* was not able to be found due to the inability to image the embryos without anaesthesia to keep them still. As initial parts of this study, possible alternatives to anaesthesia to immobilise the embryos were explored to enable non-anaesthetised imaging. One option presented in the literature was that of a glue to hold them in place (Bartlett *et al*., 2004) but after discussion and some consideration the author believed this methodology would potentially cause stress-related heart rate to increase and injure the embryos used this way. Previous work done by the author with zebrafish (*Danio rerio*) (Wyville, 2019) led to exploration of the methods utilised for that model organism and if the skills and methods could be transferred for use with *Xenopus sp*.

The methodology used when immobilising *D. rerio* is established (Bergmann *et al*., 2018; Chhabria *et al*., 2020) and consisted of making a 1-2% solution of low melting point agarose, with the liquid component being growth media the embryos are being raised in. The liquid agarose was maintained in Eppendorf tubes on heat blocks set to 27°C until ready for use. Embryos were then prepared for imaging, removed from their growth media and

placed without liquid on a petri dish. The LMP agarose solution was added using a Pasteur pipette, then the solution and embryo was drawn up into an appropriately sized transferpettor cap (Sigma, Z328510) with a piston rod (Sigma, BR701936) and left to solidify for a few seconds. When set, this would create a cylindrical agarose tube with the embryo suspended within, allowing manipulation and imaging when placed into growth media solution. The solubility of the agarose would allow the embryo to respire and not cause death through oxygen deprivation. Initial trials to test this process were done with small 1ml syringes, with the embryo being held in the hub of the syringe and with the syringe cut so the embryo could be held in the barrel of the syringe (Figure 3.7).

Figure 3.7: Xenopus agarose trials with syringes. *The embryos are held in the hub of the syringe (bottom) or the barrel (top) following modification of the syringe by cutting the hub off.*

Following curing of the agarose, the embryos were ejected into a petri dish containing 0.1X MMR, at which point the agarose cage formed in the hub of the syringe became fragmented and the embryo no longer secure (Figure 3.8).

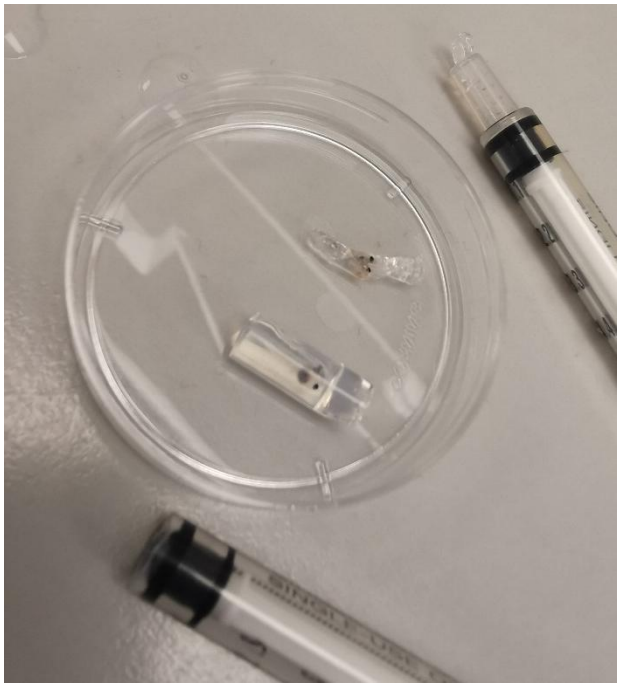

Figure 3.8: Xenopus embryos encased in agarose. *The embryo on the right was cured in the hub section of the syringe and the agarose fragmented upon ejection. The left embryo was secured using the modified syringe and remained intact upon ejection.*

The barrel method held up better physically, but when submerged in the fluid the opacity and quantity of agarose caused poor visibility of the embryo. This can be seen in Figure 3.9, and when examined under the microscope the image was blurry and unclear. It was hoped that progressing the experiment and utilising the appropriate transferpettor would resolve this problem, as it would allow for a lower volume of agarose to be utilised for the process.

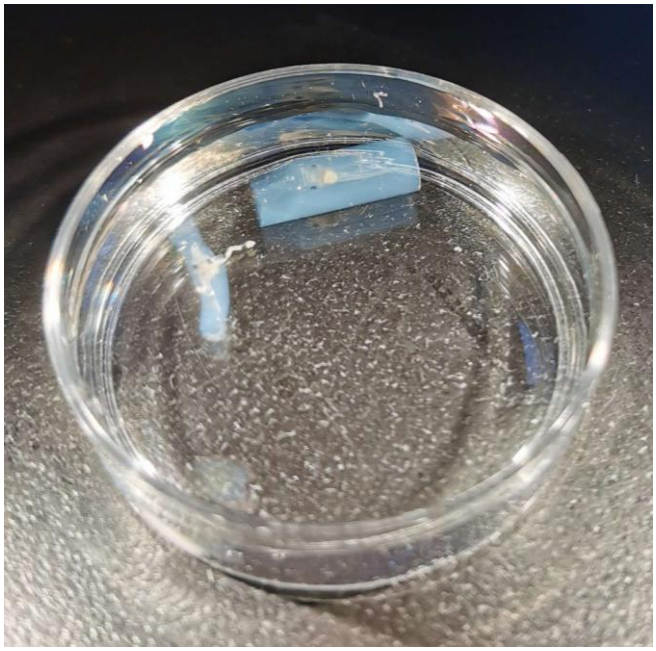

Figure 3.9: Xenopus embryos encased in agarose in MMR solution. *Under the lights, the opacity of the agarose is obvious even without the use of the microscope. Under the microscope a clear image could not be obtained.*

Problems occurred immediately using this method as zebrafish embryos are a tropical species and the temperature of the LMP agarose was around 27°C, matching the growth media temperatures and allowing the LMP agarose to gel rapidly. While *X. laevis* is tolerant to a wide range of temperatures, the highest the embryos would readily tolerate is 25°C and every attempt to use the methodology without adjustments led to immediate death of the embryo involved. *X. tropicalis* was used to see if a more heat-tolerant species would survive. There was much less risk of heat shock as they were maintained at 26°C and when used, the embryos did have a better rate of survival than the *X. laevis*. Unfortunately, the diminutive size of the *X. tropicalis* embryos and the lower levels of embryo production meant that using this species for this purpose was not a suitable option. However, it is worth noting for future work and could be developed further.

With changing the study species not able to be considered in this study, ultra-low gelling temperature agarose (Sigma) was explored as an alternative to the LMP agarose, and the holding temperature reduced to 21°C. The gelling point of this agarose is between 8-17°C. Theoretically, this would have allowed the gel to set and imaging to be conducted at around 15°C. While this did physically work and *X. laevis* embryos survived being encased in the agarose, the practicalities of this method were lacking.

Firstly, the rooms that the research was conducted in were not climate controlled; in the summer when temperatures were reaching over 38°C outside, the lab very often reached above 30°C inside, including the microscope room. Ice was available and attempts could be made to create a "cold box" to store the embryos in while imaging them but attaining and maintaining a consistent temperature would be difficult and fluctuations could potentially affect the data collected.

Secondly, when imaging attempts were made using the available embryos and the successfully utilised method to hold the embryos in place, the physical effect of the gel caused imaging problems. Due to the curve and the refraction of the gel clear images could not be gathered using the camera available; images were distorted and could not be brought clearly into focus, even when using the transferpettor to use as little agarose as possible for securing the embryo. This had not been an issue when this methodology had been used previously as it was done utilising a light sheet microscope and the embryo placed within a media-filled chamber, and the area imaged much smaller and at a much higher magnification than the light microscope used within this study. This issue could potentially be overcome in the future with the utilisation of alternative equipment but was not able to be further explored in this study.

The final problem arising with this method is the temperatures involved. *X. laevis* embryos were maintained at 23°C during incubation, and to reduce the temperature down to around 15°C for imaging would be well within the tolerance levels of the embryos and would not kill them. It is possible that the temperature change could affect the heart rate, potentially leading to inaccurate data collection- which would mean it would have to be carefully controlled throughout the experiment. Time restraints of the study meant this could not be explored further, however literature on the subject does support the idea of increased temperature increasing heart rate (and vice versa) in *Lithobates catesbeianus* (American bullfrog) embryos (Longhini *et al*., 2017).

3.4 Automation

In previous work by Saide (2018), the method of ascertaining heart rate was performed manually after processing the data and generating heart rate graphs in Microsoft Excel. Using this methodology we acquired very clear peaks and very consistent pattens in the beats, suggesting that the heart rate of those embryos was regular (Figure 3.10), and these would be straightforward to count and generate accurate results for.

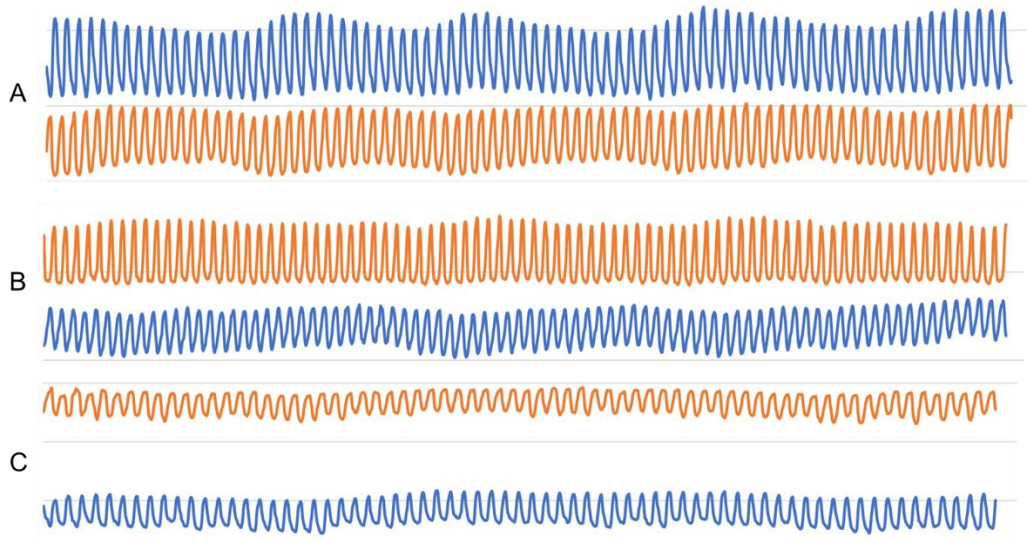

Figure 3.10: Examples of consistent heart rate graphs after processing in Microsoft Excel. *These traces show clearly defined and distinct peaks and troughs, with easy to see beats. All 3 embryos are from media only groups. The orange graphs represent the flow of blood through the ventricle and the blue the atrium.*

Unfortunately, many of the results obtained were not as clear as those shown in Figure 3.10. Often the graphs overlapped, had double peaks or unclear peaks due to the low amplitude of the peaks. Examples of unclear graphs are shown in Figure 3.11. These difficulties make counting peaks manually difficult to begin with, but in conjunction with the increase in throughput needed for the model to be developed to a commercially usable state these would increase the already high amount of time required to process the data and increase the likelihood of errors being made by the person analysing the data. For these reasons it was clear that exploring a method to automate this analysis step and determine heart rate and potentially arrhythmic heart beats was necessary.

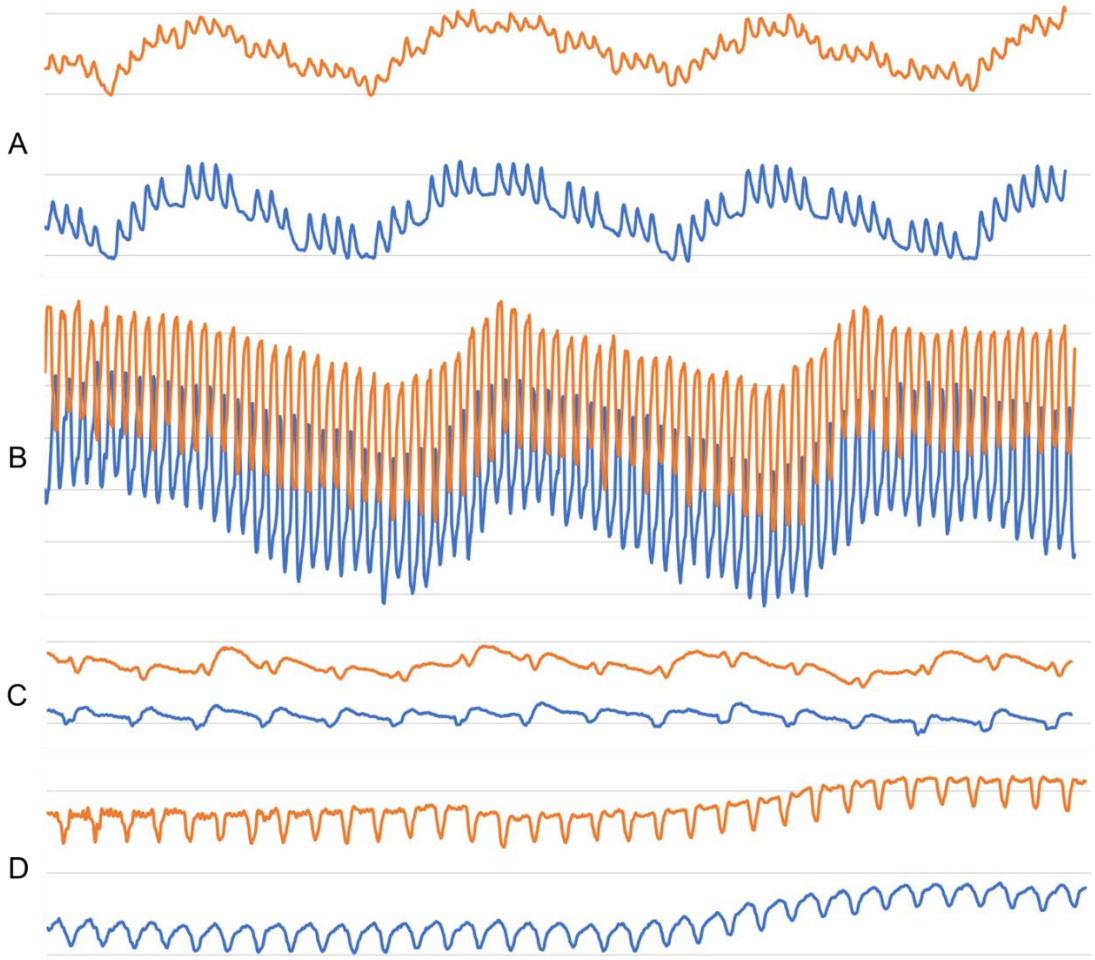

Figure 3.11: Examples of inconsistent heart rate graphs after processing in Microsoft Excel. *These traces illustrate several of the problems seen when manually counting peaks. Embryos A and B were from paracetamol experiments, 3uM and media only groups respectively. Embryos C and D were from terfenadine experiments, 50µM and 20µM respectively. The orange graphs represent the flow of blood through the ventricle and the blue the atrium. A shows irregular peak patterns, B shows the overlap of graphs that could occur, C shows inconsistent and low amplitude peaks and D shows multiple points or extended peaks.*

The problem of how to automate the process posed a unique challenge, as there are multiple software options available that could be utilised for this purpose. The author had previous experience with ImageJ, the software used to generate the heart rate data from the video. This was considered as

a strong option as the open-source nature of the software and freely available plugins created allow for excellent accessibility, and performing data collection and analysis within the same program would provide greater efficiency in the processing of data, allowing quicker and higher throughput.

The author also had previous experience with two programming languages and their respective environments, which could potentially offer greater utility in customising a code. To perform the functions needed for analysis. These languages are MATLAB and R. MATLAB is a proprietary language and development environment, and R is an open-source language with several user interfaces available, with the author being most familiar with RStudio. Both of these languages offer data processing functionality and graphical display options, but the major advantage offered by R was the open-source nature of the language and associated software. This, like ImageJ, means that there are freely available packages and documentation online offering modularity and functionality, and the open-source nature enables reduced barriers to further development. With these considerations in mind, the decision was made to initially trial creating a solution in ImageJ and if this was unsuccessful a move to RStudio would be carried out, with support in coding a program in R being provided by Dr Claudia Buhigas, a bioinformatician within the Wheeler group at the university.

3.4.1 Sine curve fitting in ImageJ

Initially, when considering automation of the heart rate analysis, the shape of the graph appeared to be similar to a sine wave in appearance. With this thought, it was considered if fitting a sine wave to the graph would provide information to allow counting the heartbeat. There would also be potential for additional information such as peak intensity may also be gained. Deviation from the expected sine curve pattern could also be utilised as an indicator of irregularity of heart rate.

As discussed, ImageJ was initially considered as the solution with the best potential for automating the heart rate analysis. Utilising the inbuilt curve fitting tool in the analyse tab of ImageJ, a formula was created in an attempt to map the sine wave. The initial formula used to map this was:

$$y = a * sin(b * x + c) + d$$

In which b would be the period of the sine wave, a is the amplitude, c helps to control the phase shift of the sine wave and d is the vertical shift of the wave. In this case, the number of beats would be determined using the value of b in the following equation:

$$heart\ rate = \frac{b}{2 * \pi}$$

The heart rate corresponds to the number of cycles the sine wave has completed along the x axis, and so to work out the beats per time recorded we designate the x axis as the value of 30 seconds. To convert into beats per minute, this can be simply multiplied by 2. Examples of the sine wave are shown in Figure 3.12.

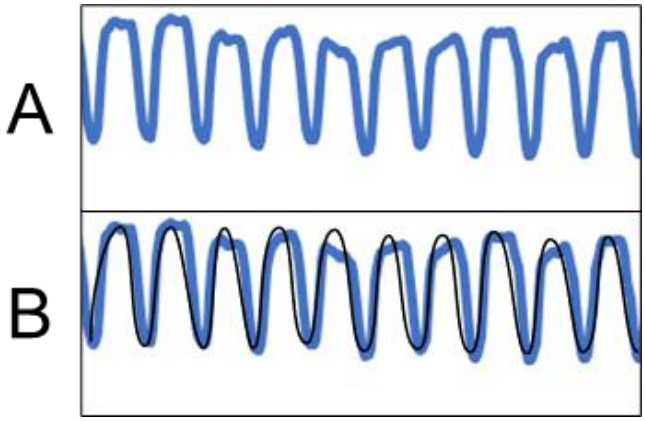

Figure 3.12: A visual example of a heart rate graph with a sine curve. *The graph section as rendered in Microsoft Excel is shown in A, with a sine curve fitted over the graph shown in B. The curve does not perfectly match the graph due to the graph being an imperfect sine curve, which is why a best fit would need to be determined for the analysis.*

This was conducted in the ImageJ software, using the built-in curve fitting tool in the analyse tab of the program. Often it would not immediately map to the datapoints and so manual adjustments to the values would be made until a curve that fit would be landed on by the software. This was incredibly time consuming as a process and the results were subjective, dependant on a “looks like” best fit rather than a true mathematical best fit. This prompted the need for further automation to increase the scale of the experiment and provide groundwork for future development of the assay to a commercial tool.

There were considerations around the possibility to create a macro to automate this process, however it was decided that generating a new code in R studio would be a better method to utilise the data, as although it would be advantageous to utilise a single piece of software from an efficiency perspective, R studio would provide greater flexibility for any future analysis.

3.4.2 Data preparation

How to prepare the raw data for analysis would prove to be a problem that needed overcoming. Initially, the processing of data entirely within ImageJ would negate these concerns as the data would be processed within the software so no further steps would necessarily need to be performed. With the shift to using RStudio however, how the data is treated became relevant.

The raw data is exported from ImageJ into Microsoft Excel, where the calculations are performed to normalise the image intensity and generate the normalised data, as was done previously for the manual counting method. Then, the values for the normalised data for each ventricle and timestamp of the video are exported into a .csv file, one per data point. It would be much more efficient to have multiple data per file but despite effort being made to do this during the study period, the author was unable to successfully make it work.

The data in the .csv files are stored in folders so that the code used to analyse them can select the files needed and pull the data in a straightforward manner.

In order to understand how the data responded to missing data, some of the data gathered was replicated with some values removed from the end of the data table. This would simulate the video ending prematurely and the full 30 seconds not being able to be gathered and allow understanding if the code is able to determine the heart rate based on this reduced data.

3.4.3 Sine curve fitting in RStudio

The full code iterations are included in the Appendices (B, C, D, E respective to each iteration), and sections highlighted in the following text where relevant.

The first iteration of the code used in RStudio focussed on attempting to fit a sine curve to the data. As part of this, the packages ‘nls’ and ‘stats’ were utilised. These allowed for estimation of the parameters of a nonlinear model and provided a range of statistical analysis functions respectively. The code was designed to gather the files with the image intensity data on which are stored as .csv’s in a set folder, it then reads and imports the file data into RStudio, before creating a data frame for the potential parameters of the sine curve equation to be put in. The next step of the code was to set control values for the maximum number of iterations to be tried- this was important as without a maximum number the code could theoretically keep attempting to find a best fit curve indefinitely. As part of this, the minimum step size factor was defined, in this instance as 1/12,000,000. The step size is the increment of change to be trialled between best fit attempts, so a large number was chosen to allow for the minimum incremental changes and maximise the likelihood of finding the best fit for the data. This section of code is shown in Figure 3.13.

```
pp <- expand.grid(b=(10:25), c=(1), A=1, D=1)
nlc <- nls.control(maxiter = 1000,minFactor = 1/12000000)
df<-data.frame()
find_parameters<-lapply(input_datasets,function(x){
  t<-x$seconds
  y<-x$R.C
  for (i in 1:nrow(pp)){
    res<- nls(y ~ A*sin(b*t+c)+D, data=data.frame(t,y),control=nlc, start=list(A=pp$A[i],b=pp$b[i],c=pp$c[i],D=pp$D[i]))
    results<-data.frame(se=sigma(res),coef_A=coef(res)[1],coef_b=coef(res)[2],coef_c=coef(res)[3],coef_D=coef(res)[4])
    df<-rbind(df,results$se,results$coef_A,results$coef_b,results$coef_c,results$coef_D)
    names(df)<-"values"
  }
  df
})
```

Figure 3.13: minFactor function use within iteration 1 of the automation code.

After this, a data frame was made to hold values of the equation that would be contained within the best fit curve. Then, the dataset of intensity values was input, along with the sine curve equation and the process of fitting curves to the data repeatedly, altering parameters each time until a best fit was determined (Figure 3.14).

```
for (i in 1:nrow(pp)){
    res<- nls(y ~ A*sin(b*t+C)+D, data=data.frame(t,y),control=nlc, start=list(A=pp$A[i],b=pp$b[i],c=pp$c[i],D=pp$D[i]))##function to fit the curve
    results<-data.frame(se=sigma(res),coef_A=coef(res)[1],coef_b=coef(res)[2],coef_c=coef(res)[3],coef_D=coef(res)[4])##retrieve the important values
    df<-rbind(df,results$se,results$coef_A,results$coef_b,results$coef_c,results$coef_D)###add these values to a data frame.
    names(df)<-"values"

}
```

Figure 3.14: Looping the parameters to fit a curve until best fit determined.

These results were reconciled into the previously created data frames to create a final results data frame, which was then utilised to generate a value for the number of heart beats using the following equation:

$$number\ of\ heart\ beats = \frac{b}{2 * pi} * time\ in\ secons$$

Wherein b is the period of the sine wave, and 30 seconds is the time used for the recording. This gives the value of number of beats in the 30 second segment used for the analysis, which can then be multiplied by 2 to generate a value of beats per minute. These results could then be analysed further for determination of change in heart rate. There were issues with the code such that when missing data was present, the code failed to function and would not return any values. This needed to be addressed in further attempts. It was thought that instead of using additional programs to analyse the data, it might be possible to introduce a process during the analysis steps to assist with flagging up irregular heart rates, which was introduced in iteration 2.

Iteration 2

The second iteration of the R code functioned mainly as the first, with additional steps included to determine if the heart rate was irregular or regular alongside other changes. These additional changes include adjusting the minFactor to 1/1024 (Figure XXX), as the original minFactor value was deemed unnecessarily small and likely slowed the code's processing speed due to this level of change between curve-fitting attempts. There was also

the introduction of a tryCatch function as part of the nls operation to return 0's if data is missing (Figure 3.15). It was hoped that this would allow the code to still function and a curve to be fitted to the data despite missing values, which tests had shown the initial code could not handle.

```
q<-lapply(input_datasets,function(x){
  t<-x$seconds
  y<-x$R.C
  for (i in 1:nrow(pp)){
    res<- tryCatch(nls(y ~ A*sin(omega*t+phi)+C, data=data.frame(t,y),control=nlc, start=list(A=pp$A[i],omega=pp$omega[i],phi=pp$phi[i],C=pp$C[i])),
                   error=function(e){return(0)})
    if (class(res)!="numeric") {
      results<-data.frame(se=sigma(res),coef_A=coef(res)[1],coef_ome=coef(res)[2],coef_phi=coef(res)[3],coef_C=coef(res)[4])
      df<-rbind(df,results$se,results$coef_A,results$coef_ome,results$coef_phi,results$coef_C)
      names(results)<-"values"
```

Figure 3.15: Utilisation of the tryCatch function in iteration 2 of the automation code.

The final major change made for this version of the code was the addition of a mutate function (Figure 3.16). The aim of this piece of code was to introduce a method of analysing the regularity of the embryo heartbeat, and to flag embryos that had an irregular heartbeat and indicate these were displaying signs of arrythmia. The preliminary heart rate results so far were showing a wide range of heart rates, from very low (<10 bpm) to very high (>150bpm). At the outset of the project, there were several uncertainties as to what a normal heart rate for an NF stage 45 embryo is, as *Xenopus* heart rate studies are sparse and produce varied results. Hou and Burggren (1995) anesthetised *Xenopus* embryos using MS-222 and measured heart rates in embryos between NF stages 41 and 66, finding heart rates ranging between 85bpm and 117bpm, with heart rates higher in younger embryos and lower in older. NF stage 45 embryo heart rates were approximately 105bpm in this paper, but work done by Boppart et al., (1997) determined that NF stage 47+ *Xenopus* embryos had a heart rate of around 128bpm; which contradicts the other findings. Other work done measuring heart rates in *Xenopus* are restricted to measuring adult heart rates, but appear more consistent as Taylor and Ihmied, (1995) and Bartlett et al., (2010) measured heart rates of 35 and 37bpm respectively.

With this range in mind, the decision was made to utilise a semi-arbitrary number to utilise as the 'cut-off' point at which embryo heart rates progressed from regular to irregular. Although not necessarily physiologically accurate, the choice of 80bpm was made as this was consistently with the range of data gathered, ensuring that some results would be returned as irregular if the code was working. This meant that the code could be tested and understood to work, and as more results were generated the number cut-off could be altered to more accurately indicate when arrythmia was present. Realistically, the results were likely to show a range of heart rates that fall into the normal condition as arrythmia could present as increased or reduced heart rates, and the code could be altered to reflect this.

```
df2<-data.frame()
for (i in q){
  df2<-rbind(df2,dim(i))
  names(df2)<-c("number.values","sample")
}
df2 <- df2 %>%
  mutate(Heartbeat = if_else(number.values==80, "Regular pattern", "Irregular pattern"))
```

Figure 3.16: Use of the mutate function in iteration 2 of the automation code.

This code seemed to handle some of the issues raised with the first iteration, but in the attempt of creating an irregular/regular flag on the data the value of 80 was chosen. If any heart rate other than 80 beats was returned it would flag as irregular using the code, which may be very inaccurate. Realistically, a study would need to be performed to determine what the normal heart rate of an NF stage 45 *Xenopus* embryo is as this was not documented in the literature. It would also be likely that a range of heart rates would fall into a normal pattern, so the code would have to be edited to include this as an option.

Another problem that became clear when analysing using this method was the secondary sine curves that were present in the data (see Figure 3.17).

These secondary waves were sometimes selected by the code instead of the primary curve as the code managed to fit a sine wave more closely to this pattern than the primary curve. This was problematic as while a human could look at the graph and clearly see the correct choice, it was uncertain how to make the code perform the same selective process. The cause of this secondary curve is unknown, it was not present in every dataset, and controlling the image recording for brightness and lighting change did not appear to make a difference to the occurrence of this phenomenon.

Work did not progress on this version as the decision was made, following extensive discussion, to explore Fourier transformations as a means of data analysis instead of fitting a sine curve to the data.

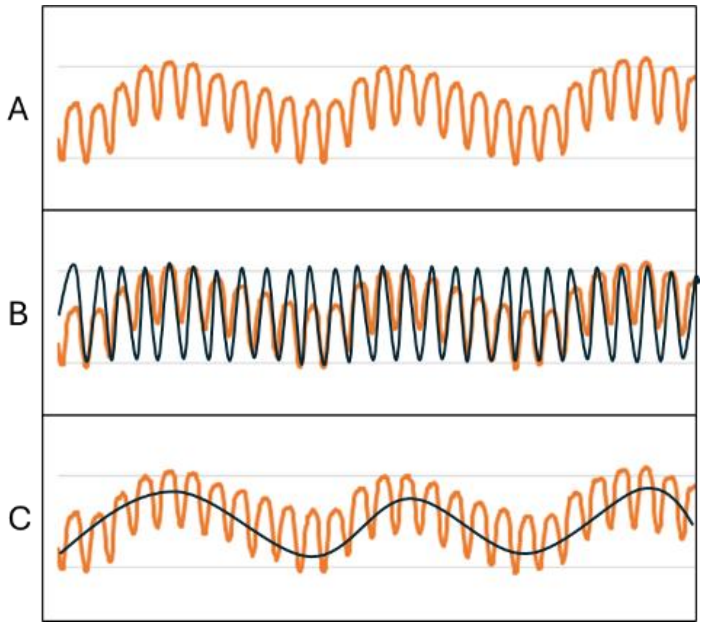

Figure 3.17: An example of a data set with a secondary sine curve. *This secondary sine curve caused the initial sine-curve fitting program to process the results incorrectly. A- Dataset as visualised graphically in Microsoft Excel. B- The anticipated sine curve fitting, following the graphical line shown in A. C- The actual sine curve pattern fitted, following the secondary sine wave within the data.*

3.4.4 Initial Results

As data was being gathered experimentally it was utilised for testing the automation as it was developed. As the focus was on sine curve fitting, analyses were performed and are presented here in Figure 3.18 and Figure 3.19 as initial data. These results showed great promise for the assay, having produced statistically significant results in the doxorubicin analysis and a strong trend in the terfenadine analysis- statistical significance was not able to be determined as only two repeats had been performed at the point the methodology was changed to Fourier transform analysis. These results are likely to be less accurate due to the issues presented with the sine curve method but are included to provide context for the work presented in this chapter.

Initial doxorubicin results are presented in Figure 3.18, with concentrations of 20, 90 and 100μM showing statistically significant differences to the control, with P values of 0.05, 0.005 and 0.005 respectively.

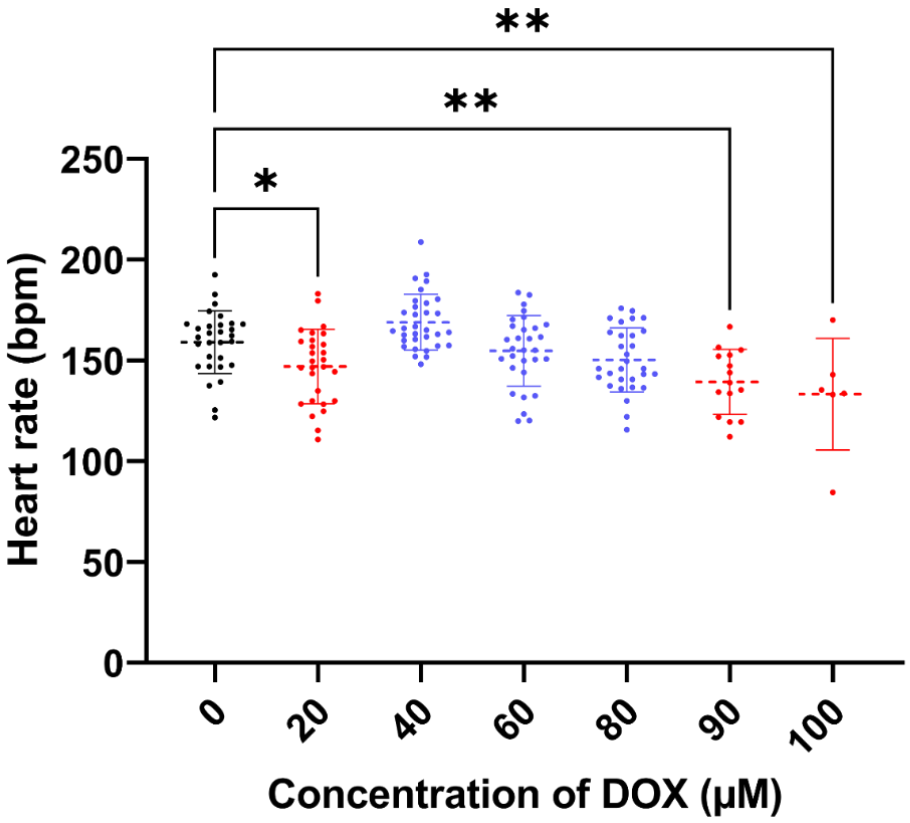

Figure 3.18: Heart rate of Xenopus embryos exposed to doxorubicin. *Xenopus embryos had been treated between NF stages 38 and 45 with doxorubicin and kept at 23°C, then heart rate measured after 15-minute treatment with MS-222 by determining number of times the heart beat for 30 seconds and adjusted into beats per minute. Average atrial heart rate ± SD of treated embryos was compared to untreated embryos (0μM) using one way ANOVA with Dunnett comparisons (*= p<0.05, **= p<0.005). 3 Biological repeats were performed with a total number of embryos measured for each concentration varying between 6 and 30.*

Initial terfenadine results (Figure 3.19) showed a strong trend toward reduction in heart rate at concentration of 10μM and above. However, the methodology of analysis changed from being analysed by sine curve fitting to Fourier transform after the second biological repeat was carried out before the third biological repeat was performed so statistics were unable to be performed at this point, but the trend indicated a strong reduction in heart rate as the concentration of terfenadine increased.

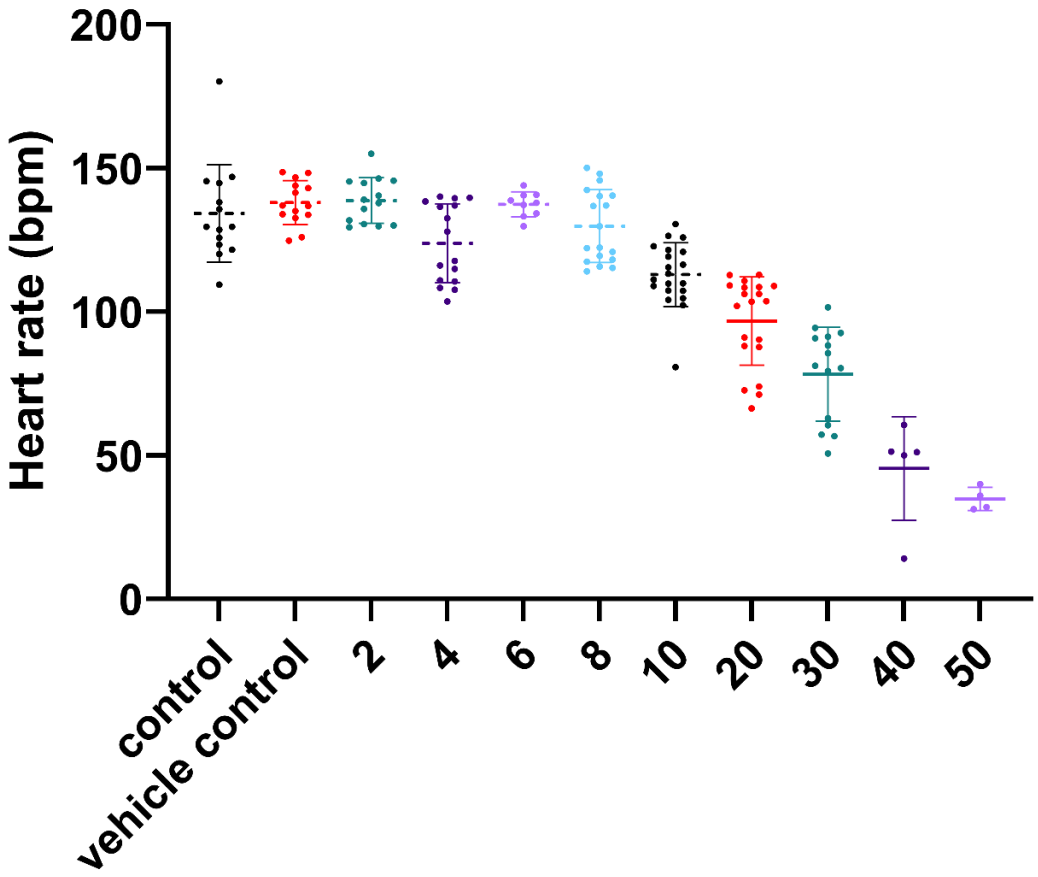

Figure 3.19: Heart rate of Xenopus embryos exposed to terfenadine. *Xenopus embryos had been treated between NF stages 38 and 45 with terfenadine and kept at 23°C, then heart rate measured after 15-minute treatment with MS-222 by determining number of times the heart beat for 30 seconds and adjusted into beats per minute. Average ventricular heart rate ± SD of treated embryos. 2 Biological repeats were performed with a total number of embryos measured for each concentration varying between 4 and 20.*

Both of these results showed very positive results, suggesting the assay was going to be beneficial and work as anticipated. It should be noted though, and this issue is continued throughout this research project, that at the highest concentrations of both drugs surveyed thus far, the number of living embryos able to be recorded and have data gathered from is much lower than those in the control groups. This is due to the high levels of toxicity

leading to increased embryo death, as was noted with the survival curves in Figures 3.2 and 3.3.

3.4.5 Fourier Transformation in RStudio

A Fourier transformation is a mathematical function that determines the base frequencies that make up a wave. As already discussed, many of the heart rate graphs had secondary sine curves within them and utilising a Fourier transform would take this into account and still allow determination of the overall heart rate. The code did this by taking the multiple signals displayed within a dataset and breaking them down into the component frequencies. By then analysing how often these frequencies occur during the dataset it was possible to determine which was the most commonly occurring frequency, which will then be used to determine the heart rate for that specific embryo.

Iteration 3

Iteration 3 of the R code was the first attempt to analyse the data by Fourier transformation. This was able to be performed again through Dr Buhigas' assistance with the R code and through discussions with Dr Timothy Grocott about Fourier transformations. The packages 'dplyr' (Wickham et al., 2025) , 'ggplot2' (Wickham et al., 2016) and 'stringr' (Wickham, 2023) were utilised in this method. These are packages designed to facilitate data frame manipulation, data visualisation, and string manipulation respectively. Data processing up until being analysed using the code was maintained as previously stated.

The first stages of the processing was conserved from the sine wave analysis, locating extracting the data from the .csv files and importing into RStudio. Then the dataset length is noted (ie. How many observations were taken), and the Fourier transform is applied to the data. Following this, a data frame was created with all the frequencies found in the sample and the mod function was used extensively to generate a plot of frequency components,

list all frequencies and determine variance of the frequencies (Figure 3.20). The mod function itself calculates the modulus of a complex number (the distance of the point on the complex plane of the complex number from the origin).

```
mod<-data.frame(values=Mod(fft_out[2 : (N/2 + 1)]))
barplot(Mod(fft_out[2 : (N/2 + 1)]))
mod$index<-as.numeric(rownames(mod))
mod$variance<-as.numeric(var(mod$values))
```

Figure 3.20: Use of the mod function in iteration 3 of the automation code.

Following this, the mod function is utilised again to determine which frequencies are the ones of most interest to the research (Figure 3.21). This was done by selecting frequencies with amplitudes higher than 0.1, as anything below this would be a weak signal and unlikely to be the one that corresponds to the peaks that indicate the blood filling the chamber. Then, the frequencies are classified into three groups; less than 25, between 25 and 85, and greater than 85. These numbers will eventually correspond to heart rates, and as with the choice of the number 80 to determine irregular or regular heart rate in iteration 2, these values could be adjusted when work had progressed further and determining the 'normality' of a heart rate, but for developing the code these values would be sufficient. One of these groups will contain the data needed to determine the number of heart beats, and we initially anticipated this would most often return as group 2 as many of the embryos analysed so far had heart rates that fell within these values. The data frame so far contained the highest amplitude, frequency, variance and group number, but a further column was added to indicate the weight of each group. This would allow for determining which was the most likely to contain the heart rate frequency, which was then chosen. The results were published listing the heart rate value, amplitude and variance.

```
 mod.selected<-mod[which(mod$values>=0.1),]
mod.selected<-mod.selected %>% mutate(Group =case_when(
  index < 25 ~ "1",
  index >= 25 & index <85 ~ "2",
  index >=85 & index <=750 ~ "3"))
df<-mod.selected %>%
  group_by(Group) %>%
  slice(which.max(values))
df$contribution<-df$values*100/sum(df$values)
df$frequency<-NA
df$frequency[df$values[2] <=1 & df$values[3]<=1 & df$Group =="1"] <- "Freq1"
df$frequency[df$values[2] <=1 & df$values[3]>=1 & df$Group =="3"] <- "Freq3"
df$frequency[df$values >=1 & df$contribution[3]>=40 & df$Group =="3"] <- "Freq3"
df$frequency[df$values >=1 & df$contribution[3]<=40 & df$Group =="2"] <- "Freq2"
df<-as.data.frame(df[complete.cases(df),])
```

Figure 3.21: Further utilisation of the mod function in iteration 3 to determine heart rate.

This code appeared to work well and provided results that appeared more accurate and truer to the manual count when compared to previous efforts on difficult samples. The largest issue found with this code was the code failed when data was missing as there was a lack of how to handle missing data in this initial attempt. This is particularly important as one failure caused the code to fail entirely for the whole group dataset, and processing the data one sample at a time was not the efficient analysis process being sought.

Iteration 4

Iteration 4, and the final code used for analysis in this project, was formed from the addition of a null data filter to remove missing data and prevent the code failing because of this. This was added as the datasets were imported to avoid problems in the analysis process as early as possible and can be seen in Figure 3.22.

```
input_datasets<-lapply(datasets, read.csv, header=TRUE, stringsAsFactors=FALSE)
a<-input_datasets[!is.na(as.numeric(input_datasets$x1)), ]
names<-list.files(path = "C:/Users/saswy/Desktop/R_Data/current data", pattern ="*csv",
                  full.names = FALSE)
names<-data.frame(names)
names(input_datasets)<-names$names
```

Figure 3.22: The null data filter utilised in iteration 4 of the automation code.

This produced data that was suitable for further analysis, giving both atrial and ventricular heart rates along with amplitude of signal (Figure 3.23). It was hoped, and some work was trialled in a very preliminary methodology, that further development could be undertaken to perform these additional analyses within R, but a lack of time prohibited this from being explored to its full potential and so remains as something to be explored in future work. Another potential area of exploration and development is the signal amplitude values produced by this method. It may be possible to utilise this as a representation of how hard the heart is pumping or as a representation of ejection fraction, but this again is something that could not be explored in this project.

	A	B	C	D	E	F	G	H	I
1		samples	atrial_heart beats	atrial_amplitude	atrial_variance	ventricular_ heartbeats	ventricular_ amplitude	ventricular_ variance	condition
2	1	0-1.csv	61	9.070489486	0.464281712	61	6.762004139	0.51832972	0-
3	2	0-10.csv	71	3.776726407	0.098817203	71	12.4277983	0.74072163	0-
4	3	0-2.csv	60	14.28323679	0.61982363	60	6.238564449	0.19805666	0-
5	4	0-4.csv	69	4.632685555	0.631000759	69	14.03584336	0.89768358	0-
6	5	0-5.csv	62	1.278575568	0.49475373	62	1.138019885	0.50678693	0-
7	6	0-6.csv	72	2.983812025	0.644957658	72	5.928706762	0.53798049	0-
8	7	0-7.csv	71	2.331182705	0.604940562	71	2.710915518	0.58146131	0-
9	8	0-8.csv	68	11.23376809	0.408879797	68	12.64020295	0.86537173	0-
10	9	0-9.csv	72	9.894299455	0.310454303	72	24.53863866	1.43258965	0-
11	10	20-1.csv	73	10.35846656	0.378922711	73	11.54758457	0.84159785	20-
12	11	20-10.csv	83	3.53803572	0.843914393	83	5.541042396	0.77007778	20-
13	12	20-2.csv	68	4.129529027	0.823361358	68	23.13723515	1.74887553	20-
14	13	20-3.csv	68	6.984158198	0.664264898	68	10.13692627	0.8021046	20-
15	14	20-4.csv	73	4.654283803	0.327627807	73	13.58645806	1.20864108	20-
16	15	20-5.csv	77	1.582924026	0.336865905	77	9.690279442	0.51720181	20-

Figure 3.23: Example of results from heart beat analysis. *Extract from the results file that the final iteration of the code generate. The file contains the original file name the data was pulled from, the heart rate, amplitude and variance for both atrium and ventricle as well as a condition column indicating what concentration of drug the embryo was exposed to.*

A summary of each iteration's process methodology is shown in Figure 3.24, with the additions or alterations of steps being highlighted as the code changed between iterations.

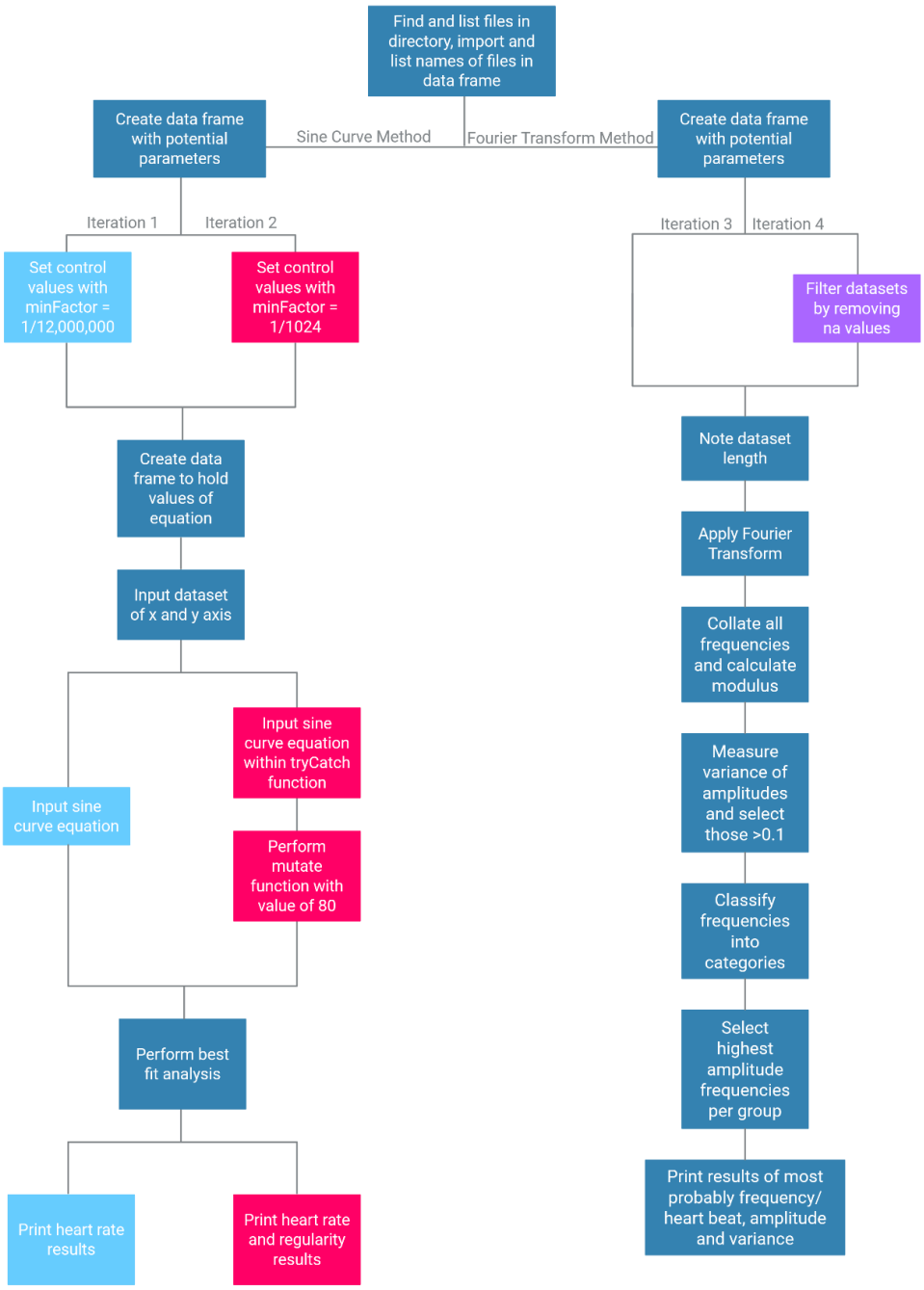

Figure 3.24: An overview of the different iterations of code used to automate the heart rate analysis. *Iterations 1 and 2 utilise the method of fitting a sine curve to the data and iterations 3 and 4 utilise the Fourier transform method. Common steps in the process between the two iterations sharing a method are in dark blue, with unique stages being highlighted in light blue (iteration 1), pink (iteration 2) or purple (iteration 4).*

3.5 Arrythmia determination

As work on the code progressed for automation of determining heart rate, one of the features sought to be included in the automation process was the detection of arrhythmias. To ensure accuracy of the automation process, the arrythmias must be determined in another manner to allow for comparison. The most straightforward way to performing this task was manually, through assessing the heart rate graphs that were produced in Microsoft Excel based on the presence and level of arrhythmia indicated in each graph.

In order to minimise the potential for bias, and to enable comparison between individuals with various levels of experience, the assessment of each graph was done on a blind basis, with dose identifier removed from each graph and provided in a randomised manner to the 3 scorers- one of whom was the author, one of whom was the authors PI and one of whom was a scientist without the specific knowledge of heart rates and arrhythmias to act as a ‘control’, with the average score being the mean of the 3. Each assessor was provided with a primer (Figure 3.25) showing examples of what would constitute no arrhythmia, mild, medium and strong arrhythmia and asked to numerically score each graph on this basis (with scores of 0, 1, 2, and 3 respectively). The intention for this analysis was to understand how subjective an arrhythmia diagnosis would be based on manual assessment of the graph.

Figure 3.25: Arrhythmia assessment primer. *This was provided to the arrythmia assessors show examples and give guidance of what would constitute a non-arrhythmic heart beat and what mild, moderate and severe arrhythmia would appear like for them to be graded with the number 0, 1, 2 or 3 respectively.*

This analysis could only be fully completed after the experimental data had been completed, and due to time constraints only the datasets for doxorubicin, terfenadine and paracetamol were able to be assessed in this manner, with the results from each compound being included in the relevant sections of this report. Finalising these results also provided the opportunity to determine the consistency between assessors, and therefore how subjective this method of manual assessment is.

Overall, there was a 40.9% complete agreement (all 3 assessors provided the same score) for the arrythmia grade given to data, with individual drugs having 60.7% (doxorubicin), 28.8% (terfenadine), and 37% (paracetamol) complete agreement. The lower levels of agreement seen in the terfenadine and paracetamol datasets are indicative of subjectivity in the assessment, as it meant each assessor determined a different severity of arrythmia was indicated- despite the primer which was created in an attempt to avoid this.

Another factor that was examined was if the 'control' assessor reached agreement with the assessors who had more experience with the project and arrythmias generally. The overall rate of control disagreement was 17.8%, with individual drugs having 16.9% (doxorubicin), 18.1% (terfenadine), and 18.5% (paracetamol) disagreement. This appears to be a low level of disagreement, and is consistent between each drug, so this could indicate that anyone performing this assessment in future work would benefit from having some experience in the topic beforehand, or a better primer and training system could be introduced to provide this. It seems likely that if these were in place the disagreement here could be reduced even further.

Also noted was the level of complete disagreement between the assessors, where all 3 produced a differing grade for datasets. The overall rate of complete disagreement was 9.5%, with individual drugs having 5.6% (doxorubicin), 13.2% (terfenadine), and 8.2% (paracetamol) disagreement.

These values are low, which indicates that although the visual assessment likely suffers from subjectivity, this is not enough to seriously compromise the results. The higher rates seen in terfenadine and paracetamol match the pattern seen with the reduced rates of complete agreement also seen with these two drugs. These results are summarised in Tables 3.2 and 3.3.

	Doxorubicin	Terfenadine	Paracetamol	Overall
Complete agreement	60.7	28.8	37	40.9
Complete Disagreement	5.6	13.2	8.2	9.5

Table 3.2: General analysis of how in agreement the three arrhythmia assessors were. *Complete agreement indicates all 3 assessors were in agreement, complete disagreement indicates all 3 assessors chose different values for arrythmia severity. Values are percentages.*

	Doxorubicin	Terfenadine	Paracetamol	Overall
Control Disagreement	16.9	18.1	18.5	17.8

Table 3.3: Analysis of control assessors' decisions. *Table indicates when both experienced assessors agreed on a value for arrythmia, but the non-expert assessor disagreed for a sample. Values are percentages.*

As there was disagreement between assessors on the levels of arrythmia, one further analysis was performed, which was to determine the agreement between assessors on a yes/no basis of if arrythmia is present or not, regardless of severity. This produced an overall agreement of 58.2%, with doxorubicin, terfenadine and paracetamol having a 66.3%, 55.6% and 52.7% agreement respectively (Table 3.4). This is a small increase for doxorubicin compared to the value of complete agreement, and a large increase for terfenadine and paracetamol. This higher rate of agreement suggests that

determining if arrythmia was present or not was clearer than determining the level of arrythmia present, and the assessors were more able to agree with each other for this.

	Doxorubicin	Terfenadine	Paracetamol	Overall
Yes/No agreement	66.3	55.6	52.7	58.2

Table 3.4: Yes/no arrythmia presence/absence analysis. *Table shows how well the three arrythmia assessors agreed when reduced to a simple yes/no analysis for presence of arrythmia. Values are percentages.*

3.6 Discussion

The assay developed so far was effective and greatly improved on the method previously utilised in Saide, (2018).

Post-experimental analysis of the vehicle control used in the project indicates that the presence of DMSO at low concentrations does not significantly affect embryo heart rate, and therefore does not impact the conclusions able to be drawn from the work, however if this is utilised in the future to better control for the DMSO it may be advisable to modulate every drug concentrations' amount of DMSO to make all doses 0.5% rather than simply the highest dose and vehicle control. This would at least ensure that any effects caused by DMSO should theoretically be maintained consistently.

As discussed earlier in the chapter, the exposure time across several developmental stages of the embryo and multiple days classifies this assay as having a mid-range exposure time, too long for acute exposure but not long enough to replicate traditional chronic exposure methods, which are typically weeks or months in duration. Chronic exposure is something that this method does not lend itself to, due to the limited amount of time spent in

the embryonic form meaning the experiment would require greater levels of ethical approval and additional complexity. This method will likely be easy to apply to measure results of an acute exposure of 1-2 hours when the embryos are NF stage 45, and an initial exploration into this was briefly performed during the period of study but no results were able to be generated due to time constraints. Future work exploring this adjustment would benefit from exploring this avenue and comparing the embryo response from the current method and the acute exposure.

Further work would also be ideal in developing a method to restrain embryos for imaging without needing to use anaesthesia. Immobilisation through agarose has worked well previously in zebrafish embryos but due to the temperature requirements of *Xenopus* along with the temperature restrictions this could not be replicated for this project. Due to the inability to measure heart rate without anaesthesia in this project, and the lack of clearly defined heart rate data in the literature involving NF stage 45 *Xenopus laevis* embryos it is impossible to confidently state if anaesthesia at the concentration utilised affected the heart rate in comparison. This is unfortunate, however mitigating the effect seen in previous work of higher anaesthesia concentrations by utilising the lowest possible concentration sufficient to immobilise the embryo was employed in this assay. Another factor to consider is the potential effects that anaesthesia could have on drug response in embryos; as although the anaesthesia is only applied at the very end of the exposure period immediately before imaging there is potential for drug interactions to occur or for anaesthetised embryos to absorb a lower amount of the drug than intended. This would be compounded if a shorter exposure time for more acute exposure were to be trialled, and is another large advantage of developing a method for measuring heart rate without the anaesthesia.

The imaging of the embryo to determine heart rate could be improved following investment in the method, as the work done in this study was

restricted to utilising the imaging equipment and software available. There are several commercial applications utilised in zebrafish research that are designed to measure cardiac function (De Luca et al., 2014; Sala et al., 2018; Santoso et al., 2020) including heart rate and may be modified for use with *Xenopus* if appropriate attention is given to making it work. A pre-existing system already validated for zebrafish may also resolve the issues identified with the use of anaesthesia, as the system videos the zebrafish without requiring the use of an anaesthetic agent.

The creation of an analysis protocol that partially automated the heart rate determination is of particular importance, as manually counting the heart rates for a piece of work this size would have been wildly impractical, and likely would have limited the amount of data able to be obtained. The automation process has scope for improvement, as there is still a significant amount of pre-processing that must be done to the data before importing it into RStudio, and the results generated using this assay could provide further indications of cardiotoxicity beyond heart rate and regularity if developed further. One potential expansion of this system is the assessment of ejection fraction- how much blood is pumped out of a heart chamber (usually ventricle) with each contraction. A reduction in left ventricular ejection fraction (LVEF) is used in human medicine to indicate cardiac damage and failure (Garg et al., 2021), and potential recapitulation of this in *Xenopus* would strengthen the model's usefulness for assessing drug-induced cardiotoxicity.

Finally, the assessment of arrythmia was suitable to produce the preliminary results included in Chapter 4, but further development must be undertaken if this assay was to be developed further, especially if seeking to utilise it at a commercial scale. As it stands, the assessment of arrythmia is very time consuming for the manual method, and the lack of effective objective analysis prevents the implementation of an automated methodology due to not being able to ensure accuracy of the code's results.

Multiple times through this chapter, references have been made to the absence of clear understanding of what a normal heart rate is in NF stage 45 *Xenopus* embryos. Using the data gathered in the course of conducting this study, the author has able to produce a value for this, which will hopefully provide beneficial for any future research performed on this model. This is expanded upon in Chapter 4.

3.7 Biomarker Assay

Biomarkers are used in determining if toxicity or damage has occurred to a particular organ. One of the most well-known of these is seen in hospitals, when a patient presents with a suspected cardiac event like myocardial infarction (heart attack). In this situation, the patients' blood is tested for a protein called cardiac troponin (Tc). Tc is present in heart tissue and is released into the bloodstream when cardiac damage occurs, such as in a heart attack event. The presence of Tc in the bloodstream therefore acts as a strong indicator that cardiac damage has occurred and enables quick and effective treatment.

One aim of this project was to determine if cardiotoxicity could be ascertained through use of biomarkers found in the bloodstream of the *Xenopus* embryo. To facilitate this, understanding of the different kinds of cardiotoxicity and what molecules could be used to detect each is imperative. It was decided to focus on miRNA biomarkers as these are an understudied area with great potential and their use in determining hepatotoxicity in *X. laevis* having been documented previously in the Wheeler lab, and results can be found in Saide *et al*., (2019).

Multiple reviews over the past decade have highlighted several potential miRNA targets that could be developed into cardiotoxicity biomarkers; see

table located in Appendix E. A summary of these findings is included in Figure 3.26.

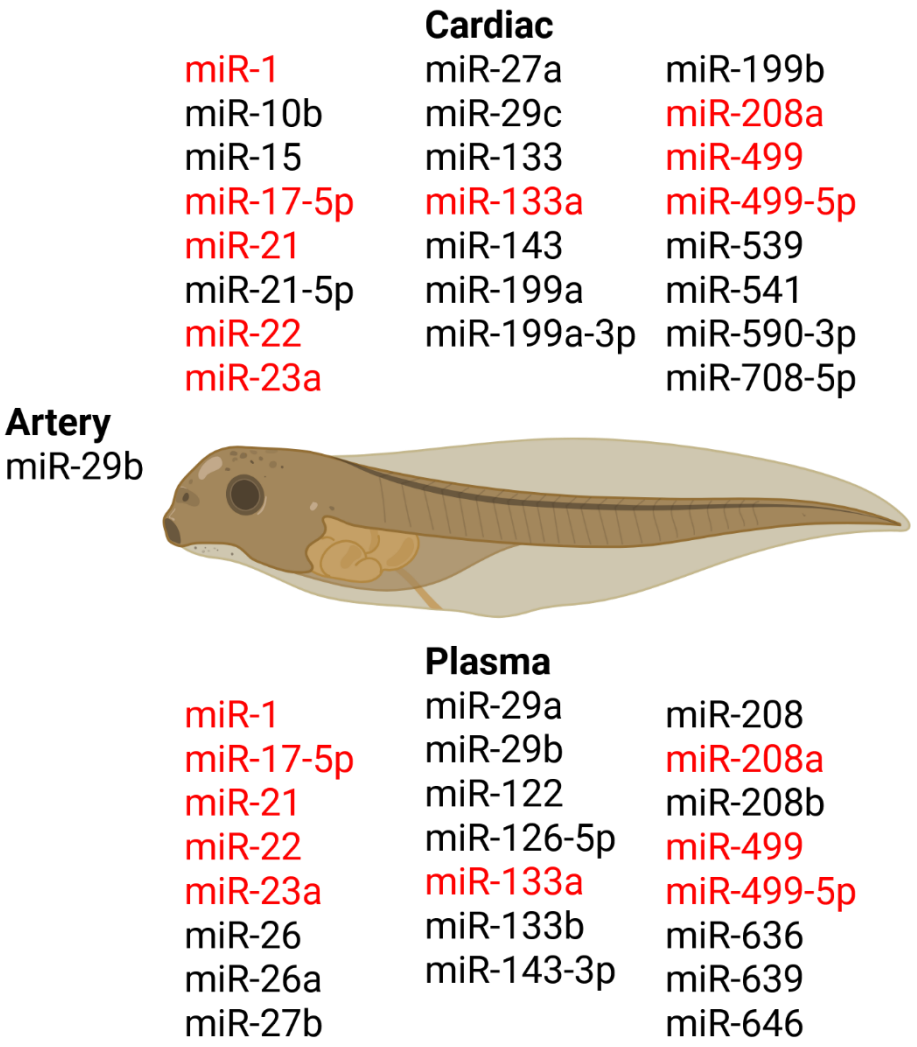

Figure 3.26: A summary of potential miRNA biomarkers of cardiotoxicity and tissues they have been identified in. *miRNAs shown in red have been identified as being affected by cardiac injury or disorder across multiple tissues. The full list of miRNAs along with the references is found in Appendix E.*

Additionally, Table 3.5 contains overlapping and further potential miRNAs that could be studied, that have been specifically noted as occurring due to doxorubicin exposure in the literature.

It should be noted that some miRNAs feature multiple times in the table, often with conflicting results- for example miR-208a was found to be upregulated both in the bloodstream and in the myocardium in work done by Wang *et al*. (2010), but Nishimura *et al*. (2015) noted a downregulation of miR-208a in the myocardium. Novak *et al.* (2017) indicated a downregulation of miR-208a in the heart ventricle, while Tong *et al*. (2015) noted an upregulation in the mouse heart following doxorubicin cancer treatment. These results are somewhat contradictory- for instance, miR-22 was noted as being both down- and up-regulated in cardiac tissue following a diagnosis of hypertrophy in different studies (Colpaert and Calore, 2019; Huang *et al*., 2013; Tu *et al*., 2013; Xu *et al*., 2012), and miR-29a was noted to be up-regulated in plasma following HCM (Colpaert and Calore, 2019; Derda *et al*., 2015; Roncarati *et al*., 2014) and down-regulated in plasma following radiotherapy (Dong *et al*., 2009; Pellegrini *et al*., 2020).

miRNA	Regulation	Tissue	Organism	Reference
miR-1	Up	Plasma	Rat	(Nishimura *et al*., 2015; Tony *et al*., 2015)
	Up	Plasma	Human	(Leger *et al*., 2017; Rigaud *et al*., 2017)
miR-21	Up	Heart	Mouse	(Desai *et al*., 2014)
	Up	Heart (myocardium)	Mouse	(Tong *et al*., 2015)
	Up	Cardiomyocytes	Rat- cell culture	(Tang *et al*., 2009)
miR-29b	Down	Myocardium, cardiomyocytes	Rat- cell culture	(Spallarossa *et al*., 2006)
	Up	Plasma	Human	(Leger *et al*., 2017)
miR-30a	Down	Heart	Rat	(Lai *et al*., 2017)
miR-30c	Down	Heart	Rat	(Lai *et al*., 2017)
miR-30e	Down	Heart	Rat	(Lai *et al*., 2017)
miR-31-5p	Up	Cardiomyocytes	Rat- cell culture	(Ji *et al*., 2020)
miR-34a	Up	CPCs, fibroblasts, RAOEC	Rat- cell culture	(Piegari *et al*., 2016)
	Up	Total cardiac tissue	mouse	(Desai *et al*., 2014)
miR-34a-5p	Up	Cardiomyocytes	Human- cell culture	(Holmgren *et al*., 2016)
miR-34b-5p	Up	Cardiomyocytes	Human- cell culture	(Holmgren *et al*., 2016)
miR-34c	Up	Total cardiac tissue	Rat	(Vacchi-Suzzi *et al*., 2012)
miR-34a-5p	Up	Myocardium	Rats	(Zhu *et al*., 2017)
	up	Cardiomyocytes	Rats- cell culture	(Zhu *et al*., 2017)
	up	Plasma	Human, rats	(Zhu *et al*., 2017)
miR-130b-3p	Up	Cardiomyocytes	Human- cell culture	(Holmgren *et al*., 2016)
miR-133a	Up	Plasma	rat	(Nishimura *et al*., 2015)
miR-133b	Up	Plasma	rat	(Nishimura *et al*., 2015)
miR-146a	Up	Cardiac myocytes	Rat- cell culture	(Horie *et al*., 2010)
miR-187-3p	up	Cardiomyocytes	Human-cell culture	(Holmgren *et al*., 2016)
miR-199a-	Down	Cardiomyocytes	Human-cell	(Holmgren *et al*.,

5p			culture	2016)
miR-199b-3p	Down	Cardiomyocytes	Human-cell culture	(Holmgren *et al*., 2016)
miR-206	Up	Plasma	Rat	(Nishimura *et al*., 2015)
miR-208a	Up	Total heart tissue	Mouse	(Tong *et al*., 2015)
miR-208b	Up	Total cardiac tissue	Rat	(Vacchi-Suzzi *et al*., 2012)
miR-208b-3p	Up	Total heart tissue	Mouse	(Desai *et al*., 2014)
miR-499	Up	Plasma	Human	(Leger *et al*., 2017)

Table 3.5: miRNAs associated with up- or down-regulation due to doxorubicin exposure.

3.7.1 miRNA selection

A thorough review of existing literature was conducted to determine suitable miRNAs to be used as both housekeeping and cardiotoxicity biomarkers; with the results of the review being summarised in Appendix A and Table 4.1.

miRNAs noted as potential options for this study were included based on multiple criteria. miRNAs were typically found through literature that was specifically researching cardiac damage or cardiac disease, but not necessarily drug-induced cardiotoxicity. This includes conditions such as myocardial infarction (MI), coronary artery disease (CAD), hypertrophic cardiomyopathy (HCM), dilated cardiomyopathy (DCM), arrhythmogenic cardiomyopathy (ACM), chronic heart failure, hypertrophy, atherosclerosis; as well as damage caused by drugs or chemicals as well as physical damage caused by ionising radiation. The reason for including such a wide variety of conditions rather than focussing only on drug-induced cardiotoxicity was to examine as many potential biomarker miRNAs as possible.

Alongside selections of biomarker miRNAs, decisions had to be made to select a housekeeping biomarker. This is typically a gene or protein that is ideally ubiquitous throughout the samples being taken and expressed at stable levels regardless of the treatment being applied. For the purposes of this study potential miRNA biomarkers were explored alongside others.

3.7.2 Housekeeping Candidates

Multiple options were presented that could be used for housekeeping purposes- which is to provide a stable expression level from which any changes of expression of the toxicity biomarkers can be determined. Some of the most promising candidates are detailed here:

U6 RNA is a small, non-coding RNA molecule that is ubiquitously expressed in the nucleus of cells and is exceptionally conserved across species. This small molecule has been recognised and utilised as a control protein for qRT-PCR in multiple studies (Bonev and Papalopulu, 2012; Causin *et al*., 2019), particularly with qRT-PCR involving miRNAs. There has been research suggesting that U6 may not be the most consistent or suitable housekeeping option (Link *et al*., 2019; Wittig, 2019; Xiang *et al*., 2014) and so others were considered and employed within this project.

5S RNA is a ribosomal RNA found within the large subunit of the ribosome across all domains of life and like U6 RNA is very strongly conserved across species. Recent literature has utilised 5S RNA as a control for examining expression changes (Fu *et al*., 2022) and so this appeared like a suitable non-miRNA control for this project.

miR-103 has been utilised previously in liver toxicity studies (Saide *et al*., 2019) as a control miRNA, and the potential for having a miRNA that is consistently expressed would be useful to perform direct miRNA to miRNA comparisons. It would also be useful to help streamline the process and

enable scaling the assay to cover multiple organ toxicities. There has been some evidence in the literature that miR-103 expression could be linked to cardiac damage or cardiac toxicity (Lian *et al*., 2016) so the suitability of this miRNA as a housekeeping option may be compromised.

miR-16 acts as a tumour suppressor gene and has been explored previously for its potential as a housekeeping gene, typically in the field of cancer research (Rice *et al*., 2015; Rinnerthaler *et al*., 2016; Yang *et al*., 2022). It was chosen for this project as a potential housekeeping gene due to its relative stable expression in the previous literature, and has been documented as being expressed in the *X. laevis* embryo (Ahmed *et al*., 2015).

RNU1A1 was suggested as a reference assay by the manufacturer of the qRT-PCR kits utilised in this study; it is a small nuclear RNA that was originally detected in mouse testes and is also expressed strongly in the adult *X. laevis* ovary. In the *Xenopus* embryo however, it has been detected at a range of stages between NF stage 8 and NF stage 40 through RNA-Seq (Session *et al*., 2016), so the potential for it being a housekeeping candidate was explored.

Let7a is a microRNA that acts as a tumour suppressor and as such is often used as an indicator miRNA in cancer studies, however, it has also been considered as a housekeeping gene in miRNA studies previously (Rice *et al*., 2015). It was decided to explore this as an option as the expression patten in *X. laevis* embryos appears to be consistent throughout the embryo (Ahmed *et al*., 2015).

3.7.2 Cardiotoxicity Biomarker Candidates

Potential biomarkers of cardiotoxicity were examined and considered following a search in the literature. The ones chosen to be used in the study are summarised in Figure 3.27, with further explanation following.

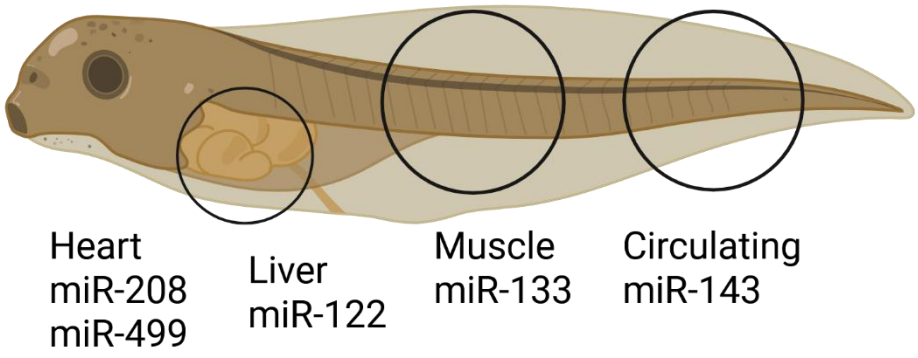

Figure 3.27: Summary of miRNAs used in the study and their locations in the Xenopus embryo. *The miRNAs chosen to be utilised are miR-208, miR-499- located in the heart, miR-122- located in the liver, miR-133- located in the muscles and miR-143- a circulating biomarker found in plasma.*

miR-208 is expressed within cardiac cells, and when the heart suffers damage, this miRNA can be released into the bloodstream, enabling detection of it through blood plasma. (Condrat *et al*., 2020; Corsten *et al*., 2010; Liu *et al*., 2015; Liu *et al*., 2017; Widera *et al*., 2011; Zhang *et al*., 2016). This miRNA has been directly implicated in doxorubicin-induced cardiotoxicity in other organisms (Desai *et al*., 2014; Tony *et al*., 2015; Vacchi-Suzzi *et al*., 2012).

miR-122 is expressed in the liver and found in multiple vertebrate species, including *X. laevis*. Previous work by the Wheeler lab (Saide *et al*., 2019) has detailed its suitability as a biomarker for paracetamol-induced liver toxicity/liver damage, and as paracetamol is being used as a control drug it

was decided to include it in the assay to confirm liver toxicity is present. It will also be useful to confirm that toxicity detected is organ specific, as generalised toxicity with multiple organ damage will theoretically see multiple organ-specific miRNAs expressed.

miR-499 is expressed in cardiomyocytes and studies have found that following cardiac injury it can be detected in the bloodstream (Wang *et al*., 2010; Zhang *et al*., 2016) and as such could prove to be a useful biomarker for this study.

miR-143 has been studied as a potential circulating biomarker of cardiac damage linked to dilated cardiomyopathy (DCM) by (Jiao *et al*., 2018) in which they showed upregulation of miR-143 in patients with DCM. It has also been studied with the context of its relationship with the hERG protein channel by (Lian *et al*., 2016); and as the hERG channel has been implicated in causing arrhythmia, particularly with terfenadine-induced cardiotoxicity, it seems as though this would be an interesting angle to approach with the inclusion of this biomarker.

miR-133 is one of the most studied microRNAs and is specifically expressed in muscles- both skeletal and cardiac in mammals, and although previous work by (Ahmed *et al*., 2015) showed a lack of expression in *Xenopus* embryo hearts at NF stage 33/34 development, it may be expressed later in the development as studied in this project. Multiple studies have implicated this miRNA as a potential biomarker of cardiac damage through various means including doxorubicin-induced cardiotoxicity, but the results of these studies are often conflicting with regards to the up- or down-regulation of this miRNA, and its presence within blood or in tissues. The inclusion of it within this study will potentially lead to some clarification of the effects drug-induced cardiotoxicity has on this miRNA.

3.8 Assay Development

miRNA primers for qRT-PCR were available commercially (Qiagen) and when compared to the target reference sequence for *X. laevis* (or *Xenopus tropicalis* if the *X. laevis* sequence was unavailable) were matched to ensure strong compatibility. Some of the primers were verified for working in *Xenopus* species but others had not, hence using the sequence comparison methodology to ensure best likelihood of success. Many miRNAs are strongly conserved between species which is why often a miRNA designed to target a mouse miRNA can be used on *Xenopus*, as the target sequence is likely to be the same or to vary by a single base.

The logical start point of assay development was to use the provided instructions within the kit (Chapter 2) and the methodology instigated by (Saide *et al*., 2019) as this has previously been shown to produce results. The same assumptions were made in this study regarding the harvesting method- cutting the embryo into two halves would produce a head sample that contained the heart and liver, and the tail sample would be filled with vasculature which could be utilised for biomarker detection.

3.8.1 Number of embryos

Initially the experiments were conducted using 20 embryos as this provided a significant quantity of RNA to analyse. After some initial work, trials were conducted using single embryos to determine if enough RNA could be extracted to perform qRT-PCR. This was done to determine if a single embryo could provide enough RNA for the experiment to work; if enough RNA could be extracted from a single embryo, then this would vastly decrease the number of embryos used within the study or enable a greater amount of data to be produced.

Unfortunately, RNA was only able to be extracted in low concentrations, if it was able to be extracted at all from a single embryo using the chosen methodology. This means that using a single embryo for the project would

not generate the data required. Furthermore, using a single embryo for the data could potentially introduce additional problems with the data being collected; individual embryos could vary greatly which means that the results generated from single embryo data may not be fully reflective of the impact the drug exposure has on the embryos. To alleviate this as an issue, pooling embryos and using multiple embryos per sample is the most logical decision, with testing taking place to determine the optimum number of embryos to include in the pool for RNA extraction.

10 embryos were trialled as an alternative to the original 20, as this would reduce the embryo availability problems that were present throughout the research whilst still, hopefully, providing enough RNA for the experiment. Experimental results however indicated that 10 embryos did not provide enough usable RNA for the study to be completed. Enough RNA could be extracted from 10 embryos for the head sample, but the tail samples did not produce a high enough concentration of RNA. This was likely due to the size differences between the two samples as the heads had more mass than the tails.

For example, in one experiment, 20 embryos produced 86.9 ng/µl and 7.0 ng/µl from the head and tail samples respectively. In contrast, 10 embryos produced 16.1 and 3.1 ng/µl RNA in the head and tail samples respectively. This is a considerable difference, and as the next stages of the experiment required a concentration of 5ng/µl there was simply not enough RNA in the tail sample from 10 embryos to be viable.

A compromise of 15 embryos was set, as this was the best solution to generate enough RNA for both samples while still utilising less embryos than the original method (data not shown).

3.8.2 cDNA dilution

The instructions for the qRT-PCR kit said that the cDNA samples were recommended to be diluted anywhere from 40x (1:40) to 80x (1:80) depending on the strength of the cDNA created and the concentration. Trials were run exploring 40x, 60x and 80x dilution to ascertain which dilution would provide the best results. It was determined that due to the small volume of RNA generated from the original samples, a lower dilution was preferential for the qRT-PCR as it generated enough cDNA to be analysed. All experiments were conducted with 40x dilution of the cDNA.

3.8.3 Housekeeping Choices

Initially, U6 was used as a housekeeping gene of choice due to the strong representation of it as a housekeeping option in the literature. However, it became clear part way through the period of research that U6 may not be as reliable a choice of housekeeper as originally thought, so while the original results for doxorubicin are included in Figure 3.43, it was clear the experiments would need to be repeated after a more suitable housekeeping candidate was found.

This was initially brought to light as throughout the initial stages of experimentation, results from the qRT-PCR revealed the U6 values to be extremely variable, an example of the results are shown in Table 3.6 where the CT values vary from 23.39 to 30.71. A good choice in housekeeping gene for this study is not variable and not affected by the drug the embryo is exposed to, meaning that throughout the study there should be little variation between the CT values detected. The CT value indicates how much of a gene's product (in this case, U6) is present in the tissue sampled- a lower CT value indicates more of the product and a higher CT value indicates less of the product- a good housekeeper would also ideally be well expressed and have a lower CT value to enable easier detection.

There was also great variability between PCR plates, but this was fixed by the switch from using a qRT-PCR machine with 96-well plates to a qRT-PCR machine that utilised 384-well plates, as this enabled the full experiment's worth of samples to be conducted in one PCR cycle rather than splitting them across multiple plates.

Sample	Repeat 1 CT value	Repeat 2 CT Value	Repeat 3 CT Value
Control	24.58	23.39	24.60
Vehicle Control	24.99	25.98	25.53
2 µm	24.15	24.59	24.58
4 µm	24.97	25.92	26.59
6 µm	27.40	27.67	28.29
8 µm	28.87	28.50	28.93
10 µm	28.83	28.84	29.04
20 µm	29.07	29.12	29.03
30 µm	30.66	30.71	30.91

Table 3.6: An example of the U6 CT values determined early in the research period. *These results showed high variability between samples. Results are from 20 pooled embryos exposed to increasing concentrations of terfenadine.*

Following further exploration into the literature, several potential candidates were found. To determine which would be the best to use, an experiment was conducted in which embryos were exposed to example concentrations of the drugs used in the study (50µM doxorubicin, 30µM terfenadine) alongside a control sample, and the CT values of 4 technical repeats mapped onto a graph, shown in Figure 3.28. In this instance, U6 RNA was relatively consistent between samples but was a high (>30) CT value throughout. Let7a was very variable, as was miR-16 and RNU1A1. 5S RNA showed some variability but the CT value remained below 30 throughout the experiment. miR-16 and Let7a also suffered from missing data points, further

affecting the reliability of these candidates. The results of this precipitated the decision to make 5S RNA the housekeeping gene of choice for the rest of the research period.

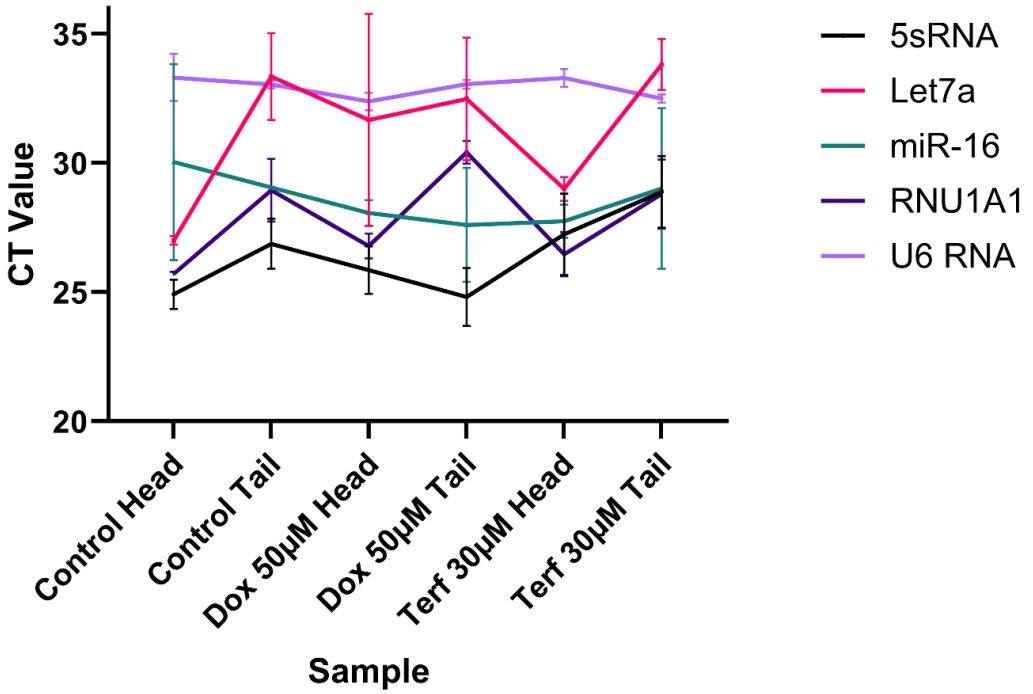

Figure 3.28: Graph showing the average CT values of various housekeeping candidates. *Average of 3 technical replicates of different housekeeping candidates for the biomarker assay, shown as CT values ± Standard Deviation.*

3.8.4 Whole Mount in Situ Hybridisation (WISH)

Whole Mount in Situ Hybridisation (WISH) is a standard technique used to determine where and when a gene of interest is expressed in a developing embryo. As part of the work conducted in this study, WISH was conducted with fixed NF stage 45 *Xenopus* embryos to determine if it was possible to visualise the miRNAs and genes of interest expression. Many examples of WISH-stained miRNAs are available to view on Xenbase, but often these are at much earlier development stages than those covered within this study.

Cardiac troponin (Tc) is a protein expressed within the heart and can therefore be used to visualise the heart of a *Xenopus* embryo, acting as a control in this experiment and serving as a comparison to the miRNAs studied to determine heart expression. As this is well studied, there were plenty of clear images of WISH expression in the literature, but none of NF stage 45 *Xenopus*. There are some images of NF stage 42 and 46 embryos (Figure 3.29) that both clearly show very distinct staining in the heart.

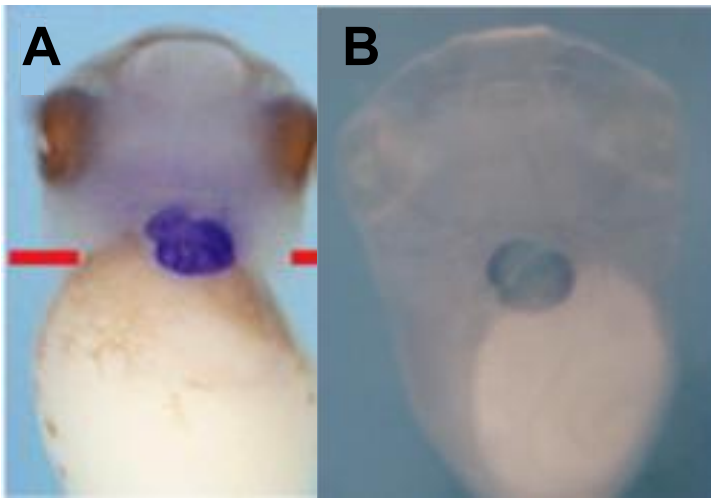

Figure 3.29: WISH of cardiac troponin in NF stages 42 (A) and 46 (B) Xenopus embryos. *A shows the heart clearly defined and well stained, with no background staining (taken from Guo et al. (2015)). B shows clear definition of heart muscle in the stain (taken from Ito et al. (2008)).*

The heart in the WISH performed during this study is clearly and distinctly stained, indicated by an arrow in Figure 3.30.

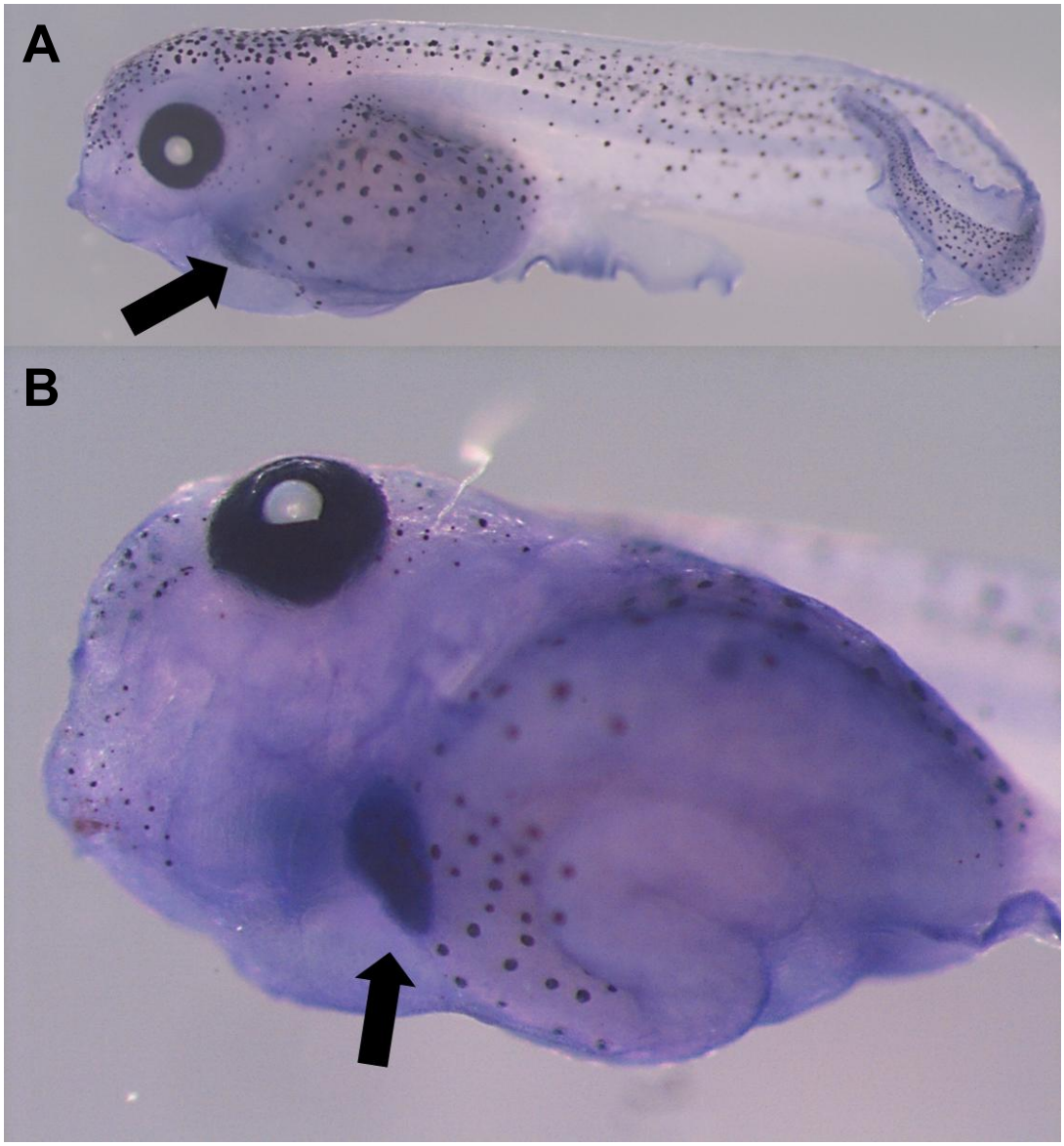

Figure 3.30: Cardiac troponin WISH of NF stage 45 Xenopus embryo*. Panel A shows a lateral view with anterior to the left. Panel B shows a ventral view with the anterior to the left. There is clear staining of the heart, indicated by the arrow in each panel.*

miR-499 was one of the miRNAs chosen to be utilised in the assay, but with conflicting data from the literature regarding its status as a tissue-specific or circulating miRNA it was hoped that seeing a successful stain from WISH would help indicate where it is expressed in *Xenopus* embryos. Existing images from Xenbase of miR-499 WISH staining showed expression in head and trunk at NF stage 33/34 or heavy, generalised staining with little no clear specificity at NF stage 36 (Figure 3.31).

Figure 3.31: WISH staining of miR-499 in NF stages 33/34 (A) and 36 (B) Xenopus embryos. *A shows clear staining in head and trunk of the embryo (taken from Ahmed et al., (2015)). B shows generalised, heavy staining with strong background (taken from Xenbase, provided through the additional data from Ahmed et al. (2015); (Fisher et al., 2023)).*

Results from the WISH performed in this study showed generalised staining with no specific cardiac staining (Figure 3.32).

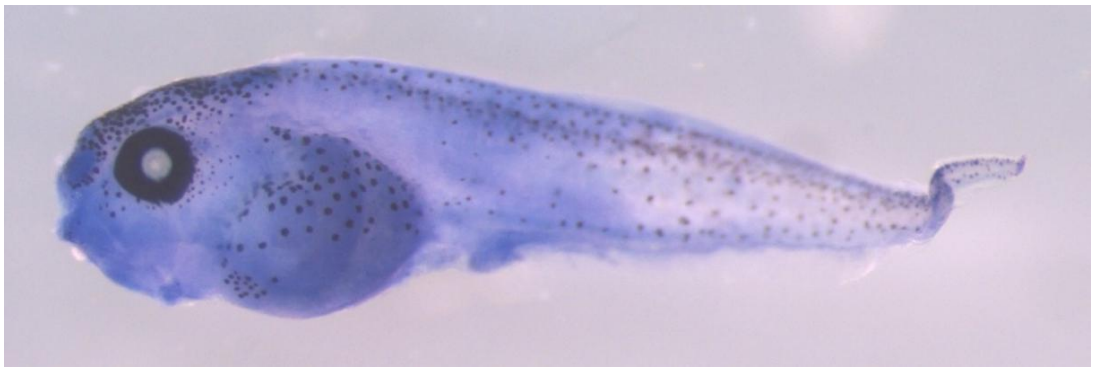

Figure 3.32: miR- 499 WISH of NF stage 45 Xenopus embryo*. Lateral view with anterior to the left, strong generalised staining is seen with no clear specific cardiac staining.*

miR-208 is referred to as a cardiac specific biomarker, however existing WISH images in embryos beyond NF stage 28 where the heart is beginning to form were lacking in the literature (Figure 3.33). This was problematic as at such an early stage the heart has yet to be fully developed in *Xenopus*, so little information relevant to this study was able to be gleaned from said images.

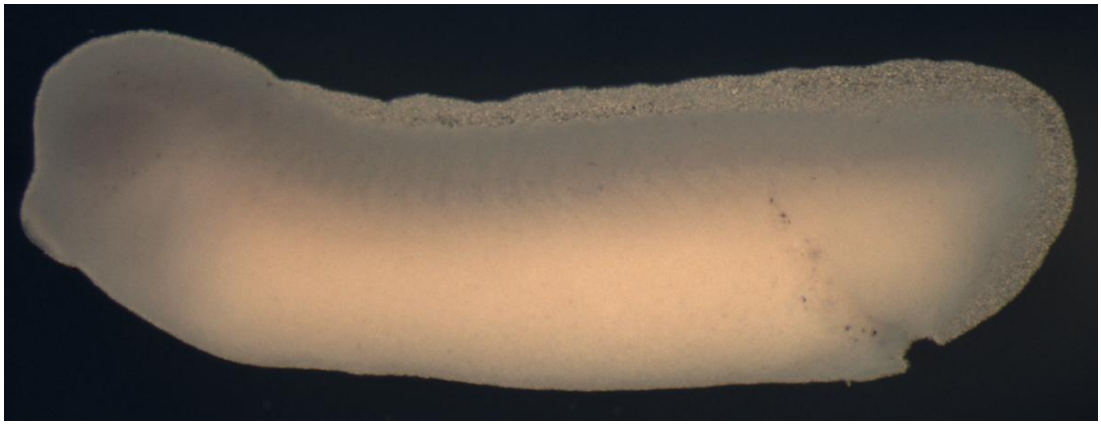

Figure 3.33: miR-208 WISH of NF stage 28 Xenopus embryo. *Image shows no visible staining in the embryo, particularly in the region surrounding the heart where miR-208 could be expected to be visualised. Image acquired from Xenbase, provided through the additional data from Ahmed et al. (2015); (Fisher et al., 2023).*

This experiment showed very strong staining in the heart (Figure 3.34), confirmed through comparison to the cardiac troponin staining shown in Figure 3.30.

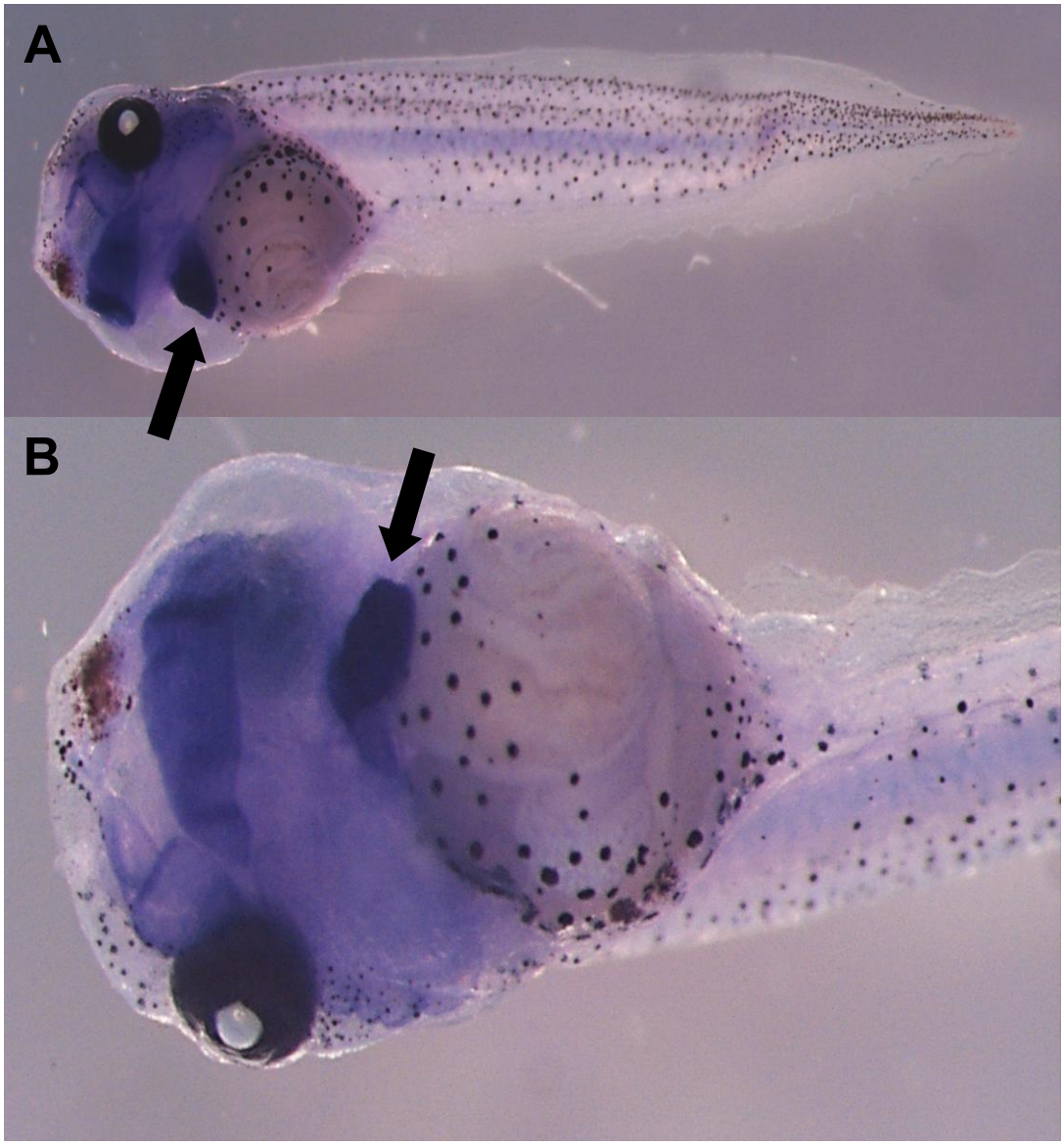

Figure 3.34: miR-208 WISH of NF stage 45 Xenopus embryo. *Panel A shows a ventro-lateral view with anterior to the left. Panel B shows a ventral view with anterior to the left. Strong cardiac staining is shown, indicated by the arrow*.

miR-143 has been linked to cardiac expression as well as having potential as a circulating biomarker. Previous WISH results show somitic expression along the spine at NF stage 30 (Figure 3.35), with a lack of information for later stage embryos.

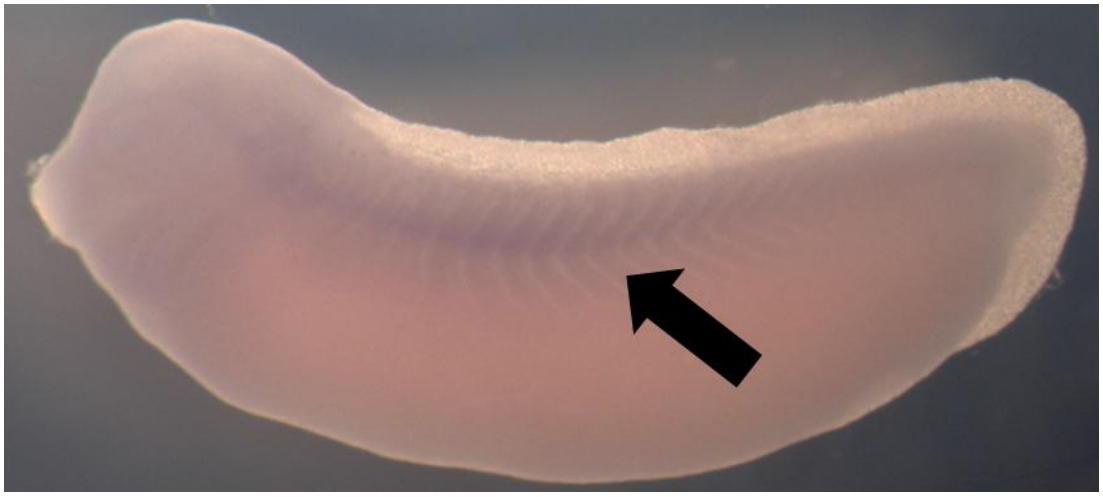

Figure 3.35: miR-143 WISH of NF stage 30 Xenopus embryo. *Some somitic expression is indicated by the staining along the somites in the spinal area. Image from Xenbase, provided through the additional data from Ahmed et al. (2015); (Fisher et al., 2023).*

This experiment showed staining present in the head and torso alongside somatic expression, with strongest staining being found in the gut and little to no staining seen in the heart (Figure 3.36).

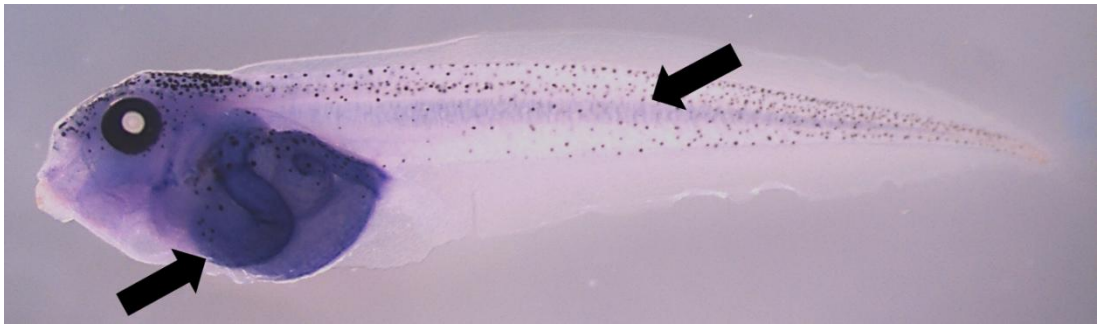

Figure 3.36: miR-143 WISH of NF stage 45 Xenopus embryo. *Lateral view with anterior to the left. Possible notochord staining was present alongside staining in the head and torso, with strongest staining present in the gut. Notochord and gut staining indicated by arrows.*

miR-133 is a muscle-specific miRNA so expression should be seen across the embryo where muscles are present, potentially including the heart. Previous images at NF stage 42 of various forms of miR-133 show a strong expression throughout the embryo in the musculature but were so heavily stained it was difficult to determine details surrounding expression (Fisher et al., 2023). This image, along with one from Ahmed et al. (2015) are included as part of Figure 3.37.

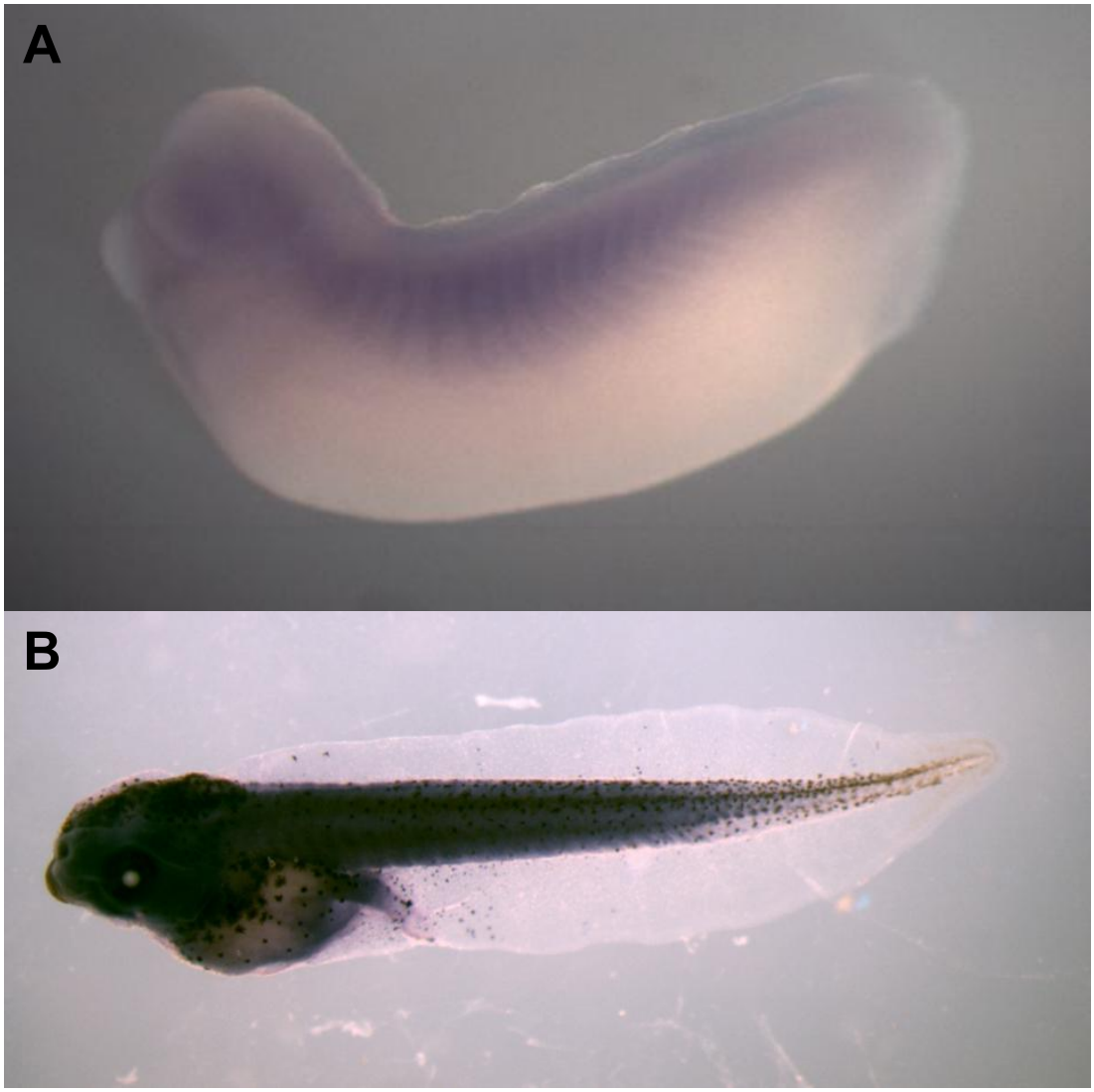

Figure 3.37: miR-133 WISH of NF stages 29 (A) and 42 (B) Xenopus embryos. *A shows possible somitic staining in the embryo across the spine and into the head, but otherwise minimal staining is present. B shows widespread, heavy staining across the embryo, possibly consistent with musculature expression but also difficult to distinguish details It is also possible that this embryo was incubated for longer than the one shown in A. Images both taken from Xenbase and provided through the additional data from Ahmed et al. (2015); (Fisher et al., 2023)*

Results for this experiment showed strongest staining throughout the tail and head, particularly around the mouth. There was no staining in the heart. Features are shown by arrows in Figure 3.38.

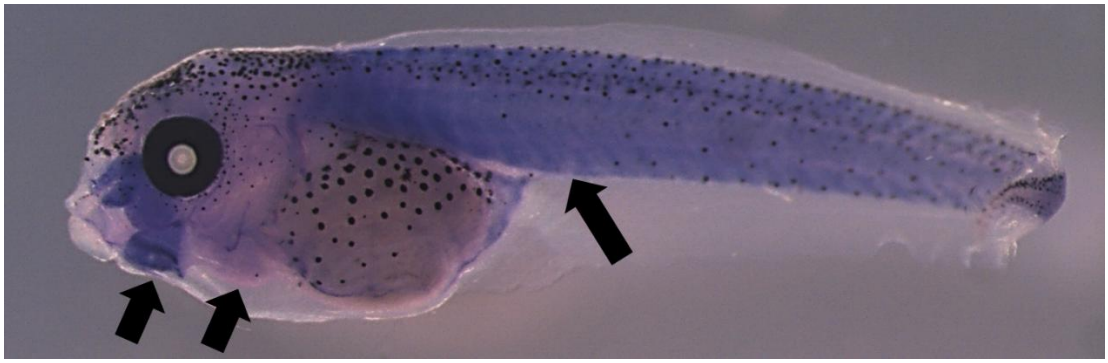

Figure 3.38: miR-133 WISH of NF stage 45 Xenopus embryo. *Lateral view with anterior to the left. Staining is shown throughout the tail and particularly in the musculature around the mouth, indicated by arrowheads. The heart is also indicated by an arrow but shows no expression.*

miR-103, despite being widely studied, does not appear to show a specific expression pattern to which it is possible to specify which tissues it is expressed in for a normal embryo. Previous WISH shows strong staining at NF stage 28 in the head and torso as well as the spinal area through the tail, with additional images at NF stage 29 showing strong somatic spinal expression. Unlike other miRNAs covered in this section, existing NF stage 45 images were available, and these show low levels of staining in the gut but very little beyond this (Figure 3.39).

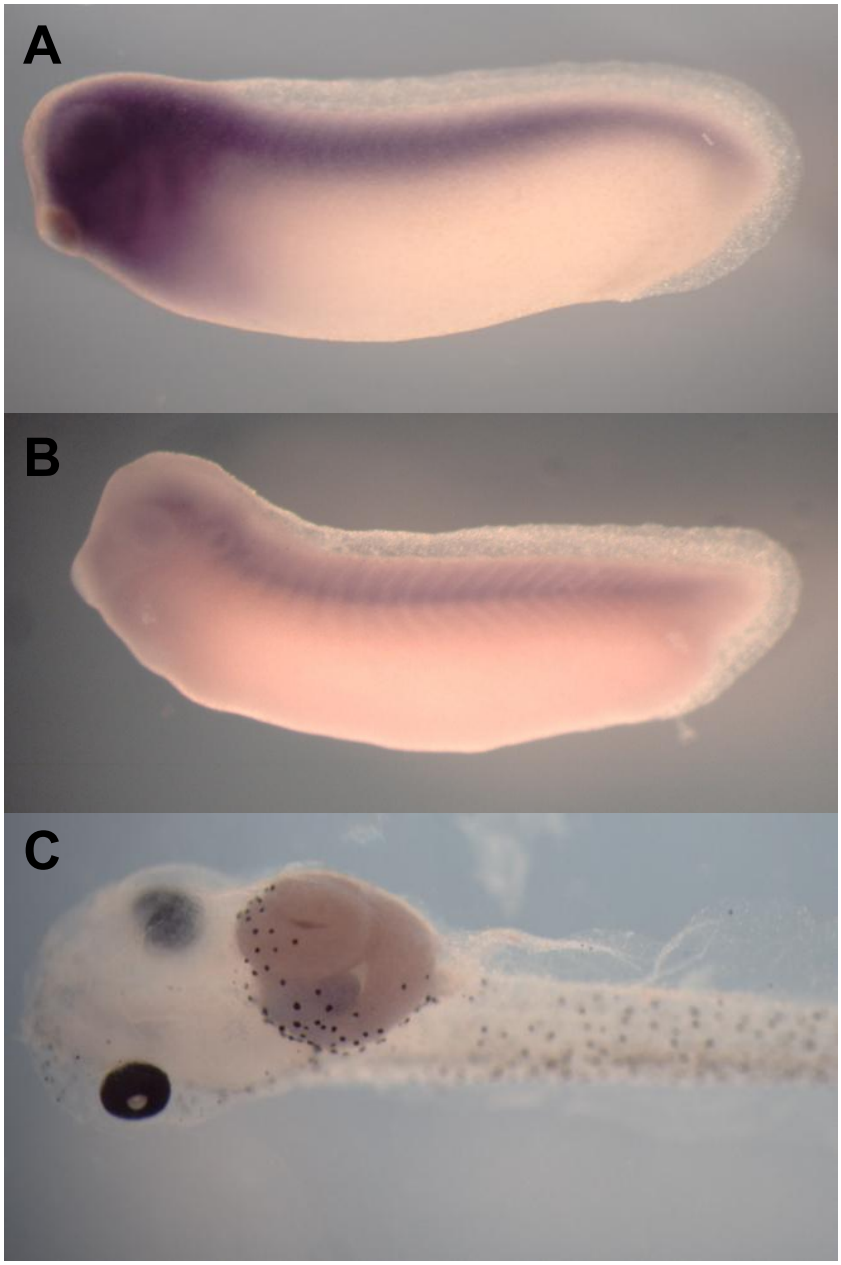

Figure 3.39: miR-103 WISH of NF stages 28 (A), 29 (B) and 45 (C) Xenopus embryos. *A shows staining in the head and torso along with staining down the spinal area and into the tail. B shows staining in the head, possibly in the brain, along with staining down the spine possibly in the somites. C shows some staining present in the gut of the embryo, but not any clear staining elsewhere. The gut staining is not particularly heavy and confined to one specific area. It is likely that the change in stain intensity between A and B is due to different incubation times during the experiment. Images taken from Xenbase, and was provided through the additional data from Ahmed et al. (2015); (Fisher et al., 2023).*

In this experiment, staining appeared to be widespread throughout the embryos' torso and head, with lighter staining throughout the tail section (Figure 3.40). There was no obvious specific staining in the heart.

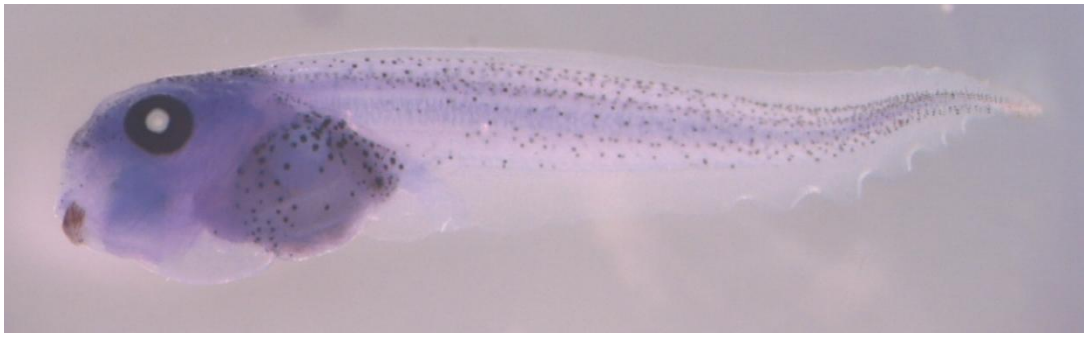

Figure 3.40: miR-103 WISH of NF stage 45 Xenopus embryo. *Lateral view with anterior to the left. Staining was widespread throughout the torso and head with lighter staining throughout the tail. No expression in the heart could be seen.*

Mir-122 is a liver specific miRNA and so would be expected to be indicated only in the liver of a WISH. Previous work carried out in the Wheeler lab has provided WISH images of *Xenopus* embryos at NF stage 38 and NF stage 45 (Figure 3.41), alongside additional images of NF stage 45 embryos obtained from Xenbase (Figure 3.42).

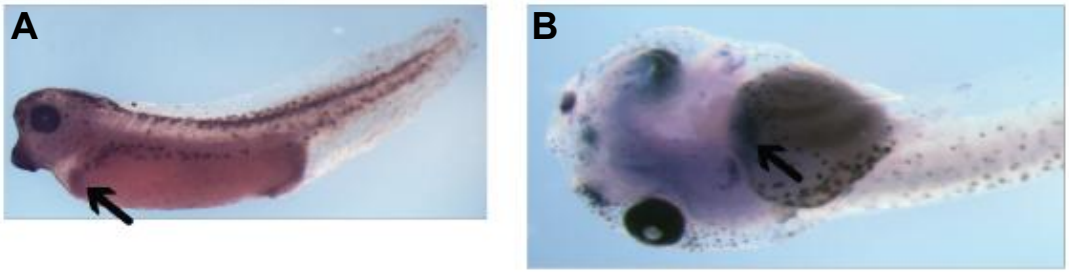

Figure 3.41: miR-122 WISH of NF stage 38 and NF stage 45 Xenopus embryos. *In both NF stage 38 (A) and NF stage (46) embryos there is staining in the liver, indicated by the arrows in each picture. Image taken from* (Saide, 2018).

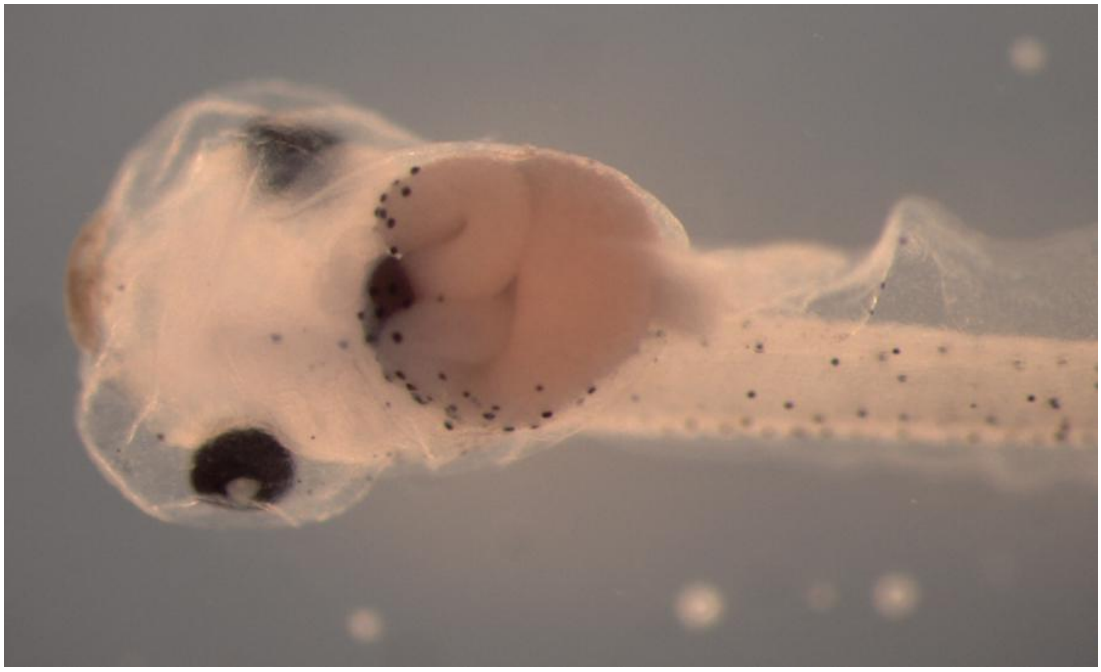

Figure 3.42: miR-122 WISH of NF stage 45 Xenopus embryo. *There is clear staining of the liver, with no background staining in the image. Image was taken from Xenbase, and was provided through the additional data from* (Ahmed et al., 2015; Fisher et al., 2023).

3.9 Initial Results

As already described, the initial results detailed in this chapter were all generated using U6 as the housekeeping gene and as such are not

comparable with the later results but are shown here to indicate the progression of the research.

Early results for doxorubicin exposure were promising, as the assay was still in development the focus was on utilising miR-208 as a marker for heart injury, as this was going to be a present/not present test of the methodology due to it potentially only being detected in the tail sample if the heart had suffered cardiac injury. The results for this are shown in Figure 3.43. Although there were not enough biological repeats conducted (only 2 were done) to perform statistics before the methodology was changed, the initial results were very interesting- taken as a simple present/not present test the indication that miR-208 was detected at all concentrations of doxorubicin above 10μM except 70μM indicates the likelihood of cardiac damage occurring is very likely. The absence of miR-208 being detected at 70μM is unexpected and unexplained- a failed extraction of miRNA is a possible reason and has been a reoccurring issue throughout the study, but for it to happen on both biological repeats is unfortunate.

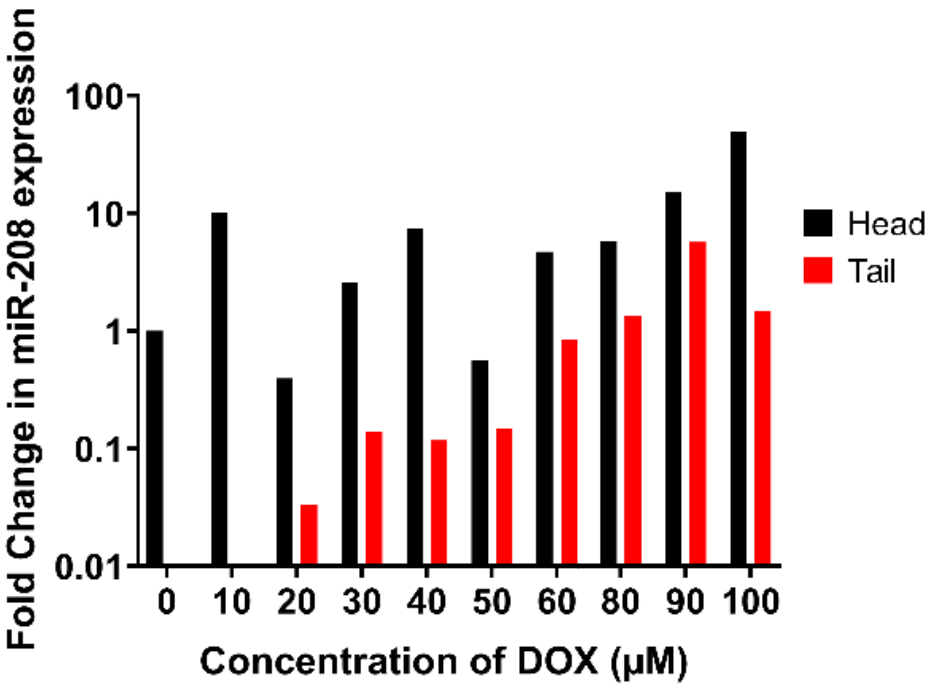

Figure 3.43: miR-208 expression in Xenopus embryos exposed to doxorubicin. *NF stage 38 embryos were exposed to doxorubicin (0-100μM), then harvested when at NF stage 45. The expression of miR-208 in the heart-containing head sample (black) and vasculature-rich tail sample (red) was measured using qRT-PCR (log (fold change ± SD)) and normalised to untreated embryos (0μM). 2 biological repeats were conducted.*

3.10 Discussion

The method development undertaken in this project to measure heart rate and expression of biomarkers was difficult and much of it was determined from trial-and-error. Overall, at the end of the research period, the methodology worked and was able to begin generating results. Throughout the development of the assay there were issues with the process, one of which was access to appropriate tools and machinery to perform experiments and scale them up to full experimental sample sets. A 96-well qRT-PCR machine was easily accessible for use, which for the first few months of development proved adequate, but as work began scaling to using more samples and larger datasets this proved inadequate, as for the largest sample collections 4 or more plates would be required to ensure the full remit of 3 technical repeats and controls, which was a potential contributor to varying results from the original housekeeping choice of U6 RNA. Obtaining access to a 384-well plate took several months, which reduced the available time for data gathering considerably.

Further problems with developing the method surrounded the ability to extract adequate amounts of RNA to perform analysis; several times over the course of creating the assay there were failures to extract enough RNA to use in the analysis, and the use of 15 embryos was decided on after several attempts at extracting RNA from higher and lower numbers of embryos. The decision to use Qiagen kits exclusively for this project was driven by several factors of convenience, experience and costs, particularly with a view to scaling the process up for industrial usage. Other options were available, including extraction methods that did not utilise a self-contained, easy to use kit, but these were rejected in favour of the convenience and scaling opportunity an off-the-shelf kit provided. Likewise, the Qiagen kits specifically have been utilised within the research group to great effect and have proved useful for the bulk of the work performed therein, so were a first choice when developing this area of work. With the benefit of hindsight, it may have been beneficial to explore other alternatives available on the market that may have

offered better extraction and functionality, as there are other kits available for purchase that offer miRNA extraction from low levels of biological sample, some as low as singe cells. In future work, it would be advisable to examine and trial these methods, as harvesting useful miRNA from a single embryo or part embryo would also benefit the 3R's principles that guided the onset of the project, utilising less embryos and generating better data.

Another expansion of the project that would have been beneficial if more time had been available to explore this is the range of drugs used in the study, both experimentally and for control purposes. A wider range of known cardiotoxic drugs, particularly those with different mechanisms of action, would assist with showing the method is robust and suitable for the widest range of potentially novel compounds to be tested. Control compounds, be they not known to cause toxicity at all, or those known to cause other forms of toxicity as per paracetamol in this assay, would also provide support for the assay. It would also allow for testing and expansion of the assay for testing more than cardiac and liver toxicity.

Chapter 4 Heart Rate Analysis

4.1 Introduction

The aim of the research covered in this chapter was to determine if cardiotoxicity could be predicted via imaging of the *Xenopus* embryos hearts after exposure to a drug. The intention was to use drugs with known cardiotoxicity to develop the assay and act as a proof of concept, before expanding onto other drugs of unknown toxicity to determine if this assay can be used for diagnosing cardiotoxicity. Ideally, this would be the case and depending on the quality of the information gleaned in the assay it may potentially provide enough information to determine what kind of cardiotoxicity is occurring.

As part of this research project, the author worked alongside two final year Undergraduate project students to incorporate mini-studies, experiments into additional toxic compounds (Paclitaxel, E4031) that the author determined would be interesting to study in *Xenopus*, however they did not have the availability to conduct a full-scale study as per the rest of the drugs covered in this chapter.

4.2 Individual drug exposure outcomes

4.2.1 Doxorubicin

When analysing the heart rate data; the atrium and ventricle were analysed individually to determine if doxorubicin concentration affected heart rate on either chamber (Figure 4.2) and then a comparison between the two were conducted (Figure 4.4). This was done to assess if the changes, if any, were isolated to a specific chamber or present across both- some forms of cardiotoxicity are noted to occur more frequently in the atrium or the ventricle, and a comparison between the two chambers may show this.

The results indicate that doxorubicin did induce cardiotoxicity in *Xenopus*, and this could be detected through reduction in heart rate and increase in

arrhythmia incidence. The results indicated that at the highest concentration of 100μM, both atrial and ventricular heart rate was reduced in a statistically significant manner and this correlated with an increase in arrhythmia detection as it rises from 0.35 to 1.66. This arrhythmia score increase signifies that the heart rate graphs have changed from being predominantly scored at a 0 (no arrhythmia) to being scored consistently high enough the average score is midway between 1 (mild) and 2 (moderate) arrhythmia.

There is also a statistically significant decrease in atrial heart rate at 20μM which is not mirrored in the ventricle, and the results in Figure 3.8 show this reduction is not statistically significant when the two chambers are compared. It is possible that this is a rogue result, but previous research has indicated that some atrial-specific pathology has been demonstrated following doxorubicin exposure (Zeiss *et al*., 2019), so further research into this could be beneficial.

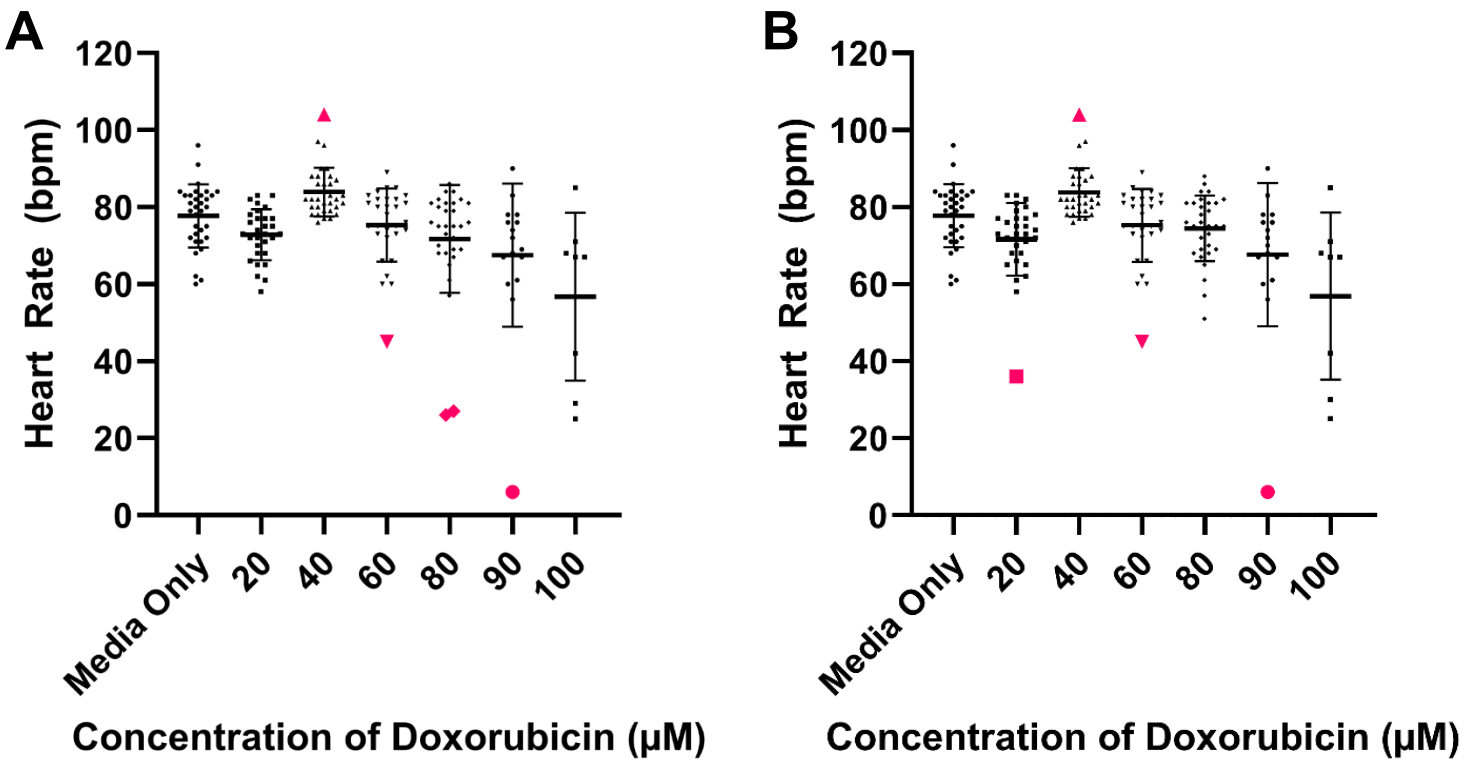

Figure 4.1: Heart rate of Xenopus embryos exposed to doxorubicin including outliers. *Xenopus embryos had been treated between NF stages 38 and 45 with doxorubicin and kept at 23°C, then atrial (A) and ventricle (B) heart rate measured after 15-minute treatment with MS-222 by determining number of times the heart had beat for 30 seconds and adjusted into beats per minute. Outliers were detected using GraphPad Prism's ROUT function with Q=1% parameters and are indicated in pink on the graph. These were removed prior to performing statistical analysis.*

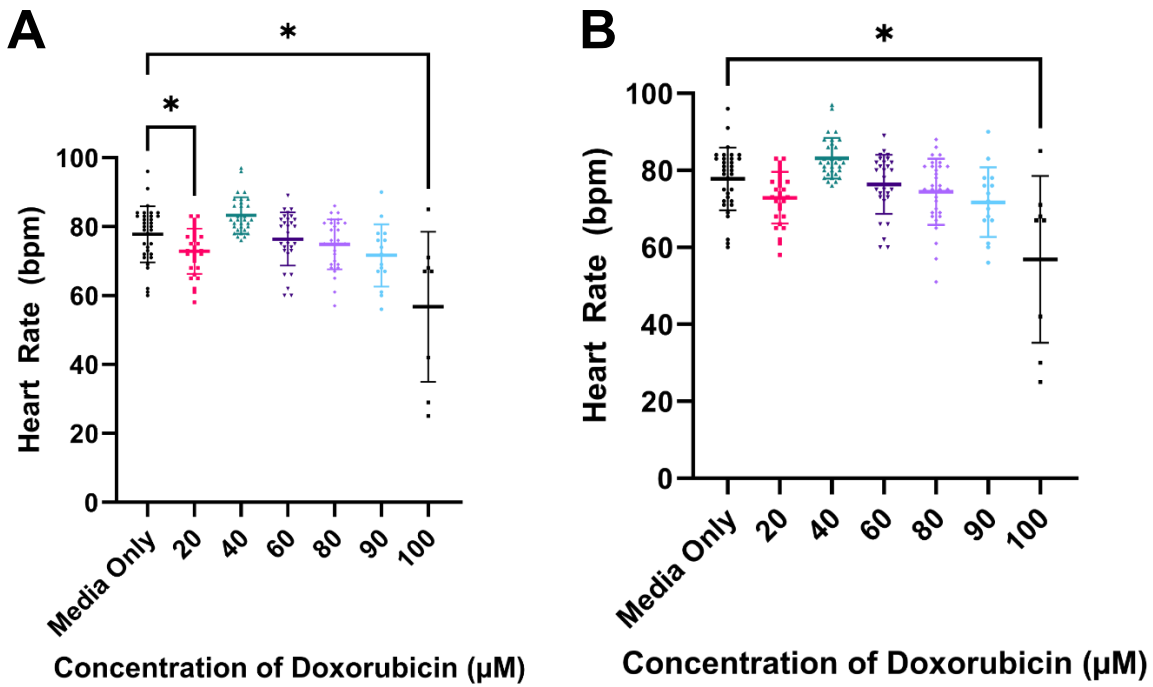

Figure 4.2: Heart rate of Xenopus embryos exposed to doxorubicin. *Xenopus embryos had been treated between NF stages 38 and 45 with doxorubicin and kept at 23°C, then atrial (A) and ventricular (B) heart rate measured after 15-minute treatment with MS-222 by determining number of times the heart had beat for 30 seconds and adjusted into beats per minute. Average atrial heart rate ± SD of treated embryos was compared to untreated embryos (0µM) using one way ANOVA (* = $p<0.05$). 3 repeats were performed with n= 8-30.*

The heart rate data following doxorubicin exposure indicates a significant reduction in heart rate (p= 0.05) in the atrium at concentrations of 20 and 100μM, and in the ventricle at 100μM (p= 0.05). When heart chamber comparison is performed there was no significant difference at any concentration.

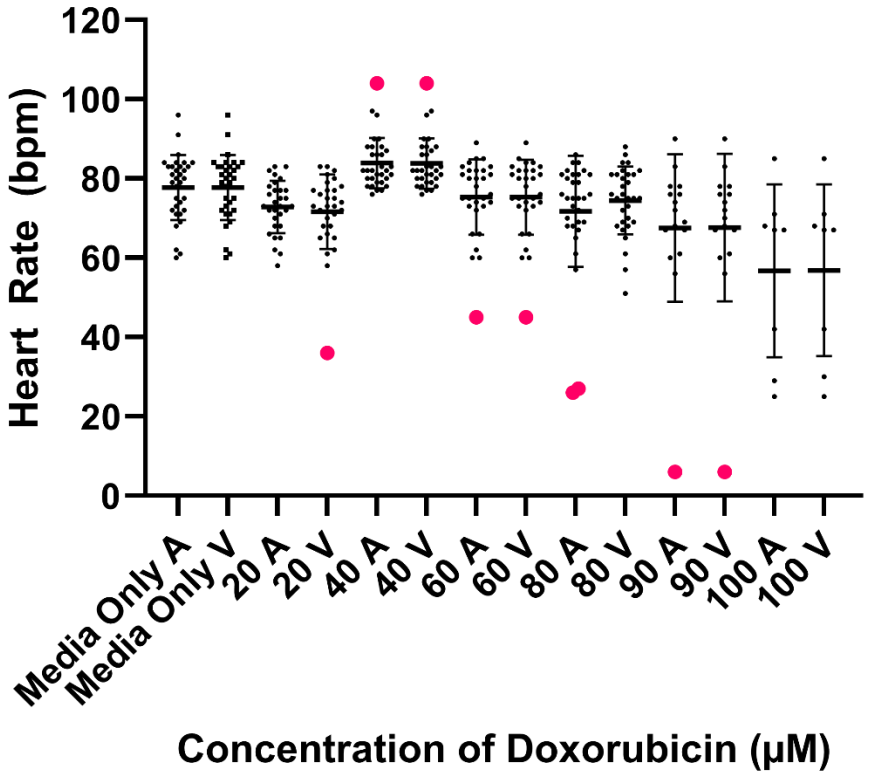

Figure 4.3: Comparison of atrial and ventricular heart rates following doxorubicin exposure. *Heart rate was measured following doxorubicin exposure. Outliers were detected using GraphPad Prism's ROUT function with Q=1% parameters and are indicated in pink on the graph. These were removed prior to performing statistical analysis.*

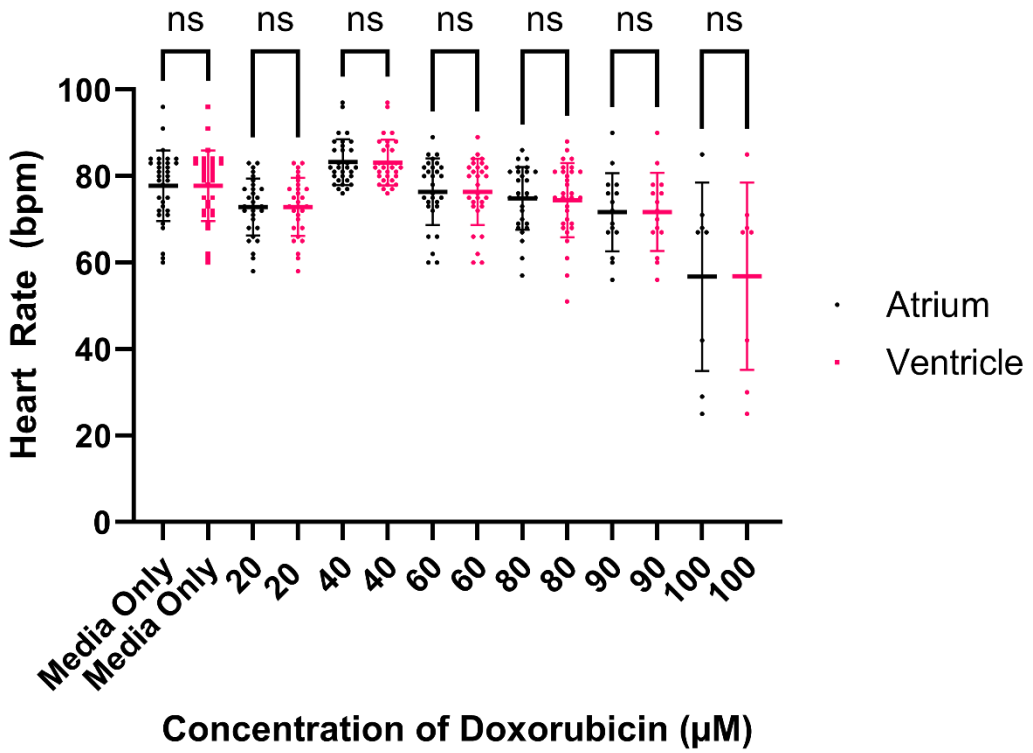

Figure 4.4: Comparison of atrial and ventricular heart rates following doxorubicin exposure. *Heart rate was measured following doxorubicin exposure and analysed by one-way ANOVA with paired comparisons between each pair of chambers at each concentration.*

The results show a significant change in average arrhythmia score at 100μM compared to the control, with an increase from 0.35 to 1.66 (Figure 4.9). Although not significantly different to the control, the graph indicates a trend of the arrhythmia score increasing from before the 100μM concentration, with 90μM having a score of 0.60. This indicates that arrhythmia may be determined through visual assessment of the heart rate graphs and that following the creation of a suitable standardised methodology this could be performed by someone without the in-depth knowledge that the author has developed over the course of the study- important for the potential to scale this process up for an industrial scale use.

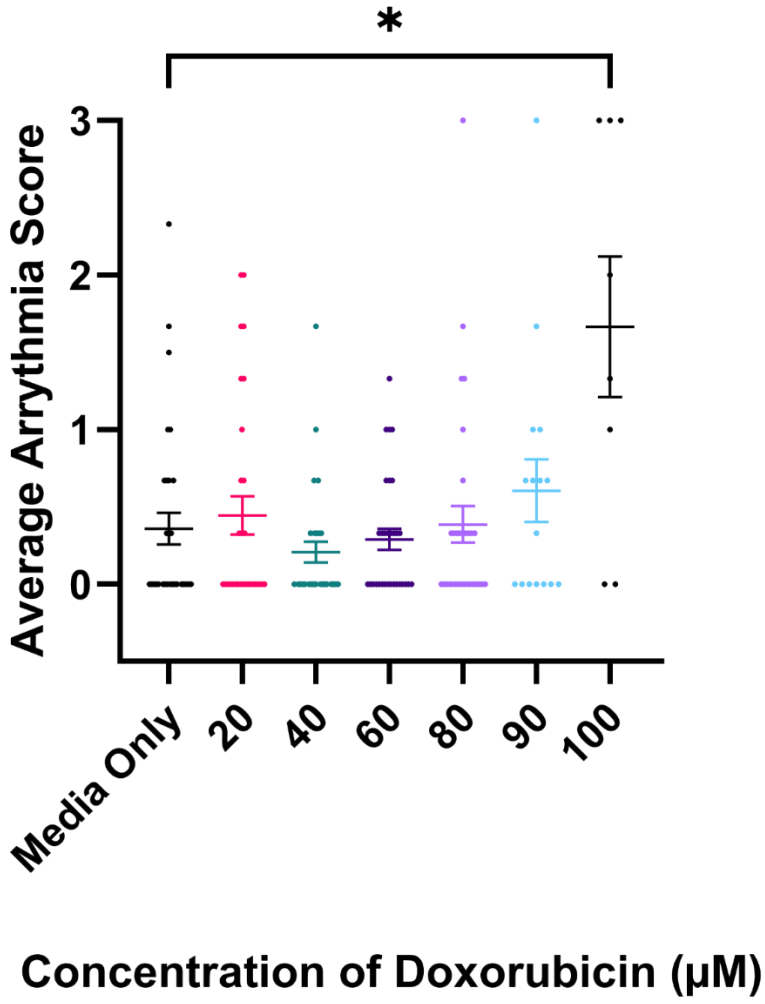

Figure 4.5: Average arrhythmia score of Xenopus embryos exposed to doxorubicin. *Xenopus embryos had been treated between NF stages 38 and 45 with doxorubicin and kept at 23°C, then heartbeat recorded after 15-minute treatment with MS-222. Heartbeat graphs were blind-assessed and given arrhythmia score from 0-3 (0- no arrhythmia, 1- mild arrhythmia, 2-moderate arrhythmia, 3- severe arrhythmia). Scores were then averaged and treated embryos were compared to untreated embryos (0μM) using one way ANOVA with Kruskal-Wallis multiple comparisons ($p<0.05$). Graph shows mean ± SEM.*

4.2.2 Terfenadine

When analysing the heart rate data; the atrium and ventricle were analysed individually to determine if doxorubicin concentration affected heart rate on either chamber (Figure 4.7) and then a comparison between the two were conducted (Figure 4.9) to assess if the changes, if any, were isolated to a specific chamber or present across both- some forms of cardiotoxicity are noted to occur more frequently in the atrium or the ventricle, and a comparison between the two chambers may show this.

The results strongly indicate that terfenadine induced cardiotoxicity in *Xenopus* embryos and that this could be detected through reduction in heart rate. The results showed that a noticeable and significant reduction in heart rate occurred at concentrations of 20μM and above, which strongly correlated with the increase in average arrhythmia score despite the latter not showing statistical significance in this study. There was no difference recorded between the two heart chambers studied, which was somewhat unexpected as in human patients terfenadine has been found to cause ventricular arrhythmias, so an alteration in ventricular output was anticipated.

Despite the lack of statistical significance, the values of the arrhythmia score indicated that there was an effect happening, as the score increased from 0.79 to an eventual 1.53 at the highest concentration of 50μM. As mentioned previously, terfenadine is known to cause ventricular arrhythmias and the results for heart rate did not indicate this also occurred in *Xenopus* embryos. Analysis of the heart rate through its shape however could be used to indicate that ventricle-specific arrhythmias are occurring, but the methodology used assessed the heart rate graph, rather than each chambers trace individually, this is not something the current analyses can confirm. It would make for a very interesting analysis should the research be taken further in later studies however.

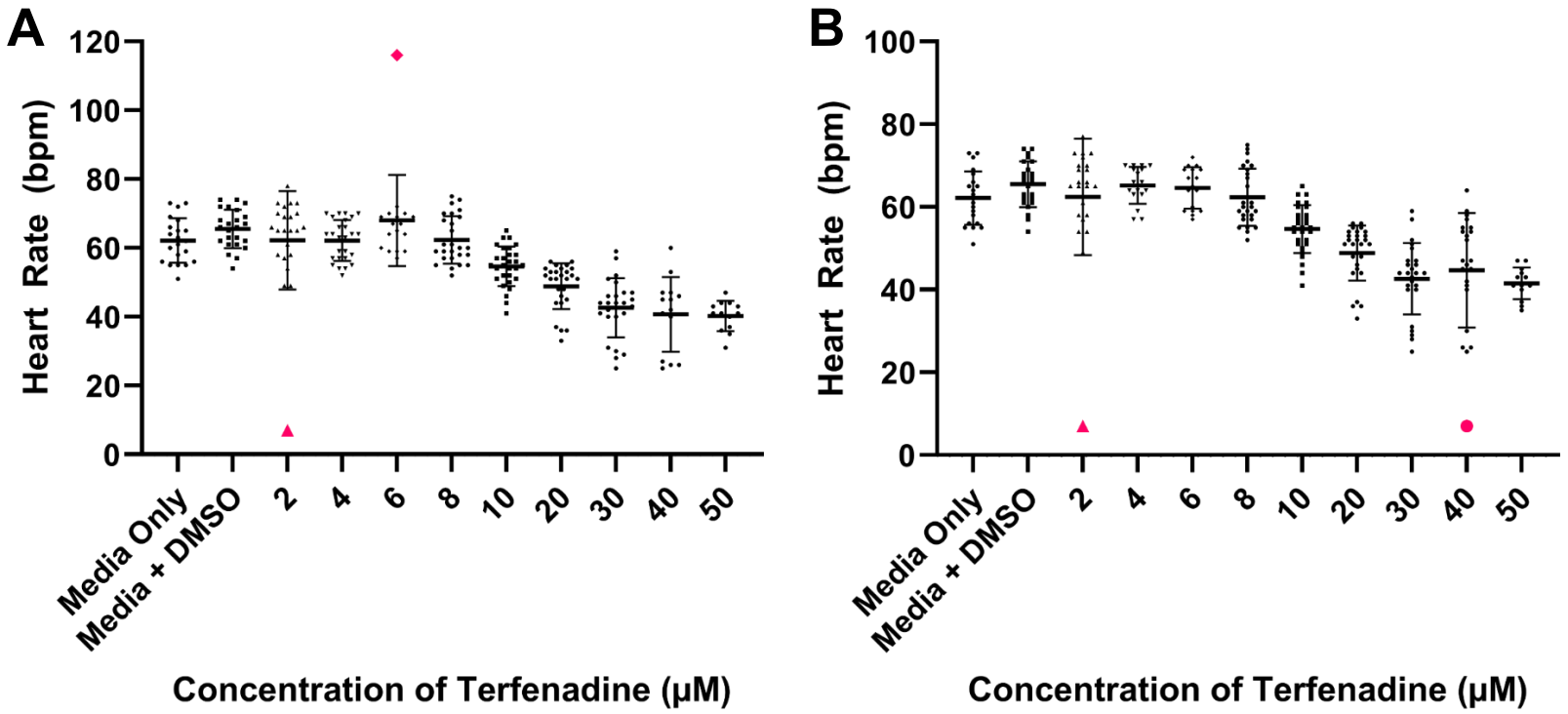

Figure 4.6: Heart rate of Xenopus embryos exposed to terfenadine including outliers. *Xenopus embryos had been treated between NF stages 38 and 45 with terfenadine and kept at 23°C, then atrial (A) and ventricular (B) heart rate measured after 15-minute treatment with MS-222 by determining number of times the heart had beat for 30 seconds and adjusted into beats per minute. Outliers were detected using GraphPad Prism's ROUT function with Q=1% parameters and are indicated in pink on the graph. These were removed prior to performing statistical analysis.*

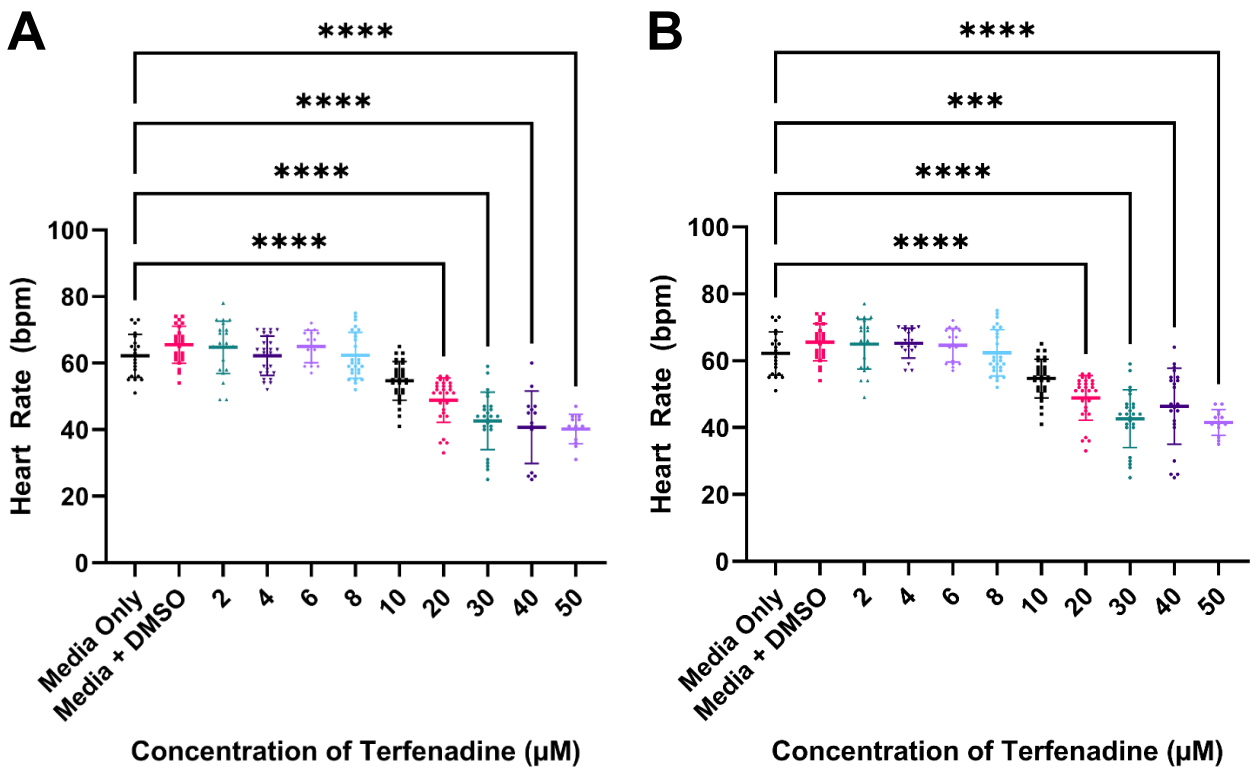

Figure 4.7: Atrial heart rate of Xenopus embryos exposed to terfenadine. *Xenopus embryos had been treated between NF stages 38 and 45 with terfenadine and kept at 23°C, then heart rate measured after 15-minute treatment with MS-222 by determining number of times the heart had beat for 30 seconds and adjusted into beats per minute. Average atrial heart rate ± SD of treated embryos was compared to untreated embryos (0μM) using one way ANOVA (****=p<0.0001). At least 3 repeats were performed, with n= 11-30.*

The heart rate data following terfenadine exposure indicated a significant reduction in heart rate ($p<0.0001$) in the atrium at concentrations of 20, 30, 40 and 50μM, and in the ventricle at 20, 30 and 50μM ($p<0.0001$) and 40μM ($p=0.0001$). When heart chamber comparison was performed there was no significant difference at any concentration.

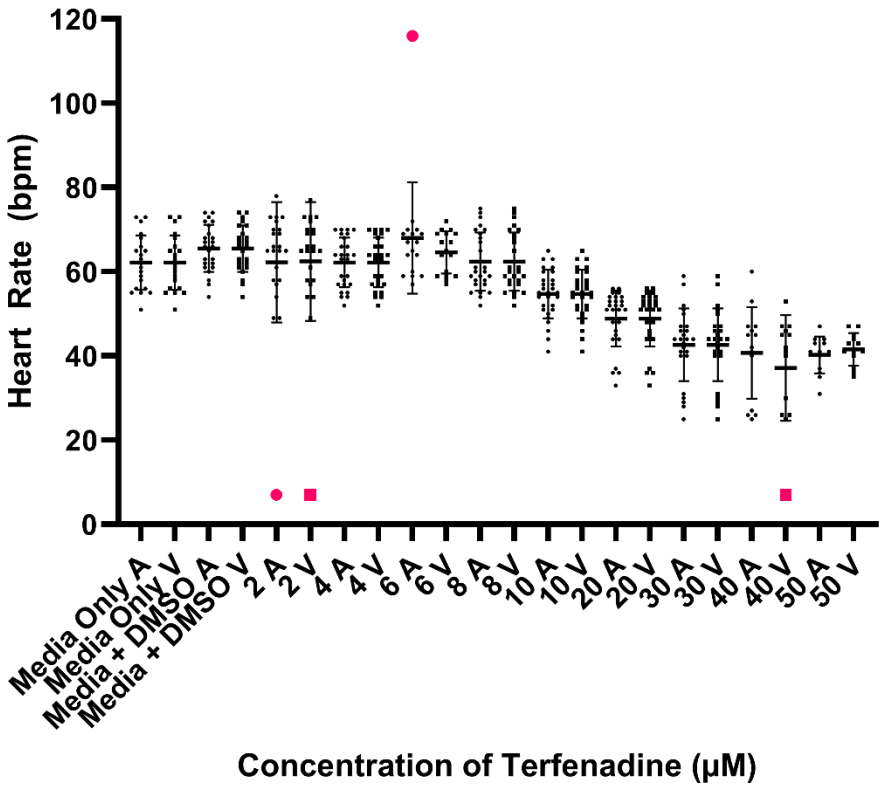

Figure 4.8: Comparison of atrial and ventricular measurements of heart rate following terfenadine exposure. *Outliers were detected using GraphPad Prism's ROUT function with Q=1% parameters and are indicated in pink on the graph. These were removed prior to performing statistical analysis.*

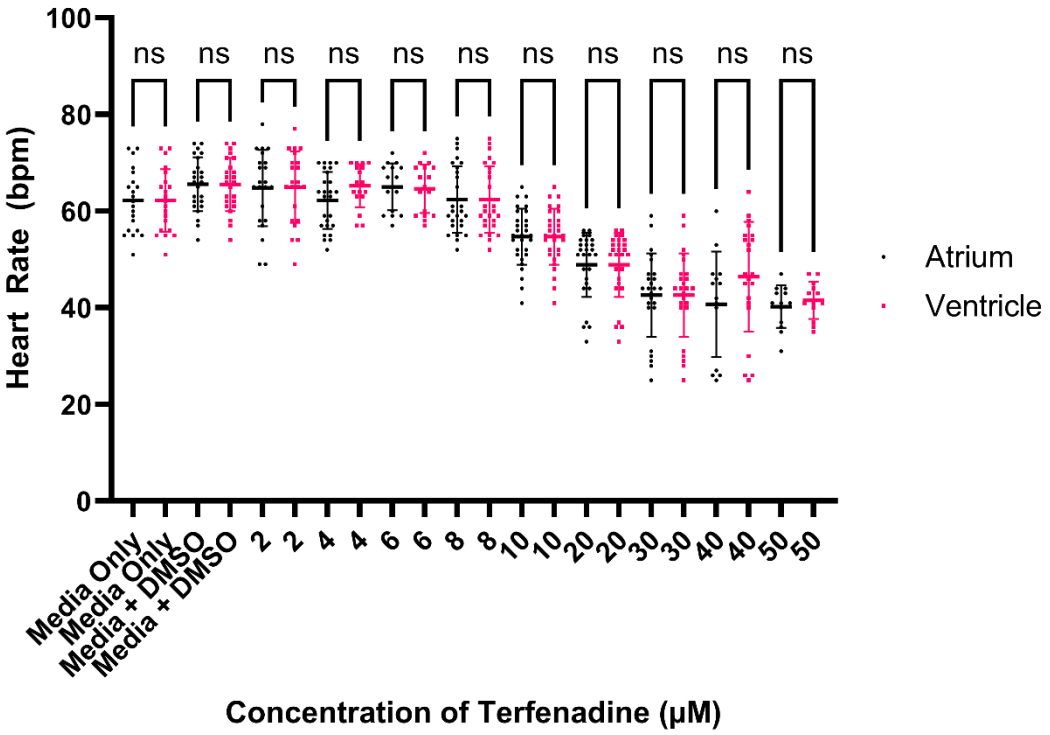

Figure 4.9: Comparison of atrial and ventricular measurements of heart rate following terfenadine exposure. *Results were analysed by one-way ANOVA with paired comparisons between each pair of chambers at each concentration.*

The last analysis undertaken was to score the heart rate graphs that were produced (see Figures 3.10 and 3.11 for examples) based on the level of arrhythmia each indicated. This was done on a blind basis, with dose identifier removed from each graph and provided in a randomised manner to the 3 scorers- one of whom was the author, one of whom was the authors PI and one of whom was a scientist without the specific knowledge of heart rates and arrhythmias to act as a 'control', with the average score being the mean of the 3. Each were provided with a primer (Figure 3.25) showing examples of what would constitute no arrhythmia, mild, medium and strong arrhythmia and asked to numerically score each graph on this basis (scores of 0, 1, 2 and 3 respectively). The intention for this analysis was to understand how subjective an arrhythmia diagnosis would be based on manual assessment of the graph.

The results showed no statistically significant differences in any group to the control, although the graph indicates a trend of the arrhythmia score increasing from around 10μM upwards; with the control having an average score of 0.79 and 20, 30, 40 and 50μM having arrhythmia scores of 0.92, 1.21, 1.35 and 1.53 respectively. With a score of 1 indicating mild arrhythmia on the scoring system, this would indicate that arrhythmia is apparent at these concentrations. These also corresponded to the concentrations in which a decrease in heart rate is observed, which supports the theory that terfenadine could be observed to cause cardiotoxicity in *Xenopus* embryos.

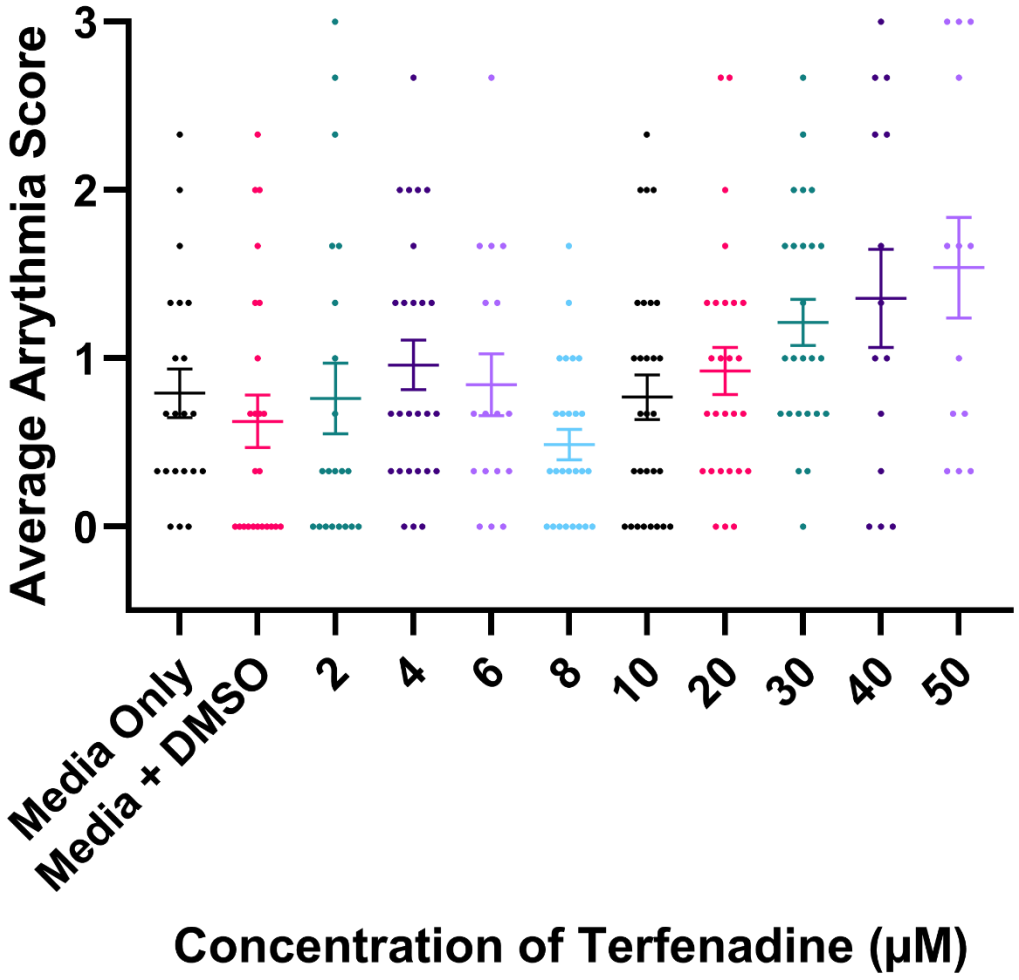

Figure 4.10: Average arrhythmia score of Xenopus embryos exposed to terfenadine. *Xenopus embryos had been treated between NF stages 38 and 45 with terfenadine and kept at 23°C, then heartbeat recorded after 15-minute treatment with MS-222. Heartbeat graphs were blind-assessed and given arrhythmia score from 0-3 (0- no arrhythmia, 1- mild arrhythmia, 2- moderate arrhythmia, 3- severe arrhythmia). Scores were then averaged and treated embryos were compared to untreated embryos (0µM) using one way ANOVA with Kruskal-Wallis multiple comparisons ($p<0.05$). Graph shows mean ± SEM.*

4.2.3 Paracetamol

When analysing the heart rate data; the atrium and ventricle were analysed individually to determine if doxorubicin concentration affected heart rate on either chamber (Figure 4.12) and then a comparison between the two was conducted (Figure 4.14) to assess if the changes, if any, were isolated to a specific chamber or present across both- some forms of cardiotoxicity are noted to occur more frequently in the atrium or the ventricle, and a comparison between the two chambers may show this.

The results presented here indicate that paracetamol did not generally appear to cause cardiotoxicity; with the alteration in heart rate seen at 1mM being an unusual and unexpected result, as paracetamol is not known to cause cardiotoxicity, and this was the lowest concentration the embryos were exposed. With that considered, if the change in heart rate was due to cardiotoxicity the change in heart rate would have been expected to be replicated across higher concentrations- this did not happen.

There were no significant differences in the arrhythmia detected and although there was some variation as the arrhythmia score seemed to decrease at the 2mM concentration, they all remained well below a score of 1, meaning most of the data were given a score of 0- no arrhythmia. These results supported the use of paracetamol as a negative control drug for this study as it supported the literature findings that it did not cause cardiotoxicity, while also being a known cause of hepatotoxicity in *Xenopus* embryos (Saide *et al*., 2019).

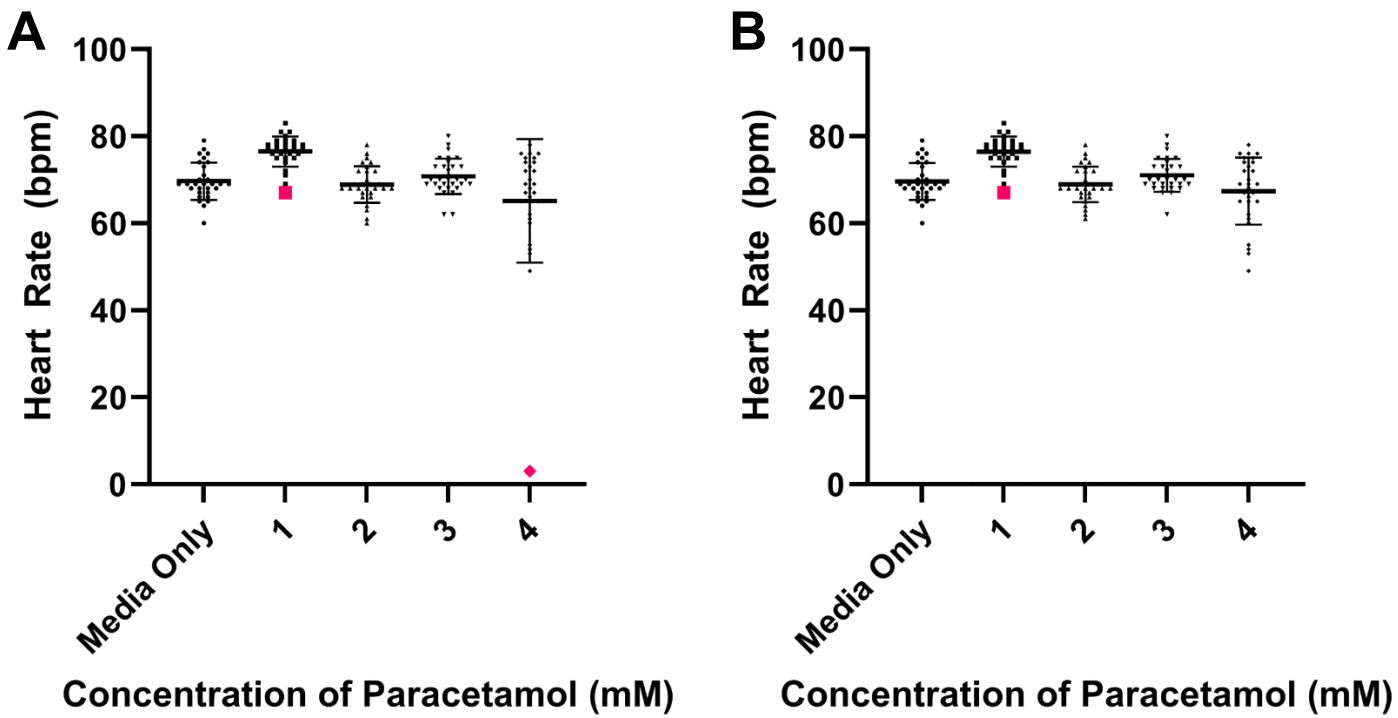

Figure 4.11: Heart rate of Xenopus embryos exposed to paracetamol including outliers. *Xenopus embryos had been treated between NF stages 38 and 45 with paracetamol and kept at 23°C, then atrial (A) and ventricular (B) heart rate measured after 15-minute treatment with MS-222 by determining number of times the heart had beat for 30 seconds and adjusted into beats per minute. Outliers were detected using GraphPad Prism's ROUT function with Q=1% parameters and are indicated in pink on the graph. These were removed prior to performing statistical analysis.*

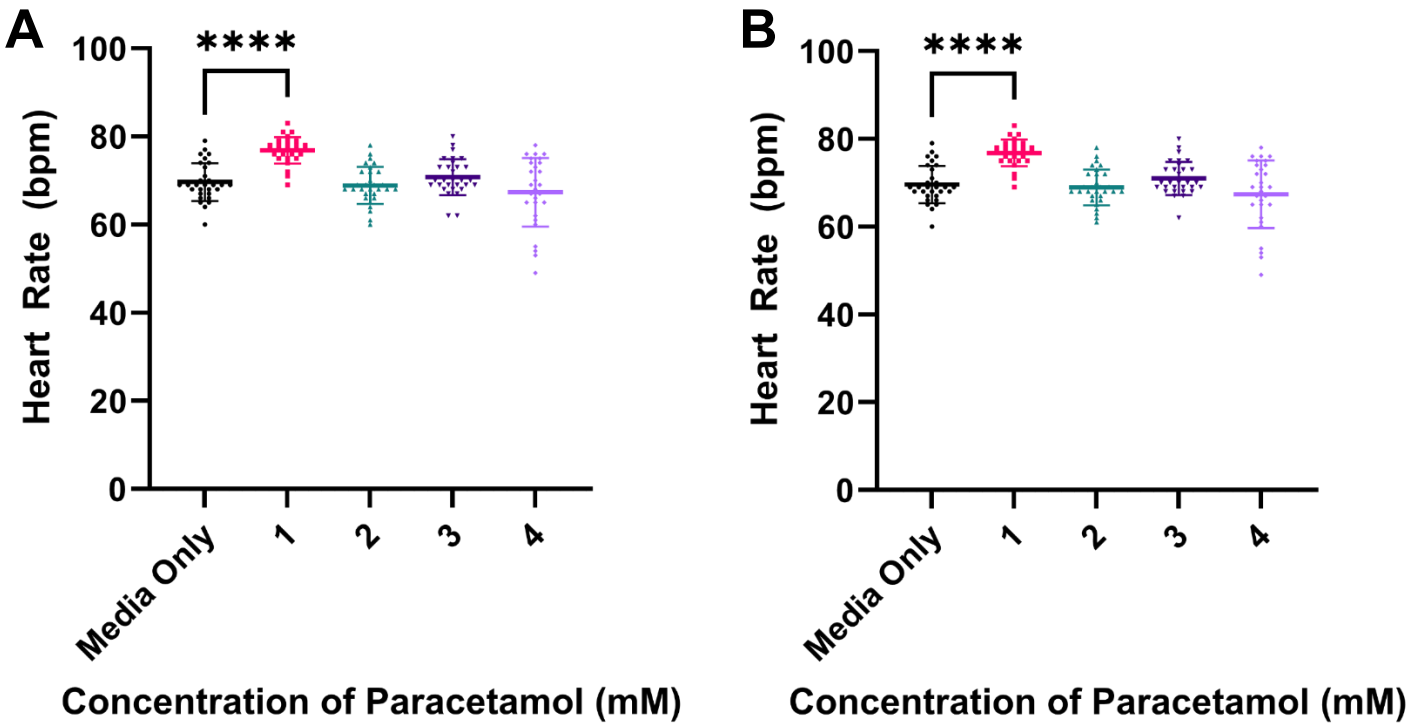

Figure 4.12: Heart rate of Xenopus embryos exposed to paracetamol. *Xenopus embryos had been treated between NF stages 38 and 45 with paracetamol and kept at 23°C, then atrial (A) and ventricular (B) heart rate measured after 15-minute treatment with MS-222 by determining number of times the heart had beat for 30 seconds and adjusted into beats per minute. Average atrial heart rate ± SD of treated embryos was compared to untreated embryos (0mM) using one way ANOVA (****= p<0.0001). At least 3 repeats were performed for an n=30.*

The heart rate data following paracetamol exposure indicated a significant increase in heart rate in the atrium and ventricle at 1mM ($p<0.0001$). When heart chamber comparison is performed there was no significant difference at any concentration.

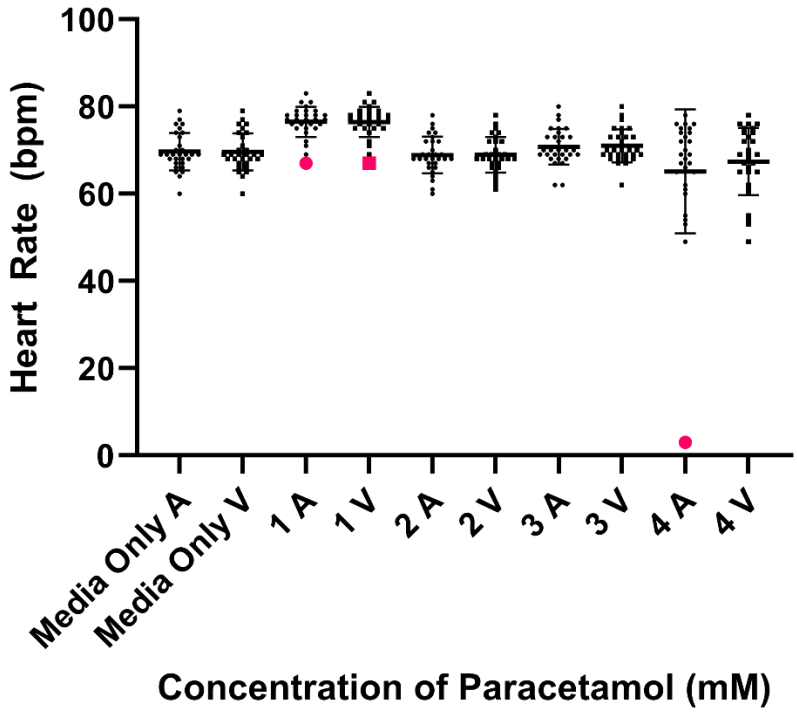

Figure 4.13: Comparison of atrial and ventricular measurements of heart rate following paracetamol exposure. *Outliers were detected using GraphPad Prism's ROUT function with Q=1% parameters and are indicated in pink on the graph. These were removed prior to performing statistical analysis.*

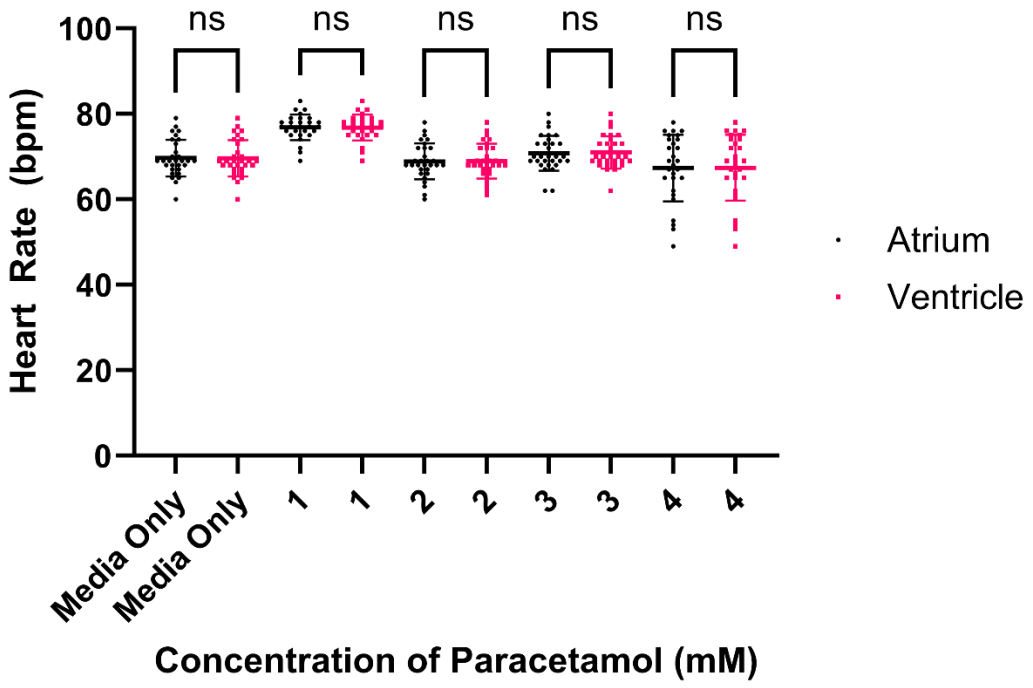

Figure 4.14: Comparison of atrial and ventricular measurements of heart rate following paracetamol exposure. *Results were analysed by one-way ANOVA with paired comparisons between each pair of chambers at each concentration.*

The last analysis undertaken was to score the heart rate graphs that were produced (see Figure 3.1 for examples) based on the level of arrhythmia each indicated. This was done on a blind basis, with dose identifier removed from each graph and provided in a randomised manner to the 3 scorers- one of whom was the author, one of whom was the authors PI and one of whom was a scientist without the specific knowledge of heart rates and arrhythmias to act as a 'control', with the average score being the mean of the 3. Each were provided with a primer (Appendix B) showing examples of what would constitute no arrhythmia, mild, medium and strong arrhythmia and asked to numerically score each graph on this basis (scores of 0,1,2 and 3 respectively). The intention for this analysis was to understand how subjective an arrhythmia diagnosis would be based on manual assessment of the graph.

The results showed no statistically significant differences in any group to the control, although there appears to be a reduction in score around the 2mM concentration. The overall score for this drug remains below 1, indicating that most of the data were consistently scored at 0 for no arrhythmia present. This result was anticipated as paracetamol is not known to cause cardiotoxicity and as such no arrhythmia was expected to be present.

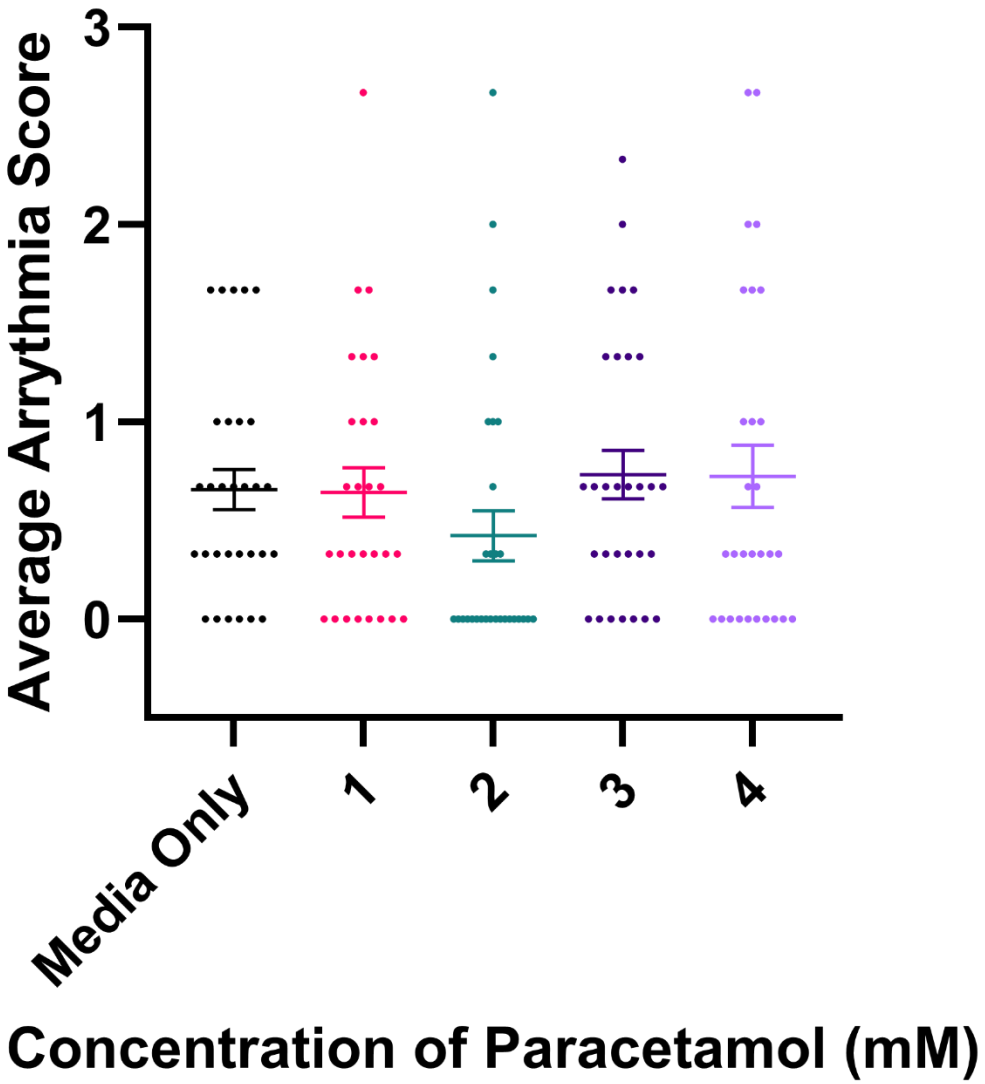

Figure 4.15: Average arrhythmia score of Xenopus embryos exposed to paracetamol. *Xenopus embryos had been treated between NF stages 38 and 45 with paracetamol and kept at 23°C, then heartbeat recorded after 15-minute treatment with MS-222. Heartbeat graphs were blind-assessed and given arrhythmia score from 0-3 (0- no arrhythmia, 1- mild arrhythmia, 2- moderate arrhythmia, 3- severe arrhythmia). Scores were then averaged and treated embryos were compared to untreated embryos (0μM) using one way ANOVA with Kruskal-Wallis multiple comparisons. Graph shows mean ± SEM.*

4.2.4 Paclitaxel

When analysing the heart rate data; the atrium and ventricle were analysed individually to determine if doxorubicin concentration affected heart rate on either chamber (Figures 3.21 and 3.22) and then a comparison between the two were conducted (Figure 3.23) to assess if the changes, if any, were isolated to a specific chamber or present across both- some forms of cardiotoxicity are noted to occur more frequently in the atrium or the ventricle, and a comparison between the two chambers may show this.

These results indicate that although paclitaxel appeared to cause toxicity due to the reduction in survival as the concentration increased (Figure 3.20), this did not appear to be cardiotoxicity as there had been no change in heart rate determined, either individually (Figures 3.21 and 3.22) or through heart chamber comparison (Figure 3.23). This was unexpected as the cardiotoxic effects of paclitaxel were quite well documented in the literature (Osman and Elkady, 2017; Pizzino et al., 2014; Valiyaveettil et al., 2023). One possible reason for this could be that the drug is not metabolised by *Xenopus* the same way that it is metabolised by humans and mammalian models and as such this is why it doesn't appear to have cardiotoxic effects. This could be addressed in future research by determining if the metabolites of the drug are present after initial exposure, something that was considered but due to the time and facility limitations was beyond the scope of this study.

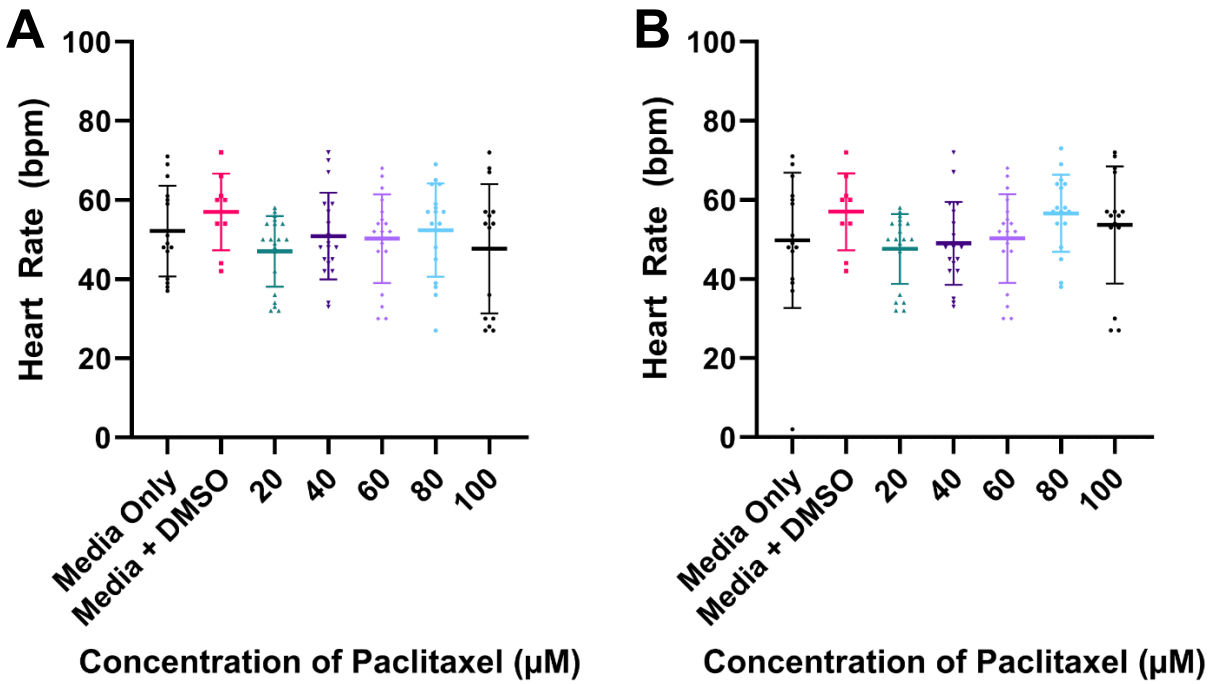

Figure 4.16: Heart rate of Xenopus embryos exposed to paclitaxel. *Xenopus embryos had been treated between NF stages 38 and 45 with paclitaxel and kept at 23°C, then atrial (A) and ventricular (B) heart rate measured after 15-minute treatment with MS-222 by determining number of times the heart had beat for 30 seconds and adjusted into beats per minute. Outliers were detected using GraphPad Prism's ROUT function with Q=1% parameters and none were present in the data. Average atrial heart rate ± SD of treated embryos was compared to untreated embryos (0µM) using one way ANOVA. 3 biological repeats of approximately 5 embryos were used in this experiment, n=15.*

The heart rate data following paracetamol exposure indicated a significant increase in heart rate in the atrium and ventricle at 1mM ($p<0.0001$). When heart chamber comparison was performed there was no significant difference at any concentration.

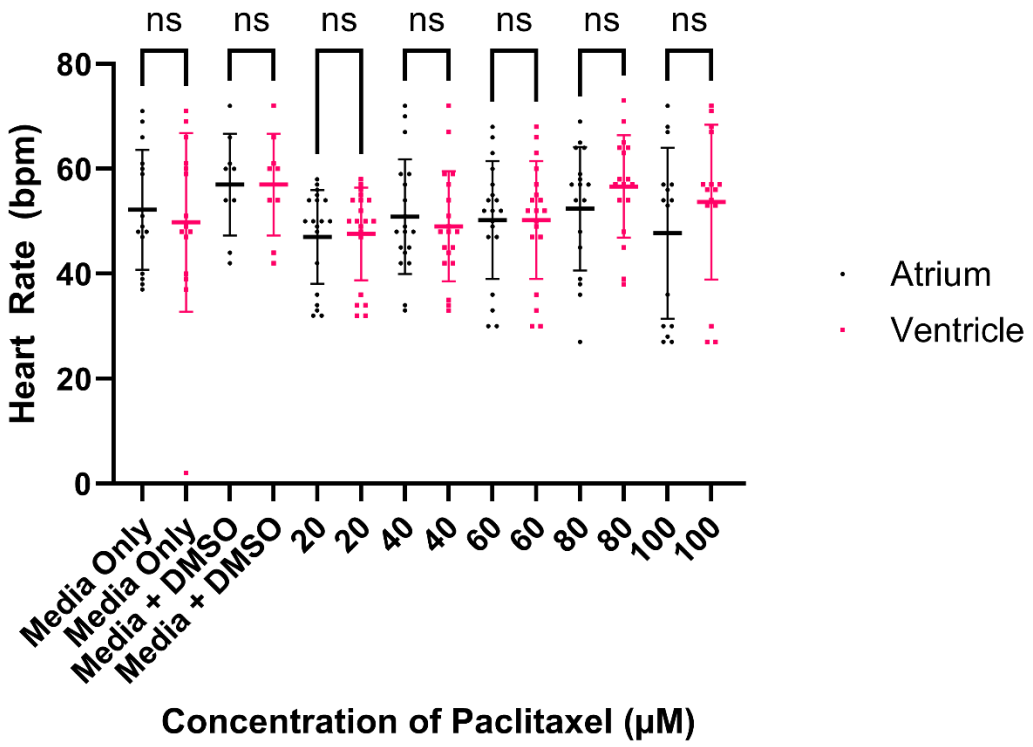

Figure 4.17: Comparison of atrial and ventricular measurements of heart rate following paclitaxel exposure. *Results were analysed by one-way ANOVA with paired comparisons between each pair of chambers at each concentration.*

4.2.5 E4031

When analysing the heart rate data; the atrium and ventricle were analysed individually to determine if doxorubicin concentration affected heart rate on either chamber (Figures 3.24 and 3.25) and then a comparison between the two was conducted (Figure 3.26) to assess if the changes, if any, were isolated to a specific chamber or present across both- some forms of cardiotoxicity are noted to occur more frequently in the atrium or the ventricle, and a comparison between the two chambers may show this.

The results shown in Section 3.5.5 suggested that there was some evidence that E4031 may cause cardiotoxicity in *Xenopus* embryos. In both atrium and ventricle there was a significant reduction in heart rate compared to the control at 40 and 80μM concentrations (Figures 3.24 and 3.25), but not at any other concentration and there was no significant difference in heart rate between the cardiac chambers at any concentration. Unfortunately, as no survival curve was performed it is not known if the concentrations used were within the physiological range for the embryos.

The fact that only two of the concentrations studied, one at the mid-range and one at the high-end of exposure levels were found to cause a reduction in heart rate does not present a clear explanation of the effect E4031 has on *Xenopus* embryos. In other drugs studied such as terfenadine (Section 3.5.2), there was a clear and consistent pattern that after a certain concentration, it and all other higher concentrations led to a decrease in heart rate which indicated a consistent effect of the drug on the embryos. The scattered effects shown by E4031 exposure may indicate that if E4031 is triggering a reduction in heart rate the effects are inconsistent and may not be wholly suggestive of sustained cardiac damage but could be caused by generalised toxicity from another cause- a dead embryo poisoning the growth media is one potential explanation. Another point of note is that the biological repeats for this experiment consisted of around five embryos being

measured at a time, which may not provide a strong enough dataset to be fully confident in the statistics conducted.

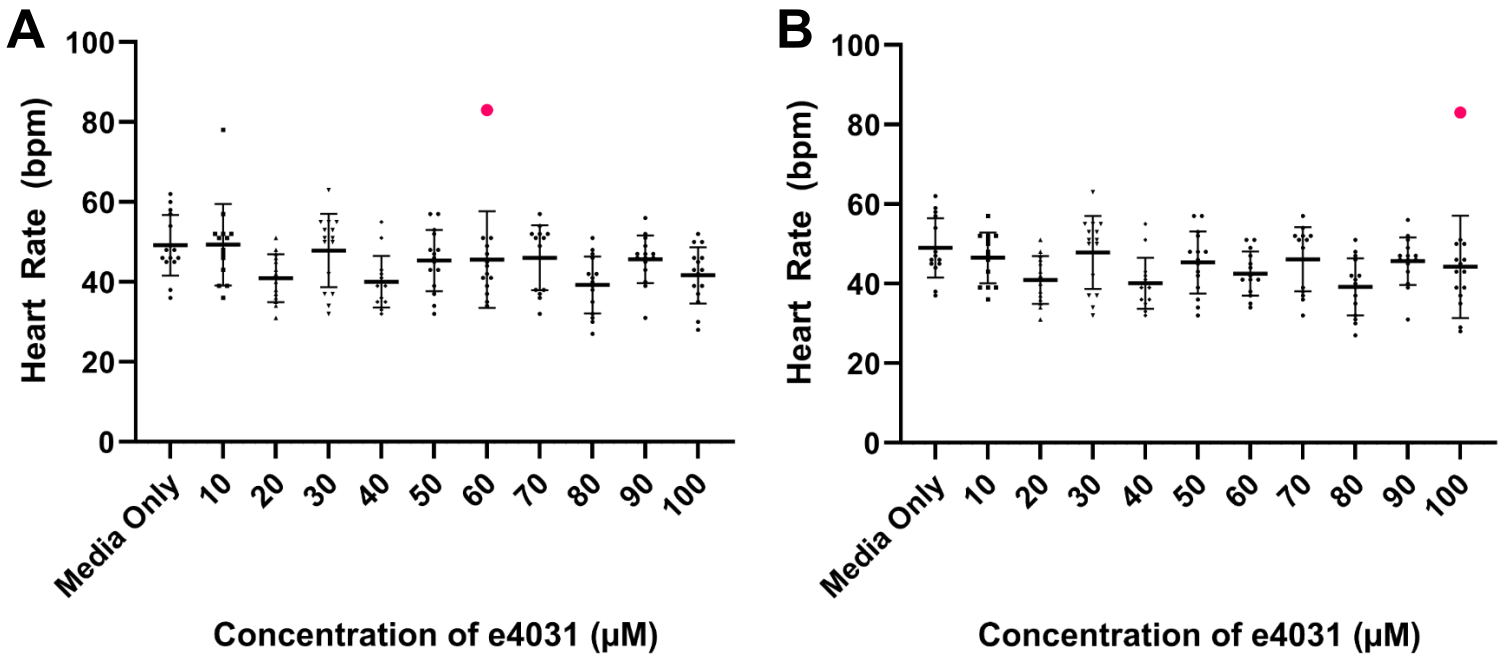

Figure 4.18: Heart rate of Xenopus embryos exposed to E4031 including outliers. *Xenopus embryos had been treated between NF stages 38 and 45 with E4031 and kept at 23°C, then atrial (A) and ventricular (B) heart rate measured after 15-minute treatment with MS-222 by determining number of times the heart had beat for 30 seconds and adjusted into beats per minute. Outliers were detected using GraphPad Prism's ROUT function with Q=1% parameters and are indicated in pink on the graph. These were removed prior to performing statistical analysis.*

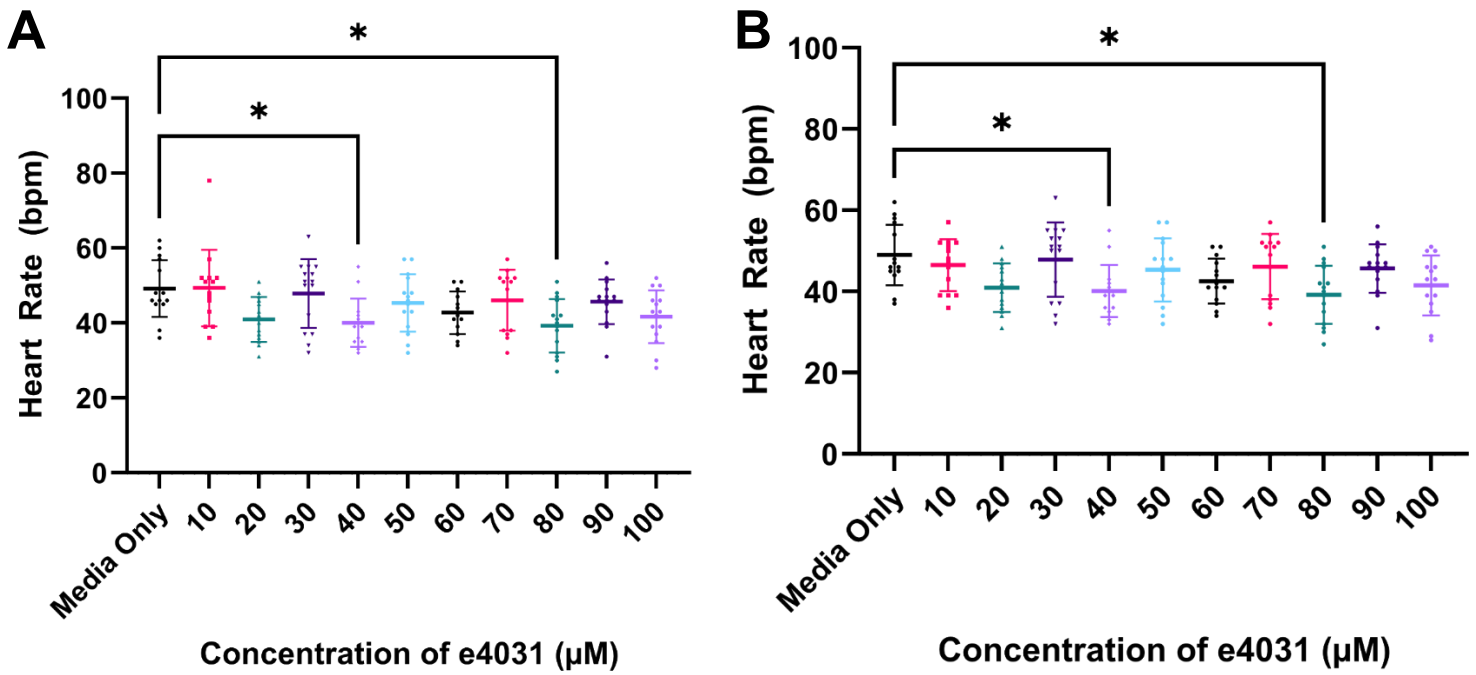

Figure 4.19: Heart rate of Xenopus embryos exposed to E4031. *Xenopus embryos had been treated between NF stages 38 and 45 with E4031 and kept at 23°C, then atrial (A) and ventricular (B) heart rate measured after 15-minute treatment with MS-222 by determining number of times the heart had beat for 30 seconds and adjusted into beats per minute. Average atrial heart rate ± SD of treated embryos was compared to untreated embryos (0μM) using one way ANOVA (*= $p<0.05$). 3 biological repeats of 5 embryos were used in this experiment, n=15.*

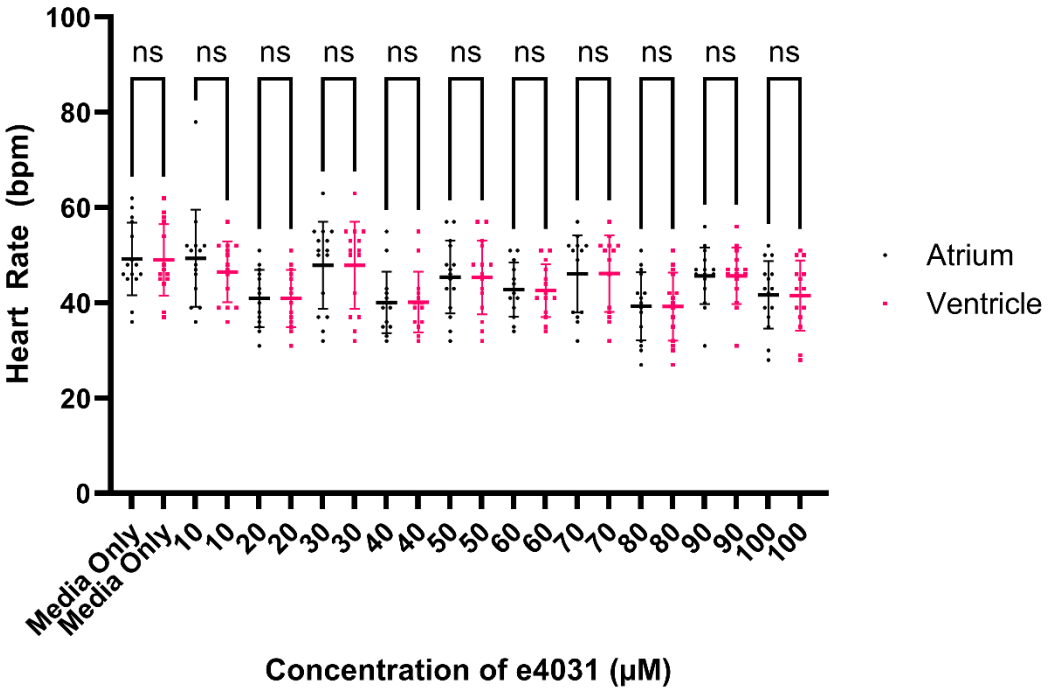

Figure 4.20: Comparison of atrial and ventricular measurements of heart rate following E4031 exposure*. Results were analysed by one-way ANOVA with paired comparisons between each pair of chambers at each concentration.*

4.3 Average Heart Rate

At the end of the study period, when all data had been gathered and analysis was in progress, it was noted that there was a lot of data collected, enough to potentially determine what the normal heart rate of a *Xenopus* embryo was. It has been mentioned throughout this report that finding heart rate data is difficult, and the information provided in the literature can be conflicting or not relevant to the stage of embryos studied.

All the data from the control/media only groups was collated together, which was a total of 228 data points. This was processed using the outlier detection tool in GraphPad, as with other data processing for the assay, which highlighted one value of 2bpm as being an outlier, so this was removed from the analysis, leaving 227 datapoints. Following further analysis using the

software, the range of heart rates seen fell between 36bpm and 96bpm. The mean heart rate for stage 45 *Xenopus* was 65.74bpm, or 66bpm when rounded to the nearest whole beat, with a standard deviation of 12.67. This is illustrated in Figure 4.21. This is provided with the caveat that this data was collected from anaesthetised embryos but provides a vital baseline for future investigation on the topic, or for researchers also working with *Xenopus* as a cardiac model.

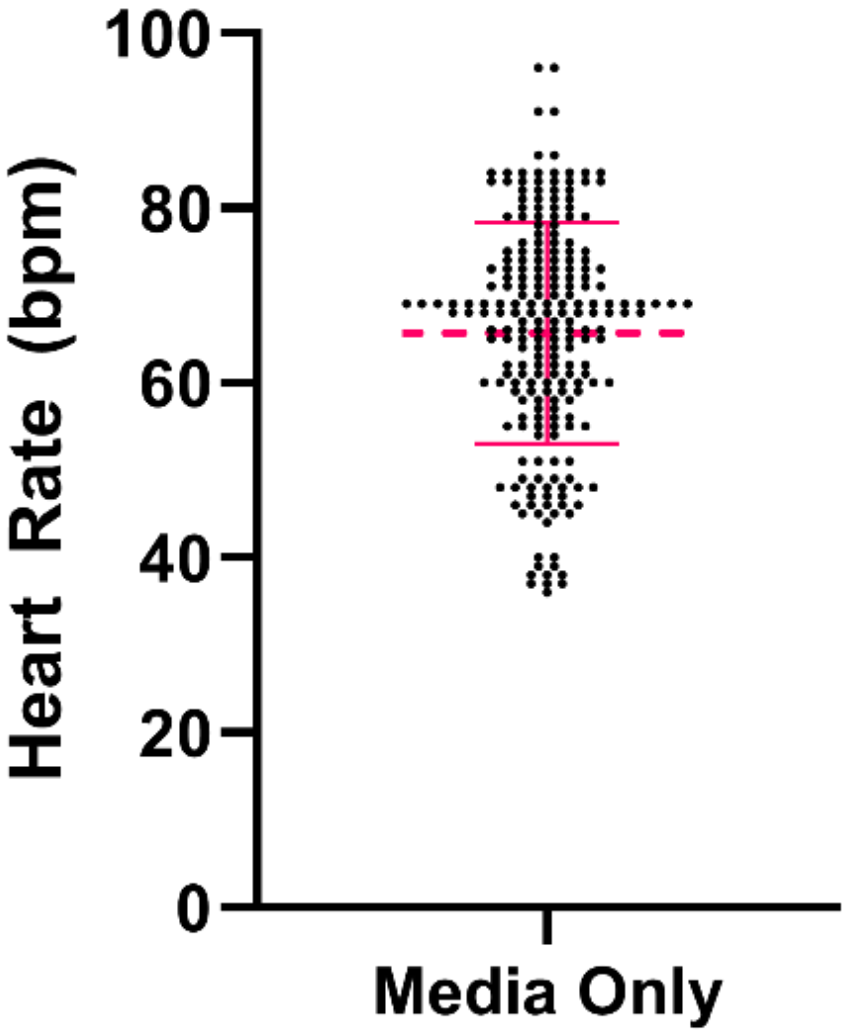

Figure 4.21 Average heart rate of NF stage 45 Xenopus laevis. *Outliers removed. Mean heart rate of 66bpm indicated with dashed pink line, and standard deviation range indicated by the solid pink line.*

4.4 Discussion

The results in this chapter were very promising for the assay, after the difficulties in development it appeared to be working well- the statistically significant changes in heart rate for the doxorubicin, terfenadine and E4031 were as anticipated, knowing these drugs were cardiotoxic it was expected that there would be an effect observed. The lack of heart rate change in paclitaxel was unexpected as cardiotoxicity following paclitaxel exposure had been well documented in the literature, as detailed previously. Paclitaxel-induced cardiotoxicity in human patients often presents as a slowed heart rate, which should have been detected by this method (Berardi et al., 2013). Additionally, the results for E4031 were inconsistent, as a reduction in heart rate was seen only at two concentrations- 40 and 80μM. This means that through this experiment there were multiple concentrations above and between these two values at which a statistically significant change in heart rate was not detected. As shown with the results from terfenadine exposure, every concentration of 20μM and higher displays a decrease in heart rate. The point at which exposure to a drug causes cardiotoxic events is typically fixed and any concentration above that would either cause the same or worse cardiotoxic effects. This would suggest that all concentrations of E4031 of 40μM and above should display reduction in heart rate and presence of cardiotoxicity, but this did not happen. There is no clear reason for this to occur, and it is an uncertainty that may be solved through further repeats or additional experimentation.

One notable issue with the assay is that it primarily focusses on heart rate and to a much lesser extent arrhythmia. This would potentially miss other manifestations of cardiotoxicity that are not constrained to heart rate, such as changes in ejection fraction (how much blood is pumped each time the heart chamber contracts). The assay could maybe be modified to measure ejection fraction as this is a measure used in human cardiac damage diagnosis. This could be done using microscope imaging and has been done in zebrafish embryos previously (Li *et al.*, 2022). This method in zebrafish has been developed to the point commercial software exists to automate the analysis

and speed up the processing of embryos (ViewPoint, France), and if a transgenic *Xenopus* can be created that produces the same GFP expression as required by zebrafish for the software to analyse, it may be possible to utilise these commercial methods for the *Xenopus* cardiac analysis.

A further marker of cardiotoxicity that was not fully explored in this study was contractility of cardiomyocytes. This is a very common feature of iPSC-based assays and being able to measure any effects *in vivo* would further help the model corroborate results seen *in vitro*. One of the advantages of exploring this as an opportunity is that there are well established methods to measure contractility and several high-throughput systems that already exist which could potentially be utilised in this model. One of these systems is MUSCLEMOTION, an open-source software developed to perform contractility measuring and identify changes in this following drug development (Sala et al., 2018). The open-source nature of the software lends itself to customisation and development to suit research needs, and the advantage for future work on this *Xenopus* method is that the authors have already developed a method of using the software to analyse in vivo zebrafish hearts and so a lot of the groundwork has already been done to prepare for modifying the system.

Another potential issue with the heart rate assay was the consistency of the computerised analysis. The initial method of sine wave fitting struggled due to the secondary curve that was present in many- but not all- of the data. The cause of the secondary curve was unknown and attempts to correct for it or to avoid it being present in the data failed. This was the main reason for changing methods to using Fourier transformations, which provided much clearer results. Very late into the writing process, the author came across work by Milan and colleagues (2011). This work devised and implemented a method of recording the ECG of adult zebrafish and during the process experienced some similar interference patterns as those found in this work. This is shown in Figure 4.22. The authors of this paper determined that their

source of interference was due to skeletal muscle movements despite the individuals being anaesthetised. Specifically, they posit that gill movement of the fish is the main contributor of the regular, sinusoidal wave pattern seen in their ECG. In *Xenopus* embryos, gills are developed and in use by NF stage 40 of development and only begin to be resorbed as part of the embryo metamorphosis project at NF stage 46 and beyond. This means that during the imaging for the heart rate assay used in this project, gill movement could be a contributing factor to the secondary wave seen in the results. The exact mechanism the gills would cause this interference is unknown, as the measure outputs are different, with this assay measuring blood passage in and out of the heart chambers. Despite further reading on the subject, the author of this report was unable to find clear instruction on how the data was normalised and analysed in this process and so was unable to attempt processing of the data generated for this report using the methodology noted in Milan *et al.* (2011).

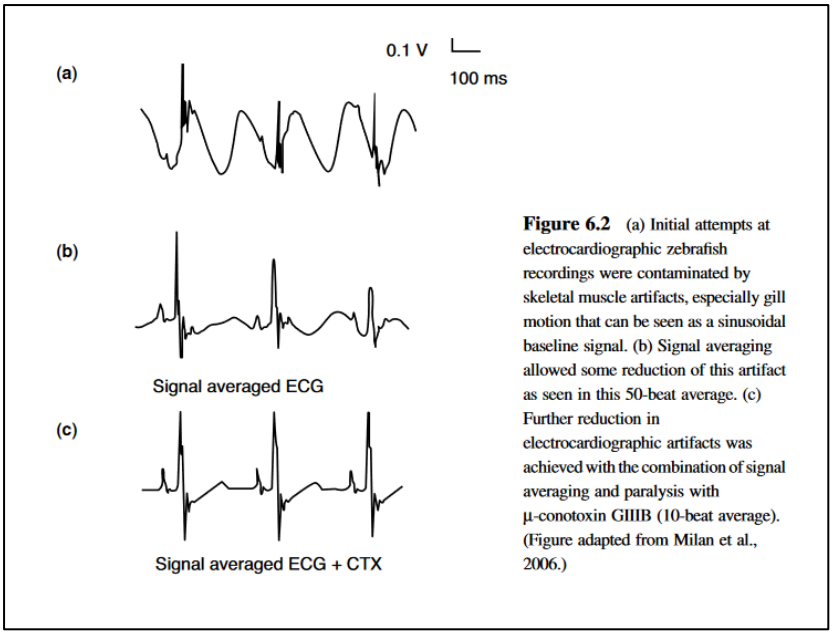

Figure 6.2 (a) Initial attempts at electrocardiographic zebrafish recordings were contaminated by skeletal muscle artifacts, especially gill motion that can be seen as a sinusoidal baseline signal. (b) Signal averaging allowed some reduction of this artifact as seen in this 50-beat average. (c) Further reduction in electrocardiographic artifacts was achieved with the combination of signal averaging and paralysis with μ-conotoxin GIIIB (10-beat average). (Figure adapted from Milan et al., 2006.)

Figure 4.22: ECG of anaesthetised adult zebrafish. *Sine wave contamination shown clearly in A, with similar appearance to that seen in this projects heart rate assay. Methods to remove these artefacts are shown in B and C. Taken from Milan et al. (2011).*

Additional caveats with the data obtained within this chapters' work that need to be considered include the reduction of data obtained at the highest concentrations of drug exposure. Using doxorubicin as an example; while the control group had excellent survival rates (reflected in Figure 3.5), at the highest concentrations where embryos were able to survive, the survival rate plummeted to around 25%. With only around a quarter of embryos surviving, this impacted the number of data points available for analysis. Using the same example, while the same number of embryos were exposed to the drug at each concentration initially, the increased death rate means the highest concentrations only had 16 and 8 datapoints respectively. This lends some uncertainty to the results obtained from a statistical standpoint, but by the same token the increase in deaths served as a form of proof of toxicity, although if this counts as acute or chronic toxicity is up for debate.

The determination of an average heart rate for NF stage 45 *Xenopus laevis* embryos represents a distinct addition to wider knowledge, as throughout the previous chapters it has been noted on several occasions that much of the research into *Xenopus* has not been done at this stage, and nobody had attempted to measure heart rate at this specific stage. This information will hopefully be useful for future cardiac research in *Xenopus laevis*.

Chapter 5 Biomarker Analysis

5.1 Introduction

The aim of the research conducted in this chapter was to determine if cardiotoxicity could be determined through analysing miRNAs selected as biomarkers of cardiotoxicity using a qRT-PCR assay. This method used the same drugs utilised in the previous chapter for consistency, and with the intention to streamline the process when scaled up as embryos could be imaged for the heart rate assay then harvested for the biomarker assay, maximising the amount of data gathered from each embryo and reducing the overall number of embryos used in the process.

5.2 Individual drug exposure outcomes

5.2.1 Doxorubicin

The results for doxorubicin exposure were mixed (Figure 5.1); the data for miR-208 being particularly poor quality, with lack of detection across all tail samples and many head samples in which there should have been strong detection. miR-499 results show a potential effect of doxorubicin exposure with the detection levels dropping off considerably at the higher concentrations of 80 and 100μM after appearing to rise in the mid-range concentrations from the control. miR-143 showed poor results with an absence of detection across multiple samples and very low levels of detection in the few it was present in. It is possible that miR-143 is genuinely expressed at very low levels in *Xenopus* embryos, which would be problematic in its use as a biomarker as at such low levels of detection it is difficult to see a change in the levels of miRNA detected. U6RNA was detected across most samples and the levels of detection vary greatly from sample to sample, which indicates that the suspicions surrounding U6 being a poor choice for housekeeping discussed in Section 3.8.3 may have been correct, and as such the decision to change the housekeeping gene to 5SRNA appears to have been a sensible option. miR-122 was detected in the head sample and not the tail sample for the control, which was as expected. It was consistently detected in other head samples but at very

varied levels and surprisingly detected also in tail samples at the 20 and 40μM concentrations. miR-103 was detected in all samples at varying levels but there appears to be a trend in a reduction of detection at the highest concentrations which could potentially be linked to cardiotoxicity.

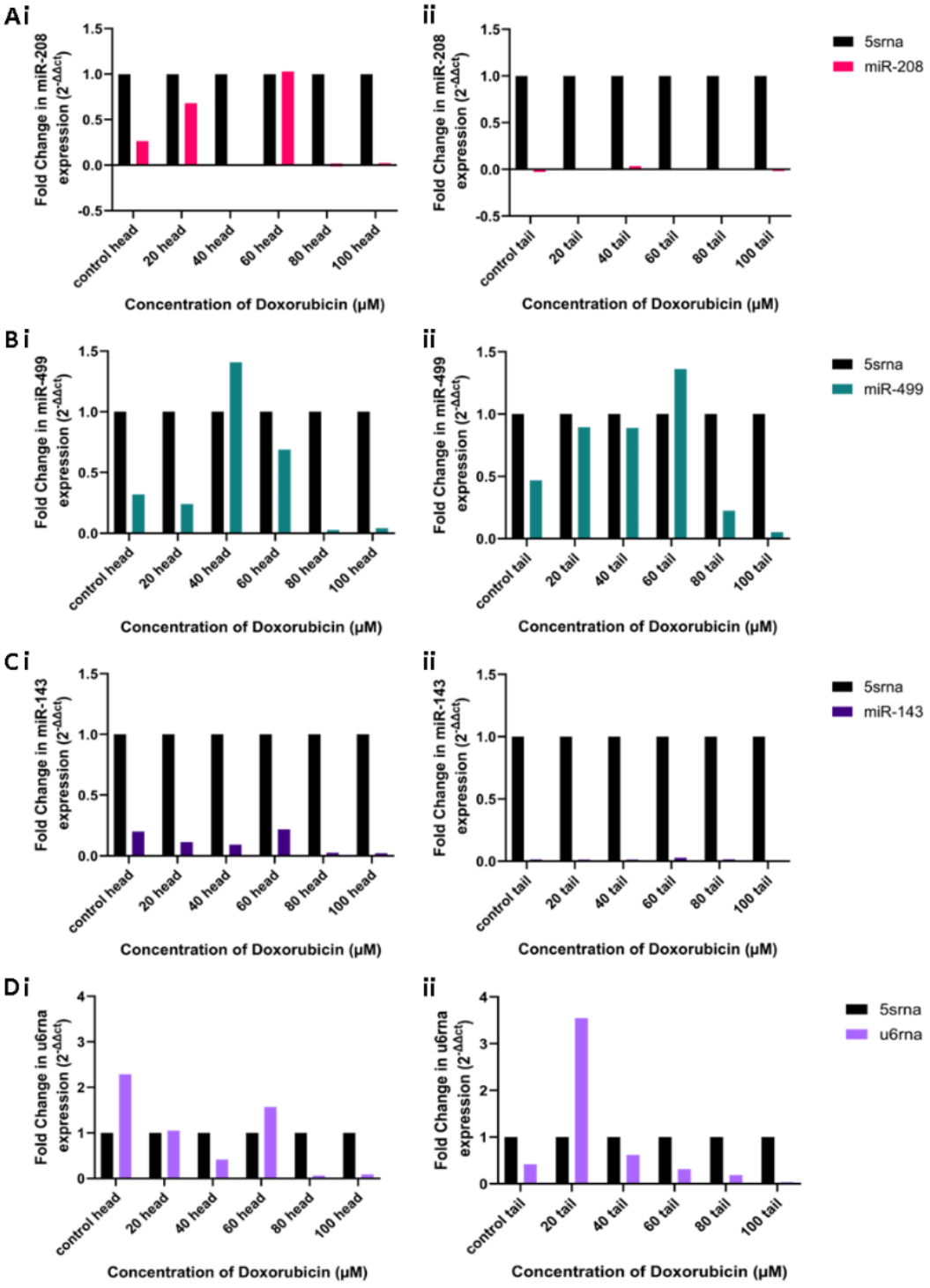
Ai
ii
Fold Change in miR-208 expression ($2^{-\Delta\Delta ct}$)
1.5
1.0
0.5
0.0
-0.5
control head
20 head
40 head
60 head
80 head
100 head
control tail
20 tail
40 tail
60 tail
80 tail
100 tail
Concentration of Doxorubicin (μM)
5srna
miR-208
Bi
ii
Fold Change in miR-499 expression ($2^{-\Delta\Delta ct}$)
miR-499
Ci
ii
Fold Change in miR-143 expression ($2^{-\Delta\Delta ct}$)
miR-143
Di
ii
Fold Change in u6rna expression ($2^{-\Delta\Delta ct}$)
4
3
2
1
0
u6rna

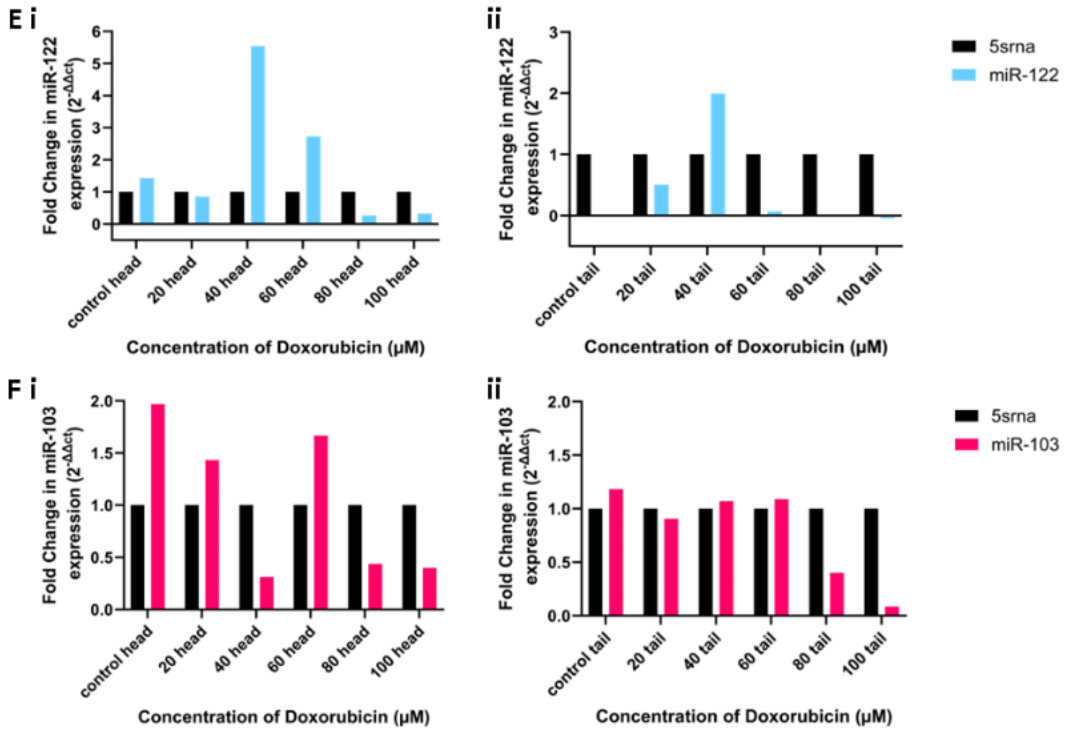

Figure 5.1: Expression levels of multiple miRNAs and U6RNA in Xenopus embryos exposed to doxorubicin. *Embryos were exposed to doxorubicin (0-100μM) at NF stage 38 and harvested at NF stage 45; with 15 embryos being sampled and pooled per biological repeat. The expression of each biomarker was measured using qRT-PCR and normalised against the head sample of the untreated embryos, using 5S RNA as a housekeeping marker. 2 biological repeats were conducted so statistics were unable to be performed.* ***A****- miR-208 expression.* ***B****- miR-499 expression.* ***C****- miR-143 expression.* ***D****- U6RNA expression.* ***E****- miR-122 expression.* ***F****- miR-103 expression. Head samples are shown in graph i for each biomarker, and tail samples are shown in graph ii for each biomarker.*

5.2.2 Terfenadine

Extremely high levels of miR-208 were detected in head samples for the vehicle control, 10 and 40μM (Figure 5.2). These high levels make it difficult to assess the much lower levels of detection in the other concentrations studied, but it is clear enough that miR-208 was detected in both control tail samples and many of the drug-containing tail samples. As miR-208 is found in the heart, it should not have been detected in the tail samples unless cardiac damage had taken place. This could indicate problems with the embryos used in the experiment, potentially already having suffered cardiac damage without drug exposure. As a result, these results are presented with low confidence of their accuracy. miR-499 was consistently detected in all samples except the tail sample at the highest concentration (100μM). The levels of detection increased in the 30μM samples and above, which could be a potential indication of cardiotoxicity. miR-143 was consistently detected across all head samples but again had very variable levels of detection, with values peaking at the 40 and 50μM head samples. This could possibly be linked to cardiotoxicity occurring but the lack of consistency across the head and tail samples and the noted lack of biological repeats prohibits any concrete conclusions being made. U6RNA detection was varied across all samples with a large spike in the 50μM head sample, which again indicated the decision to move away from U6RNA as a housekeeping choice was made on a sound basis. miR-122 had some interesting results, as there was detection in the head sample of the control concentration and not in the tail as would be expected from a sample of healthy *Xenopus* embryos while in the highest concentration of 50μM there was massively increased detection in the head sample and some detection in the tail sample, albeit quite low. This could be a very strong indication of hepatotoxicity, the only caveat being that terfenadine is not known to be a hepatotoxic drug, so potentially this was a sign of more generalised toxicity. One potential explanation however could be noted in the increase in miR-122 detection noted in the vehicle control sample- it is possible that the vehicle used to enable terfenadine to become soluble in the water-based growth media (DMSO) is responsible for this increase and may potentially be hepatotoxic. This potential confounding factor is further explored in Section 4.6. miR-103 levels appeared to increase

as the concentration of terfenadine increased, with notable increases after 30μM exposure.

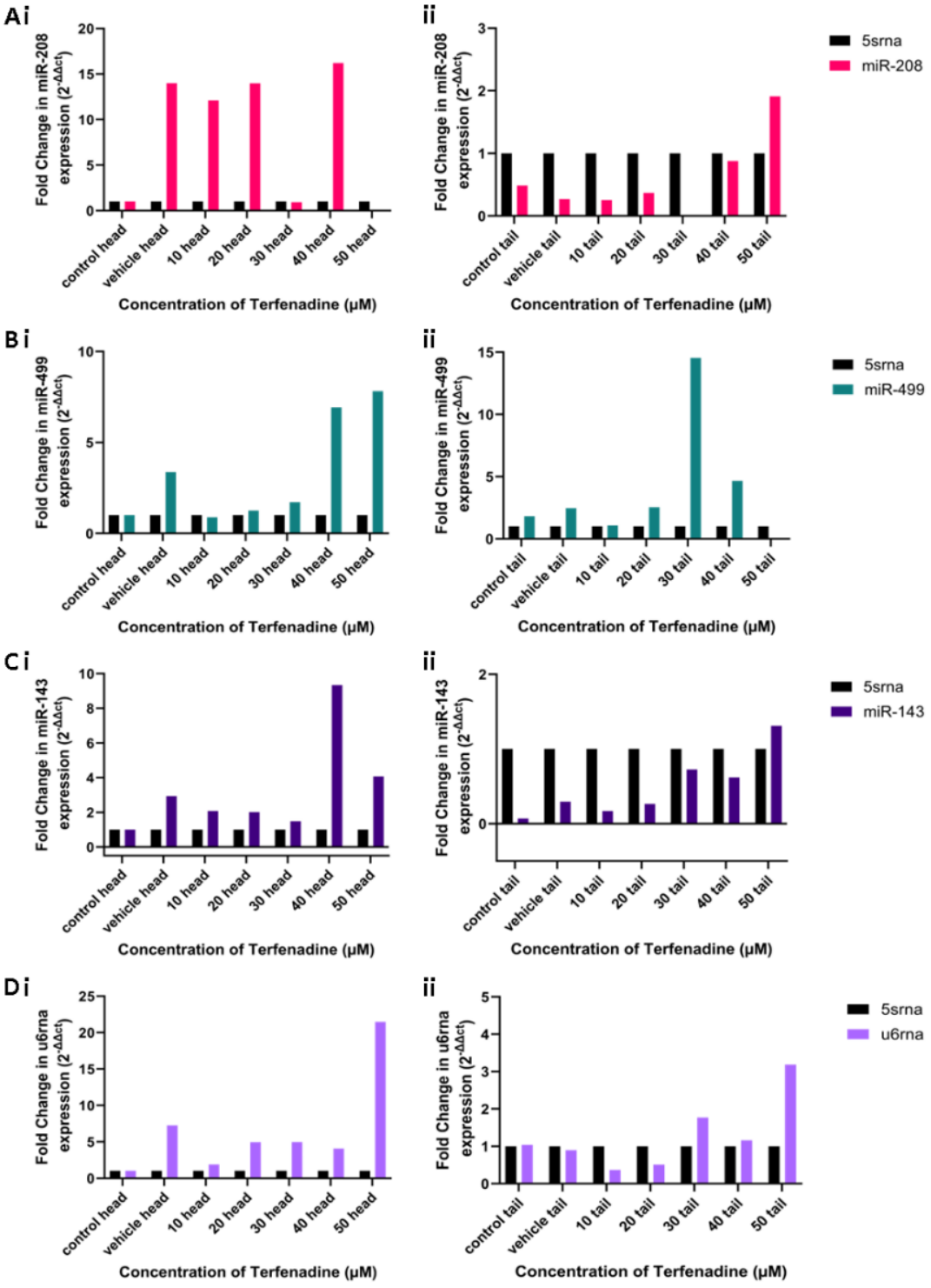
Ai
Fold Change in miR-208 expression ($2^{-\Delta\Delta ct}$)
20
15
10
5
0
control head
vehicle head
10 head
20 head
30 head
40 head
50 head
Concentration of Terfenadine (μM)
ii
Fold Change in miR-208 expression ($2^{-\Delta\Delta ct}$)
3
2
1
0
control tail
vehicle tail
10 tail
20 tail
30 tail
40 tail
50 tail
Concentration of Terfenadine (μM)
5srna
miR-208
Bi
Fold Change in miR-499 expression ($2^{-\Delta\Delta ct}$)
10
5
0
control head
vehicle head
10 head
20 head
30 head
40 head
50 head
Concentration of Terfenadine (μM)
ii
Fold Change in miR-499 expression ($2^{-\Delta\Delta ct}$)
15
10
5
0
control tail
vehicle tail
10 tail
20 tail
30 tail
40 tail
50 tail
Concentration of Terfenadine (μM)
5srna
miR-499
Ci
Fold Change in miR-143 expression ($2^{-\Delta\Delta ct}$)
10
8
6
4
2
0
control head
vehicle head
10 head
20 head
30 head
40 head
50 head
Concentration of Terfenadine (μM)
ii
Fold Change in miR-143 expression ($2^{-\Delta\Delta ct}$)
2
0
control tail
vehicle tail
10 tail
20 tail
30 tail
40 tail
50 tail
Concentration of Terfenadine (μM)
5srna
miR-143
Di
Fold Change in u6rna expression ($2^{-\Delta\Delta ct}$)
25
20
15
10
5
0
control head
vehicle head
10 head
20 head
30 head
40 head
50 head
Concentration of Terfenadine (μM)
ii
Fold Change in u6rna expression ($2^{-\Delta\Delta ct}$)
5
4
3
2
1
0
control tail
vehicle tail
10 tail
20 tail
30 tail
40 tail
50 tail
Concentration of Terfenadine (μM)
5srna
u6rna

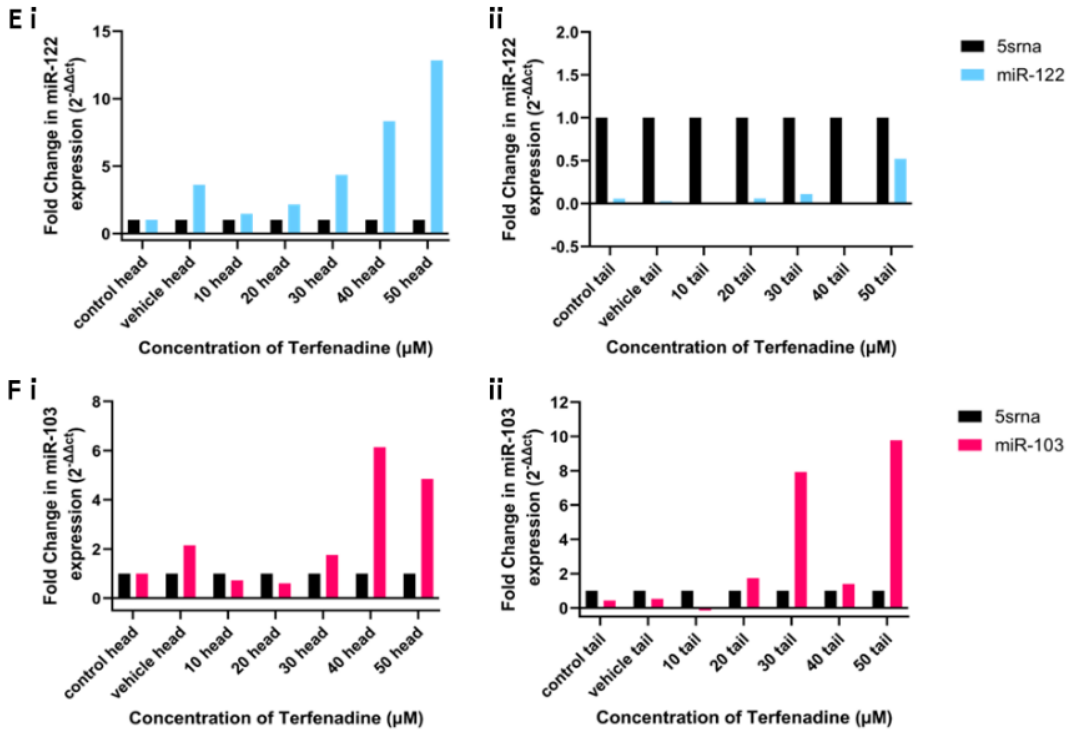

Figure 5.2: Expression levels of multiple miRNAs and U6RNA in Xenopus embryos exposed to terfenadine. *Embryos were exposed to doxorubicin (0-50μM) at NF stage 38 and harvested at NF stage 45; with 15 embryos being sampled and pooled per biological repeat. The expression of each biomarker was measured using qRT-PCR and normalised against the head sample of the untreated embryos, using 5S RNA as a housekeeping marker. 1 biological repeat was performed so statistics were unable to be performed.* ***A****- miR-208 expression.* ***B****- miR-499 expression.* ***C****- miR-143 expression.* ***D****- U6RNA expression.* ***E****- miR-122 expression.* ***F****- miR-103 expression. Head samples are shown in graph i for each biomarker, and tail samples are shown in graph ii for each biomarker.*

5.2.3 Paracetamol

miR-208 detection levels were very varied, with no consistent detection across the head samples as would be expected due to the presence of the heart in those samples (Figure 5.3). The tail samples were consistently at zero detection however, which matches the expectations for this miRNA. miR-499 was present and detected at very low levels throughout the concentrations of paracetamol used in the study; the levels were so low that no real conclusions or suggestions can be drawn from this data. This situation repeated for miR-143, U6RNA and miR-103 as the detected levels varied and are very low when they were detected. In an ideal experiment given that the drug used here is paracetamol, miR-122 would be present in all head samples and present at the higher concentrations in the tail samples as well, where hepatoxicity would have occurred. This did not happen in this experiment, with detection present across all head samples but at varied, low levels, and no detection in tail samples. It is possible that the explanation for this is simply the fact that no hepatotoxicity occurred, but this would mean a failure to recapitulate the results found previously by Saide *et al*. (2019).

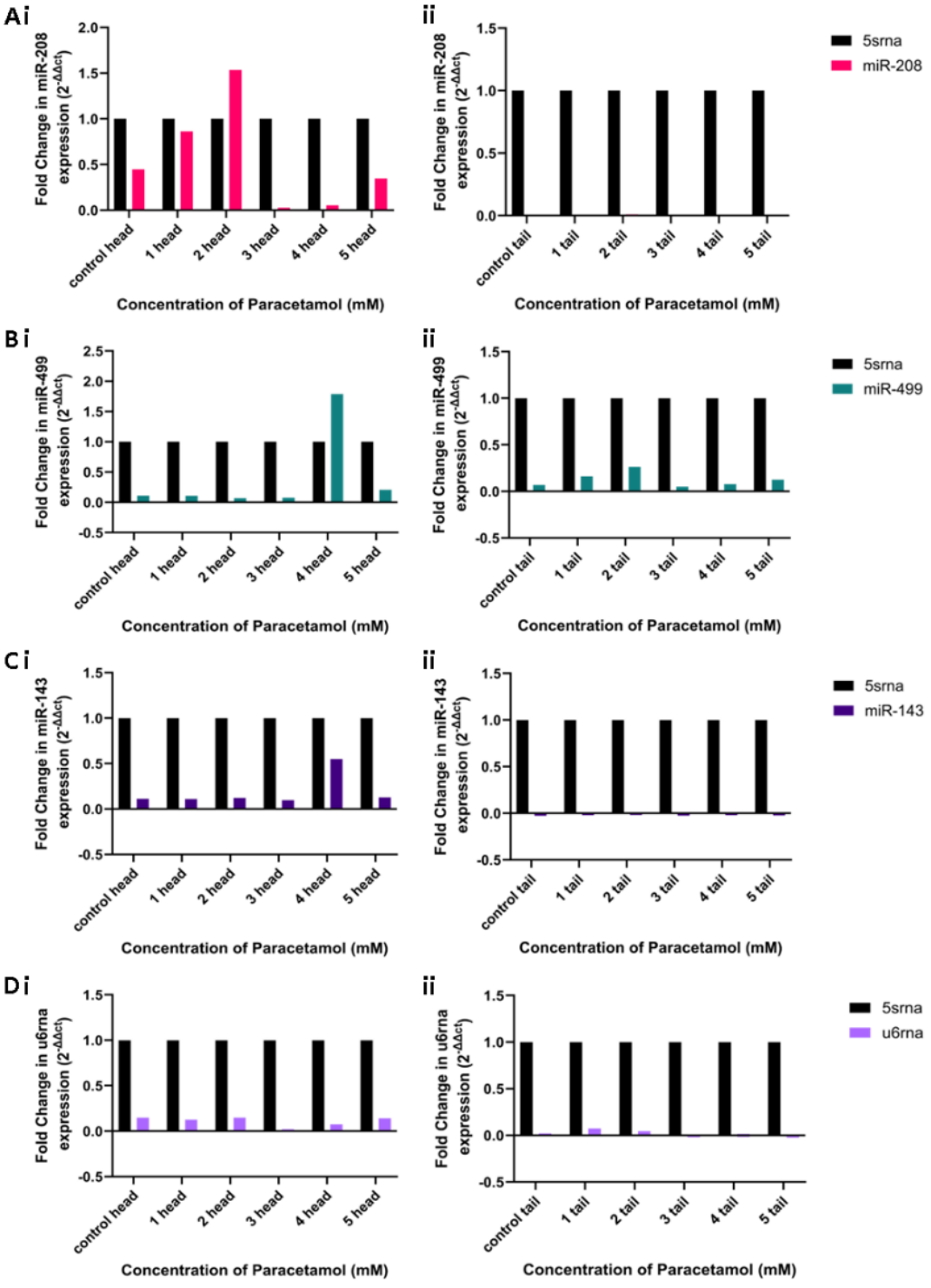
Ai
Fold Change in miR-208 expression ($2^{-\Delta\Delta ct}$)
2.0
1.5
1.0
0.5
0.0
control head
1 head
2 head
3 head
4 head
5 head
Concentration of Paracetamol (mM)
ii
Fold Change in miR-208 expression ($2^{-\Delta\Delta ct}$)
1.5
1.0
0.5
0.0
control tail
1 tail
2 tail
3 tail
4 tail
5 tail
Concentration of Paracetamol (mM)
5srna
miR-208
Bi
Fold Change in miR-499 expression ($2^{-\Delta\Delta ct}$)
2.5
2.0
1.5
1.0
0.5
0.0
-0.5
control head
1 head
2 head
3 head
4 head
5 head
Concentration of Paracetamol (mM)
ii
Fold Change in miR-499 expression ($2^{-\Delta\Delta ct}$)
1.5
1.0
0.5
0.0
-0.5
control tail
1 tail
2 tail
3 tail
4 tail
5 tail
Concentration of Paracetamol (mM)
5srna
miR-499
Ci
Fold Change in miR-143 expression ($2^{-\Delta\Delta ct}$)
1.5
1.0
0.5
0.0
-0.5
control head
1 head
2 head
3 head
4 head
5 head
Concentration of Paracetamol (mM)
ii
Fold Change in miR-143 expression ($2^{-\Delta\Delta ct}$)
1.5
1.0
0.5
0.0
-0.5
control tail
1 tail
2 tail
3 tail
4 tail
5 tail
Concentration of Paracetamol (mM)
5srna
miR-143
Di
Fold Change in u6rna expression ($2^{-\Delta\Delta ct}$)
1.5
1.0
0.5
0.0
-0.5
control head
1 head
2 head
3 head
4 head
5 head
Concentration of Paracetamol (mM)
ii
Fold Change in u6rna expression ($2^{-\Delta\Delta ct}$)
1.5
1.0
0.5
0.0
-0.5
control tail
1 tail
2 tail
3 tail
4 tail
5 tail
Concentration of Paracetamol (mM)
5srna
u6rna

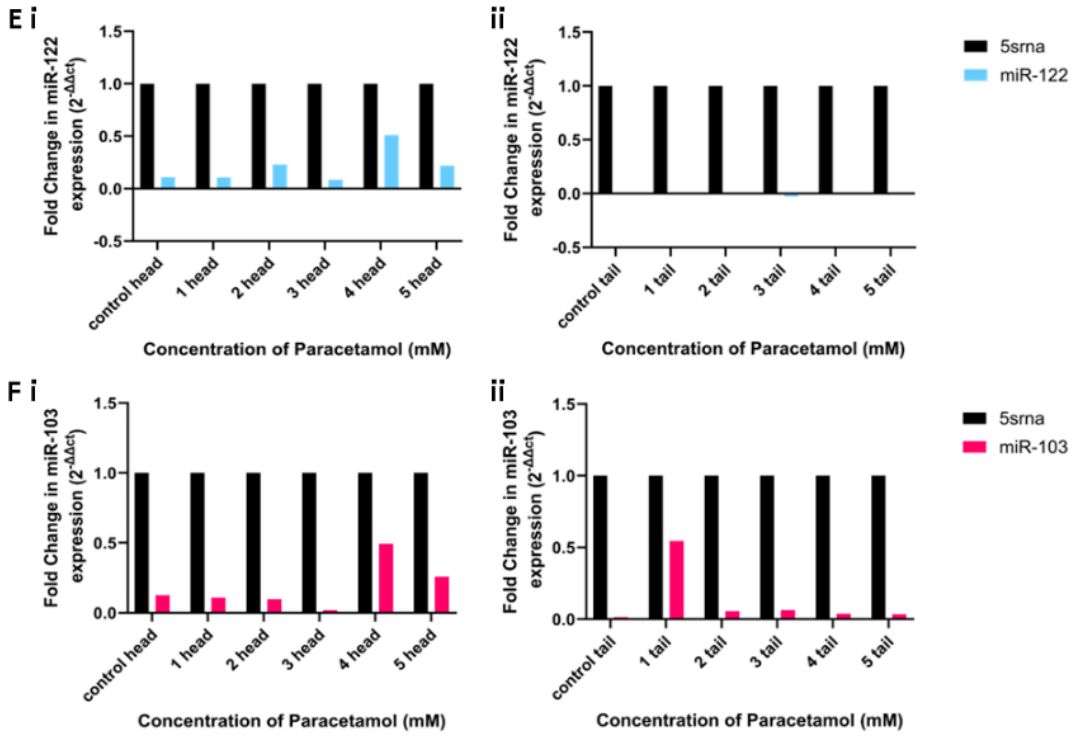

Figure 5.3: Expression levels of multiple miRNAs and U6RNA in Xenopus embryos exposed to paracetamol. *Embryos were exposed to doxorubicin (0-5mM) at NF stage 38 and harvested at NF stage 45; with 15 embryos being sampled and pooled per biological repeat. The expression of each biomarker was measured using qRT-PCR fold and normalised against the head sample of the untreated embryos, using 5S RNA as a housekeeping marker. 1-2 biological repeats were performed so statistics were unable to be performed.* ***A****- miR-208 expression.* ***B****- miR-499 expression.* ***C****- miR-143 expression.* ***D****- U6RNA expression.* ***E****- miR-122 expression.* ***F****- miR-103 expression. Head samples are shown in graph i for each biomarker, and tail samples are shown in graph ii for each biomarker.*

5.3 Summary

A summary of the results generated in this chapter can be found in Table 5.1.

		miR-208	miR-499	miR-143	miR-122	miR-103
Doxorubicin	Head	Up	Down	Down	Up	Down
	Tail	No change	Down	No Change	Up	Down
Terfenadine	Head	Up	Up	Up	Up	Up
	Tail	Up	Up	Up	Up	Up
Paracetamol	Head	Down	Up	Up	Up	Up
	Tail	No change	No change	No change	No change	Up

Table 5.1: A summary of effects seen on miRNA expression.

5.4 Discussion

In this chapter, we sought to determine if miRNAs were suitable biomarkers to detect drug-induced cardiotoxicity in *Xenopus* embryos. To this end, the results obtained showed promise in answering this question but are stymied by the lack of biological repeats able to be conducted during the study period. While patterns of expression appear to be present the lack of statistical significance able to be placed on these mean they remain as suggestions of effect.

The primary issue with the results generated in this chapter is the lack of repeats performed. This occurred due to multiple reasons, the most prominent being the availability of embryos from which to sample and generate datapoints from. The issues surrounding embryo availability are expanded upon in Chapter 6, but a small explanation is included here. To use terfenadine as an example, there were 7 concentrations of the drug (including both controls) utilised for the biomarker analysis assay, whereas in the heart rate assay 11 concentrations were utilised. The reason for this reduction was the availability of embryos; each concentration required 15 embryos to provide enough RNA for a single sample, and the survival rate dropped off at concentrations above 10μM, as per Figure 3.3 from a previous chapter. This meant that for every concentration studied in this assay there

was an expectation of a less than 100% survival rate, down to under 25% at the highest concentration of 50μM. So, to achieve a single RNA sample, more than 15 embryos must be exposed each time. To assume an average of a perfect 50% survival rate for the non-control concentrations, 30 embryos would need to be exposed per sample. With the addition of an assumed 100% survival rate for the control samples this would require 180 embryos per biological repeat. With the knowledge that a single *Xenopus* can lay hundreds of eggs in one day this may not seem excessive, but the reality faced during this research project was that demand for embryos was consistently high, but yields were often much lower than anticipated, resulting in a reduced number of embryos available for experiments. Under ideal circumstances, the full range of concentrations explored in Chapter 3 would also have been explored here, with the intention of searching for biomarker changes before physical changes in heart rate were observed, but the pressure of embryo numbers ultimately precluded this and in combination with time constraints of the research period prevented multiple biological repeats occurring.

As part of the review of the results of this study, questions surrounding the miRNAs chosen were brought forward. Although the rationale behind choosing each miRNA is discussed in Chapter 3, it is worth discussing the similarities between human and *Xenopus* miRNAs to determine if the results anticipated would be consistent with that seen in the literature on human disease. A summary of the miRNA sequences in *Xenopus* and humans is shown in Table 5.2, with differences between the sequences highlighted. As can be seen by this data, there are differences in sequences between the two species, but these are generally restricted to single base changes, with the most drastic difference being in miR-208. miR-208b in humans has 4 bases different to the miR-208 in *Xenopus*, and 3 differences than miR-208a in humans. This could theoretically lead to differences as miRNAs are only around 20 bases long, so 4 differences could theoretically lead to changes in function, but in this instance, this seems unlikely especially as the changed bases do not occur as a block but as individual base changes. It is also more

likely that the miR-208 in this instance is a conservation of miR-208a in humans rather than miR-208b, as there is only a single base difference.

miRNA	*Xenopus* sequence taken from Xenbase (Fisher et al., 2023)	Human Sequence taken from miRbase (Kozomara et al., 2019)
miR-208	AUAAGACGA**G**CA**U**AA**A**G**C**UUGU	a- AUAAGACGAGCA**A**AAAGCUUGU b- AUAAGACGA**A**CA**A**AA**G**G**U**UUGU
miR-103	AGCAGCAUUGUACAGGGCUAUGA	AGCAGCAUUGUACAGGGCUAUGA
miR-122-5p	UGGAGUGUGACAAUGGUGUUUGU	UGGAGUGUGACAAUGGUGUUUGU
miR-133-3p	a- **?**UUGGUCCCCUUCAACCAGCUG**U** b- **?**UUGGUCCCCUUCAACCAGCU**A?** c- **?**UUGGUCCCCUUCAACCAGCUG**C** d- **?**UUGGUCCCCUUCAACCAGC**C**G**C**	a1- **U**UUGGUCCCCUUCAACCAGCUG**?** a2- **U**UUGGUCCCCUUCAACCAGCUG**?** b- **U**UUGGUCCCCUUCAACCAGCU**A?**
miR-17-5p	CAAAGUGCUUACAGUGCAGGUAG**U**	CAAAGUGCUUACAGUGCAGGUAG**?**
miR-31-5p	AGGCAAGAUG**U**UGGCAUAGCU**G**	AGGCAAGAUG**C**UGGCAUAGCU**?**
miR-143	UGAGAUGAAGCACUGUAGCUC**G**	UGAGAUGAAGCACUGUAGCUC**A**
miR-499-5p	UUAAGACUUGCAGUGAUGUUU**AG**	UUAAGACUUGCAGUGAUGUU**U?**
miR-16	a- UAGCAGCACGUAAAUAUUGG**U**G b- UAGCAGCACGUAAAUAUUGG**GU** c- UAGCAGCACGUAAAUA**C**UGGAG	1- UAGCAGCACGUAAAUA**U**UGG**C**G 2- UAGCAGCACGUAAAUA**U**UGG**CG**

Table 5.2: miRNA sequences for miRNAs studied in this project in both Xenopus and human. *A comparison of the miRNA sequences published for both Xenopus sp. and humans, with differences between the two highlighted in blue and bolded for visibility. Question marks are used to denote gaps in the sequences provided.*

A further problem found in this chapter was the PCR assay, as it was extremely inconsistent in its output. There was significant time spent on developing the method and attempting to solve these issues detailed in Chapter 3, but it is clear from the results generated in this chapter that

although progress was made and some results were able to be gathered, there were still outstanding issues with the method. A potential cause for PCR failure could be the probes used in the analysis. The desire to use off-the-shelf probes was derived from wanting to create and develop an assay that could be easily replicated or scaled for industrial use, so off-the-shelf products would facilitate this. The products chosen were chosen carefully, with Table 5.3 indicating that the miRNA sequences of the products differed little from the published *Xenopus* sequences. In fact, for most products the sequences were identical and so should have had no issues with binding to the target miRNA, whereas the ones that did differ varied by one or two bases at most. These also tended to occur in miRNA 133-3p and miRNA-16, in which different forms of the miRNA have been observed in *Xenopus*. It would be possible to create miRNA probes that were custom designed for each miRNA, and this may be preferable if the assay was scaled up to an industrial scale as it would ensure consistency without relying on a third-party product.

miRNA	*Xenopus* sequence taken from Xenbase (Fisher et al., 2023)	Product sequence
miR-208	AUAAGACGAGCAUAAAGCUUGU	AUAAGACGAGCAUAAAGCUUGU
miR-103	AGCAGCAUUGUACAGGGCUAUGA	AGCAGCAUUGUACAGGGCUAUGA
miR-122-5p	UGGAGUGUGACAAUGGUGUUUGU	UGGAGUGUGACAAUGGUGUUUGU
miR-133-3p	a- UUGGUCCCCUUCAACCAGCUGU b- UUGGUCCCCUUCAACCAGCU**A?** c- UUGGUCCCCUUCAACCAGCUG**C** d- UUGGUCCCCUUCAACCAGC**C**G**C**	UUGGUCCCCUUCAACCAGCU**GU**
miR-17-5p	CAAAGUGCUUACAGUGCAGGUAGU	CAAAGUGCUUACAGUGCAGGUAGU
miR-31-5p	AGGCAAGAUGUUGGCAUAGCUG	AGGCAAGAUGUUGGCAUAGCUG
miR-143	UGAGAUGAAGCACUGUAGCUCG	UGAGAUGAAGCACUGUAGCUCG
miR-499-5p	UUAAGACUUGCAGUGAUGUUUA**G**	UUAAGACUUGCAGUGAUGUUUA**?**
miR-16	a- UAGCAGCACGUAAAUAUUGGUG b- UAGCAGCACGUAAAUAUUGG**GU** c- UAGCAGCACGUAAAUA**C**UGG**A**G	UAGCAGCACGUAAAUA**U**UGG**UG**

Table 5.3: miRNA sequences for miRNAs studied in this project. *A comparison of the miRNA sequences published are compared to the target miRNA sequences of the products used, with differences between the two sequences being highlighted in blue and bolded for visibility. Question marks are used to denote gaps in the sequences provided.*

Chapter 6 Discussion

6.1 Project Aims and Hypotheses

This chapter will discuss the key findings from each results chapter, followed by discussion of these results within the wider context of the project. Finally, conclusions will be drawn and areas of future research considered.

It was hypothesised that *Xenopus laevis* would be a useful model organism for ascertaining cardiotoxicity early in the drug development process. To test this hypothesis, key aims were developed:

- To determine if drugs known to cause cardiotoxicity in humans can be observed to cause cardiotoxicity in embryonic amphibians
- To evaluate the appropriateness of an embryonic amphibian model of cardiotoxicity and its potential for use in an industrial setting

Over the course of the creation of this thesis, novel research has been conducted and data gathered that would provide answers to the question of whether *Xenopus* can be used to accurately predict the cardiotoxicity of a drug.

6.2 Key findings

6.2.1 Assay Development

The work performed in Chapter 3 was instrumental in the creation of an improved method of measuring heart rate in *Xenopus* embryos. The development of code that can automate the analysis of heart rate is critical to the future success and application of the assay as without this in place the workload of counting heart rate becomes a significant limiting factor for scaling of the process. Alongside this, initial steps have been taken to develop a standardised method for assessing the arrhythmic state of the heart rate data gathered, with weaknesses identified for awareness of future research in the topic.

Further findings in this chapter was the development of a biomarker assay and identification of miRNAs that could be utilised as markers of cardiotoxicity.

6.2.2 Heart Rate Assay

To summarise the results found in this assay and detailed in Chapter 4, statistically significant decreases in heart rate was seen in both heart chambers for doxorubicin, terfenadine, paracetamol and e4031. There was no change in heart rate seen following exposure to paclitaxel. There were no differences between heart chambers across all drugs studied. A statistically significant increase in arrythmia was seen in doxorubicin, with no change in arrythmia seen in paracetamol. Terfenadine results showed a trend of increase in arrythmia, but this was not statistically significant. For the first time, a value for a normal heart rate of NF stage 45 *Xenopus laevis* embryos was determined, with the normal heart rate falling between 53-79bpm, and a mean of 66bpm.

A change in heart rate was used as an indicator of cardiotoxicity, so doxorubicin, terfenadine, paracetamol and e4031 were seen to cause cardiotoxicity in this experiment. This occurred at the highest concentrations of doxorubicin, mid-to-high concentrations of terfenadine, mid and high concentrations of e4031 and a low concentration of paracetamol. Paclitaxel was not found to be cardiotoxic based off this criteria. The increase in arrythmia was also used as an indicator of cardiotoxicity for doxorubicin. The results for terfenadine exposure was suggestive of cardiotoxicity despite the lack of statistical significance.

6.2.3 Biomarker Assay

The full results from this assay are presented in Chapter 5. No statistically significant results were determined from the experiments conducted. Some changes in miRNA expression were seen, but these were inconsistent and

inconclusive with limited conclusions able to be made. Further discussion and considerations on how to improve the assay are included in Section 5.4.

6.2.4 Further context

The results presented in this report sought to determine if cardiotoxic effects of compounds seen in *Xenopus* embryos were replicated to those reported in human patients and seen in mammalian model organisms. Doxorubicin, in humans, leads to cell apoptosis and cardiac damage, which can present through a variety of symptoms including cardiac swelling, ejection fraction reduction and arrythmias. The assay as it currently stands is unable to measure ejection fraction, and so this is a factor that was not seen replicated in the *Xenopus* for both doxorubicin and paclitaxel (for whom reduction in ejection fraction is also a key indicator of cardiotoxicity). The assay does appear to detect arrythmias and the change in heart rate can be used as an indicator of cardiac damage. Terfenadine cardiotoxicity is characterised by arrythmias caused by long QT syndrome, which the *Xenopus* assay indicated successfully although the diagnosis of long QT syndrome is not possible without directly measuring electrical conductivity within the heart. Paracetamol is not known to cause cardiotoxicity in humans and as already discussed the presence of a change in heart rate is unexpected, with a change in heart rate being used as a marker of cardiotoxicity in this assay. Paclitaxel-induced cardiotoxicity in humans presents as reduction in ejection fraction, bradycardia arrythmias and changes in blood pressure (both hypo- and hypertension have been reported). Blood pressure was not a factor that could be accounted for in this assay, and unfortunately the results presented did not recapitulate a change in heart rate. E4031 is a research compound and not a medical drug, and therefore has not been given to human subjects, but in other mammal species HERG-ion channel blocking has been noted, leading to long QT intervals. These indicate that the experiments performed as part of this study had mixed success in replicating the physiological responses seen in human and mammalian models, with failures being partly due to factors that the assay could not detect and sometimes without clear explanation.

In the grander scheme of *Xenopus* research, these results show great promise in developing the model further. During the period covered by this study, *Xenopus* research generally continued taking place and further interest in *Xenopus* picked up pace. This is shown by the continuation of several existing *Xenopus*-focussed conferences, some of which have now entered their second decade of existence, and the creation of a new conference focussed on *Xenopus* as a model – the 1st Asian *Xenopus* Conference, which took place in late 2024 (Jang et al., 2025). This increase in interest shows that the animal model is gaining popularity and further interest in developing in this particular area of research is likely to be well-received and taken up by future researchers. Further use of *Xenopus* models as human disease analogues has also increased in popularity, particularly with *X. tropicalis* as they can be readily utilised for genetic disorders (Willsey et al., 2024) alongside even greater development of the model for toxicity testing (Gao and Shen, 2021).

Although interest in *Xenopus* as an animal model has increased over the past few years, further research has also taken place in the area of non-animal models. Of particular interest to the field of toxicity is the successful development of complex cardiac organoids that showed self-organising behaviour, which at the outset of this project remained elusive (Schutgens and Clevers, 2020). The need for self-organising organoids stems from the desire to recapitulate the in vivo environment and development of organs, alongside the complex chamber system of the real heart. The first self-organising cardiac organoid was published in 2021 (Hofbauer et al., 2021). This paper has since led to further development of the cardiac organoid system, with additional work from (Schmidt et al., 2023) taking the model further and creating multi-chambered organoids, as well as increasing the number of assays these organoids can be utilised in (Huang et al., 2025). Alongside these organoids, further work with IPSC-derived methods have developed and novel organ-on-a-chip models are becoming more sophisticated and physiologically relevant (Raniga et al., 2024). The increasing number and complexity of these non-animal models, combined

with the improvement of them as they become closer to reproducing the in vivo environment could very well lead to the supplanting of some in vivo models as no longer necessary. This is unlikely to occur in the very near future, as several fundamental hurdles need to be overcome by these models before being suitable for scaling and widespread use, such as vascularisation issues and standardisation of methods, but once these have been addressed there is no reason the models could not be utilised to replicate *in vivo*, *in vitro*.

Further support of this eventual overtake of in vitro methods includes increasing support for these methods from industry and regulatory bodies. In 2022, the FDS 2.0 act was signed into law in the USA, which removes the legal requirement of extensive animal testing to demonstrate drug safety if enough in vitro evidence has been collected to allow bypassing these requirements (Han, 2023). This goes one step further than the ICH guidelines that theoretically allows such bypassing by being explicit in encouraging it where appropriate.

Viewing these advances from a 3Rs perspective, as the original question set out by this study was built on 3Rs foundations, the potential shown by non-animal methods is great and would be the favoured option, all things being equal between methods. The reality for the moment is that despite rapid improvement in alternative methods, as of 2025 they are not currently able to truly replace animal models in the cardiotoxicity assessment of novel compounds. Likewise, this model requires work to develop its capability for industrial scaling, but this is much closer to deployment than cardiac organoids, for example. It seems likely that the *Xenopus* model could be deployed as a first-*in-vivo* model following extensive *in vitro* testing and could potentially be utilised as a less animal intensive model where animal testing is a necessity.

6.3 Limitations

There were several issues that arose over the course of this study that were common to both assays. Of note, the availability of *Xenopus* embryos to perform experiments with was a consistent problem throughout the period of research. Various causes can be attributed to this, including disturbances due to necessary building work, an aging frog colony and outbreaks of illness within the colony all contributed to low or absent egg laying behaviour. These instances of lower egg numbers meant there were often cases where desired egg numbers were higher than available, so a rationing system had to be put in place. Events such as the building work and illness were unavoidable, and a combination of reduced operations due to the Covid-19 pandemic and illness at the supplier meant that younger animals were unable to be purchased and introduced to refresh the colony as planned in 2020. The delays caused by this were long reaching, with young animals only being introduced midway through 2023. With younger frogs in a colony, these issues would largely be solved, and in the event of scaling this process up to industry standards either increasing the size of the colony or creation of a dedicated colony would easily provide for the needs of the assay.

When embryos were exposed to drugs, significant embryo death was observed. This data can be found in the dose response curves found in Chapter 3. This was problematic as it compounded the issues with embryo availability and meant that there were times that a less-than-optimal number of embryos survived drug treatment to be analysed. Embryo death is not inherently negative, as this indicates toxicity, but if too many embryos died this pushed the balance into not having enough embryos remaining for analysis. This could be mitigated by performing multiple repeats of experiments, but this cycles back into the issue of embryo availability. The results of this situation in practical terms are that for some of the experiments conducted, the overall n numbers were lower than desired.

Another consideration to be taken with the higher death rate is the nature of the surviving embryos- by virtue of the fact they remain alive when others have died, they are likely less susceptible to the toxic effects of the drugs. This may indicate the results are not fully representative of a “typical” embryo. This is, unfortunately, something that cannot realistically be mitigated but is worth considering when analysing the data.

Additionally, the current assay has no way of determining that the toxic effects leading to embryo death are specifically cardiotoxic or if there is general toxicity occurring. Investigation into this may be beneficial in future work. Further experiments providing comparisons to controls would also be beneficial, as although paracetamol was used in this research, this was primarily to determine if the same assay could be used to detect both hepatotoxicity and cardiotoxicity in the same experiment. Using non-toxic compounds would be very beneficial to provide a true comparison, especially when utilising an array of compounds that are used in existing *in vitro* models such as those seen in (De Korte et al., 2020)

The method of drug application in these assays was to add the drug to the embryo growth media and the assumption was made that the drug was taken up from the media into the embryo and metabolised. Work was begun previously by the lab (Saide, 2018) to assess the capability of *Xenopus* embryos to metabolise human drugs- in that case, paracetamol. To assess this, Saide (2018) used high performance liquid chromatography-tandem mass spectrometry (HPLC-MS/MS) to determine if metabolites of paracetamol were present in the exposed embryos and in what concentrations/proportions. The work was not fully completed, but the initial results were promising, indicating that *Xenopus* embryos could metabolise paracetamol and that predicted metabolites appeared to be present in similar ratios to humans, albeit ratios seen in child metabolism rather than adults. These results are presented with the caveat of low repeat numbers but indicate that the methodology was working and could be employed in this

area of research too. Unfortunately, lack of access to a mass spectrometer and time prevented these experiments from being performed during this period of research. Other methods of drug provision could be explored if it was discovered that there was lack of uptake or metabolisation of the drug, such as microinjection, but the options are limited as the embryos do not eat at the stages used in this study.

Additionally, dosage considerations for the drugs used in this study were based on survival curves. This allowed a suitable concentration to be used for the *Xenopus* embryos, but there is no clear way to determine the human dose equivalent of these concentrations. The concept of knowing an equivalent human dose is important as many drugs could be toxic in very high concentrations but at therapeutic levels provide no real risk to health. If the concentrations being given to the *Xenopus* in this assay that proved toxic were within the estimated therapeutic range for humans, this would indicate a stronger need to disregard the compound for future development, whereas if the dose corresponded to something much higher than would be therapeutic there is the potential for further development if the positive clinical effects were beneficial. The Food and Drug Administration (FDA) of the United States provides guidance for industry on estimating the maximum safe starting dose in initial clinical trials (Food and Drug Administration, 2005). This document contains a table, shown in Figure 6.1, that provides conversion ratios to convert human dosages to animal dosages and vice versa for use in drug toxicity studies. As can be seen in the figure, the animal species covered by this table are the most used in research and are exclusively mammalian. This is a useful resource and would be made more relevant had it included non-mammalian animals, such as zebrafish or *Xenopus*. Helpfully, the document includes explanations as to how the figures were reached, and these methods could theoretically be used for determining a dose conversion factor for *Xenopus*, both adult and embryo. Unfortunately, the methodology involves determining body surface area, which is incredibly difficult for *Xenopus* embryos due to their size, as well as information regarding toxicity from studies of the specific animal, which as

covered in the introduction to this report is lacking for *Xenopus*. This clear gap in the literature could form the basis for additional study.

Table 1: Conversion of Animal Doses to Human Equivalent Doses Based on Body Surface Area

Species	To Convert Animal Dose in mg/kg to Dose in mg/m^2, Multiply by k_m	To Convert Animal Dose in mg/kg to HED[a] in mg/kg, Either:	
		Divide Animal Dose By	Multiply Animal Dose By
Human	37	---	---
Child (20 kg)[b]	25	---	---
Mouse	3	12.3	0.08
Hamster	5	7.4	0.13
Rat	6	6.2	0.16
Ferret	7	5.3	0.19
Guinea pig	8	4.6	0.22
Rabbit	12	3.1	0.32
Dog	20	1.8	0.54
Primates:			
Monkeys[c]	12	3.1	0.32
Marmoset	6	6.2	0.16
Squirrel monkey	7	5.3	0.19
Baboon	20	1.8	0.54
Micro-pig	27	1.4	0.73
Mini-pig	35	1.1	0.95

[a] Assumes 60 kg human. For species not listed or for weights outside the standard ranges, HED can be calculated from the following formula:

$$HED = \text{animal dose in mg/kg} \times (\text{animal weight in kg/human weight in kg})^{0.33}.$$

[b] This k_m value is provided for reference only since healthy children will rarely be volunteers for phase 1 trials.

[c] For example, cynomolgus, rhesus, and stumptail.

***Figure 6.1: Human dose equivalent table**. Table showing ratio values to determine human-animal dose conversions for use in drug toxicity studies. Taken from Food and Drug Administration (2005).*

6.4 Future work

The research covered so far in this report has provided promising results, but additional development is required to improve the system further should future researchers wish to build upon the work done in this report.

First and foremost, the biomarker assay requires refinement to improve the consistency of the assay and allow for a greater number of results to be

obtained. Developing the qRT-PCR assay to be more efficient would be the authors preferred option, following the steps discussed in Section 5.3.2, as this would allow for effective quantification of the miRNA, allow for incorporation with previous work on liver toxicity and be expandable as required.

An alternative to this could be done by trialling alternatives to qRT-PCR. miRNAs have excellent potential as a clinical biomarker generally and this is reflected in the potential for cardiotoxicity indication, and qRT-PCR is not the only method available for their detection. One alternative method of detecting miRNAs that has recently been developed is the use of ELISA (Lei *et al*., 2022). ELISA itself is a well-established method for detection of proteins but has only recently been utilised for miRNA detection. Although a new ELISA would need to be made for each novel miRNA to be detected, ELISA kits for other compounds are readily available and it is likely that with appropriate industry collaboration a commercialised kit could be created for miRNAs of interest. The easy availability of ELISA kits for other compounds would allow the methodology to be incorporated as part of a comprehensive assay system.

Some other cardiotoxicity indicators that are available for ELISA detection include Cardiac Troponin and CDF-15; a protein found in increased concentrations in cardiac toxicity. A potential hurdle to overcome with the ELISA assay would be cross-reaction of antibodies and ensuring the reactivity for *Xenopus* is present, as many ELISA kits are designed for human protein reaction.

The time at which the *Xenopus* is exposed to the drugs was determined based on previous work in the lab (Saide *et al*., 2019). A good experiment to conduct would be to expose the embryos to the drug for 24 hours, starting at NF stage 43 of development, in order to compare to the current assay which

begins exposure at NF stage 38 of development and exposure to the drug lasts 72 hours. This could represent the difference between acute exposure and chronic exposure, and any potential differences in toxicity due to the different exposure times could be elucidated. Preliminary work began on this during the period but was left incomplete due to the embryo availability problems already covered and prioritising the main subject of the research.

As discussed previously, the use of HPLC-MS/MS had been used previously to determine the ability of *Xenopus* embryos to metabolise paracetamol. This was assessed by determining the presence and concentration of paracetamol metabolites in *Xenopus* embryos exposed to the drug. Understanding how *Xenopus* embryos metabolize drugs and if they produce the same metabolites as are found in humans would be useful information, as often toxic effects are triggered by a drug metabolite rather than the drug itself. If toxic metabolites are produced in different proportions in different species the drug will be more or less toxic despite similar doses.

A natural next step in the process of developing *Xenopus* embryos as a model of organ toxicity is to begin examination of additional organ systems with *Xenopus*. One such organ with strong potential is the kidney, as often the kidneys are damaged by novel drugs.

The final step in developing the model would be commercialising it to be suitable for large scale use by the pharmaceutical industry. This could be done by creation and validation of a series of methodologies that can then be taken and used by the companies themselves, or through the development of a spin out company within the University, expanding the *Xenopus* colony and training of specialised staff members to perform these assays on a contract basis. If the first method was chosen, the necessity of using off-the-shelf products would need to be considered. In order to meet the needs of pharma companies it would be important to develop a relationship with these

companies. During this study, it was considered to take part in the Innovate UK ICURe program, which would have allowed for direct conversation and evaluation of the model by contacts within the industry and a business plan developed should the model meet the needs of the companies. This could potentially lead to the creation of the previously mentioned spinout and would have been an excellent opportunity for both model and researcher. Unfortunately, due to circumstances outside of the control of the author, this could not be done but would be highly recommended for future researchers on the subject.

6.5 Final Conclusions

The project began out of a desire to develop *Xenopus* as a model organism suitable for assessing organ toxicity of novel compounds, and this project represents the exploration of cardiotoxicity specifically. The aims of the project were two-fold; firstly, to determine if cardiotoxicity can be observed in *Xenopus* embryos and secondly if the model is appropriate for use at an industrial scale for drug development.

The results obtained over the course of this research indicates that cardiotoxic drugs in humans do cause cardiotoxicity in *Xenopus* embryos, and this was most clearly seen in the heart rate assay. The methods used are clear and well thought out, with results that clearly indicate cardiotoxicity in drugs known to cause cardiotoxic effects in humans. The methodology of utilising imaging followed by computer analysis of the heart rate was effective, and additional development in automation would enable this to be scaled up to an appropriate size for large scale drug assessment. Additional development will also allow for more information to be gained from the results such as arrhythmia. The biomarker assay was less successful, despite being based on sound technical foundations, but with additional refinement should enhance the ability to detect cardiotoxicity and quantify the cardiotoxic effects.

Overall, *Xenopus* is to be a very promising model for cardiotoxicity detection in drug development. It has previously shown usefulness in hepatoxicity testing, proving the use of *Xenopus* as an organ toxicity model that can be utilised at a greater level by the addition of further organ systems into the process. This model further enhances the support of the *Xenopus* as a model meeting NC3Rs standards, as drug toxicity to multiple organs can be tested from the same assay, demonstrating both a reduction in embryos used (even though they are not subject to ASPA (1986) protection) and a refinement principle of utilising the embryos efficiently for data generation. To this end, once fully developed as a commercial method, use of *Xenopus* embryos for drug discovery will lead to a reduction in the need for further mammalian models being used unnecessarily for toxicity testing.

Glossary/Abbreviations

AMBP- alpha-1-microglobulin/bikunin precursor

ANP- atrial natriuretic peptide

ASPA- Animals (Scientific Procedures) Act 1986

BCIP- 5-Bromo-4-chloro-3-indolyl phosphate p-toluidine salt

BNP- cerebral natriuretic peptide

cDNA- copy deoxyribonucleic acid

CiPA- Comprehensive in vitro Proarrythmia assay

CNP- type c natriuretic peptide

DILI- drug induced liver injurt

DMF- Dimethylformamide

DMSO- dimethyl sulphoxide

DNA- deoxyribonucleic acid

ECG- electrocardiogram

ECHO- echocardiography

EXRC- European *Xenopus* resource centre

FBS- foetal bovine serum

FETAX- Frog Embryo Teratogenesis Assay *Xenopus*

Fps- frames per second

GSH- glutathione

hCG- human chorionic gonadotropin

HEPES- 2-[4-(2-Hydroxyethyl)piperazin-1-yl]ethane-1-sulfonic acid

hERG- human Ether-à-go-go-related gene

HYB- hybridisation buffer

Ikr- rapidly activating delayed rectifier potassium ion current

IKs- slow delayed rectifier current

IPSCs- induced pluripotent stem cells

JiCSA- Japan iPSC Cardiac Safety Assessment

LB- luria broth

LVEF- left ventricular ejection fraction

MI- myocardial infarction

MMR- marks modified ringers

MS-222 -tricaine methane sulphonate

NBT- Nitro Blue Tetrazolium

NF- Nieuwkoop-Faber

NPs- natriuretic peptides

NTC- no template control

PCR- polymerase chain reaction

PMSG- pregnant mare serum gonadotropin

QRT-PCR- quantitative reverse transcriptase polymerase chain reaction

ROI- region of interest

Rpm- revolutions per minute

SSC- saline sodium citrate buffer

Tc- cardiac troponin

TdP- Torsade de Pointes

WISH- whole mount in situ hybridisation

Bibliography

Abu-Elmagd, M., Mulvaney, J. and Wheeler, G. N. (2017). Frizzled-7 is required for Xenopus heart development. *Biology Open* bio.026963.

Adachi, T., Nakanishi, M., Otsuka, Y., Nishimura, K., Hirokawa, G., Goto, Y., Nonogi, H. and Iwai, N. (2010). Plasma MicroRNA 499 as a Biomarker of Acute Myocardial Infarction. *Clinical Chemistry* **56**, 1183–1185.

Ahmed, A., Ward, N. J., Moxon, S., Lopez-Gomollon, S., Viaut, C., Tomlinson, M. L., Patrushev, I., Gilchrist, M. J., Dalmay, T., Dotlic, D., et al. (2015). A database of microRNA expression patterns in Xenopus laevis. *PLoS ONE* **10**, 1–10.

Andrysiak, K., St, J. and Dulak, J. (2021). Human-induced pluripotent stem cell-derived cardiomyocytes , 3D cardiac structures , and heart-on-a-chip as tools for drug research. 1061–1085.

Animals (Scientific Procedures) Act (1986).

Balaji, J. (2006). ImajeJ Time Series Analyzer Plugin.

Bartlett, H. L., Scholz, T. D., Lamb, F. S. and Weeks, D. L. (2004). Characterization of embryonic cardiac pacemaker and atrioventricular conduction physiology in Xenopus laevis using noninvasive imaging. *American Journal of Physiology - Heart and Circulatory Physiology* **286**, 2035–2041.

Bartlett, H. L., Escalera, R. B., Patel, S. S., Wedemeyer, E. W., Volk, K. A., Lohr, J. L. and Reinking, B. E. (2010). Echocardiographic Assessment of Cardiac Morphology and Function in Xenopus. *Comparative Medicine* **60**,.

Belevych, A. E., Sansom, S. E., Terentyeva, R., Ho, H.-T., Nishijima, Y., Martin, M. M., Jindal, H. K., Rochira, J. A., Kunitomo, Y., Abdellatif, M., et al. (2011). MicroRNA-1 and -133 Increase Arrhythmogenesis in Heart Failure by Dissociating Phosphatase Activity from RyR2 Complex. *PLoS ONE* **6**, e28324.

Bell, R. M., Mocanu, M. M. and Yellon, D. M. (2011). Retrograde heart perfusion: The Langendorff technique of isolated heart perfusion. *Journal of Molecular and Cellular Cardiology* **50**, 940–950.

Berg, E. L. (2019). Human Cell-Based in vitro Phenotypic Profiling for Drug Safety-Related Attrition. *Frontiers in Big Data* **2**, 1–8.

Bergmann, K., Meza Santoscoy, P., Lygdas, K., Nikolaeva, Y., MacDonald, R., Cunliffe, V. and Nikolaev, A. (2018). Imaging Neuronal Activity in the Optic Tectum of Late Stage Larval Zebrafish. *JDB* **6**, 6.

Blass, B. E. (2015). *Basic principles of drug discovery and development*. Amsterdam ; Boston: Elsevier/AP, Academic Press is an imprint of Elsevier.

Bonaventura, G., Iemmolo, R., Attaguile, G. A., La Cognata, V., Pistone, B. S., Raudino, G., D'Agata, V., Cantarella, G., Barcellona, M. L. and Cavallaro, S. (2021). iPSCs: A Preclinical Drug Research Tool for Neurological Disorders. *IJMS* **22**, 4596.

Bonev, B. and Papalopulu, N. (2012). Methods to Analyze microRNA Expression and Function During Xenopus Development. In *Xenopus Protocols: Post-Genomic Approaches*, pp. 445–459.

Boppart, S. A., Tearney, G. J., Bouma, B. E., Southern, J. F., Brezinski, M. E. and Fujimoto, J. G. (1997). Noninvasive assessment of the developing *Xenopus* cardiovascular system using optical coherence tomography. *Proc. Natl. Acad. Sci. U.S.A.* **94**, 4256–4261.

Boštjančič, E., Zidar, N., Štajer, D. and Glavač, D. (2010). MicroRNA miR-1 is Up-regulated in Remote Myocardium in Patients with Myocardial Infarction. *Fol. Biol.* **56**, 27–31.

Bowley, G., Kugler, E., Wilkinson, R., Lawrie, A., Van Eeden, F., Chico, T. J. A., Evans, P. C., Noël, E. S. and Serbanovic-Canic, J. (2022). Zebrafish as a tractable model of human cardiovascular disease. *British J Pharmacology* **179**, 900–917.

Brändli, A. W. (2004). Prospects for the Xenopus embryo model in therapeutics technologies. *Chimia* **58**, 694–702.

Bristow, M. R., Billingham, M. E., Mason, J. W. and Daniels, J. R. (1978). Clinical spectrum of anthracycline antibiotic cardiotoxicity. *Cancer Treatment Reports*.

Brunning, A. (2016). Understanding the Drug Discovery Process.

Calore, M., Lorenzon, A., Vitiello, L., Poloni, G., Khan, M. A. F., Beffagna, G., Dazzo, E., Sacchetto, C., Polishchuk, R., Sabatelli, P., et al. (2019). A novel murine model for arrhythmogenic cardiomyopathy points to a pathogenic role of Wnt signalling and miRNA dysregulation. *Cardiovascular Research* **115**, 739–751.

Calvano, J., Achanzar, W., Murphy, B., DiPiero, J., Hixson, C., Parrula, C., Burr, H., Mangipudy, R. and Tirmenstein, M. (2016). Evaluation of microRNAs−208 and 133a/b as differential biomarkers of acute cardiac and skeletal muscle toxicity in rats. *Toxicology and Applied Pharmacology* **312**, 53–60.

Cardoso-Vera, J. D., Islas-Flores, H., SanJuan-Reyes, N., Montero-Castro, E. I., Galar-Martínez, M., García-Medina, S., Elizalde-Velázquez, A., Dublán-García, O. and Gómez-Oliván, L. M. (2017). Comparative study of diclofenac-induced embryotoxicity and teratogenesis in Xenopus laevis and Lithobates catesbeianus, using the frog embryo teratogenesis assay: Xenopus (FETAX). *Science of The Total Environment* **574**, 467–475.

Carotenuto, R., Pallotta, M. M., Tussellino, M. and Fogliano, C. (2023a). Xenopus laevis (Daudin, 1802) as a Model Organism for Bioscience: A Historic Review and Perspective. *Biology* **12**, 890.

Carotenuto, R., Tussellino, M., Fusco, S., Benvenuto, G., Formiggini, F., Avallone, B., Motta, C. M., Fogliano, C. and Netti, P. A. (2023b). Adverse Effect of Metallic Gold and Silver Nanoparticles on Xenopus laevis Embryogenesis. *Nanomaterials* **13**, 2488.

Causin, R., Pess□a-Pereira, D., Souza, K., Evangelista, A., Reis, R., Fregnani, J. and Marques, M. (2019). Identification and performance evaluation of housekeeping

genes for microRNA expression normalization by reverse transcription-quantitative PCR using liquid-based cervical cytology samples. *Oncol Lett*.

Chatterjee, K., Zhang, J., Honbo, N. and Karliner, J. S. (2010). Doxorubicin Cardiomyopathy. *Cardiology* **115**, 155–162.

Chen, Y., Zhao, Y., Chen, W., Xie, L., Zhao, Z.-A., Yang, J., Chen, Y., Lei, W. and Shen, Z. (2017). MicroRNA-133 overexpression promotes the therapeutic efficacy of mesenchymal stem cells on acute myocardial infarction. *Stem Cell Res Ther* **8**, 268.

Cheng, H. and Force, T. (2010). Molecular Mechanisms of Cardiovascular Toxicity of Targeted Cancer Therapeutics. *Circulation Research* **106**, 21–34.

Chhabria, K., Plant, K., Bandmann, O., Wilkinson, R. N., Martin, C., Kugler, E., Armitage, P. A., Santoscoy, P. L., Cunliffe, V. T., Huisken, J., et al. (2020). The effect of hyperglycemia on neurovascular coupling and cerebrovascular patterning in zebrafish. *J Cereb Blood Flow Metab* **40**, 298–313.

Collyer, E. (2024). *Comparative heart anatomy*.

Colpaert, R. M. W. and Calore, M. (2019). MicroRNAs in Cardiac Diseases. *Cells* **8**, 737.

Condrat, C. E., Thompson, D. C., Barbu, M. G., Bugnar, O. L., Boboc, A., Cretoiu, D., Suciu, N., Cretoiu, S. M. and Voinea, S. C. (2020). miRNAs as Biomarkers in Disease: Latest Findings Regarding Their Role in Diagnosis and Prognosis. *Cells* **9**, 276.

Corsten, M. F., Dennert, R., Jochems, S., Kuznetsova, T., Devaux, Y., Hofstra, L., Wagner, D. R., Staessen, J. A., Heymans, S. and Schroen, B. (2010). Circulating MicroRNA-208b and MicroRNA-499 reflect myocardial damage in cardiovascular disease. *Circulation: Cardiovascular Genetics* **3**, 499–506.

Crumb, J., Arnold, J., Payne, P. and Brown, M. Blockade of Multiple Human Cardiac Potassium Currents by the Antihistamine Terlenadine: Possible Mechanism for Terfenadine-Associated Cardiotoxicity.

Da Costa Martins, P. A., Salic, K., Gladka, M. M., Armand, A.-S., Leptidis, S., El Azzouzi, H., Hansen, A., Coenen-de Roo, C. J., Bierhuizen, M. F., Van Der Nagel, R., et al. (2010). MicroRNA-199b targets the nuclear kinase Dyrk1a in an auto-amplification loop promoting calcineurin/NFAT signalling. *Nat Cell Biol* **12**, 1220–1227.

D'Alessandra, Y., Devanna, P., Limana, F., Straino, S., Di Carlo, A., Brambilla, P. G., Rubino, M., Carena, M. C., Spazzafumo, L., De Simone, M., et al. (2010). Circulating microRNAs are new and sensitive biomarkers of myocardial infarction. *European Heart Journal* **31**, 2765–2773.

D'Amico, L., Seng, W. L., Yang, Y. and Suter, W. (2011). Assessment of Drug-Induced Cardiotoxicity in Zebrafish. In *Zebrafish: Methods for Assessing Drug Safety and Toxicity*, pp. 45–54.

Darbar, D. and Roden, D. M. (2013). Genetic mechanisms of atrial fibrillation: impact on response to treatment. *Nat Rev Cardiol* **10**, 317–329.

De Korte, T., Katili, P. A., Mohd Yusof, N. A. N., Van Meer, B. J., Saleem, U., Burton, F. L., Smith, G. L., Clements, P., Mummery, C. L., Eschenhagen, T., et al. (2020). Unlocking Personalized Biomedicine and Drug Discovery with Human Induced Pluripotent Stem Cell–Derived Cardiomyocytes: Fit for Purpose or Forever Elusive? *Annu. Rev. Pharmacol. Toxicol.* **60**, 529–551.

De Luca, E., Zaccaria, G. M., Hadhoud, M., Rizzo, G., Ponzini, R., Morbiducci, U. and Santoro, M. M. (2014). ZebraBeat: a flexible platform for the analysis of the cardiac rate in zebrafish embryos. *Sci Rep* **4**, 4898.

Derda, A. A., Thum, S., Lorenzen, J. M., Bavendiek, U., Heineke, J., Keyser, B., Stuhrmann, M., Givens, R. C., Kennel, P. J., Christian Schulze, P., et al. (2015). Blood-based microRNA signatures differentiate various forms of cardiac hypertrophy. *International Journal of Cardiology* **196**, 115–122.

Desai, V. G., C. Kwekel, J., Vijay, V., Moland, C. L., Herman, E. H., Lee, T., Han, T., Lewis, S. M., Davis, K. J., Muskhelishvili, L., et al. (2014). Early biomarkers of doxorubicin-induced heart injury in a mouse model. *Toxicology and Applied Pharmacology* **281**, 221–229.

Deshmukh, R. S., Kovács, K. A. and Dinnyés, A. (2012). Drug Discovery Models and Toxicity Testing Using Embryonic and Induced Pluripotent Stem-Cell-Derived Cardiac and Neuronal Cells. *Stem Cells International* **2012**, 1–9.

Dessertenne, F. (1966). Ventricular tachycardia with 2 cariable opposing foci. *Archives des Maladies du Coeur et des Vaisseaux* **59**, 263–272.

Dhingra, A. K., Chopra, B., Bhardwaj, S., Grewal, A. S. and Guarve, K. (2023). Virtual screening. In *Computational Approaches in Drug Discovery, Development and Systems Pharmacology*, pp. 223–236. Elsevier.

Diniz, G. P., Lino, C. A., Guedes, E. C., Nascimento Moreira, L. D. and Barreto-Chaves, M. L. M. (2015). Cardiac microRNA-133 is down-regulated in thyroid hormone-mediated cardiac hypertrophy partially via Type 1 Angiotensin II receptor. *Basic Res Cardiol* **110**, 49.

Doka, G., Malikova, E., Galkova, K., La Rocca, G., Kruzliak, P., Adamek, M., Rodrigo, L., Krenek, P. and Klimas, J. (2017). Downregulation of myogenic microRNAs in sub-chronic but not in sub-acute model of daunorubicin-induced cardiomyopathy. *Mol Cell Biochem* **432**, 79–89.

Dong, S., Cheng, Y., Yang, J., Li, J., Liu, X., Wang, X., Wang, D., Krall, T. J., Delphin, E. S. and Zhang, C. (2009). MicroRNA Expression Signature and the Role of MicroRNA-21 in the Early Phase of Acute Myocardial Infarction. *Journal of Biological Chemistry* **284**, 29514–29525.

Drawnel, F. M., Wachten, D., Molkentin, J. D., Maillet, M., Aronsen, J. M., Swift, F., Sjaastad, I., Liu, N., Catalucci, D., Mikoshiba, K., et al. (2012). Mutual antagonism between IP3RII and miRNA-133a regulates calcium signals and cardiac hypertrophy. *Journal of Cell Biology* **199**, 783–798.

Eakins, S. and Xu, J. J. eds. (2009). *Drug Efficacy, Safety, and Biologics Discovery: Emerging Technologies and Tools*. Hoboken, New Jersey: John Wiley & Sons.

Eitel, I., Adams, V., Dieterich, P., Fuernau, G., De Waha, S., Desch, S., Schuler, G. and Thiele, H. (2012). Relation of circulating MicroRNA-133a concentrations with myocardial damage and clinical prognosis in ST-elevation myocardial infarction. *American Heart Journal* **164**, 706–714.

Eken, S. M., Christersdottir, T., Winski, G., Sangsuwan, T., Jin, H., Chernogubova, E., Pirault, J., Sun, C., Simon, N., Winter, H., et al. (2019). miR-29b Mediates the Chronic Inflammatory Response in Radiotherapy-Induced Vascular Disease. *JACC: Basic to Translational Science* **4**, 72–82.

Eulalio, A., Mano, M., Ferro, M. D., Zentilin, L., Sinagra, G., Zacchigna, S. and Giacca, M. (2012). Functional screening identifies miRNAs inducing cardiac regeneration. *Nature* **492**, 376–381.

European Commission (2003). Directive 2003/63/EC. *Official Journal of the European Union* **L**, 46–94.

Feldman, A., Moreira, D. A. R., Gun, C., Wang, H.-T. L., Hirata, M. H., De Freitas Germano, J., Leite, G. G. S. and Farsky, P. (2017). Analysis of Circulating miR-1, miR-23a, and miR-26a in Atrial Fibrillation Patients Undergoing Coronary Bypass Artery Grafting Surgery: Atrial Fibrillation Patients Undergoing Coronary Bypass Artery Grafting Surgery. *Annals of Human Genetics* **81**, 99–105.

Ferreira, A. L. A., Matsubara, L. S. and Matsubara, B. B. (2008). Anthracycline-Induced Cardiotoxicity. *Cardiovascular & Hematological Agents in Medicinal Chemistry* **6**,.

Fisher, M., James-Zorn, C., Ponferrada, V., Bell, A. J., Sundararaj, N., Segerdell, E., Chaturvedi, P., Bayyari, N., Chu, S., Pells, T., et al. (2023). Xenbase: key features and resources of the *Xenopus* model organism knowledgebase. *GENETICS* **224**, iyad018.

Food and Drug Administration (2005). Guidance for Industry.

Fort, D. J., Rogers, R. L., Thomas, J. H., Buzzard, B. O., Noll, A. M. and Spaulding, C. D. (2004). Comparative sensitivity of *Xenopus tropicalis* and *Xenopus laevis* as test species for the FETAX model. *J of Applied Toxicology* **24**, 443–457.

Fu, J., Chen, Y. and Li, F. (2018). Attenuation of MicroRNA-495 Derepressed PTEN to Effectively Protect Rat Cardiomyocytes from Hypertrophy. *Cardiology* **139**, 245–254.

Fu, J., Zhu, W., Wang, L., Luo, M., Jiang, B. and Dong, Z. (2022). Dynamic Expression and Gene Regulation of MicroRNAs During Bighead Carp (Hypophthalmichthys nobilis) Early Development. *Front. Genet.* **12**, 821403.

Gao, J. and Shen, W. (2021). Xenopus in revealing developmental toxicity and modeling human diseases. *Environmental Pollution* **268**, 115809.

Garg, P., Lewis, R. A., Johns, C. S., Swift, A. J., Capener, D., Rajaram, S., Thompson, A. A. R., Condliffe, R., Elliot, C. A., Charalampopoulos, A., et al. (2021). Cardiovascular magnetic resonance predicts all-cause mortality in pulmonary hypertension associated with heart failure with preserved ejection fraction. *Int J Cardiovasc Imaging* **37**, 3019–3025.

Gintant, G. A., Limberis, J. T., McDermott, J. S., Wegner, C. D. and Cox, B. F. (2001). The canine Purkinje fiber: An in vitro model system for acquired long QT syndrome and drug-induced arrhythmogenesis. *Journal of Cardiovascular Pharmacology* **37**, 607–618.

Giunti Editorial Group ed. (2005). *Atlas of Anatomy*. Herron Books (Distributed Titles).

Godden, A. M., Antonaci, M., Ward, N. J., Van Der Lee, M., Abu-Daya, A., Guille, M. and Wheeler, G. N. (2022). An efficient miRNA knockout approach using CRISPR-Cas9 in Xenopus. *Developmental Biology* **483**, 66–75.

Goren, Y., Kushnir, M., Zafrir, B., Tabak, S., Lewis, B. S. and Amir, O. (2012). Serum levels of microRNAs in patients with heart failure. *European Journal of Heart Failure* **14**, 147–154.

Guo, R., Liu, G., Du, M., Shi, Y., Jiang, P., Liu, X., Liu, L., Liu, J. and Xu, Y. (2015). Early ketamine exposure results in cardiac enlargement and heart dysfunction in Xenopus embryos. *BMC Anesthesiol* **16**,.

Gutiérrez-Lovera, C., Martínez-Val, J., Cabezas-Sainz, P., López, R., Rubiolo, J. A. and Sánchez, L. (2019). *In vivo* toxicity assays in zebrafish embryos: a pre-requisite for xenograft preclinical studies. *Toxicology Mechanisms and Methods* **29**, 478–487.

Han, J. J. (2023). FDA Modernization Act 2.0 allows for alternatives to animal testing. *Artificial Organs* **47**, 449–450.

He, R., Ding, C., Yin, P., He, L., Xu, Q., Wu, Z., Shi, Y. and Su, L. (2019). MiR-1a-3p mitigates isoproterenol-induced heart failure by enhancing the expression of mitochondrial ND1 and COX1. *Experimental Cell Research* **378**, 87–97.

Hempel, A. and Kühl, M. (2016). A Matter of the Heart: The African Clawed Frog Xenopus as a Model for Studying Vertebrate Cardiogenesis and Congenital Heart Defects. *Journal of Cardiovascular Development and Disease* **3**, 21.

Hofbauer, P., Jahnel, S. M., Papai, N., Giesshammer, M., Deyett, A., Schmidt, C., Penc, M., Tavernini, K., Grdseloff, N., Meledeth, C., et al. (2021). Cardioids reveal self-organizing principles of human cardiogenesis. *Cell* **184**, 3299-3317.e22.

Holmgren, G., Synnergren, J., Andersson, C. X., Lindahl, A. and Sartipy, P. (2016). Toxicology in Vitro MicroRNAs as potential biomarkers for doxorubicin-induced cardiotoxicity. *Toxicology in Vitro* **34**, 26–34.

Hoppler, S. and Conlon, F. L. (2020). Xenopus: Experimental access to cardiovascular development, regeneration discovery, and cardiovascular heart-defect modeling. *Cold Spring Harbor Perspectives in Biology* **12**, 1–10.

Horie, T., Ono, K., Nishi, H., Nagao, K., Kinoshita, M., Watanabe, S., Kuwabara, Y., Nakashima, Y., Takanabe-Mori, R., Nishi, E., et al. (2010). Acute doxorubicin cardiotoxicity is associated with miR-146a-induced inhibition of the neuregulin-ErbB pathway. *Cardiovascular Research* **87**, 656–664.

Hou, P. C. and Burggren, W. W. (1995). Blood pressures and heart rate during larval development in the anuran amphibian Xenopus laevis. *American Journal of Physiology-Regulatory, Integrative and Comparative Physiology* **269**, R1120–R1125.

Huang, Z.-P., Chen, J., Seok, H. Y., Zhang, Z., Kataoka, M., Hu, X. and Wang, D.-Z. (2013). MicroRNA-22 Regulates Cardiac Hypertrophy and Remodeling in Response to Stress. *Circulation Research* **112**, 1234–1243.

Huang, Z., Jia, K., Tan, Y., Yu, Y., Xiao, W., Zhou, X., Yi, J. and Zhang, C. (2025). Advances in cardiac organoid research: implications for cardiovascular disease treatment. *Cardiovasc Diabetol* **24**, 25.

Hubrecht, R. C. and Carter, E. (2019). The 3Rs and Humane Experimental Technique: Implementing Change. *Animals* **9**, 754.

Hydbring, P. and Badalian-Very, G. (2013). Clinical applications of microRNAs. *F1000 Research* **2**,.

ICH Harmonised Tripartite Guideline (1994). Dose Response Information to Support Drug Registration E4.

ICH Harmonised Tripartite Guideline (1998). Duration of Chronic Toxicity Testing in Animals (Rodent and Non-Rodent Toxicity Testing) S4.

ICH Harmonised Tripartite Guideline (2000). Safety Pharmacology Studies for Human Pharmaceuticals S7A.

ICH Harmonised Tripartite Guideline (2005a). The Non-Clinical Evaluation of the Potential for Delayed Ventricular Repolarization (QT Interval Prolongation) by Human Pharmaceuticals S7B.

ICH Harmonised Tripartite Guideline (2005b). The Clinical Evaluation of QT/QTc Interval Prolongation and Proarrhythmic Potential for Non-Antiarrhythmic Drugs E14.

ICH Harmonised Tripartite Guideline (2009a). Guidance on Nonclinical Safety Studies for the Conduct of Human Clinical Trials and Marketing Authorisation for Pharmaceuticals M3(R2).

ICH Harmonised Tripartite Guideline (2009b). Nonclinical Evaluation for Anticancer Pharmaceuticals S9.

Ito, Y., Seno, S., Nakamura, H., Fukui, A. and Asashima, M. (2008). XHAPLN3 plays a key role in cardiogenesis by maintaining the hyaluronan matrix around heart anlage. *Developmental Biology* **319**, 34–45.

Jang, D. G., Sim, H. J. and Kwon, K. Y. (2025). Integrative approaches in Xenopus-based research: A report from the 1st Asian Xenopus Conference. *Development, Growth & Differentiation* **67**, 186–191.

Ji, X., Ding, W., Xu, T., Zheng, X., Zhang, J., Liu, M., Liu, G. and Wang, J. (2020). MicroRNA-31-5p attenuates doxorubicin-induced cardiotoxicity via quaking and circular RNA Pan3. *Journal of Molecular and Cellular Cardiology* **140**, 56–67.

Jiao, M., You, H.-Z., Yang, X.-Y., Yuan, H., Li, Y.-L., Liu, W.-X., Jin, M. and Du, J. (2018). Circulating microRNA signature for the diagnosis of childhood dilated cardiomyopathy. *Sci Rep* **8**, 724.

Jost, N., Papp, J. G. and Varró, A. (2007). Slow delayed rectifier potassium current (IKs) and the repolarization reserve. *Annals of Noninvasive Electrocardiology* **12**, 64–78.

Karakikes, I., Chaanine, A. H., Kang, S., Mukete, B. N., Jeong, D., Zhang, S., Hajjar, R. J. and Lebeche, D. (2013). Therapeutic Cardiac-Targeted Delivery of *miR-1* Reverses Pressure Overload–Induced Cardiac Hypertrophy and Attenuates Pathological Remodeling. *JAHA* **2**, e000078.

Khan, S. U., Khan, A. U., Kamal, M. A. and Htar, T. T. (2023). Computer-aided drug designing illuminate polypharmacology of natural products against multiple estrogen receptor. In *Computational Approaches in Drug Discovery, Development and Systems Pharmacology*, pp. 281–333. Elsevier.

Kim, I., Boyle, K. M. and Carroll, J. L. (2005). Postnatal development of E-4031-sensitive potassium current in rat carotid chemoreceptor cells. *Journal of Applied Physiology* **98**, 1469–1477.

Kodama, I., Kamiya, K. and Toyama, J. (1997). Cellular electropharmacology of amiodarone. *Cardiovascular Research* **35**, 13–29.

Kolker, S. J., Tajchman, U. and Weeks, D. L. (2000). Confocal Imaging of Early Heart Development in Xenopus laevis. *Developmental Biology* **218**, 64–73.

Kozomara, A., Birgaoanu, M. and Griffiths-Jones, S. (2019). miRBase: from microRNA sequences to function. *Nucleic Acids Research* **47**, D155–D162.

Kuwabara, Y., Ono, K., Horie, T., Nishi, H., Nagao, K., Kinoshita, M., Watanabe, S., Baba, O., Kojima, Y., Shizuta, S., et al. (2011). Increased MicroRNA-1 and MicroRNA-133a Levels in Serum of Patients With Cardiovascular Disease Indicate Myocardial Damage. *Circ Cardiovasc Genet* **4**, 446–454.

Laboratory Animal Welfare Act (1966).

Lai, L., Chen, J., Wang, N., Zhu, G., Duan, X. and Ling, F. (2017). MiRNA-30e mediated cardioprotection of ACE2 in rats with Doxorubicin-induced heart failure through inhibiting cardiomyocytes autophagy. *Life Sciences* **169**, 69–75.

Leger, K. J., Leonard, D., Nielson, D., De Lemos, J. A., Mammen, P. P. A. and Winick, N. J. (2017). Circulating microRNAs: Potential Markers of Cardiotoxicity in Children and Young Adults Treated With Anthracycline Chemotherapy. *JAHA* **6**, e004653.

Lei, J., He, M., Li, J., Li, H., Wang, W., Gopinath, S. C. B. and Xu, L. (2022). miRNA identification by nuclease digestion in ELISA for diagnosis of osteosarcoma. *Biotech and App Biochem* **69**, 1365–1372.

Li, X., Zhang, R., Zhao, B., Lossin, C. and Cao, Z. (2016). Cardiotoxicity screening: a review of rapid-throughput in vitro approaches. *Archives of Toxicology* **90**, 1803–1816.

Li, Z., Song, Y., Liu, L., Hou, N., An, X., Zhan, D., Li, Y., Zhou, L., Li, P., Yu, L., et al. (2017). miR-199a impairs autophagy and induces cardiac hypertrophy through mTOR activation. *Cell Death Differ* **24**, 1205–1213.

Li, R. A., Keung, W., Cashman, T. J., Backeris, P. C., Johnson, B. V., Bardot, E. S., Wong, A. O. T., Chan, P. K. W., Chan, C. W. Y. and Costa, K. D. (2018a). Bioengineering an electro-mechanically functional miniature ventricular heart chamber from human pluripotent stem cells. *Biomaterials* **163**, 116–127.

Li, M., Chen, X., Chen, L., Chen, K., Zhou, J. and Song, J. (2018b). MiR-1-3p that correlates with left ventricular function of HCM can serve as a potential target and differentiate HCM from DCM. *J Transl Med* **16**, 161.

Li, J., Zhang, Y., Song, X., Li, R., Yang, W., Tian, M., Zhang, S., Cao, G., Song, L., Chen, Y., et al. (2022). The mechanism and effects of remdesivir-induced developmental toxicity in zebrafish: Blood flow dysfunction and behavioral alterations. *Journal of Applied Toxicology* **42**, 1688–1700.

Lian, Q., Chow, Y., Esteban, M., Pei, D. and Tse, H. F. (2010). Future perspective of induced pluripotent stem cells for diagnosis, drug screening and treatment of human diseases. *Thrombosis and haemostasis* **104**, 39–44.

Lian, J., Guo, J., Huang, X., Yang, X., Huang, G., Mao, H., Sun, H. H., Ba, Y. and Zhou, J. (2016). miRNAs Regulate hERG. *Journal of Cardiovascular Electrophysiology* **27**, 1472–1482.

Liang, P., Lan, F., Lee, A. S., Gong, T., Sanchez-Freire, S.-F., Wang, Y., Diecke, S., Sallam, K., Knowles, J. W., Wang, P. J., et al. (2013). Drug screening using a library of human induced pluripotent stem cell-derived cardiomyocytes reveals disease-specific patterns of cardiotoxicity. *Circulation* **127**, 1677–1691.

Link, F., Krohn, K. and Schumann, J. (2019). Identification of stably expressed housekeeping miRNAs in endothelial cells and macrophages in an inflammatory setting. *Sci Rep* **9**, 12786.

Liu, X., Fan, Z., Zhao, T., Cao, W., Zhang, L., Li, H., Xie, Q., Tian, Y. and Wang, B. (2015). Plasma miR-1, miR-208, miR-499 as potential predictive biomarkers for acute myocardial infarction: An independent study of Han population. *Experimental Gerontology* **72**, 230–238.

Liu, L., Ning, B., Cui, J., Zhang, T. and Chen, Y. (2017). miR-29c is implicated in the cardioprotective activity of Panax notoginseng saponins against isoproterenol-induced myocardial fibrogenesis. *Journal of Ethnopharmacology* **198**, 1–4.

Livak, K. J. and Schmittgen, T. D. (2001). Analysis of relative gene expression data using real-time quantitative PCR and the 2-ΔΔCT method. *Methods* **25**, 402–408.

Lohr, J. L. and Yost, H. J. (2000). Vertebrate model systems in the study of early heart development:Xenopus and zebrafish. *Am. J. Med. Genet.* **97**, 248–257.

Longhini, L. S., Zena, L. A., Da Silva, G. S. F., Bícego, K. C. and Gargaglioni, L. H. (2017). Temperature effects on the cardiorespiratory control of American bullfrog tadpoles based on a non-invasive methodology. *Journal of Experimental Biology* jeb.160911.

Lu, F. C. and Kacew, S. (2002). *Lu's Basic Toxicology*. London, UK: Taylor & Francis.

Marín-Barba, M., Gavilán, H., Gutiérrez, L., Lozano-Velasco, E., Rodríguez-Ramiro, I., Wheeler, G. N., Morris, C. J., Morales, M. P. and Ruiz, A. (2018). Unravelling the mechanisms that determine the uptake and metabolism of magnetic single and multicore nanoparticles in a *Xenopus laevis* model. *Nanoscale* **10**, 690–704.

Martini, F., Tarazona, J. V. and Pablos, M. V. (2012). Are Fish and Standardized FETAX Assays Protective Enough for Amphibians? A Case Study on *Xenopus laevis* Larvae Assay with Biologically Active Substances Present in Livestock Wastes. *The Scientific World Journal* **2012**, 1–6.

Mathur, A., Loskill, P., Shao, K., Huebsch, N., Hong, S., Marcus, S. G., Marks, N., Mandegar, M., Conklin, B. R., Lee, L. P., et al. (2015). Human iPSC-based Cardiac Microphysiological System For Drug Screening Applications. *Sci Rep* **5**, 8883.

McGill, M. R. and Jaeschke, H. (2013). Metabolism and Disposition of Acetaminophen: Recent Advances in Relation to Hepatotoxicity and Diagnosis. *Pharm Res* **30**, 2174–2187.

Meng, C., Fan, L., Wang, X., Wang, Y., Li, Y., Pang, S., Lv, S. and Zhang, J. (2022). Preparation and Evaluation of Animal Models of Cardiotoxicity in Antineoplastic Therapy. *Oxidative Medicine and Cellular Longevity* **2022**, 1–16.

Milan, D. J. and MacRae, C. A. (2011). In Vivo Recording of the Adult Zebrafish Electrocardiogram. In *Zebrafish: Methods for Assessing Drug Safety and Toxicity*, .

Ministry of Science and Technology (1988). *Statute on the Administration of Laboratory Animal Use*.

Ministry of Science and Technology (2006). *Guideline on the Humane Treatment of Laboratory Animals*.

Mittal, P., Chopra, H., Kaur, K. P. and Gautam, R. K. (2023). New drug discovery pipeline. In *Computational Approaches in Drug Discovery, Development and Systems Pharmacology*, pp. 197–222. Elsevier.

Mohun, T. (2003). The Origins of Cardiac Tissue in the Amphibian, Xenopus laevis. *Trends in Cardiovascular Medicine* **13**, 244–248.

Mohun, T. J., Leong, L. M., Weninger, W. J. and Sparrow, D. B. (2000). The Morphology of Heart Development in Xenopus laevis. *Developmental Biology* **218**, 74–88.

Monahan, B. P., Ferguson, C. L., Killeavy, E. S., Lloyd, B. K., Troy, J. and Cantilena Jr, L. R. (1990). Torsades de pointes occurring in association with terfenadine use. *JAMA: Journal of the American Medical Association* **264**, 2788–2790.

Moonen, M., Frere, P., Lancellotti, P. and Jerusalem, G. (2017). *Cardiac Monitoring During Clinical Trials*. Elsevier Inc.

Morais, F., Pires, V., Almeida, M., Martins, M. A., Oliveira, M. and Lopes, I. (2024). Influence of polystyrene nanoplastics on the toxicity of haloperidol to amphibians: An in vivo and in vitro approach. *Science of The Total Environment* **951**, 175375.

Moser, B. and Rayburn, J. (2007). Research Article: Evaluation of developmental toxicity of interaction between caffeine and pseudoephedrine using frog embryo teratogenesis assay-Xenopus (Fetax). *BIOS* **78**, 1–9.

Mouche, I., Malesic, L. and Gillardeaux, O. (2011). FETAX Assay for Evaluation of Developmental Toxicity. In *Drug Safety Evaluation: Methods and Protocols*, pp. 257–269. Humana Press.

Nerbonne, J. M., Nichols, C. G., Schwarz, T. L. and Escande, D. (2001). Genetic Manipulation of Cardiac K^+ Channel Function in Mice: What Have We Learned, and Where Do We Go From Here? *Circulation Research* **89**, 944–956.

Nieuwkoop, P. D. and Faber, J. (1958). Normal Table of Xenopus Laevis (Daudin). *Copeia*.

Ning, B., Zhang, Y., Wu, D., Cui, J., Liu, L., Wang, P., Wang, W., Zhu, W., Chen, Y. and Zhang, T. (2017). Luteolin-7-diglucuronide attenuates isoproterenol-induced myocardial injury and fibrosis in mice. *Acta Pharmacol Sin* **38**, 331–341.

Nishi, H., Ono, K., Horie, T., Nagao, K., Kinoshita, M., Kuwabara, Y., Watanabe, S., Takaya, T., Tamaki, Y., Takanabe-Mori, R., et al. (2011). MicroRNA-27a Regulates Beta Cardiac Myosin Heavy Chain Gene Expression by Targeting Thyroid Hormone Receptor β1 in Neonatal Rat Ventricular Myocytes. *Molecular and Cellular Biology* **31**, 744–755.

Nishimura, Y., Kondo, C., Morikawa, Y., Tonomura, Y., Torii, M., Yamate, J. and Uehara, T. (2015). Plasma miR-208 as a useful biomarker for drug-induced cardiotoxicity in rats. *J of Applied Toxicology* **35**, 173–180.

Novak, J., Sana, J., Stracina, T., Novakova, M. and Slaby, O. (2017). Doxorubicin and Liposomal Doxorubicin Differentially Affect Expression of miR-208a and let-7g in Rat Ventricles and Atria. *Cardiovasc Toxicol* **17**, 355–359.

Obiol-Pardo, C., Gomis-Tena, J., Sanz, F., Saiz, J. and Pastor, M. (2011). A multiscale simulation system for the prediction of drug-induced cardiotoxicity. *Journal of Chemical Information and Modeling* **51**, 483–492.

Ok Song, M., Fort, D. J., McLaughlin, D. L., Rogers, R. L., Thomas, J. H., Buzzard, B. O., Noll, A. M. and Myers, N. K. (2003). Evaluation of *Xenopus tropicalis* as an Alternative Test Organism for Frog Embryo Teratogenesis Assay— *Xenopus* (FETAX). *Drug and Chemical Toxicology* **26**, 177–189.

Oleaga, C., Bernabini, C., Smith, A. S. T., Srinivasan, B., Jackson, M., McLamb, W., Platt, V., Bridges, R., Cai, Y., Santhanam, N., et al. (2016). Multi-Organ toxicity demonstration in a functional human in vitro system composed of four organs. *Sci Rep* **6**, 20030.

Osman, M. and Elkady, M. (2017). A Prospective Study to Evaluate the Effect of Paclitaxel on Cardiac Ejection Fraction. *Breast Care* **12**, 255–259.

Ostapowicz, G. (2002). Results of a Prospective Study of Acute Liver Failure at 17 Tertiary Care Centers in the United States. *Ann Intern Med* **137**, 947.

Park, M. J., Chae, J.-P., Woo, D., Kim, J. Y., Bae, Y. C., Lee, J. Y., Lee, S. Y., Nam, E. J. and Nam, S.-W. (2024). Ibuprofen-induced multiorgan malformation during embryogenesis in Xenopus laevis (FETAX). *Biochemical and Biophysical Research Communications* **703**, 149565.

Pathak, S., Mishra, A., Sonawane, G., Sonawane, K., Rawat, S., Raizaday, A., Singh, S. K. and Gupta, G. (2023). In silico pharmacology. In *Computational Approaches in Drug Discovery, Development and Systems Pharmacology*, pp. 1–52. Elsevier.

Pellegrini, L., Sileno, S., D'Agostino, M., Foglio, E., Florio, M. C., Guzzanti, V., Russo, M. A., Limana, F. and Magenta, A. (2020). MicroRNAs in Cancer Treatment-Induced Cardiotoxicity. *Cancers* **12**, 704.

Piegari, E., Russo, R., Cappetta, D., Esposito, G., Urbanek, K., Dell'Aversana, C., Altucci, L., Berrino, L., Rossi, F. and De Angelis, A. (2016). MicroRNA-34a regulates doxorubicin-induced cardiotoxicity in rat. *Oncotarget* **7**, 62312–62326.

Pizzino, F., Vizzari, G., Bomzer, C. A., Qamar, R., Carerj, S., Zito, C. and Khandheria, B. K. (2014). Diagnosis of Chemotherapy-Induced Cardiotoxicity. *Journal of Patient-Centered Research and Reviews* **1**, 121–127.

Podyacheva, E. Y., Kushnareva, E. A., Karpov, A. A. and Toropova, Y. G. (2021). Analysis of Models of Doxorubicin-Induced Cardiomyopathy in Rats and Mice. A Modern View From the Perspective of the Pathophysiologist and the Clinician. *Front. Pharmacol.* **12**, 670479.

Raniga, K., Nasir, A., Vo, N. T. N., Vaidyanathan, R., Dickerson, S., Hilcove, S., Mosqueira, D., Mirams, G. R., Clements, P., Hicks, R., et al. (2024). Strengthening cardiac therapy pipelines using human pluripotent stem cell-derived cardiomyocytes. *Cell Stem Cell* **31**, 292–311.

Rawal, S., Nagesh, P. T., Coffey, S., Van Hout, I., Galvin, I. F., Bunton, R. W., Davis, P., Williams, M. J. A. and Katare, R. (2019). Early dysregulation of cardiac-specific microRNA-208a is linked to maladaptive cardiac remodelling in diabetic myocardium. *Cardiovasc Diabetol* **18**, 13.

Redfern, W. S., Carlsson, L., Davis, A. S., Lynch, W. G., MacKenzie, I., Palethorpe, S., Siegl, P. K. S., Strang, I., Sullivan, A. T., Wallis, R., et al. (2003). Relationships between preclinical cardiac electrophysiology, clinical QT interval prolongation and torsade de pointes for a broad range of drugs: Evidence for a provisional safety margin in drug development. *Cardiovascular Research* **58**, 32–45.

Rice, J., Roberts, H., Rai, S. N. and Galandiuk, S. (2015). Housekeeping genes for studies of plasma microRNA: A need for more precise standardization. *Surgery* **158**, 1345–1351.

Rigaud, V. O. C., Ferreira, L. R. P., Ayub-Ferreira, S. M., ávila, M. S., Brandão, S. M. G., Cruz, F. D., Santos, M. H. H., Cruz, C. B. B. V., Alves, M. S. L., Issa, V. S., et al. (2017). Circulating miR-1 as a potential biomarker of doxorubicininduced cardiotoxicity in breast cancer patients. *Oncotarget* **8**, 6994–7002.

Rinnerthaler, G., Hackl, H., Gampenrieder, S., Hamacher, F., Hufnagl, C., Hauser-Kronberger, C., Zehentmayr, F., Fastner, G., Sedlmayer, F., Mlineritsch, B., et al.

(2016). miR-16-5p Is a Stably-Expressed Housekeeping MicroRNA in Breast Cancer Tissues from Primary Tumors and from Metastatic Sites. *IJMS* **17**, 156.

Roncarati, R., Viviani Anselmi, C., Losi, M. A., Papa, L., Cavarretta, E., Da Costa Martins, P., Contaldi, C., Saccani Jotti, G., Franzone, A., Galastri, L., et al. (2014). Circulating miR-29a, Among Other Up-Regulated MicroRNAs, Is the Only Biomarker for Both Hypertrophy and Fibrosis in Patients With Hypertrophic Cardiomyopathy. *Journal of the American College of Cardiology* **63**, 920–927.

Roy, M.-L., Dumaine, R. and Brown, A. M. (1996). HERG, a Primary Human Ventricular Target of the Nonsedating Antihistamine Terfenadine. *CIRCULATION* **94**, 817–823.

Rubiś, P., Totoń-Żurańska, J., Wiśniowska-Śmiałek, S., Holcman, K., Kołton-Wróż, M., Wołkow, P., Wypasek, E., Natorska, J., Rudnicka-Sosin, L., Pawlak, A., et al. (2017). Relations between circulating microRNAs (miR-21, miR-26, miR-29, miR-30 and miR-133a), extracellular matrix fibrosis and serum markers of fibrosis in dilated cardiomyopathy. *International Journal of Cardiology* **231**, 201–206.

Rubiś, P., Totoń-Żurańska, J., Wiśniowska-Śmiałek, S., Dziewięcka, E., Kołton-Wróż, M., Wołkow, P., Pitera, E., Rudnicka-Sosin, L., Garlitski, A. C., Gackowski, A., et al. (2018). The relationship between myocardial fibrosis and myocardial micro RNA s in dilated cardiomyopathy: A link between mir-133a and cardiovascular events. *J Cellular Molecular Medi* **22**, 2514–2517.

Saide, K. (2018). Development of a non-mammalian, pre-clinical screening tool for the predictive analysis of drug toxicity.

Saide, K., Sherwood, V. and Wheeler, G. N. (2019). Paracetamol-induced liver injury modelled in Xenopus laevis embryos. *Toxicology Letters* **302**, 83–91.

Sakai, K., Shimba, K., Ishizuka, K., Yang, Z., Oiwa, K., Takeuchi, A., Kotani, K. and Jimbo, Y. (2017). Functional innervation of human induced pluripotent stem cell-derived cardiomyocytes by co-culture with sympathetic neurons developed using a microtunnel technique. *Biochemical and Biophysical Research Communications* **494**, 138–143.

Sala, L., Van Meer, B. J., Tertoolen, L. G. J., Bakkers, J., Bellin, M., Davis, R. P., Denning, C., Dieben, M. A. E., Eschenhagen, T., Giacomelli, E., et al. (2018). MUSCLEMOTION: A Versatile Open Software Tool to Quantify Cardiomyocyte and Cardiac Muscle Contraction In Vitro and In Vivo. *Circulation Research* **122**,.

Salata, J. J., Jurkiewicz, N. K., Wallace, A. A., Stupienski, R. F., Guinosso, P. J. and Lynch, J. J. (1995). Cardiac Electrophysiological Actions of the Histamine H 1 -Receptor Antagonists Astemizole and Terfenadine Compared With Chlorpheniramine and Pyrilamine. *Circulation Research* **76**, 110–119.

Salkoff, L., Baker, K., Butler, A., Covarrubias, M., Pak, M. D. and Wei, A. (1992). An essential “set” of K+ channels conserved in flies, mice and humans. *Trends Neurosci* **15**, 161–6.

Sanguinetti, M. C., Jiang, C., Curran, M. E. and Keating, M. T. (1995). A mechanistic link between an inherited and an acquird cardiac arrthytmia: HERG encodes the IKr potassium channel. *Cell* **81**, 299–307.

Santoso, F., Farhan, A., Castillo, A. L., Malhotra, N., Saputra, F., Kurnia, K. A., Chen, K. H.-C., Huang, J.-C., Chen, J.-R. and Hsiao, C.-D. (2020). An Overview of Methods for Cardiac Rhythm Detection in Zebrafish. *Biomedicines* **8**, 329.

Schindelin, J., Arganda-Carreras, I., Frise, E., Kaynig, V., Longair, M., Pietzsch, T., Preibisch, S., Rueden, C., Saalfeld, S., Schmid, B., et al. (2012). Fiji: An open-source platform for biological-image analysis. *Nature Methods* **9**, 676–682.

Schmidt, C., Deyett, A., Ilmer, T., Haendeler, S., Torres Caballero, A., Novatchkova, M., Netzer, M. A., Ceci Ginistrelli, L., Mancheno Juncosa, E., Bhattacharya, T., et al. (2023). Multi-chamber cardioids unravel human heart development and cardiac defects. *Cell* **186**, 5587-5605.e27.

Schutgens, F. and Clevers, H. (2020). Human Organoids: Tools for Understanding Biology and Treating Diseases. *Annu. Rev. Pathol. Mech. Dis.* **15**, 211–234.

Session, A. M., Uno, Y., Kwon, T., Chapman, J. A., Toyoda, A., Takahashi, S., Fukui, A., Hikosaka, A., Suzuki, A., Kondo, M., et al. (2016). Genome evolution in the allotetraploid frog Xenopus laevis. *Nature* **538**, 336–343.

Shan, Z.-X., Lin, Q.-X., Fu, Y.-H., Deng, C.-Y., Zhou, Z.-L., Zhu, J.-N., Liu, X.-Y., Zhang, Y.-Y., Li, Y., Lin, S.-G., et al. (2009). Upregulated expression of miR-1/miR-206 in a rat model of myocardial infarction. *Biochemical and Biophysical Research Communications* **381**, 597–601.

Sharma, S., Kumaravel, J., Kaur, G., Prakash, A. and Medhi, B. (2023). Target identification for potential drug discovery. In *Computational Approaches in Drug Discovery, Development and Systems Pharmacology*, pp. 183–196. Elsevier.

Shi, H., Li, J., Song, Q., Cheng, L., Sun, H., Fan, W., Li, J., Wang, Z. and Zhang, G. (2019). Systematic identification and analysis of dysregulated mi RNA and transcription factor feed-forward loops in hypertrophic cardiomyopathy. *J Cellular Molecular Medi* **23**, 306–316.

Singal, P. K. and Iliskovic, N. (1998). Current Concepts: Doxorubicin-Induced Cardiomyopathy. *NEW ENGLAND JOURNAL OF MEDICINE* **339**, 900–905.

Skála, M., Hanousková, B., Skálová, L. and Matoušková, P. (2019). MicroRNAs in the diagnosis and prevention of drug-induced cardiotoxicity. *Archives of Toxicology* **93**, 1–9.

Spallarossa, P., Altieri, P., Garibaldi, S., Ghigliotti, G., Barisione, C., Manca, V., Fabbi, P., Ballestrero, A., Brunelli, C. and Barsotti, A. (2006). Matrix metalloproteinase-2 and -9 are induced differently by doxorubicin in H9c2 cells: The role of MAP kinases and NAD(P)H oxidase. *Cardiovascular Research* **69**, 736–745.

Steinherz, L. J., Steinherz, P. G., Tan, C. T. C., Murphy, M. L. and Heller, G. (1991). Cardiac Toxicity 4 to 20 Years After Completing Anthracycline Therapy. *JAMA: The Journal of the American Medical Association*.

Strauss, D. G., Wu, W. W., Li, Z., Koerner, J. and Garnett, C. (2021). Translational Models and Tools to Reduce Clinical Trials and Improve Regulatory Decision Making for QTc

and Proarrhythmia Risk (ICH E14/S7B Updates). *Clin Pharma and Therapeutics* **109**, 319–333.

Tang, Y., Zheng, J., Sun, Y., Wu, Z., Liu, Z. and Huang, G. (2009). MicroRNA-1 Regulates Cardiomyocyte Apoptosis by Targeting Bcl-2. *Int. Heart J.* **50**, 377–387.

Taylor, E. W. and Ihmied, Y. M. (1995). Vagal and adrenergic tone on the heart of Xenopus laevis at different temperatures. *Journal of Thermal Biology* **20**, 55–59.

Tijsen, A. J., Creemers, E. E., Moerland, P. D., De Windt, L. J., Van Der Wal, A. C., Kok, W. E. and Pinto, Y. M. (2010). MiR423-5p as a circulating biomarker for heart failure. *Circulation Research* **106**, 1035–1039.

Tomlinson, M. L., Field, R. A. and Wheeler, G. N. (2005). Xenopus as a model organism in developmental chemical genetic screens. *Molecular BioSystems* **1**, 223–228.

Tomlinson, M. L., Guan, P., Morris, R. J., Fidock, M. D., Rejzek, M., Garcia-Morales, C., Field, R. A. and Wheeler, G. N. (2009). A Chemical Genomic Approach Identifies Matrix Metalloproteinases as Playing an Essential and Specific Role in Xenopus Melanophore Migration. *Chemistry and Biology* **16**, 93–104.

Tong, Z., Jiang, B., Wu, Y., Liu, Y., Li, Y., Gao, M., Jiang, Y., Lv, Q. and Xiao, X. (2015). MiR-21 Protected Cardiomyocytes against Doxorubicin-Induced Apoptosis by Targeting BTG2. *IJMS* **16**, 14511–14525.

Tony, H., Yu, K. and Qiutang, Z. (2015). MicroRNA-208a Silencing Attenuates Doxorubicin Induced Myocyte Apoptosis and Cardiac Dysfunction. *Oxidative Medicine and Cellular Longevity* **2015**, 1–6.

Tu, Y., Wan, L., Bu, L., Zhao, D., Dong, D., Huang, T., Cheng, Z. and Shen, B. (2013). MicroRNA-22 Downregulation by Atorvastatin in a Mouse Model of Cardiac Hypertrophy: a new Mechanism for Antihypertrophic Intervention. *Cell Physiol Biochem* **31**, 997–1008.

Tu, Y., Wan, L., Zhao, D., Bu, L., Dong, D., Yin, Z., Cheng, Z. and Shen, B. (2014). In vitro and in vivo direct monitoring of miRNA-22 expression in isoproterenol-induced cardiac hypertrophy by bioluminescence imaging. *Eur J Nucl Med Mol Imaging* **41**, 972–984.

U.S Food & Drug Administration (2018). The Drug Development Process.

Vacchi-Suzzi, C., Bauer, Y., Berridge, B. R., Bongiovanni, S., Gerrish, K., Hamadeh, H. K., Letzkus, M., Lyon, J., Moggs, J., Paules, R. S., et al. (2012). Perturbation of microRNAs in Rat Heart during Chronic Doxorubicin Treatment. *PLoS ONE* **7**, e40395.

Valentin, J. P., Hoffmann, P., De Clerck, F., Hammond, T. G. and Hondeghem, L. (2004). Review of the predictive value of the Langendorff heart model (Screenit system) in assessing the proarrhythmic potential of drugs. *Journal of Pharmacological and Toxicological Methods* **49**, 171–181.

Valiyaveettil, D., Joseph, D. and Malik, M. (2023). Cardiotoxicity in breast cancer treatment: Causes and mitigation. *Cancer Treatment and Research Communications* **37**, 100760.

Van Acker, S. A. B. E., Kramer, K., Voest, E. E., Grimbergen, J. A., Zhang, J., Van Der Vijgh, W. J. F., Bast, A. and Van Acker, S. A. B. E. (1996). Doxorubicin-induced cardiotoxicity monitored by ECG in freely moving mice. *Cancer Chemotherapy and Pharmacology* **38**, 95–101.

Van Rooij, E., Quiat, D., Johnson, B. A., Sutherland, L. B., Qi, X., Richardson, J. A., Kelm, R. J. and Olson, E. N. (2009). A Family of microRNAs Encoded by Myosin Genes Governs Myosin Expression and Muscle Performance. *Developmental Cell* **17**, 662–673.

Wang, G. K., Zhu, J. Q., Zhang, J. T., Li, Q., Li, Y., He, J., Qin, Y. W. and Jing, Q. (2010). Circulating microRNA: A novel potential biomarker for early diagnosis of acute myocardial infarction in humans. *European Heart Journal* **31**, 659–666.

Wang, W., Shi, Q., Mattes, W. B., Mendrick, D. L. and Yang, X. (2015). Translating extracellular microRNA into clinical biomarkers for drug-induced toxicity: From high-throughput profiling to validation. *Biomarkers in Medicine* **9**, 1177–1188.

Webster, C. A., Di Silvio, D., Devarajan, A., Bigini, P., Micotti, E., Giudice, C., Salmona, M., Wheeler, G. N., Sherwood, V. and Bombelli, F. B. (2016). An Early Developmental Vertebrate Model for Nanomaterial Safety: Bridging Cell-Based and Mammalian Toxicity Assessment. *Nanomedicine (Lond.)* **11**, 643–656.

Weinsberg, F., Bauer, C. K. and Schwarz, J. R. (1997). The class III antiarrhythmic agent E-4031 selectively blocks the inactivating inward-rectifying potassium current in rat anterior pituitary tumor cells (GH 3 /B 6 cells). *Pfl gers Archiv European Journal of Physiology* **434**, 1–10.

Wheeler, G. N. and Brändli, A. W. (2009). Simple vertebrate models for chemical genetics and drug discovery screens: Lessons from zebrafish and Xenopus. *Developmental Dynamics* **238**, 1287–1308.

Wickham, H. (2023). stringr: Simple, Consistent Wrappers for Common String Operations.

Wickham, H., Chang, W., Henry, L., Pedersen, T. L., Takahashi, K., Wilke, C., Woo, K., Yutani, H., Dunnington, D. and van den Brand, T. (2016). ggplot2: Elegant Graphics for Data Analysis.

Wickham, H., François, R., Henry, L., Müller, K. and Vaughanh, D. (2025). dplyr: A Grammar of Data Manipulation.

Widera, C., Gupta, S. K., Lorenzen, J. M., Bang, C., Bauersachs, J., Bethmann, K., Kempf, T., Wollert, K. C. and Thum, T. (2011). Diagnostic and prognostic impact of six circulating microRNAs in acute coronary syndrome. *Journal of Molecular and Cellular Cardiology* **51**, 872–875.

Willsey, H. R., Seaby, E. G., Godwin, A., Ennis, S., Guille, M. and Grainger, R. M. (2024). Modelling human genetic disorders in *Xenopus tropicalis*. *Disease Models & Mechanisms* **17**, dmm050754.

Wittig, J. (2019). Investigating a microRNA-499-5p network during cardiac development.

Wolpert, L., Tickle, C. and Arias, alfonso martinez (2015). *Principles of Development*. Oxford: oxford university press.

Woosley, R. L., Chen, Y., Freiman, J. P. and Gillis, R. A. (1993). Mechanism of the Cardiotoxic Actions Of Terfenadine. *JAMA The Journal of the American Medical Association* **269**, 1532–1536.

Wyville, S. (2019). Characterisation of the neuro-glial-vascular unit in the developing and diseased retina using zebrafish (Danio rerio) as a model organism.

Xiang, M., Zeng, Y., Yang, R., Xu, H., Chen, Z., Zhong, J., Xie, H., Xu, Y. and Zeng, X. (2014). U6 is not a suitable endogenous control for the quantification of circulating microRNAs. *Biochemical and Biophysical Research Communications* **454**, 210–214.

Xiao, Y., Zhao, J., Tuazon, J. P., Borlongan, C. V. and Yu, G. (2019). MicroRNA-133a and Myocardial Infarction. *Cell Transplant* **28**, 831–838.

Xin, Y., Yang, C. and Han, Z. (2016). Circulating miR-499 as a potential biomarker for acute myocardial infarction. *Ann. Transl. Med.* **4**, 135–135.

Xu, X., Song, X., Li, Q., Wang, G., Jing, Q. and Qin, Y. (2012). Attenuation of MicroRNA-22 derepressed PTEN to effectively protect rat cardiomyocytes from hypertrophy. *Journal Cellular Physiology* **227**, 1391–1398.

Xu, C., Hu, Y., Hou, L., Ju, J., Li, X., Du, N., Guan, X., Liu, Z., Zhang, T., Qin, W., et al. (2014). β-Blocker carvedilol protects cardiomyocytes against oxidative stress-induced apoptosis by up-regulating miR-133 expression. *Journal of Molecular and Cellular Cardiology* **75**, 111–121.

Xue, S., Liu, D., Zhu, W., Su, Z., Zhang, L., Zhou, C. and Li, P. (2019). Circulating miR-17-5p, miR-126-5p and miR-145-3p are novel biomarkers for diagnosis of acute myocardial infarction. *Frontiers in Physiology* **10**, 1–11.

Yang, T., Prakash, C., Roden, D. M. and Snyders, D. J. (1995). Mechanism of block of a human cardiac potassium channel by terfenadine racemate and enantiomers. *British J Pharmacology* **115**, 267–274.

Yang, Q., Cui, J., Wang, P., Du, X., Wang, W., Zhang, T. and Chen, Y. (2016). Changes in interconnected pathways implicating microRNAs are associated with the activity of apocynin in attenuating myocardial fibrogenesis. *European Journal of Pharmacology* **784**, 22–32.

Yang, C.-L., Tsai, F.-M., Chen, C.-W., Hsiao, K.-H., Chen, J.-H. and Kao, W.-Y. (2022). Comparing miR-16 and miR-1228 as an optimal endogenous control for quantification of circulating microRNAs in colorectal cancer patients. *Tzu Chi Med J* **34**, 318.

Yin, C., Salloum, F. N. and Kukreja, R. C. (2009). A Novel Role of MicroRNA in Late Preconditioning: Upregulation of Endothelial Nitric Oxide Synthase and Heat Shock Protein 70. *Circulation Research* **104**, 572–575.

Yu, Y., Liu, H., Yang, D., He, F., Yuan, Y., Guo, J., Hu, J., Yu, J., Yan, X., Wang, S., et al. (2019). Aloe-emodin attenuates myocardial infarction and apoptosis via up-regulating miR-133 expression. *Pharmacological Research* **146**, 104315.

Zahn, N., James-Zorn, C., Ponferrada, V. G., Adams, D. S., Grzymkowski, J., Buchholz, D. R., Nascone-Yoder, N. M., Horb, M., Moody, S. A., Vize, P. D., et al. (2022). Normal Table of Xenopus development: a new graphical resource. *Deveopment* **149**,.

Zeiss, C. J., Gatti, D. M., Toro-Salazar, O., Davis, C., Lutz, C. M., Spinale, F., Stearns, T., Furtado, M. B. and Churchill, G. A. (2019). Doxorubicin-Induced Cardiotoxicity in Collaborative Cross (CC) Mice Recapitulates Individual Cardiotoxicity in Humans. *G3 Genes|Genomes|Genetics* **9**, 2637–2646.

Zhang, H., Liu, S., Dong, T., Yang, J., Xie, Y., Wu, Y., Kang, K., Hu, S., Gou, D. and Wei, Y. (2016). Profiling of differentially expressed microRNAs in arrhythmogenic right ventricular cardiomyopathy. *Sci Rep* **6**, 28101.

Zhang, X., Sun, Y., Zhang, Y., Fang, F., Liu, J., Xia, Y. and Liu, Y. (2022). Cardiac Biomarkers for the Detection and Management of Cancer Therapy-Related Cardiovascular Toxicity. *JCDD* **9**, 372.

Zhao, L. and Zhang, B. (2017). Doxorubicin induces cardiotoxicity through upregulation of death receptors mediated apoptosis in cardiomyocytes. *Scientific Reports* **7**, 1–11.

Zhao, C. H., Cheng, G.-C., He, R. L., Hong, Y., Wan, Q. L., Wang, Z.-Z. and Pan, Z.-Y. (2015). Analysis and clinical significance of microRNA-499 expression levels in serum of patients with acute myocardial infarction. *Genet. Mol. Res.* **14**, 4027–4034.

Zhao, D., Lei, W. and Hu, S. (2021). Cardiac organoid — a promising perspective of preclinical model. *Stem Cell Research and Therapy* **12**, 1–11.

Zhou, X., Li, X. and Wu, M. (2018). miRNAs reshape immunity and inflammatory responses in bacterial infection. *Sig Transduct Target Ther* **3**, 14.

Zhu, J.-N., Fu, Y.-H., Hu, Z., Li, W.-Y., Tang, C.-M., Fei, H.-W., Yang, H., Lin, Q., Gou, D.-M., Wu, S.-L., et al. (2017). Activation of miR-34a-5p/Sirt1/p66shc pathway contributes to doxorubicin-induced cardiotoxicity. *Sci Rep* **7**, 11879.

Zimmerman, M., Duruz, H., Guinand, O., Broccard, O., Levy, P., Lacatis, D. and Bloch, A. (1992). Torsades de Pointes after treatment with terfenadine and ketoconazole. *European Heart Journal* **13**, 1002–1003.

Zorn, A. M. and Mason, J. (2001). Gene expression in the embryonic Xenopus liver. *Mechanisms of Development* **103**, 153–157.

Appendix

Appendix A: First iteration of automation code.

```r
install.packages('nls')
library(stats)
###fiting sine curve to dataset
datasets <- list.files(path="C:/Users/saswy/Desktop/R_Data/current data", pattern="*csv", full.names=TRUE, recursive=FALSE)###list all the files in the working directory
input_datasets<-lapply(datasets, read.csv, header=TRUE, stringsAsFactors=FALSE)##read/import all the files listed before (all datasets in the dorectory)
names<-list.files(path = "C:/Users/saswy/Desktop/R_Data/current data", pattern ="*csv",
                  full.names = FALSE)###list with names of the files
names<-data.frame(names)##convert to data frame
pp <- expand.grid(b=(10:25), c=(1), A=1, D=1)##create data frame with potential parameters to try to fit the model with
nlc <- nls.control(maxiter = 1000,minFactor = 1/12000000)
df<-data.frame()
find_parameters<-lapply(input_datasets,function(x){
  t<-x$seconds
  y<-x$R.C
  for (i in 1:nrow(pp)){
    res<- nls(y ~ A*sin(b*t+c)+D, data=data.frame(t,y),control=nlc, start=list(A=pp$A[i],b=pp$b[i],c=pp$c[i],D=pp$D[i]))
    results<-data.frame(se=sigma(res),coef_A=coef(res)[1],coef_b=coef(res)[2],coef_c=coef(res)[3],coef_D=coef(res)[4])
    df<-rbind(df,results$se,results$coef_A,results$coef_b,results$coef_c,results$coef_D)
    names(df)<-"values"
  }
  df
})
final_parameters<-data.frame()
extract_values<-lapply(find_parameters,function(x){
  df_model<-as.data.frame(unlist(x))
  names(df_model)<-"values"
  df_model<-data.frame(se= df_model$values[c(TRUE, FALSE,FALSE,FALSE,FALSE)], coef_A = df_model$values[c(FALSE, TRUE,FALSE,FALSE,FALSE)],
                       coef_b = df_model$values[c(FALSE, FALSE,TRUE,FALSE,FALSE)],coef_c = df_model$values[c(FALSE, FALSE,FALSE,TRUE,FALSE)],
                       coef_D = df_model$values[c(FALSE, FALSE,FALSE,FALSE,TRUE)])
  best_fit<-df_model[df_model$se==min(df_model$se),]
  #print(df_model)
  final_parameters<-rbind(final_parameters,best_fit)
  #print(final_parameters)
})
results<-as.data.frame(unlist(extract_values))
names(results)<-"values"
results<-data.frame(se= results$values[c(TRUE, FALSE,FALSE,FALSE,FALSE)], coef_A = results$values[c(FALSE, TRUE,FALSE,FALSE,FALSE)],
                    coef_b = results$values[c(FALSE, FALSE,TRUE,FALSE,FALSE)],coef_c = results$values[c(FALSE, FALSE,FALSE,TRUE,FALSE)],
                    coef_D = results$values[c(FALSE, FALSE,FALSE,FALSE,TRUE)])
results$dataset<-names$names
results$number_of_beats<-results$coef_b/(2*pi)*30

##fit the curve by trying potential parameters specified in a data frame pp. This is automated instead of manual
pp <- expand.grid(b=(10:25), c=(1), A=1, D=1) ##create data frame with potential parameters
nlc <- nls.control(maxiter = 1000,minFactor = 1/12000000)##parameters for the fitting function
df<-data.frame()##data frame object to store results
for (i in 1:nrow(pp)){##loop over the parameters in pp to fit the sine curve until all of them have been used.
  res<- nls(y ~ A*sin(b*t+c)+D, data=data.frame(t,y),control=nlc, start=list(A=pp$A[i],b=pp$b[i],c=pp$c[i],D=pp$D[i]))##function to fit the curve
  results<-data.frame(se=sigma(res),coef_A=coef(res)[1],coef_b=coef(res)[2],coef_c=coef(res)[3],coef_D=coef(res)[4])##retrieve the important values
  df<-rbind(df,results$se,results$coef_A,results$coef_b,results$coef_c,results$coef_D)###add these values to a data frame.
  names(df)<-"values"

}

df_model<-data.frame(se= df$values[c(TRUE, FALSE,FALSE,FALSE,FALSE)], coef_A = df$values[c(FALSE, TRUE,FALSE,FALSE,FALSE)],
                     coef_b = df$values[c(FALSE, FALSE,TRUE,FALSE,FALSE)],coef_c = df$values[c(FALSE, FALSE,FALSE,TRUE,FALSE)],
                     coef_D = df$values[c(FALSE, FALSE,FALSE,FALSE,TRUE)])###organise the values (coeficients, standard error) in a data frame with columns.
best_fit<-df_model[df_model$se==min(df_model$se),]###retrieve the best fit values by choosing the model fit witht he lowest standard error.

```

Appendix B: Second iteration of automation code.

```r
install.packages('nls')
library(nls)
library(stats)
###fiting sine curve to dataset
datasets <- list.files(path="C:/Users/saswy/Desktop/R_Data/current data", pattern="*csv", full.names=TRUE, recursive=FALSE)
input_datasets<-lapply(datasets, read.csv, header=TRUE, stringsAsFactors=FALSE)
names<-list.files(path = "C:/Users/saswy/Desktop/R_Data/current data", pattern ="*csv",
                  full.names = FALSE)
names<-data.frame(names)
names(input_datasets)<-names$names
pp <- expand.grid(omega=(10:25), phi=(1), A=1, C=1)
nlc <- nls.control(maxiter = 1000,minFactor = 1/1024)
mf <- nls.control(minFactor = 0.000976562)
df<-data.frame()
q<-lapply(input_datasets,function(x){
  t<-x$seconds
  y<-x$R.C
  for (i in 1:nrow(pp)){
    res<- tryCatch(nls(y ~ A*sin(omega*t+phi)+C, data=data.frame(t,y),control=nlc, start=list(A=pp$A[i],omega=pp$omega[i],phi=pp$phi[i],C=pp$C[i])),
                   error=function(e){return(0)})
    if (class(res)!="numeric") {
      results<-data.frame(se=sigma(res),coef_A=coef(res)[1],coef_ome=coef(res)[2],coef_phi=coef(res)[3],coef_C=coef(res)[4])
      df<-rbind(df,results$se,results$coef_A,results$coef_ome,results$coef_phi,results$coef_C)
      names(results)<-"values"
    }
  }
  df
})
df2<-data.frame()
for (i in q){
  df2<-rbind(df2,dim(i))
  names(df2)<-c("number.values","sample")
}
df2 <- df2 %>%
  mutate(Heartbeat = if_else(number.values==80, "Regular pattern", "Irregular pattern"))

models<-data.frame()
final_parameters<-data.frame()
w<-lapply(q,function(x){
  df_model<-as.data.frame(unlist(x))
  names(df_model)<-"values"
  df_model<-data.frame(se= df_model$values[c(TRUE, FALSE,FALSE,FALSE,FALSE)], coef_A = df_model$values[c(FALSE, TRUE,FALSE,FALSE,FALSE)],
                       coef_ome = df_model$values[c(FALSE, FALSE,TRUE,FALSE,FALSE)],coef_phi = df_model$values[c(FALSE, FALSE,FALSE,TRUE,FALSE)],
                       coef_C = df_model$values[c(FALSE, FALSE,FALSE,FALSE,TRUE)])
  best_fit<-df_model[df_model$se==min(df_model$se),]
  #print(df_model)
  final_parameters<-rbind(final_parameters,best_fit)
  #models<-rbind(models,df_model)
  #print(final_parameters)
})
results<-as.data.frame(unlist(w))
names(results)<-"values"
results<-data.frame(se= results$values[c(TRUE, FALSE,FALSE,FALSE,FALSE)], coef_A = results$values[c(FALSE, TRUE,FALSE,FALSE,FALSE)],
                    coef_ome = results$values[c(FALSE, FALSE,TRUE,FALSE,FALSE)],coef_phi = results$values[c(FALSE, FALSE,FALSE,TRUE,FALSE)],
                    coef_C = results$values[c(FALSE, FALSE,FALSE,FALSE,TRUE)])
results$dataset<-names$names
results$number_of_beats<-results$coef_ome/(2*pi)*30
results$Heartbeat<-df2$Heartbeat
###END OF SCRIPT
```

Appendix C: Third iteration of automation code.

```r
#install.packages("dplyr")
#install.packages("ggplot2")
#install.packages("stringr")
library(dplyr)
library(ggplot2)
library(stringr)
slice <- dplyr::slice

#List all the paths to each csv file
datasets <- list.files(path="C:/Users/saswy/Desktop/R_Data/current data", pattern="*csv", full.names=TRUE, recursive=FALSE)
#Read all csv. This object is a list that has the contents of each csv as items of the list.
input_datasets<-lapply(datasets, read.csv, header=TRUE, stringsAsFactors=FALSE)
#Get names for each csv and use them to name each item of "input_datasets". Now we can identify each csv by name on this list.
names<-list.files(path = "C:/Users/saswy/Desktop/R_Data/current data", pattern ="*csv",
                  full.names = FALSE)
names<-data.frame(names)
names(input_datasets)<-names$names## add names to each object of the lsit

###Function that process the csv for each sample
process_sample<-function(time,beat){
  #Create data frame containing the time (seconds) and beats (L.C or R.C).
  data <- data.frame(x = time, y = beat)
  N <- length(data$x) #the number of samples or observations taken
  fft_in <- data$y
  #Apply fourier transform
  fft_out <- fft(fft_in)
  #Generate ata frame with frequencies. Mod function is calculating the modulus of a complex number, which is the distance of the point on
  #the argand plane of the complex number from the origin.
  mod<-data.frame(values=Mod(fft_out[2 : (N/2 + 1)]))
  #Generate plot of frequency components
  barplot(Mod(fft_out[2 : (N/2 + 1)]))
  #Add a column with all frequencies.
  mod$index<-as.numeric(rownames(mod))#contains all the frequencies
  #Variance of the amplitude of all frequencies.
  mod$variance<-as.numeric(var(mod$values))
  #Select amplitudes higher than 0.1. The lower the amplitude the less intense the signal. We are interested in strong signals.
  mod.selected<-mod[which(mod$values>=0.1),]
  #Classification of frequencies based on chosen criteria. Frequencies lower than 25 = 1; >= 25 & < 85 =2 and >= 85 = 3. We need to select one
  #of these Groups to determine the number of beats. In most cases we expect the frequency to be "2", beats ranging from 25 to 85.
  mod.selected<-mod.selected %>% mutate(Group =case_when(
    index < 25 ~ "1",
    index >= 25 & index <85 ~ "2",
    index >=85 & index <=750 ~ "3"))
  #For each Group (1,2,3), we are interested in selecting the strongest frequencies, which are the ones with the  highest amplitude or signal.
  #Data frame df is composed of three rows, one for each Group (1,2,3) and 4 columns (highest amplitude, frequency, variance and Group).
  df<-mod.selected %>%
    group_by(Group) %>%
    slice(which.max(values))
  ##Add column that indicates the weight of each Group. Based on the amplitude value, it indicates how much each frequency contributes to the
  #global signal.
  df$contribution<-df$values*100/sum(df$values)
  df$frequency<-NA
  #Selection of the most probable frequency
  df$frequency[df$values[2] <=1 & df$values[3]<=1 & df$Group =="1"] <- "Freq1"
  df$frequency[df$values[2] <=1 & df$values[3]>=1 & df$Group =="3"] <- "Freq3"
  df$frequency[df$values >=1 & df$contribution[3]>=40 & df$Group =="3"] <- "Freq3"
  df$frequency[df$values >=1 & df$contribution[3]<=40 & df$Group =="2"] <- "Freq2"
  df<-as.data.frame(df[complete.cases(df),])
  #Generate final data frame
  df_final<-data.frame(heartbeat=df$index,amplitude=df$values, variance=df$variance)
}
###process one sample
dat5 <- read.csv("C:/Users/saswy/Desktop/R_Data/current data")
process_sample(dat5$seconds,dat5$L.C)
##process all samples
lc<-lapply(input_datasets,function(x){
  process_sample(x$seconds,x$L.C)
}
)
rc<-lapply(input_datasets,function(x){
  process_sample(x$seconds,x$R.C)
}
)
final_dataset.lc<-unlist(lc)
df.lc<-data.frame(heartbeat=final_dataset.lc)
df.lc<-data.frame(heartbeat= df.lc$heartbeat[c(TRUE,FALSE,FALSE)], amplitude = df.lc$heartbeat[c(FALSE,TRUE,FALSE)],
                  variance = df.lc$heartbeat[c(FALSE,FALSE,TRUE)])
final_dataset.rc<-unlist(rc)
df.rc<-data.frame(heartbeat=final_dataset.rc)
df.rc<-data.frame(heartbeat= df.rc$heartbeat[c(TRUE, FALSE,FALSE)], amplitude = df.rc$heartbeat[c(FALSE, TRUE,FALSE)],
                  variance = df.rc$heartbeat[c(FALSE, FALSE,TRUE)],variance1=df.rc$heartbeat[c(FALSE, FALSE,TRUE)])
df_all<-data.frame(samples=names$names,atrial_heartbeats=as.numeric(df.lc$heartbeat),atrial_amplitude=as.numeric(df.lc$amplitude),
                   atrial_variance=as.numeric(df.lc$variance),
                   ventricular_heartbeats=as.numeric(df.rc$heartbeat),ventricular_amplitude=as.numeric(df.rc$amplitude),
                   ventricular_variance=as.numeric(df.rc$variance))
df_all$condition<-str_extract(df_all$samples, "0umtad|100umtad|90umtad|20umtad|40umtad|60umtad|80umtad")
write.csv(df_all, "C:/Users/saswy/Desktop/R_Data/results")
```

Appendix D: Final iteration of automation code.

```r
#install.packages("dplyr")
#install.packages("ggplot2")
#install.packages("stringr")
library(dplyr)
library(ggplot2)
library(stringr)
slice <- dplyr::slice

datasets <- list.files(path="C:/Users/saswy/Desktop/R_Data/current data", pattern="*csv", full.names=TRUE, recursive=FALSE)
input_datasets<-lapply(datasets, read.csv, header=TRUE, stringsAsFactors=FALSE)#a list of csv
a<-input_datasets[!is.na(as.numeric(input_datasets$x1)), ]
names<-list.files(path = "C:/Users/saswy/Desktop/R_Data/current data", pattern ="*csv",
                  full.names = FALSE)
names<-data.frame(names)
names(input_datasets)<-names$names## add names to each object of the lsit
omega <- (2*pi)/30

datasets <- list.files(path="C:/Users/saswy/Desktop/R_Data/current data", pattern="*csv", full.names=TRUE, recursive=FALSE)
input_datasets<-lapply(datasets, read.csv, header=TRUE, stringsAsFactors=FALSE)#a list of csv
names<-list.files(path = "C:/Users/saswy/Desktop/R_Data/current data", pattern ="*csv",
                  full.names = FALSE)
names<-data.frame(names)
names(input_datasets)<-names$names## add names to each object of the lsit
omega <- (2*pi)/30
###function that process the csv for each sample
process_sample<-function(time,beat){
  data <- data.frame(x = time, y = beat)
  rumeric<-class(data$y)
  N <- length(data$x)
  fft_in <- as.numeric(data$y)
  fft_out <- fft(fft_in)##apply fourier tranform
  mod<-data.frame(values=Mod(fft_out[2 : (N/2 + 1)]))
  #get plot
  #barplot(Mod(fft_out[2 : (N/2 + 1)]))
  mod$index<-as.numeric(rownames(mod))
  mod$variance<-as.numeric(var(mod$values))
  mod.selected<-mod[which(mod$values>=0.1),]##select amplitudes higher than 0.1
  mod.selected<-mod.selected %>% mutate(Group =case_when(
    index < 25 ~ "1",
    index >= 25 & index <85 ~ "2",
    index >=85 & index <=750 ~ "3"))
  df<-mod.selected %>%
    group_by(Group) %>%
    slice(which.max(values))
  df$contribution<-df$values*100/sum(df$values)
  df$frequency<-NA
  #selection of the most probable frequency
  df$frequency[df$values[2] <=1 & df$values[3]<=1 & df$Group =="1"] <- "Freq1"
  df$frequency[df$values[2] <=1 & df$values[3]>=1 & df$Group =="3"] <- "Freq3"
  df$frequency[df$values >=1 & df$contribution[3]>=40 & df$Group =="3"] <- "Freq3"
  df$frequency[df$values >=1 & df$contribution[3]<=40 & df$Group =="2"] <- "Freq2"
  df<-as.data.frame(df[complete.cases(df),])
  print(df)
  df_final<-data.frame(heartbeat=df$index,amplitude=df$values, variance=df$variance)

}
##process all samples
lc<-lapply(input_datasets,function(x){
  process_sample(x$seconds,x$L.C)
}
)
rc<-lapply(input_datasets,function(x){
  #x<-x[!is.na(as.numeric(x$R.C)),]
  process_sample(x$seconds,x$R.C)
}
)
final_dataset.lc<-unlist(lc)
processed_samples<-data.frame(processed=gsub("\\.heartbeat*|\\.variance*|\\.amplitude*","",names(final_dataset.lc)))
al_input<-data.frame(failed=names(lc))
final_names<-al_input[al_input$failed %in% processed_samples$processed,]
failed<-failed[!failed$failed %in% processed_samples$processed,]
df.lc<-data.frame(heartbeat=final_dataset.lc)
df.lc<-data.frame(heartbeat= df.lc$heartbeat[c(TRUE,FALSE,FALSE)], amplitude = df.lc$heartbeat[c(FALSE,TRUE,FALSE)],
                  variance = df.lc$heartbeat[c(FALSE,FALSE,TRUE)])
final_dataset.rc<-unlist(rc)
df.rc<-data.frame(heartbeat=final_dataset.rc)
df.rc<-data.frame(heartbeat= df.rc$heartbeat[c(TRUE, FALSE,FALSE)], amplitude = df.rc$heartbeat[c(FALSE, TRUE,FALSE)],
                  variance = df.rc$heartbeat[c(FALSE, FALSE,TRUE)],variance1=df.rc$heartbeat[c(FALSE, FALSE,TRUE)])
df_all<-data.frame(samples=final_names,atrial_heartbeats=as.numeric(df.lc$heartbeat),atrial_amplitude=as.numeric(df.lc$amplitude),
                   atrial_variance=as.numeric(df.lc$variance),
                   ventricular_heartbeats=as.numeric(df.rc$heartbeat),ventricular_amplitude=as.numeric(df.rc$amplitude),
                   ventricular_variance=as.numeric(df.rc$variance))
df_all$condition<-str_extract(df_all$samples, "10-|70-|40-")
write.csv(df_all, "C:/Users/saswy/Desktop/R_Data/results/results.csv")
```

Appendix E: miRNAs associated with up- or down-regulation due to cardiac damage or cardiotoxicity. *Treatment/damage includes myocardial infarction (MI), coronary artery disease (CAD), hypertrophic cardiomyopathy (HCM), dilated cardiomyopathy (DCM), arrhythmogenic cardiomyopathy (ACM), long QT syndrome (LQTS).*

miRNA	Treatment/Damage	Regulation	Tissue	Reference
miR-1	MI	Up	Cardiac, Plasma	(Condrat *et al*., 2020; Corsten *et al*., 2010; Liu *et al*., 2015; Tijsen *et al*., 2010; Wang *et al*., 2010; Widera *et al*., 2011)
	MI	Up	Plasma	(D'Alessandra *et al*., 2010; Wang *et al*., 2015)
	CAD	Up	Plasma	(Wang *et al*., 2010; Wang *et al*., 2015)
	Daunorubicin	Down	Heart	(Doka *et al*., 2017; Skála *et al*., 2019)
	Hypertrophy	Down	Cardiac	(Colpaert and Calore, 2019; Karakikes *et al*., 2013)
miR-10b	HCM, DCM	Up	Cardiac	(Colpaert and Calore, 2019; Li *et al*., 2018a)
miR-15 family	MI	Down	Cardiac	(Colpaert and Calore, 2019; Hydbring and Badalian-Very, 2013)
miR-17-5p	HCM	Up	Cardiac	(Colpaert and Calore, 2019; Shi *et al*., 2019)
	MI	Up	Circulating	(Xue *et al*., 2019)
miR-21	Arrhythmia	Up	Plasma	(Colpaert and Calore, 2019)
	DCM	Down	Plasma	(Colpaert and Calore, 2019; Rubiś *et al*., 2017; Rubiś *et al*., 2018)
	DCM	Up	Cardiac	(Colpaert and Calore, 2019; Li *et al*., 2018a)
	Ionising Radiation	Up	Fibroblasts	(Pellegrini *et al*., 2020; Tang *et al*., 2009)
	Ionising Radiation	Up	Myocardium	(Pellegrini *et al*., 2020; Shan *et al*., 2009)
	Isoproterenol	Up	Heart	(Ning *et al*., 2017; Skála *et al*., 2019; Yang *et al*., 2016)
	Radiotherapy	Up	PBMCs	(Boštjančič *et al*., 2010; Pellegrini *et al*., 2020)
miR-21-5p	ACM	Up	Cardiac	(Colpaert and Calore, 2019; Zhang *et al*., 2016)
miR-22	Hypertrophy	Down/Up	Cardiac	(Colpaert and Calore, 2019; Huang *et al*., 2013; Tu *et al*., 2013; Xu *et al*., 2012)
	Isoproterenol	Up	Cardiomyocytes	(Skála *et al*., 2019; Tu *et al*., 2014)
	Heart Failure	Up	Plasma	(Goren *et al*., 2012; Wang *et al*., 2015)
miR-23a	Arrhythmia	Down	Plasma	(Colpaert and Calore,

				2019; Feldman *et al*., 2017)
	HCM, DCM	Up	Cardiac	(Colpaert and Calore, 2019; Li *et al*., 2018b)
miR-26	DCM	Down	Plasma	(Colpaert and Calore, 2019; Rubiś *et al*., 2017; Rubiś *et al*., 2018)
miR-26a	Arrhythmia	Down	Plasma	(Colpaert and Calore, 2019; Feldman *et al*., 2017)
miR-27a	Contractility	Up	Cardiac	(Colpaert and Calore, 2019; Nishi *et al*., 2011)
	HCM	Down	Cardiac	(Colpaert and Calore, 2019; Li *et al*., 2018b)
miR-27b	DCM	Down	Plasma	(Colpaert and Calore, 2019; Jiao *et al*., 2018)
miR-29a	HCM	Up	Plasma	(Colpaert and Calore, 2019; Derda *et al*., 2015; Roncarati *et al*., 2014)
	Radiotherapy	Down	Plasma	(Dong *et al*., 2009; Pellegrini *et al*., 2020)
miR-29b	Anthracycline Chemotherapy	Up	Plasma	(Eken *et al*., 2019; Pellegrini *et al*., 2020)
	Ionising Radiation	Down	Arteries	(Pellegrini *et al*., 2020; Yin *et al*., 2009)
miR-29c	Isoproterenol	Down	Heart	(Liu *et al*., 2017; Ning *et al*., 2017; Skála *et al*., 2019; Yang *et al*., 2016)
miR-122	MI	Down	Plasma	(D'Alessandra *et al*., 2010)
miR-126-3p	DCM	Up	Plasma	(Colpaert and Calore, 2019; Jiao *et al*., 2018)
miR-126-5p	MI	Up	Plasma	(Xue *et al*., 2019)
miR-133	Chronic Heart Failure	Up	Cardiac	(Belevych *et al*., 2011; Colpaert and Calore, 2019)
	MI	Up/Down	Cardiac	(Chen *et al*., 2017; Colpaert and Calore, 2019; Xu *et al*., 2014; Yu *et al*., 2019)
	Hypertrophy	Down	Cardiac	(Colpaert and Calore, 2019; Diniz *et al*., 2015; Drawnel *et al*., 2012; He *et al*., 2019)
miR-133a	DCM	Down	Plasma	(Colpaert and Calore, 2019; Rubiś *et al*., 2017; Rubiś *et al*., 2018)
	MI	Up	Plasma	(Condrat *et al*., 2020; Eitel *et al*., 2012; Kuwabara *et al*., 2011; Widera *et al*., 2011; Xiao *et al*., 2019; Zhou *et al*., 2018)
	Daunorubicin	Down	Heart	(Doka *et al*., 2017; Skála *et al*., 2019)
	MI	Up	Plasma	(D'Alessandra *et al*.,

				2010; Wang *et al*., 2015)
	CAD	Up	Plasma	(Wang *et al*., 2010; Wang *et al*., 2015)
	MI	Up	Plasma	(Corsten *et al*., 2010; Wang *et al*., 2015)
miR-133b	MI	Up	Plasma	(D'Alessandra *et al*., 2010; Wang *et al*., 2015)
miR-143	LQTS	Up	Cardiac	(Colpaert and Calore, 2019; Lian *et al*., 2016)
miR-143-3p	DCM	Up	Plasma	(Colpaert and Calore, 2019; Jiao *et al*., 2018)
miR-199a	Hypertrophy	Up	Cardiac	(Colpaert and Calore, 2019; Li *et al*., 2017)
miR-199a-3p	MI	Down	Cardiac	(Colpaert and Calore, 2019; Eulalio *et al*., 2012)
miR-199b	Hypertrophy	Up	Cardiac	(Colpaert and Calore, 2019; Da Costa Martins *et al*., 2010)
miR-208	Ionising Radiation	Up	Plasma	(Calvano *et al*., 2016; Nishimura *et al*., 2015; Skála *et al*., 2019)
miR-208a	Contractility	Up	Cardiac	(Colpaert and Calore, 2019; Rawal *et al*., 2019; Van Rooij *et al*., 2009)
	Daunorubicin	Down	Heart	(Doka *et al*., 2017; Skála *et al*., 2019)
	Isoproterenol	Up	Plasma	(Liu *et al*., 2015)
	CAD	Up	Plasma	(Wang *et al*., 2010; Wang *et al*., 2015)
miR-208b	MI	Up	Plasma	(Corsten *et al*., 2010; Wang *et al*., 2015)
miR-499	MI	Up	Plasma	(Colpaert and Calore, 2019; Corsten *et al*., 2010; Xin *et al*., 2016)
	MI	Up	Plasma/cardiac	(Adachi *et al*., 2010; Condrat *et al*., 2020; Corsten *et al*., 2010; Liu *et al*., 2015; Zhao *et al*., 2015)
	CAD	Up	Plasma	(Wang *et al*., 2010; Wang *et al*., 2015)
	MI	Up	Plasma	(Corsten *et al*., 2010; Wang *et al*., 2015)
miR-499-5p	ACM	Down	Cardiac	Colapert 2019 (Colpaert and Calore, 2019)
		Up	Plasma	(D'Alessandra *et al*., 2010; Wang *et al*., 2015)
miR-539	MI	Up	Cardiac	(Colpaert and Calore, 2019; Wang *et al*., 2015)
miR-541	Hypertrophy	Down	Cardiac	(Colpaert and Calore, 2019; Fu *et al*., 2018)
miR-590-3p	MI	Down	Cardiac	(Colpaert and Calore, 2019; Eulalio *et al*., 2012)
miR-636	DCM	Up	Plasma	(Colpaert and Calore,

				2019)
miR-639	DCM	Down	Plasma	(Colpaert and Calore, 2019)
miR-646	DCM	Down	Plasma	(Colpaert and Calore, 2019)
miR-708-5p	ACM	Up	Cardiac	(Calore *et al*., 2019; Colpaert and Calore, 2019)